



# Kent Academic Repository

**Johnson, Chloe Anne (2019) *Functional Investigation into the Physiology and Pathology of Myosin Class II Isoforms*. Doctor of Philosophy (PhD) thesis, University of Kent,.**

## Downloaded from

<https://kar.kent.ac.uk/80793/> The University of Kent's Academic Repository KAR

## The version of record is available from

## This document version

UNSPECIFIED

## DOI for this version

## Licence for this version

UNSPECIFIED

## Additional information

## Versions of research works

### Versions of Record

If this version is the version of record, it is the same as the published version available on the publisher's web site. Cite as the published version.

### Author Accepted Manuscripts

If this document is identified as the Author Accepted Manuscript it is the version after peer review but before type setting, copy editing or publisher branding. Cite as Surname, Initial. (Year) 'Title of article'. To be published in *Title of Journal*, Volume and issue numbers [peer-reviewed accepted version]. Available at: DOI or URL (Accessed: date).

### Enquiries

If you have questions about this document contact [ResearchSupport@kent.ac.uk](mailto:ResearchSupport@kent.ac.uk). Please include the URL of the record in KAR. If you believe that your, or a third party's rights have been compromised through this document please see our [Take Down policy](https://www.kent.ac.uk/guides/kar-the-kent-academic-repository#policies) (available from <https://www.kent.ac.uk/guides/kar-the-kent-academic-repository#policies>).

# Functional Investigation into the Physiology and Pathology of Myosin Class II Isoforms

Chloe Anne Johnson

2019

A thesis submitted to the University of Kent for the degree of

Doctor of Philosophy in Biochemistry

School of Biosciences

Faculty of Sciences

University of Kent

## ***Declaration***

This thesis contains 4 published works. Each publication was part of a collaborative effort with multiple laboratories. The studies of the functional differences between myosin class II isoforms (Chapter 3), the sequence changes in beta myosin that alter velocity (Chapter 4) and Hypertrophic Cardiomyopathy-causing mutations (Chapter 5) were part of a collaboration with Professor Leinwand from the University of Colorado, USA. The computational modelling in Chapter 3 and Chapter 5 were performed with assistance from Dr Mijailovich's group at the Illinois Institute of Technology, USA and University of Kragujevac, Serbia. The investigation into the function of UNC-45 and a *C. elegans* myosin called MHC-B (Chapter 6) was a collaborative project with Dr Clausen's group at the Institute for Molecular Pathology, Vienna.

My precise contribution to each publication is outlined in detail at the beginning of each results chapter.

No part of this thesis has been submitted in support of an application for any degree or qualification of the University of Kent or any other University or Institute of learning.

Chloe Anne Johnson

October 2019

## ***Acknowledgements***

First and foremost I wish to express my special thanks to my supervisor, Professor Michael Geeves. It has been an honour to be your last student, and a real pleasure to work with you for the past three years. You have shaped me into the scientist I am today, and I will miss working with you. Your continued wisdom, support and encouragement has made this whole endeavour possible.

I would also like to thank Professor Daniel Mulvihill and members of his lab, past and present, for welcoming me into the lab when I joined and making the lab a great environment. I am particularly grateful to Dr Karen Baker, Alia Dos Santos and Dr Jonathan Walklate for being great friends to me.

I have been incredibly fortunate to have had many opportunities to collaborate with world-leading labs. My thanks go to Professor Leslie Leinwand, Dr Carlos Vera, Dr Tim Clausen, Renato Arnese, Dr Srboljub Mijailovich and Marina Svcevic and for facilitating the work presented in this thesis.

To Mum, Pops & Em – thank you for always being such loving constants in my life. I hope I've made you proud.

And finally, to Shanur, who has made this whole process worth it. I cannot wait for our next adventure. Thank you for always being you.

In loving memory of my dear friend, Niken Pam.

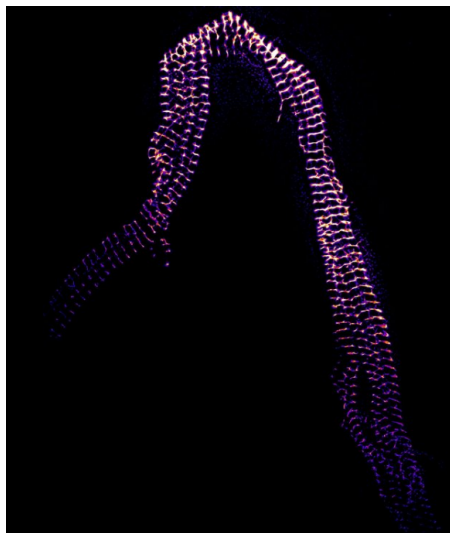


## **Table of contents**

|  |            |
|--|------------|
| <b>Declaration</b> .....   | <b>ii</b>  |
| <b>Acknowledgements</b> .....  | <b>iii</b> |
| <b>Table of contents</b> .....                                       | <b>iv</b>  |
| <b>Abstract</b> .....  | <b>1</b>   |
| <b>Abbreviations</b> .....   | <b>2</b>   |
| <br>   |            |
| <b><u>1. INTRODUCTION</u></b> .....                                  | <b>4</b>   |
| <b>Preface</b> .....   | <b>4</b>   |
| <b>1.1 General properties of myosin</b> .....                        | <b>5</b>   |
| 1.1.1 Myosin.....  | 5          |
| 1.1.2 Sarcomeric myosin.....   | 6          |
| 1.1.3 Structure of class II myosin .....                             | 7          |
| 1.1.4 Structure of the sarcomere.....                                | 11         |
| 1.1.5 ATPase cross-bridge cycle .....                                | 18         |
| <b>1.2 Myosin class II isoforms</b> .....                            | <b>20</b>  |
| 1.2.1 Isoform genes .....  | 20         |
| 1.2.2 Cardiac isoforms .....   | 23         |
| 1.2.3 Developmental isoforms.....                                    | 24         |
| 1.2.4 Skeletal isoforms.....   | 25         |
| 1.2.5 Extraocular isoform .....                                      | 25         |
| 1.2.6 MyHC-7b .....  | 26         |
| 1.2.7 Expression of isoforms.....                                    | 26         |
| <b>1.3 Myosin evolution</b> .....                                    | <b>28</b>  |
| 1.3.1 Myosin superfamily evolution .....                             | 28         |
| 1.3.2 Adaptation to body mass in mammals .....                       | 31         |
| 1.3.3 Velocity and ADP release .....                                 | 34         |
| <b>1.4 Cardiomyopathies</b> .....                                    | <b>37</b>  |
| 1.4.1 Hypertrophic cardiomyopathy .....                              | 38         |
| 1.4.2 Early and late onset mutations.....                            | 40         |
| <b>1.5 Myosin folding</b> .....                                      | <b>42</b>  |
| 1.5.1 UCS family .....   | 42         |
| 1.5.2 <i>C. elegans</i> UNC-45 structure .....                       | 44         |
| 1.5.3 UNC-45 function.....   | 46         |
| <b>1.6 Techniques to probe functional properties of myosin</b> ..... | <b>48</b>  |

|   |            |
|---|------------|
| 1.6.1 Stopped-flow spectroscopy .....   | 48         |
| 1.6.2 Kinetic modelling .....   | 50         |
| <b>1.7 Themes.....</b>  | <b>52</b>  |
| <br>  |            |
| <b><u>2. MATERIALS AND METHODS .....</u></b>  | <b>54</b>  |
| <b>2.1 Materials.....</b>   | <b>54</b>  |
| 2.1.1 Materials.....  | 54         |
| 2.1.2 Buffers.....  | 55         |
| <b>2.2 Protein preparation .....</b>  | <b>56</b>  |
| 2.2.1 Rabbit psoas and rat soleus myosin and S1 preparation.....  | 56         |
| 2.2.2 Rabbit actin preparation .....  | 57         |
| 2.2.3 C2C12 cell protein expression and purification.....   | 58         |
| 2.2.4 SDS PAGE gels .....   | 60         |
| <b>2.3 Kinetic measurements.....</b>  | <b>61</b>  |
| 2.3.1 Stopped-flow and fluorescence.....  | 61         |
| 2.3.2 Transient kinetics .....  | 62         |
| 2.3.3 Pseudo-first order reactions .....  | 63         |
| 2.3.4 S1 affinity for actin.....  | 65         |
| <b>2.4 Modelling .....</b>  | <b>66</b>  |
| <b>2.5 In vitro motility assay .....</b>  | <b>68</b>  |
| <br>  |            |
| <b><u>3. The ATPASE cycle of Human Muscle Myosin II isoforms: Adaptation of a single mechanochemical cycle for different physiological roles .....</u></b>                    | <b>69</b>  |
| <b>3.1 Context of research .....</b>  | <b>69</b>  |
| <b>3.2 Aims of research .....</b>   | <b>69</b>  |
| <b>3.3. Contribution to publication.....</b>  | <b>70</b>  |
| <b>3.4 Publication.....</b>   | <b>70</b>  |
| <br>  |            |
| <b><u>4. Cardiac/slow muscle contraction velocity has evolved to match heart rate with body size through variation in <math>\beta</math>-cardiac myosin sequence.....</u></b> | <b>95</b>  |
| <b>4.1 Context of research .....</b>  | <b>95</b>  |
| <b>4.2 Aims of research .....</b>   | <b>95</b>  |
| <b>4.3 Contribution to publication.....</b>   | <b>96</b>  |
| <b>4.4 Publication.....</b>   | <b>96</b>  |
| <br>  |            |
| <b><u>5. Myosin motor domains carrying mutations implicated in early or late onset hypertrophic cardiomyopathy have similar properties.....</u></b>                           | <b>134</b> |

|   |            |
|---|------------|
| <b>5.1 Context of research .....</b>  | <b>134</b> |
| <b>5.2 Aims of research .....</b>   | <b>135</b> |
| <b>5.3 Contribution to publication .....</b>  | <b>135</b> |
| <b>5.4 Publication .....</b>  | <b>135</b> |
| <br>  |            |
| <b><u>6. Molecular features of the UNC-45 chaperone critical for binding and folding muscle myosin.....</u></b>   | <b>171</b> |
| <b>6.1 Context of research .....</b>  | <b>171</b> |
| <b>6.2 Aims of research .....</b>   | <b>171</b> |
| <b>6.3 Contribution to publication .....</b>  | <b>172</b> |
| <b>6.4 Publication .....</b>  | <b>172</b> |
| <br>  |            |
| <b><u>7. Discussion .....</u></b>   | <b>198</b> |
| <b>7.1 The ATPASE cycle of Human Muscle Myosin II isoforms: Adaptation of a single mechanochemical cycle for different physiological roles .....</b>                    | <b>198</b> |
| <b>7.2 Cardiac/slow muscle contraction velocity has evolved to match heart rate with body size through variation in <math>\beta</math>-cardiac myosin sequence.....</b> | <b>203</b> |
| <b>7.3 Myosin motor domains carrying mutations implicated in early or late onset hypertrophic cardiomyopathy have similar properties .....</b>                          | <b>208</b> |
| <b>7.4 Molecular features of the UNC-45 chaperone critical for binding and folding muscle myosin .....</b>  | <b>213</b> |
| <b>7.5 Concluding remarks and future perspectives.....</b>  | <b>217</b> |
| <br>  |            |
| <b><u>8. Non-publication references.....</u></b>  | <b>218</b> |

## **Abstract**

Myosin is a cytoskeletal motor that uses metabolic energy stored in ATP to do mechanical work. Muscle myosin in all mammals consists of a variety of isoforms, each expressed from its own gene. All of the striated muscle myosin sequences are highly conserved, but each myosin isoform confers distinct contractile characteristics to distinct muscle fibre types. How each myosin is tuned for its specific function is not well understood. We combined detailed biochemical characterisation with a novel kinetic modelling approach to probe how sarcomeric myosin isoforms adapt their mechanochemical cross-bridge cycle to perform different functions.

The next question from this was how the sequences of these highly conserved isoforms give rise to these contractile differences. Focussing on the  $\beta$  cardiac myosin (MyHC- $\beta$ ), we investigated how the sequence of the protein can drive adaptation to changes in body mass by altering the rate of ADP-release and velocity of contraction. Bioinformatics analysis identified the sequence variants in MyHC- $\beta$  that directly control its velocity and the biochemical validations are presented. This demonstrates how a protein can adapt over evolutionary time frames to meet different physiological requirements, which remains one of the fundamental questions in structural and molecular biology.

Mutations in the same protein (MyHC- $\beta$ ) are a major cause of the life-threatening disease, Hypertrophic Cardiomyopathy (HCM). The specific mechanistic changes to myosin function that lead to this disease remain incompletely understood. We hypothesised that mutations that result in early onset disease would have more severe changes in function than do later onset mutations. Contrary to our hypothesis, no clear distinction was observed in the molecular behaviour of MyHC- $\beta$  between early and late onset HCM mutations. One of the existing challenges of a study of this scale is the difficulty in producing recombinant myosin protein. This thesis will describe the development of an innovative expression system in insect cells which produce *C. elegans* body wall myosin in a non-muscle environment. The approach was validated by the biochemical characterisation of the resulting protein, which was found to be homologous to human MyHC- $\beta$ , suggesting it could be used as a new model protein to study human disease.

My thesis describes how sarcomeric myosins have fine-tuned their properties to give rise to different physiological functions, and how these processes are disrupted in diseased-states.



### ***Non-publication abbreviations***

|           |   |
|-----------|---|
| A-band    | Anisotropic band                                |
| AM        | Actin-myosin complex                            |
| AMD       | Actin-myosin-ADP complex                        |
| AMDPi     | Actin-myosin-ADP-phosphate complex              |
| AMT       | Actin-myosin-ATP                                |
| ARM       | Armadillo repeat                                |
| ARVC      | Arrhythmogenic right ventricular cardiomyopathy |
| DCM       | Dilated cardiomyopathy                          |
| dpc       | Days post coitum                                |
| DR        | Duty ratio                                      |
| ELC       | Essential light chain                           |
| EOM       | Extraocular muscle                              |
| F-actin   | Filamentous-actin                               |
| G-actin   | Globular-actin                                  |
| HCM       | Hypertrophic cardiomyopathy                     |
| HMM       | Heavy meromyosin                                |
| I-band    | Isotropic bands                                 |
| IHM       | Interacting heads motif                         |
| $k_{obs}$ | Observed rate constant                          |
| L50       | Lower 50 kDa subdomain of myosin                |
| LECA      | Last eukaryotic common ancestor                 |
| LMM       | Light meromyosin                                |
| sS1       | Short subfragment 1 of myosin                   |
| S1        | Subfragment 1 of myosin                         |
| S2        | Subfragment 2 of myosin                         |
| MDPi      | Myosin-ADP-phosphate complex                    |
| MT        | Myosin-ATP complex                              |
| MUSICO    | Muscle Simulation Code                          |
| MyBP      | Myosin-binding protein                          |

|                |                                  |
|----------------|----------------------------------|
| MyBP-C         | Myosin-binding protein C         |
| MyHC           | Myosin heavy chain               |
| MyHC-emb       | Myosin heavy chain embryonic     |
| MyHC-EO        | Myosin heavy chain extraocular   |
| MyHC-IIa       | Myosin heavy chain IIa           |
| MyHC-IIb       | Myosin heavy chain IIb           |
| MyHC-IId       | Myosin heavy chain II d          |
| MyHC-peri      | Myosin heavy chain perinatal     |
| MyHC- $\alpha$ | Myosin heavy chain alpha         |
| MyHC- $\beta$  | Myosin heavy chain beta          |
| PMSF           | Phenylmethylsulfonyl fluorid     |
| Pyrene         | N-(1-pyrenyl)-iodoacetamide      |
| RLC            | Regulatory light chain           |
| SRX            | Super-relaxed state              |
| TnC            | Troponin-C                       |
| TnI            | Troponin-I                       |
| TnT            | Troponin-T                       |
| TPR            | N-terminal tetratricopeptide     |
| U50            | Upper 50 kDa subdomain of myosin |
| UCS            | UNC-45/CRO1/She4p                |
| UNC-45         | Uncoordinated mutant-45          |

# **1. Introduction**

## ***Preface***

Understanding the relationship between protein structure and function remains a primary focus in many fields of biology, including (but not limited to) genetics, molecular biology, biochemistry and cell biology. The discovery of the motor protein myosin and the fundamental mechanism underlying muscle contraction many decades ago led to a surge in research to characterise its mechanochemical activity. Underlying this activity is the protein's highly conserved structure, of which we now know many details. The functional repertoire of myosin is very diverse - but how has the protein been engineered to enable this? This is a question that remains unanswered. The sequence differences between muscle myosin isoforms can be very small, yet there exists a plethora of functions that the family can perform. Whilst the sequences contain all the genomic information necessary for a protein to perform its function, studying these sequences alone does not yield insights into how myosin isoforms are able to adapt their behaviour to suit the functional demands of the muscle in which they exist. The differences tend to manifest themselves on a biochemical or functional level, indicative of a mechanism of 'fine-tuning' of the highly-conserved myosin protein, which most likely occurs on a molecular level. Gaining a deeper understanding of this process of fine-tuning of myosin class II isoforms is the basis for the studies undertaken in this thesis.

## 1.1 General properties of myosin

### 1.1.1 Myosin

Myosin is a ubiquitous and multifunctional motor protein that converts the energy generated from the hydrolysis of ATP to power movement. The myosin superfamily comprises 35 different sub groups, 13 of which have been identified in humans (Odrionitz and Kollmar 2007). Figure 1.1 demonstrates the myriad of known myosin groups. Myosins are involved in a wide range of cellular processes including cargo interactions, actin-based projections, membrane compartments, cell division, and what this thesis will predominantly focus on, muscle contraction.

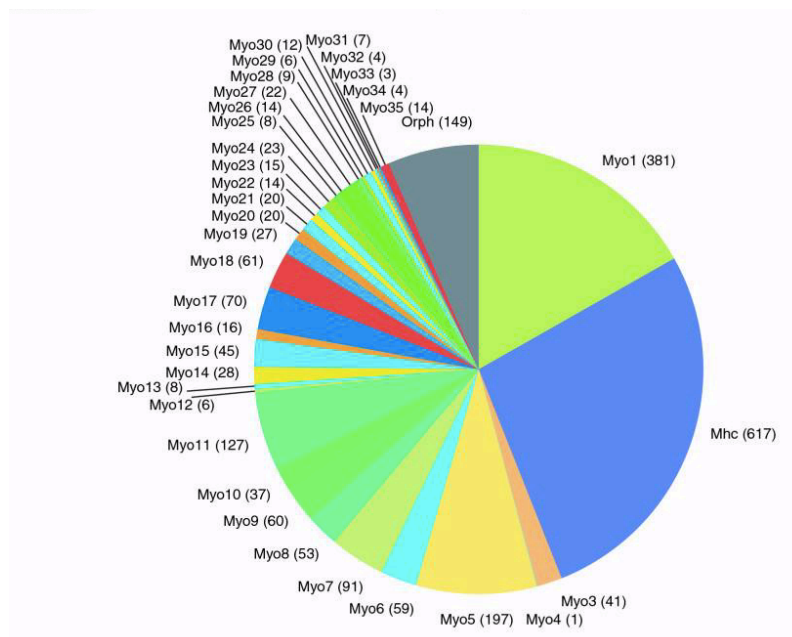


**Figure 1.1 The number of myosins per class. Exact numbers are given in brackets. Figure from (Odrionitz and Kollmar 2007).**

Myosins are structurally related, actin-based molecular motors which can exist either as a single or a double headed dimer. They move towards the plus-end of actin filaments, with the exception of myosin class VI, which are directed towards the minus-end (Park et al. 2007). They have a conserved myosin ATPase cycle, even across different families (Sellers 2000). The enzymatic activity of these motors is coupled to structural changes associated with track interactions, to produce motile movement.

Myosins share a common structure comprised of head, neck and tail regions, as shown in Figure 1.2. The head domain is composed of the motor domain, so-called because it contains the sites for catalytic activity, and the lever arm. The motor domain

contains the nucleotide- and actin-binding sites. The neck region contains a variable number of IQ motifs, which are units of 23 amino acids with the sequence IQXXXRGXXXR that serve as a binding site for calmodulin, or calmodulin-like proteins such as myosin light chains (Bähler and Rhoads 2002). The binding of light chains stabilises the lever arm and allows for some regulation of the myosin protein. Some myosin classes have a cargo binding domain at the C-terminal end, to facilitate intracellular transport of vesicles or organelles – myosin V is an example (Masters, Kendrick-Jones, and Buss 2016).

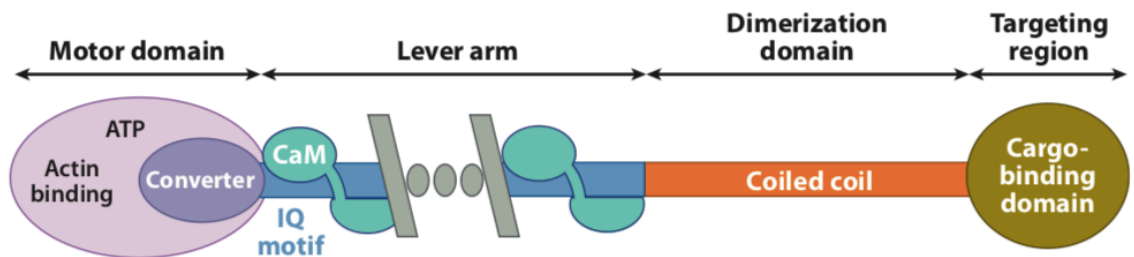


**Figure 1.2. Schematic of the organization of the typical myosin molecule. All myosin sequences contain a motor domain with conserved elements able to bind ATP as well as more variable regions involved in actin binding. The sequence of the tail region is more variable, depending on the myosin class, but can contain coiled-coil sequences for dimerization. The most C-terminal regions can play a role in targeting the myosin to specific cargos in the cell for certain myosin classes. Figure adapted from (Sweeney and Houdusse 2010).**

### 1.1.2 Sarcomeric myosin

Myosins were traditionally termed conventional or unconventional. Class II myosins make up the conventional myosins, and are responsible for muscle contraction. Class II myosins are hexameric protein complexes, composed of 2 heavy chains, 2 essential light chains (ELC) and 2 regulatory light chains (RLC). The 2 heavy chains form a dimer, with the motor domain found at the N-terminal part. The IQ motifs on the heavy chains facilitate binding of the essential and regulatory light chains. The C-terminal region of the heavy chain forms a rod-like coiled-coil structure. Proteolytic digestion of the myosin dimer with the enzyme papain can generate heavy meromyosin (HMM) and light meromyosin (LMM) (Figure 1.3) (Kominz et al. 1965). The HMM fragment consists of the 2 globular head domains, the 2 neck regions, and a short portion of the coiled-coil tail, leaving the remaining coiled-coil portion of the tail in the LMM fragment. HMM interacts with many components of the sarcomere, predominantly with actin in the thin filament. The head and tail portions of HMM can be separated by further digestion with  $\alpha$ -chymotrypsin to generate subfragment 1 (S1)

and subfragment 2 (S2) (Gergely, Gouvea, and Karibian 1955; Mihalyi and Harrington 1959). The S1 is a monomeric motor domain; the remaining dimeric neck region makes up S2.

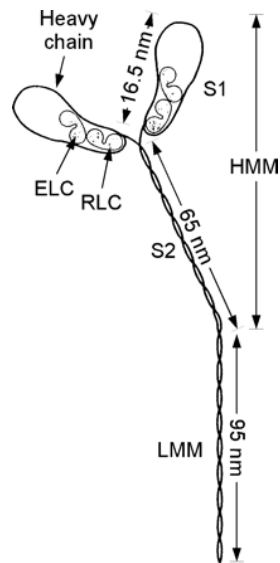


**Figure 1.3. Schematic representation of cleavage products of a myosin molecule to generate HMM and LMM. HMM can be further digested with  $\alpha$ -chymotrypsin to generate subfragment 1 (S1) and subfragment 2 (S2). Figure from (Hooper and Thuma 2005).**

### 1.1.3 Structure of class II myosin

The first crystal structure of an S1 molecule was obtained in 1994 for chicken skeletal S1, in what is now termed the post-rigor state of the cross-bridge cycle (Rayment et al. 1993). Since then, more high-resolution crystal structures have become available of myosin in different nucleotide-bound states, yielding insights into structural changes that the myosin motor is subjected to during the cross-bridge cycle (see section 1.15, Figure 1.12). To note, all residue numbers hereafter in this section are referring to the chicken skeletal S1 structure.

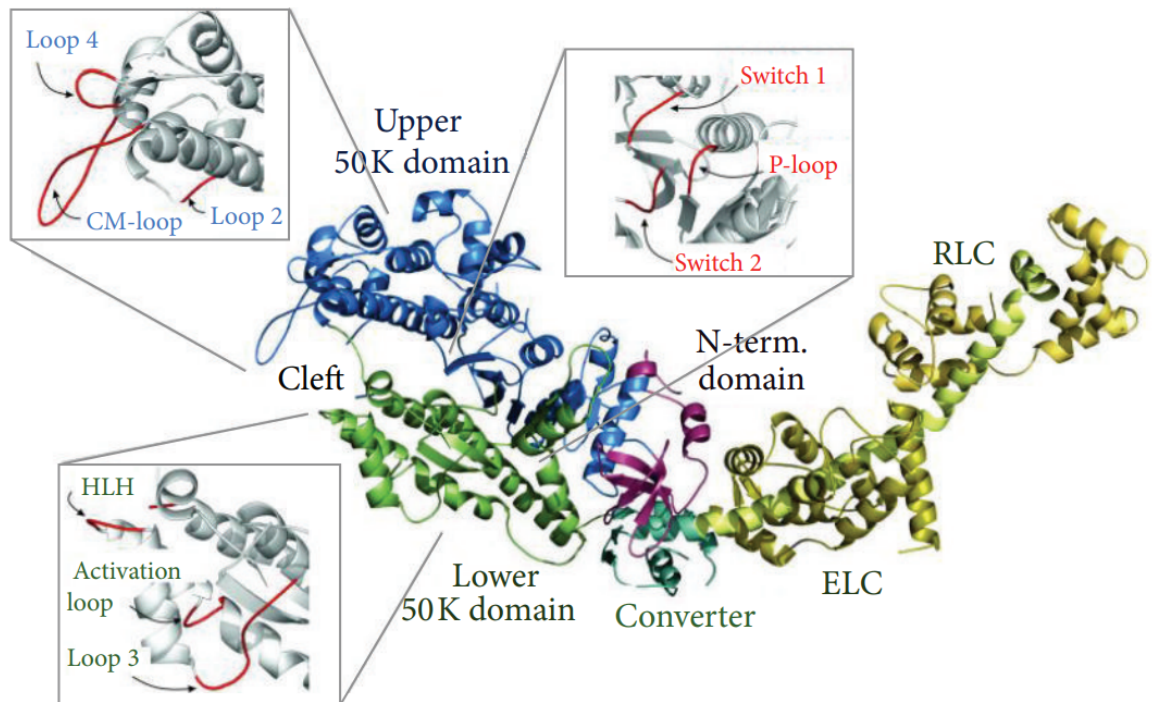


**Figure 1.4. Crystal structure of a chicken skeletal myosin motor domain in a post-rigor complex. The lower 50 kDa subdomain is shown in green, the upper 50 kDa subdomain in blue, the converter domain in cyan and the essential and regulatory light chains in yellow. Figure from (Mansson, Rassier, and Tsiavaliaris 2015).**

S1 can be proteolytically digested into 3 fragments, which are named by their apparent molecular weights; a 25 kDa N-terminal domain, a central 50 kDa and a 20 kDa C-terminal domain (Mornet et al. 1979) (see Figure 1.4). The central 50 kDa fragment is composed of the upper 50 kDa and lower 50 kDa subdomains (U50 and L50, respectively). The U50 and L50 subdomains are separated by the central beta sheet and surrounding alpha helices, which together form a 4-5 nm deep cleft, extending from the nucleotide binding site to the actin-binding site. The actin- and nucleotide-binding sites are therefore on opposite sides of the seven-stranded  $\beta$ -sheet and are separated by 40–50 Å (Geeves, Fedorov, and Manstein 2005). The central  $\beta$ -sheet is composed of 7 strands, 6 of which are found in the U50 subdomain, and 1 from the L50 subdomain (Figure 1.5).

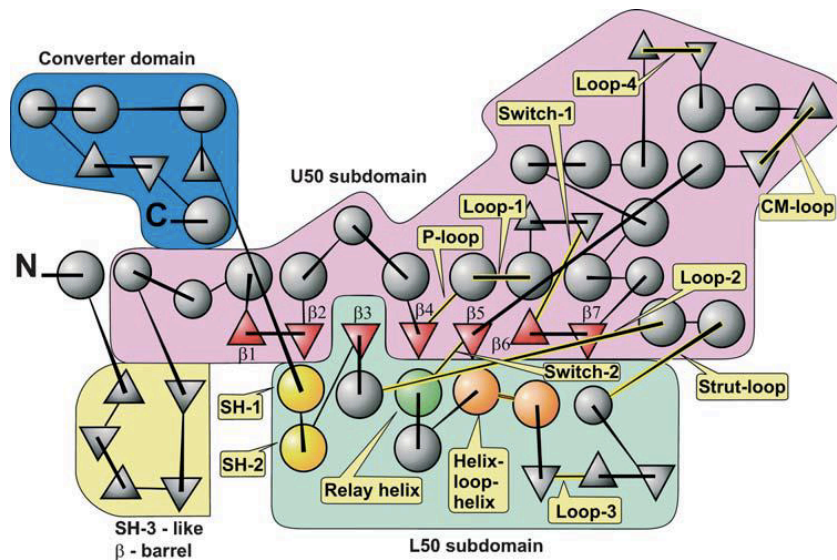


**Figure 1.5. Topological map of the myosin motor domain. Helices are shown as circles,  $\beta$  strands are shown as triangles. The N-terminal SH-3-like  $\beta$  barrel is coloured yellow, the U50 subdomain in pink, the L50 subdomain in green and the converter domain in blue. Figure from (Geeves, Fedorov, and Manstein 2005).**

The L50 subdomain contains a major portion of the actin-binding site. The U50 subdomain contains the nucleotide binding pocket, which is made up of switch 1 and switch 2 and the P-loop. These switches move relative to one another depending on which nucleotide is present during the cross-bridge cycle. Switch 1 is positioned at the bottom of the actin-binding cleft, and communicates between the nucleotide- and actin-binding sites. The conformation of this switch determines whether the cleft is in a 'closed' or 'open' conformation. Switch 2 recognises  $\gamma$ -phosphate of a nucleotide bound in the pocket. The conformation of switch 2 is dictated by the conformation of the active site. Movement of the switch 2 helix forces the SH1-SH2 helices to adjust, causing a 60 degree rotation of the converter and lever arm, which generates a 5 nm step size (Koppole, Smith, and Fischer 2006).

The 20 kDa fragment contains a long alpha helix (residues 648-689) that spans the structure from loop 2 to the third strand in the central beta sheet, followed by a turn and a broken helix. This broken helix is referred to as the SH1-SH2 as it contains two reactive thiols at positions 697 (SH2) and 707 (SH1). The distal end of the SH1 helix forms a hinge for the ensuing converter domain (Rayment et al. 1993).

The converter domain is juxtaposed to the lever arm, and is located close to the essential light chain binding site (Dominguez et al. 1998). The converter domain acts as a fulcrum for the lever arm, and amplifies small conformational changes that occur in the active site by as much as 10 times. To do this, the converter domain links to the relay helix,



which is found in the L50 subdomain. Switch 2 is at the end of the relay helix, which when bound to a  $\gamma$ -phosphate will cause a twisting and bending of the relay helix, so that the distal end goes through a large movement. The distal end is in close contact with the converter domain, and so the converter domain moves with it to generate a 5-10 nm translation of the tip of the IQ domain. Therefore, the position of the relay helix determines the movement of the converter domain.

A number of surface loops are present within the structure to provide physical links that mediate conformational changes as a result of actin- and nucleotide-binding. Switch 2 and the P-loop are involved in nucleotide binding, whilst loop 2, loop 3, loop 4 and the cardiomyopathy loop are involved in actin binding (Figure 1.4, 1.5). There are a number of important linkers in the motor domain such as the SH1 helix, relay helix and the strut loop, all of which are joined by key structural domains.

The cardiomyopathy loop (CM loop) is found at positions 406-416, shown at the top-right of Figure 1.5. Its sequence is important for correct myosin function (Liu et al. 2005). The name comes from the hypertrophic cardiomyopathy causing-mutation found at the human 403 residue, which is an arginine to glutamine substitution. This was the first missense point mutation to be identified in human  $\beta$ -cardiac myosin (Geisterfer-Lowrance et al. 1990). Unconventional myosins can be regulated via this loop due to phosphorylation of a serine or threonine (termed TEDS site) by members of the p21-activated kinase family (Attanapola, Alexander, and Mulvihill 2009; Fujita-Becker et al. 2005; Novak and Titus 1998). Phosphorylation at this site stimulates actin-activated ATPase and motor activity; motors without a negative charge at this position display low ATPase and motility (De La Cruz, Ostap, and Sweeney 2001; Ostap et al. 2002; Fujita-Becker et al. 2005). The CM loop forms an antiparallel  $\beta$ -strand that is the major site of interaction of the upper 50-kDa motor domain with actin.

Another loop in the motor domain is the strut loop, composed of 4 amino acids at positions 590-593 which is found on the surface near the actin-binding site. A single insertion or deletion into this loop abolished strong binding to actin, although the motor activity in the absence of actin was unchanged, showing the loop is important for actin binding (Sasaki, Ohkura, and Sutoh 2000).

#### 1.1.4 Structure of the sarcomere

The mammalian muscular system contains 3 types of muscles – skeletal, cardiac and smooth. The underlying contractile mechanism is conserved across all 3 types, but they differ in their structural ordering and regulation. Smooth muscle is an involuntary, non-striated muscle. It is present in the walls of hollow organs such as the intestines and the bladder, and is controlled by the autonomous nervous system. In contrast, cardiac and skeletal muscle have a highly structured appearance when viewed under the microscope. The work of this thesis will focus on the skeletal and cardiac muscle systems.

Cardiac and skeletal muscles have a striated appearance, and are composed of muscle fibres, which are individually comprised of myofibrils. It is myofibrils that contain repeating units of the basic, contractile unit of a muscle cell – the sarcomere. An electron micrograph is shown in Figure 1.6 – the alternating light and dark bands are visible which are responsible for the striated pattern. A sarcomere is typically 1.5 - 3.2 microns in length (Burkholder and Lieber 2001), depending on muscle type and is composed of thin and thick filaments.

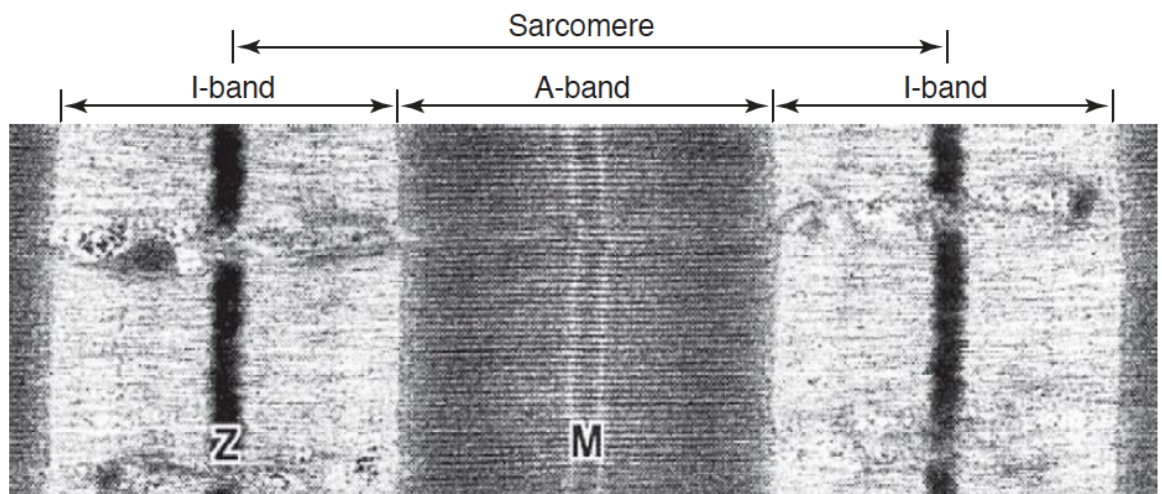


**Figure 1.6. Electron micrograph of a sarcomere from skeletal muscle. The A-band corresponds to the region containing overlapping thin and thick filaments, the I-band contains just the thin filaments. The Z-disc and M-bands are where thin and thick filaments respectively are anchored. (Agarkova and Perriard 2005).**

The thin filaments are seen as light bands, or isotropic bands (I-bands). The thin filaments are composed predominantly of actin, tropomyosin and troponin. Running through the middle of the I-band is the Z-disc, which in Figure 1.6 can be seen as a dark, thick line. The Z-disc anchors the thin filaments in the sarcomere. The dark bands, or anisotropic bands (A-bands) are composed of overlapping thin and thick filaments. The thick filament is composed of mostly myosin, myosin light chains and myosin binding

protein-C (MyBP-C). The slightly darker line running through the middle of the A-band represents the M-band, which is where thick filaments are anchored. The H-zone corresponds to the part of the A-band that contains no thin filaments. The sliding filament theory obtained its name due to the phenomenon by which, when viewed under a microscope, the thick filaments slide past the thin filaments during contraction, resulting in the I-band and H-zone shortening but the A-band remaining the same length (Huxley and Hanson 1953). Myosin thick filaments are bipolar with a bare zone halfway along their length, where there is antiparallel packing of myosin molecules (Figure 1.7). The myosin heads then appear in the two outer parts of the filaments, termed the bridge regions (AL-Khayat et al. 2013).

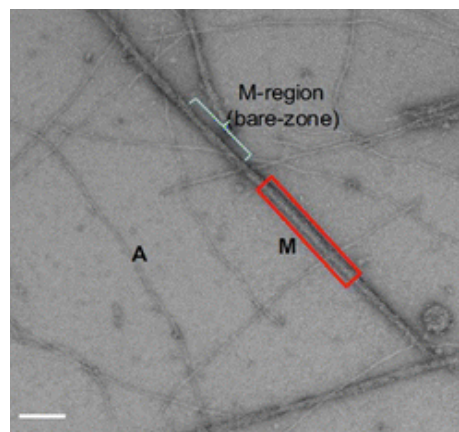


**Figure 1.7. Electron micrograph of isolated myosin filaments (M) from the ventricular muscle of a human heart. Some actin filaments can be seen in the background, labelled (A). Scale bar is 200 nM. Adapted from (AL-Khayat et al. 2013)**

As well as the major components of the thin and thick filaments, there are a number of accessory proteins found within the sarcomere that confer stability on the structure. This is fundamental for skeletal and cardiac muscles to function. Titin is one example, which is a “giant” protein 1  $\mu$ M in length, spanning half the length of a sarcomere. It is thought to act like a molecular spring, maintaining a continuous filament structure throughout a myofibril. The elastic I-band region of titin consists of immunoglobulin sequences with intermittent unique regions. Titin’s elastic properties are a result of a region that contains 70% proline, glutamic acid, valine and lysine residues (Labeit and Kolmerer 1995). In the A-band, titin interacts with MyBP-C and the myosin tail domains, thus linking titin to the thick filaments (Houmeida et al. 1995; Soteriou, Gamage, and Trinick 1993). The A-band region of titin is composed of super repeats of seven fibronectin III domains and four immunoglobulin domains. These domains correspond to the C-zone thick filament repeats and may define

the number and position of myosin and MyBP-C (Freiburg and Gautel 1996). Titin has also been found to interact with actin (Chung et al. 2011; Nishikawa et al. 2019).

Anchored at the Z-disc is a protein called nebulin. Nebulin has a chain weight of around 600–900 kDa and runs along the thin filaments in the I-band from the Z-disc to the actin filament tip. Nebulin occurs in many splice isoforms of varying length and this length has been shown to determine the length of the actin filaments in the I-band of skeletal muscle (Siegfried, Ottenheijm, and Granzier 2011). The thin filament is terminated at the end toward the M-band (the pointed end) by the protein tropomodulin (McElhinny et al. 2001). At the Z-disc, the barbed ends of actin-based thin filaments are cross-linked via  $\alpha$ -actinin (Maruyama and Ebashi 1965). A schematic of the sarcomere containing thick filaments, thin filaments and titin is shown in Figure 1.8.

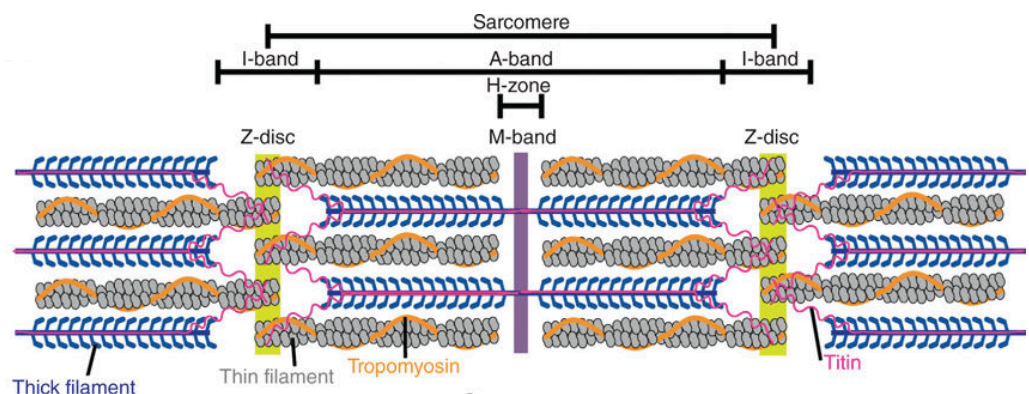


**Figure 1.8. Schematic representation of the sarcomere. Actin (grey) forms thin filaments with tropomyosin (orange) and troponin. Thick filaments are depicted blue. The lateral boundaries of the sarcomere are at the Z-disc (yellow). The I-bands surround the Z-disc, and correspond to thin filaments with no over-lapping thick filaments. The M-band is shown in purple, and constitutes where thick filaments are anchored. The A-band region contains both thin and thick filaments, whereas the H-zone contains only thick filaments. Titin (pink) extends the length of a half-sarcomere. Figure from (Henderson and Gregorio 2015).**

Another component of the thick filament is the myosin-binding protein family (MyBP). This family consists of myosin-binding protein C (MyBP-C) and myosin-binding protein H (MyBP-H). Both are located in the C zone (A-band region containing cross-bridges) and are restricted to transverse stripes spaced at 43 nm intervals (Bennett et al. 1986; Craig and Offer 1976). The structure of MyBPs includes a series of immunoglobulin and fibronectin type III repeat domains (Flashman et al. 2004). MyBPs interact with the thick, thin, and titin filament systems. The highly conserved C-terminal C10 domain of both MyBP-C and MyBP-H allows for interaction with myosin tails contributing to the

maintenance and stability of the thick filament (Kampourakis et al. 2014; Moos et al. 1975; Mouton et al. 2015). Additionally, the C-terminus binds titin and is necessary to localize MyBPs to the A-band (Gilbert et al. 1999; Labeit et al. 1992). The N-terminus of MyBP-C binds actin filaments, potentially regulating contraction by altering the actin-activated myosin ATPase activity (Hartzell 1985; Squire, Luther, and Knupp 2003), while MyBP-C's N-terminal M-motif interacts with the S2 region of myosin (Gruen and Gautel 1999; Starr and Offer 1978). Although the precise function is still being elucidated, MyBPs are involved in filament assembly and in regulation of contraction (Weith et al. 2012). MyBP-C is thought to link the thick and thin filament systems and further regulate cross-bridge cycling by displacing tropomyosin and competing with myosin for actin binding (Ackermann and Kontogianni-Konstantopoulos 2011).

The myosin-containing thick filaments interact with the thin filament in a sarcomere to produce movement. The thin filament is primarily composed of three proteins; actin, tropomyosin and troponin. Actin is one of the major structural elements of muscle. Actin is an activator of myosin; in the absence of actin, myosin can hydrolyse ATP, but its presence increases the ATPase rate by a factor of 100 for fast adult skeletal isoforms. Vertebrates express 3 main actin isoforms –  $\alpha$ ,  $\beta$ , and  $\gamma$ .  $\alpha$ -actin is predominantly expressed in skeletal and cardiac muscles during adulthood, whilst  $\gamma$ -actin is expressed in smooth muscles of blood vessels and internal organs. Cytoplasmic  $\beta$ - and  $\gamma$ -actin are ubiquitous and have a role in the cytoskeleton with expression occurring in all cells in different ratios (Dugina, Shagieva, and Kopnin 2019; Garrels and Gibson 1976).

Actin is a highly conserved protein with a sequence identity of 85% between the most divergent family members. Over 50 actin binding proteins have been identified in both lower and higher eukaryotes (Geeves, Fedorov, and Manstein 2005); distant but undisputable prokaryotic homologues of actin have been identified (van den Ent, Amos, and Löwe 2001; Jones, Carballido-López, and Errington 2001). Multiple actin monomers (globular actin, G-actin) polymerise to form filaments (filamentous actin, or F-actin), which forms the backbone of the thin filament. The critical protein concentration ( $C_c$ , concentration of monomers) for actin polymerisation is  $0.1 \mu\text{M}$  – above this concentration G-actin will spontaneously form F-actin (Tilney 1976; Vinson et al. 1998).

The first crystal structure of G-actin was achieved in 1990 (Kabsch et al. 1990). Figure 1.9 shows the structure of G-actin at atomic resolution (Geeves, Fedorov, and Manstein 2005). The monomer consists of two subunits, called the 'small' and 'large' domains. These domains are separated by a central cleft which contains the nucleotide

and cation binding site (Gordon, Homsher, and Regnier 2000). Each domain can be further subdivided; the small domain contains subdomain 1 and 2, and the large domain contains subunits 3 and 4. Two parallel strands of F-actin can form a double helical structure (as seen in Figure 1.10). Subdomains 3 and 4 are located internally in the helix whereas subdomains 1 and 2 are solvent-exposed as they are located on the surface of the filament, where interaction with myosin heads can occur. The helix repeats every 13 actin monomers, or every 360 Å (Graceffa and Dominguez 2003).

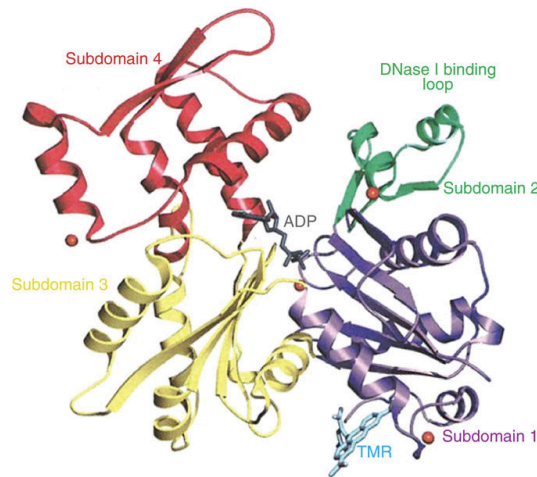


**Figure 1.9. Crystal structure of an actin-monomer, or globular actin, showing the 4 subdomains. An ADP nucleotide and magnesium cations are shown. Figure from (Otterbein, Graceffa, and Dominguez 2001).**

An extended, fibrous molecule called tropomyosin is also found in the thin filament with actin (see Figure 1.10). It is composed of two right-handed  $\alpha$ -helices, which form a left-handed coiled-coil structure. The formation of a coiled-coil is energetically favorable as hydrophobic interactions of non-polar residues in the two chains stabilize the molecule. Tropomyosin can exist either as homo- or heterodimers (Janco et al. 2013). Mammalian fast skeletal and cardiac tissues express variable ratios of  $\alpha$ - and  $\beta$ -tropomyosin and assemble as  $\alpha\alpha$  and  $\alpha\beta$  dimers.  $\beta\beta$  heterodimers have low thermal stability, and so are not typically found in most muscle tissues (Janco et al. 2013). Tropomyosin molecules extend over and interact with seven actin monomers, which together with troponin subunits confer regulation of the thin filament. The formation of an extended filament is achieved through N-terminal to C-terminal aggregation of the tropomyosin dimer via an 8-11 amino acid residue overlap. Tropomyosin spans seven actin monomers on each strand of an F-actin polymer (Gordon et al. 2000). Tropomyosin regulates the binding of myosin to actin as a result of structural changes in the troponin complex.

The troponin complex is composed of three subunits – troponin-C (TnC), troponin-I (TnI) and troponin-T (TnT) (Greaser and Gergely 1973), which are named after their specific functions in the complex. The positions of these three subunits are shown in Figure 1.10. TnC consists of two globular regions, which are connected through a long  $\alpha$ -helix. TnC binds  $\text{Ca}^{2+}$  via calcium-binding EF-hand motifs. Binding of calcium to the EF-motif leads to conformational changes allowing the N-terminal domain of TnC to interact with TnI (McKay et al. 1997). TnI is the inhibitory subunit of the troponin complex and is able to block actin.myosin ATPase activity in the presence of tropomyosin (Leavis and Gergely 1984). When TnC interacts with TnI, it dissociates from actin, shifting tropomyosin to allow for weak binding of myosin to actin. The calcium state of TnI changes its affinity for binding partners based on the binding of calcium to TnC and its subsequent conformational shift (Lehman et al. 2001). TnT is the third component of the complex, which anchors the troponin complex to tropomyosin (Franklin et al. 2012; Kobayashi, Jin, and de Tombe 2008). The function of TnT is somewhat controversial. It is thought to organize the regulatory complex as a whole, by anchoring TnC and TnI to the thin filament; however TnT may also have roles in muscle contraction through regulation of actin.myosin ATPase activity, calcium sensitivity, and force generation in the sarcomere (Potter et al. 1995; Willott et al. 2010).

As detailed above, there are a plethora of interactions that occur between the numerous proteins of the thin and thick filaments of a sarcomere. These interactions are summarized in Figure 1.10.

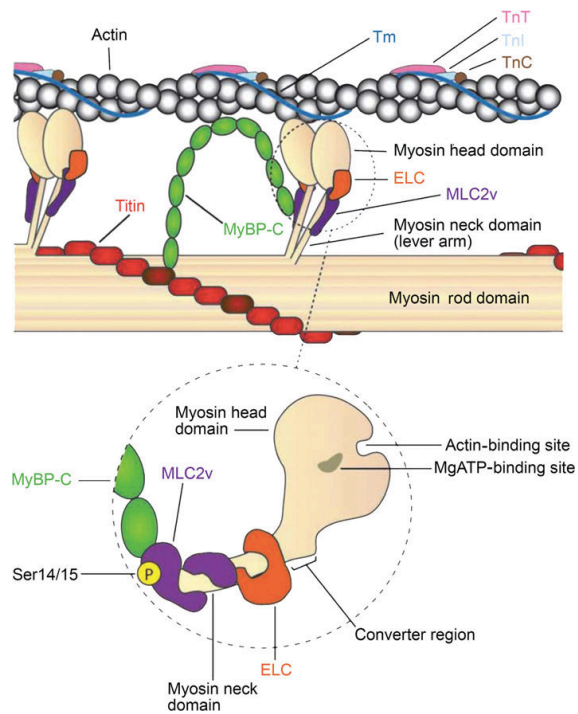


**Figure 1.10. Summary of interactions occurring in thick and thin filaments in a striated muscle. Muscle contraction is dependent on the interactions between myosin-based thick filament via the head domain and actin-based thin filament. The troponin complex, composed of troponin T, troponin C and troponin I (TnT, TnC, TnI, respectively) and tropomyosin regulate actin.myosin ATPase in a  $\text{Ca}^{2+}$ -sensitive manner. Thick filament regulator proteins - myosin essential light chain (ELC) and myosin regulatory light chain-2 (MLC2v) and MyBP-C - regulate myosin activation and function. MyBP-C interactions with actin, the myosin rod domain, MLC2v and titin are shown. The magnified, dashed circle highlights MyBP-C interacting with MLC2v, the actin- and nucleotide-binding sites in the myosin motor domain, and the phosphorylation site found at Ser14/15. Figure adapted from (Sweeney and Houdusse 2010).**



### 1.1.5 ATPase cross-bridge cycle

The fundamental mechanism of muscle contraction was first described by Huxley and colleagues in 1954, who put forward the sliding filament theory when they observed sarcomere shortening under a light microscope (Huxley and Niedergerke 1953). The sliding filament theory was further expanded by Lymn and Taylor as a cycle containing 4 steps (Lymn and Taylor 1971). This is summarised in Figure 1.11. Briefly, myosin is bound to actin in the rigor complex (free of nucleotide). ATP binds, which leads to very fast dissociation of myosin from actin. The hydrolysis of ATP to ADP and  $P_i$  leads to formation of a stable myosin.ADP. $P_i$  complex, whereupon actin can rebind. This leads to release of the products and return to the rigor state. In the last transition, myosin slides past actin in a rowing-like stroke – this event is referred to as the powerstroke.

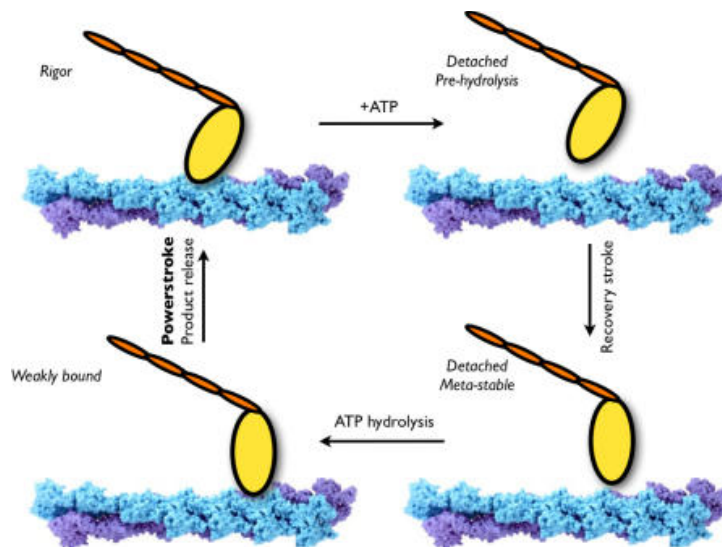


**Figure 1.11. The Lymn-Taylor actin.myosin ATPase cycle. The binding of ATP to actin.myosin (in a rigor complex) leads to dissociation of myosin from actin. Structural changes in the lever arm orientation leads to the recovery stroke, followed by ATP hydrolysis. Myosin now rebinds actin weakly. Subsequent phosphate release is coupled to the powerstroke. Changes in the orientation of the lever arm and ADP release increases the affinity of myosin for actin, returning the complex to a rigor state. Figure from (Yu et al. 2007).**

Today's widely accepted model of the actin.myosin ATPase cycle, also known as the cross-bridge cycle, is composed of coupled mechanical and biochemical events, converting biochemical energy into movement. Since the Lymn-Taylor model was proposed, numerous structures have been characterised for myosin in different parts of the cross-bridge cycle. This has provided insight into how the kinetic cycle is related to

structural changes in the myosin molecule, as shown in Figure 1.12. The work in this thesis is based upon an 8-step cycle, which will be discussed in further detail in section 1.6.2.

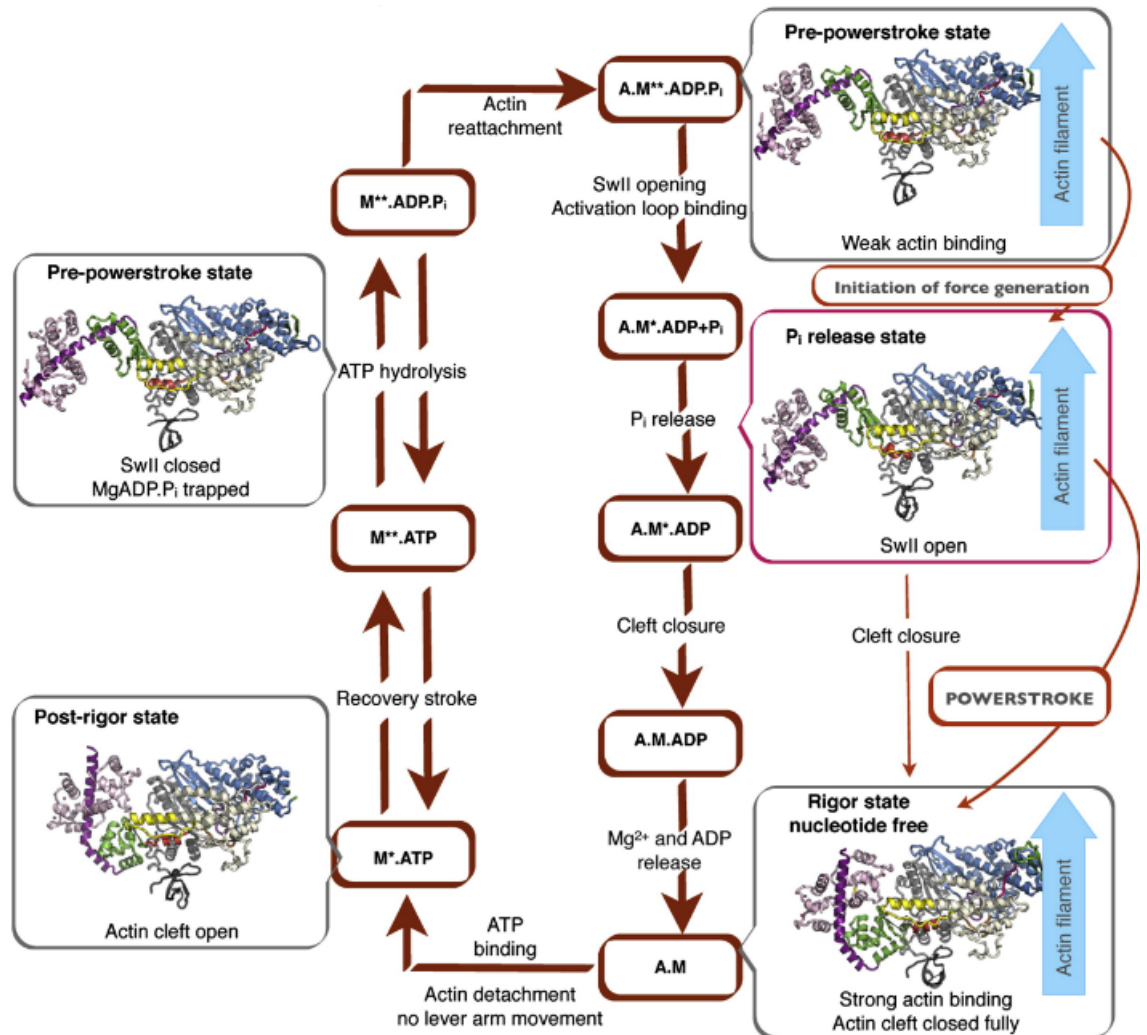


**Figure 1.12. Actin-myosin ATPase cycle showing the known structural states of Myosin VI in the force-generating cross-bridge cycle. The motor domain of Myosin VI is depicted in four structural states: Rigor (nucleotide free, on F-actin); Post-Rigor (detached from F-actin, bound to an ATP analog); pre-powerstroke (bound to ADP.Pi, representing post hydrolysis with ADP.Pi trapped in the active site) and the Pi release state. Figure adapted from (Linas et al. 2015).**

## **1.2 Myosin class II isoforms**

### 1.2.1 Isoform genes

The myosin class II family contain 13 isoforms in humans, which can be divided into three groups: smooth, striated and non-muscle. Nine of these 13 isoforms are striated, which this thesis will focus on (see Table 1.1). Expression levels vary across species, developmental time point and muscle type (Bottinelli and Reggiani 2000; Lu et al. 1999; Toniolo et al. 2004). ATP turnover and force production vary between different isoforms. Fatigue tolerance is also a property of the isoform being expressed (Karatzafiri, Adamek, and Geeves 2017). These variations confer unique characteristics to different muscle types, and the varied myosin composition within skeletal muscle fibres allows for a wide range of contractile velocities and forces among different muscle types.

The relative proportions of isoforms varies between different muscle types (Harridge et al. 1996). In humans, adult muscle fibres may contain predominantly one myosin isoform (beta, IIa or IIc), or they can be found of mixtures of fibre types (beta/IIa, IIa/IIc for example (Bottinelli and Reggiani 2000)). Early expression patterns define adult fibre types, although changes in isoform composition can occur in response to neural, hormonal and mechanical factors (Loughna et al. 1990; Pette and Vrbová 1985). A skeletal muscle will have a range of mechanical & energy demands exerted upon it – thus, diversity in fibre composition is required to meet these demands.

The human *MYH* genes are highly conserved, sharing 77-95% sequence homology when excluding the MyHC-7b (Table 1.2). This is true for both the motor and tail domains of myosin isoforms. There is even higher conservation across mammalian species – Table 1.3 shows the % sequence identity of beta and embryonic isoforms between rat, rabbit, human and bovine species. For both isoforms, the sequence homology is 97-98% identical.

| <b>Gene</b>  | <b>Protein</b> | <b>Abbrev.</b> | <b>Chromosome position</b> | <b>Class</b> | <b>Human Tissue Expression</b>                 |
|--------------|----------------|----------------|----------------------------|--------------|--|
| <i>MYH2</i>  | MyHC-IIa       | Ila            | 17                         | Striated     | Skeletal muscle post birth                     |
| <i>MYH4</i>  | MyHC-IIb       | IIb            | 17                         | Striated     | Unknown  |
| <i>MYH1</i>  | MyHC-IIc       | IId            | 17                         | Striated     | Skeletal muscle post birth                     |
| <i>MYH6</i>  | MyHC- $\alpha$ | Alpha          | 14                         | Striated     | Atrial myocardium                              |
| <i>MYH7</i>  | MyHC- $\beta$  | Beta           | 14                         | Striated     | Ventricular myocardium and slow skeletal       |
| <i>MYH3</i>  | MyHC-emb       | Embryonic      | 17                         | Striated     | Embryo skeletal muscle and regenerating muscle |
| <i>MYH8</i>  | MyHC-peri      | Perinatal      | 17                         | Striated     | Embryo skeletal muscle and regenerating muscle |
| <i>MYH13</i> | MyHC-EO        | Extraocular    | 17                         | Striated     | Extraocular and specialised muscles            |
| <i>MYH7b</i> | MyHC-7B        | 7b             | 20                         | Striated     | Unknown  |
| <i>MYH9</i>  | NMMHC-IIa      | Non-muscle IIa | 22                         | Non-muscle   | Cytoplasm                                      |
| <i>MYH10</i> | NMMHC-IIb      | Non-muscle IIb | 17                         | Non-muscle   | Cytoplasm                                      |
| <i>MYH11</i> | SMMHC          | Smooth         | 16                         | Smooth       | Smooth muscles                                 |
| <i>MYH14</i> | NNMHC-IIc      | Non-muscle IIc | 19                         | Non-muscle   | Cytoplasm                                      |

**Table 1.1. Summary of myosin class II genes and the proteins they encode. Data in table taken from (Schiaffino and Reggiani 2011; Lee et al. 2019).**

|    |                |          |          |          |                |               |           |          |         |         |
|----|----------------|----------|----------|----------|----------------|---------------|-----------|----------|---------|---------|
| A. | MyHC-IIa       | MyHC-IIa |          |          |                |               |           |          |         |         |
|    | MyHC-IIb       | 92       | MyHC-IIb |          |                |               |           |          |         |         |
|    | MyHC-IIc       | 95       | 94       | MyHC-IIc |                |               |           |          |         |         |
|    | MyHC- $\alpha$ | 80       | 80       | 81       | MyHC- $\alpha$ |               |           |          |         |         |
|    | MyHC- $\beta$  | 81       | 81       | 81       | 93             | MyHC- $\beta$ |           |          |         |         |
|    | MyHC-Peri      | 93       | 90       | 92       | 80             | 79            | MyHC-Peri |          |         |         |
|    | MyHC-Emb       | 85       | 83       | 84       | 79             | 81            | 85        | MyHC-Emb |         |         |
|    | MyHC-EO        | 81       | 81       | 82       | 77             | 77            | 82        | 79       | MyHC-EO |         |
|    | MyHC-7b        | 67       | 67       | 67       | 68             | 69            | 67        | 67       | 66      | MyHC-7b |

|    |                |          |          |          |                |               |           |          |         |         |
|----|----------------|----------|----------|----------|----------------|---------------|-----------|----------|---------|---------|
| B. | MyHC-IIa       | MyHC-IIa |          |          |                |               |           |          |         |         |
|    | MyHC-IIb       | 92       | MyHC-IIb |          |                |               |           |          |         |         |
|    | MyHC-IIc       | 93       | 96       | MyHC-IIc |                |               |           |          |         |         |
|    | MyHC- $\alpha$ | 79       | 81       | 80       | MyHC- $\alpha$ |               |           |          |         |         |
|    | MyHC- $\beta$  | 80       | 80       | 81       | 91             | MyHC- $\beta$ |           |          |         |         |
|    | MyHC-Peri      | 94       | 92       | 93       | 81             | 81            | MyHC-Peri |          |         |         |
|    | MyHC-Emb       | 86       | 85       | 85       | 79             | 79            | 86        | MyHC-Emb |         |         |
|    | MyHC-EO        | 85       | 85       | 85       | 80             | 79            | 86        | 82       | MyHC-EO |         |
|    | MyHC-7b        | 66       | 66       | 66       | 68             | 69            | 67        | 66       | 66      | MyHC-7b |

|    |                |          |          |          |                |               |           |          |         |         |
|----|----------------|----------|----------|----------|----------------|---------------|-----------|----------|---------|---------|
| C. | MyHC-IIa       | MyHC-IIa |          |          |                |               |           |          |         |         |
|    | MyHC-IIb       | 91       | MyHC-IIb |          |                |               |           |          |         |         |
|    | MyHC-IIc       | 96       | 93       | MyHC-IIc |                |               |           |          |         |         |
|    | MyHC- $\alpha$ | 81       | 80       | 81       | MyHC- $\alpha$ |               |           |          |         |         |
|    | MyHC- $\beta$  | 82       | 81       | 82       | 95             | MyHC- $\beta$ |           |          |         |         |
|    | MyHC-Peri      | 92       | 89       | 92       | 80             | 81            | MyHC-Peri |          |         |         |
|    | MyHC-Emb       | 84       | 82       | 84       | 79             | 79            | 84        | MyHC-Emb |         |         |
|    | MyHC-EO        | 78       | 77       | 79       | 76             | 75            | 79        | 77       | MyHC-EO |         |
|    | MyHC-7b        | 57       | 57       | 57       | 60             | 59            | 57        | 56       | 57      | MyHC-7b |

**Table 1.2. Sequence identities for A) full length, B) motor domain and C) rod domains of human class II myosin isoforms. Sequences were obtained from NCBI and alignments were performed using NCBI protein BLAST.**

|    |        |     |        |       |        |  |  |  |  |  |
|----|--------|-----|--------|-------|--------|--|--|--|--|--|
| A. | Rat    | Rat |        |       |        |  |  |  |  |  |
|    | Rabbit | 98  | Rabbit |       |        |  |  |  |  |  |
|    | Human  | 97  | 98     | Human |        |  |  |  |  |  |
|    | Bovine | 97  | 98     | 98    | Bovine |  |  |  |  |  |

|    |        |     |        |       |        |  |  |  |  |  |
|----|--------|-----|--------|-------|--------|--|--|--|--|--|
| B. | Rat    | Rat |        |       |        |  |  |  |  |  |
|    | Rabbit | 92  | Rabbit |       |        |  |  |  |  |  |
|    | Human  | 98  | 97     | Human |        |  |  |  |  |  |
|    | Bovine | 97  | 97     | 98    | Bovine |  |  |  |  |  |

**Table 1.3. Sequence identities between 4 mammalian species for A) MyHC- $\beta$  and B) MyHC-emb full length myosin. Sequences were obtained from NCBI and alignments were performed using NCBI protein BLAST.**

### 1.2.2 Cardiac isoforms

The myocardium of mammalian hearts contains two cardiac isoforms of myosin; alpha (MyHC- $\alpha$ ) and beta (MyHC- $\beta$ ). The two cardiac proteins are encoded by the genes *MYH6* and *MYH7*, respectively, which are found as a gene cluster on chromosome 14 at position 12. MyHC- $\alpha$  is the major isoform expressed in atrial myocardium in mammals, although a small proportion is also expressed in ventricular myocardium (Lompré, Nadal-Ginard, and Mahdavi 1984). MyHC- $\beta$  is the major isoform expressed in ventricular myocardium in mammals, although it is also expressed in slow skeletal muscle fibres, such as the soleus muscle fibre (Weiss 1996).

The two cardiac myosin genes are differentially regulated during development and respond opposingly to various hormonal stimuli, hemodynamic stress and exercise (summarised in Table 2). The ratio of expressed isoforms varies between species - larger mammals, including humans, express predominantly  $\beta$ -MyHC in their cardiac ventricles while small mammals such as rats and mice express predominantly  $\alpha$ -MyHC.

| Stimuli                    | MyHC- $\alpha$ | MyHC- $\beta$ |
|----------------------------|----------------|---------------|
| ↑ Triiodothyronine Hormone | ↑              | ↓             |
| ↓ Triiodothyronine Hormone | ↓              | ↑             |
| Exercise                   | ↑              | ↓             |
| Pressure overload          | ↓              | ↑             |
| Ageing                     | ↓              | ↑             |

**Table 1.4. Summary of directional regulation of cardiac *MYH6* and *MYH7* genes. Adapted from (Weiss 1996).**

Defining the properties of cardiac isoforms in detail has been limited by the availability of pure samples of the individual proteins. Unlike skeletal myosins, the cardiac isoforms are unstable and typically generate small quantities of protein. The recent advancements in recombinant human muscle myosin production enabled the kinetic characterisation of the two cardiac isoforms (Deacon et al. 2012). This work demonstrated that the MyHC- $\alpha$  isoform has a 10-fold faster ADP release rate than the MyHC- $\beta$ , indicative of a fast-type myosin. This is supported by the work of Piroddi et al, who showed that single human atrial myofibrils have a five-fold faster rate of tension development after a period of

rapid shortening than single ventricular myofibrils (Piroddi et al. 2007). MyHC- $\alpha$  also has a ~10-fold faster ATP hydrolysis step and exhibits a ~five-fold weaker actin affinity than MyHC- $\beta$ . These kinetic differences distinguish the two isoforms, and confers the contractility characteristics of the chambers of the heart in which they are found.

The ratio of cardiac myosin isoforms play a major role in the determination of cardiac contractility, as demonstrated by Herron et al, who showed that myocyte fragments expressing ~12% MyHC- $\alpha$  developed ~52% greater peak power output than fragments expressing 0% MyHC- $\alpha$  (Herron and McDonald 2002). There is evidence to suggest that a lower expression of MyHC- $\alpha$  is a hallmark of pathology – healthy human hearts contain ~10% MyHC- $\alpha$ , but end-stage failing hearts contain no detectable MyHC- $\alpha$  (Miyata et al. 2000; Nakao et al. 1997). As will be discussed in section 1.4, both isoforms have been implicated in cardiomyopathies.

### 1.2.3 Developmental isoforms

Humans contain two developmental isoforms, embryonic (MyHC-emb) and perinatal (MyHC-peri), which are encoded by the genes *MYH3* and *MYH8* respectively. Both isoforms are found in the developing embryo (along with MyHC- $\beta$ ) (Whalen et al. 1981) and regenerating muscles (Sartore, Gorza, and Schiaffino 1982). Their expression is down-regulated after birth when they are replaced by adult skeletal isoforms (Schiaffino et al. 2015). The embryonic isoform was characterised in 2016 by Walklate et al, who demonstrated it is a slow-type motor with similar kinetic properties to the MyHC- $\beta$  (J. Walklate et al. 2016). For example, both have a slow ADP release rate.

MyHC-peri is predicted to be a fast-type isoform, due to the motor domain sequence in the *MYH8* gene having considerable sequence similarity with skeletal fast *MYH* genes (Weiss, Schiaffino, and Leinwand 1999). Further supporting this is ATPase data, which was collected on the two isoforms by Resnicow et al in 2010, and it was observed that the MyHC-peri isoform had a  $V_{max}$  similar to the adult skeletal isoforms, whereas the embryonic isoform was slower (Resnicow et al. 2010). The kinetic properties of the perinatal isoform will be explored in more detail in chapter 3.

#### 1.2.4 Skeletal isoforms

In vertebrates, 3 skeletal myosin isoforms exist, MyHC-IId, MyHC-IIa and MyHC-IIb, encoded by the genes *MYH1*, *MYH2* and *MYH4* respectively. The sequence homology between the 3 isoforms is 91-96% for both the motor and rod domains. Whilst humans encode the *MYH4* gene and the mRNA has been detected in extraocular and jaw muscles (Horton et al. 2001; Horton et al. 2008), MyHC-IIb is not expressed at the protein level in humans (Ennion et al. 1995; Smerdu et al. 1994). However, the MyHC-IIb is expressed in skeletal muscles of small mammals such as mouse, rat and rabbit. Interestingly, MyHC-IIb is expressed in pig, a mammal similar in size to humans (Lefaucheur et al. 1998); this suggests the expression of MyHC-IIb is not simply size-dependent. Kinetic characterisation has been conducted for these isoforms, which showed all three had similar properties. In particular, the ADP release rate was more than  $100 \text{ s}^{-1}$  for these isoforms, which is characteristic of a fast-type myosin.

#### 1.2.5 Extraocular isoform

Extraocular muscles (EOMs) surround the eye ball and are responsible for stabilization of the eye and for several distinct voluntary and reflex movements. There are six EOMs in mammals, the contractile properties of which differ significantly from typical skeletal muscles. The specific tension (the maximum muscle force normalised with respect to muscle cross sectional area) is lower for EOMs than that observed in limb muscles whilst also having a very high speed of contraction alongside a relatively high resistance to fatigue (Close and Luff 1974; Lynch, Frueh, and Williams 1994; Porter and Baker 1996).

Many fibres in EOMs express multiple class II isoforms, and localise them differentially along the length of the fibre (Walro and Kucera 1999; Wieczorek et al. 1985; Park et al. 2012). Mammalian extraocular muscles express all nine of striated myosin isoforms (Jacoby et al. 1990; Rubinstein, Porter, and Hoh 2004; Zhou, Liu, and Kaminski 2010), one of which includes MyHC-EO, the protein product of the *MYH13* gene. MyHC-EO is a specialised isoform of myosin that is specific for extraocular muscle (Sartore et al. 1987), although it is has also been found to be expressed in laryngeal muscles (Lucas, Rughani, and Hoh 1995). It was first categorized as a fast type myosin likely contributing to rapid eye movements (Briggs and Schachat 2000; Schachat and Briggs 2002). This was supported by the work of Resnicow et al, who demonstrated that a recombinant MyHC-EO had an ATPase rate similar to recombinant adult skeletal isoforms (Resnicow et al. 2010).



The same construct also had a weak ADP affinity and fast ADP release rate, which also matches the properties of adult fast skeletal isoforms (Bloemink et al. 2013).

### 1.2.6 MyHC-7b

MyHC-7b was first identified by Nagase et al, and the expression profile of the genes revealed that MyHC-7b RNA is expressed in cardiac and skeletal muscle, foetal and adult brain tissues (Nagase et al. 1998). Low expression levels were also identified in the liver, pancreas, spleen, lung, kidney and ovary. MyHC-7b shares the highest sequence homology to MyHC- $\beta$  and MyHC- $\alpha$  (69% and 68% respectively – see Table 1.2). Interestingly, each of these myosin genes encodes an intronic microRNA - micro RNAs derived from introns can suppress intracellular RNA homologues and regulate the gene function. These intronic microRNAs play a role in cardiac stress response, and the MyHC- $\alpha$  and MyHC-7b intronic microRNAs also have redundant roles in skeletal muscle fibre-type specification (van Rooij et al. 2009; van Rooij, Liu, and Olson 2008). Despite this, MyHC-7b is not detected at the protein level in mammalian cardiac or skeletal muscle. The discrepancy between RNA and protein expression is due to a splicing event in which the transcript is produced, but undergoes some nonsense mediated decay, while the intronic microRNA is still expressed (Bell, Buvoli, and Leinwand 2010).

### 1.2.7 Expression of isoforms

The expression pattern of the two developmental isoforms have been well characterised in the mouse and rat models. In mice, MyHC-emb appears 9.5 days post coitum (dpc) and MyHC-peri 10.5 dpc (Lyons et al. 1990). In rats, MyHC-emb and MyHC- $\beta$  are expressed in the first muscle fibres to form, so called primary generation fibres (Narusawa et al. 1987; Rubinstein and Kelly 1981). Secondary generation fibres express MyHC-emb and MyHC-peri (Condon et al. 1990). The developmental isoforms disappear at the same time as the adult skeletal myosin isoforms (MyHC-IIa, MyHC-IIc, and MyHC-IIb) are expressed. In rats, the protein is detected a few days after birth (DeNardi et al. 1993) while in mice the transcripts can be detected before birth (Lu et al. 1999). The timing of the downregulation of the developmental isoforms appears to be dependent on the body muscle at both the mRNA and protein level (Agbulut et al. 2003; Lu et al. 1999).

Human muscle developmental pattern of myosin isoform expression has yet to be fully elucidated. Figure 1.13 shows in situ hybridisation studies of *MYH* transcripts in developing human skeletal muscle. At week 8 of gestation, primary generation fibre is

present in the human skeletal muscle, containing MyHC-emb and MyHC- $\beta$  (Barbet, Thornell, and Butler-Browne 1991; Draeger, Weeds, and Fitzsimons 1987). Secondary generation fibres are formed after week 10 and express only MyHC-emb at week 12, MyHC-peri protein being detected at later stages (Cho, Webster, and Blau 1993). *MYH3* transcripts account for about 81 % of all *MYH* transcripts in the human foetal skeletal muscle at week 15 of gestation (Racca et al. 2013). At week 16 to 17, a tertiary fibre population has been identified, initially composed of adult fast myofibres (Draeger et al. 1987; Ecob-Prince, Hill, and Brown 1989). In situ hybridization indicates that MyHC-IIa transcripts are weakly expressed at week 19 and more strongly at birth, whereas MyHC-IId transcripts are barely present at birth but expressed at 30 days after birth. ~95% of human skeletal muscle fibres appear to derive from secondary and tertiary fibres and their diversification into the fast type IIa or beta lineage occurs before birth, during the third trimester of gestation, whereas the differentiation of type IId fibres takes place in the first week after birth (Schiaffino et al. 2015).

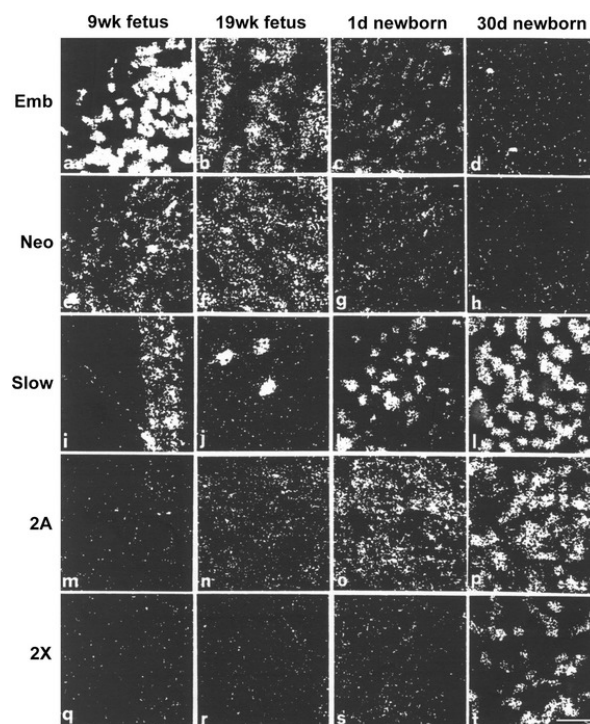


**Figure 1.13.** MyHC transcripts in developing human skeletal muscle. The transcripts were revealed by in situ hybridization using probes specific for the following MYH genes: *MYH3* (MyHC-emb, a–d), *MYH8* (MyHC-peri, e–h), *MYH7* (MyHC- $\beta$ , i–l), *MYH2* (MyHC-IIa m–p), and *MYH1* (MyHC-IId, q–t). Muscles examined were quadriceps femoris from 9 and 19-week-old fetuses and vastus lateralis from 1-day- and 1-month-old newborns. Scale bar = 30  $\mu$ m. Figure from (Schiaffino et al. 2015).

### **1.3 Myosin evolution**

#### 1.3.1 Myosin superfamily evolution

Myosins are molecular motors that diversified very early during eukaryotic evolution (Thompson and Langford 2002; Richards and Cavalier-Smith 2005). Most eukaryotes rely on myosins, and only a few taxonomic groups, e.g., red algae and diplomonad protists appear to live without them (Vale 2003). Prokaryotes do not contain myosin - a shift in nucleotide-binding specificity from GTP to ATP is thought to have occurred to form the myosin–kinesin ATPase ancestor at the very origin of eukaryotes (Cavalier-Smith 2002).

To understand the class distribution of myosin in different taxa, Odrionitz and Kollmar compared the genomic analysis of 2,269 myosins found in 328 organisms (Odrionitz and Kollmar 2007). Based on the myosin class content of each organism and the positions of each organism's single myosins in the phylogenetic tree of the myosin motor domains, a eukaryotic tree of life was reconstructed, as shown in Figure 1.14. This identified 35 sub groups of myosin. They also identified five new classes, class-XX, class-XXI, class-XXII, class-XXVIII, and class-XXXV, which are specific to Metazoan species. 13 of the 35 sub groups have been identified in humans. The data show that several taxa have evolved asynchronously, for example the Mammalia and the Fungi.

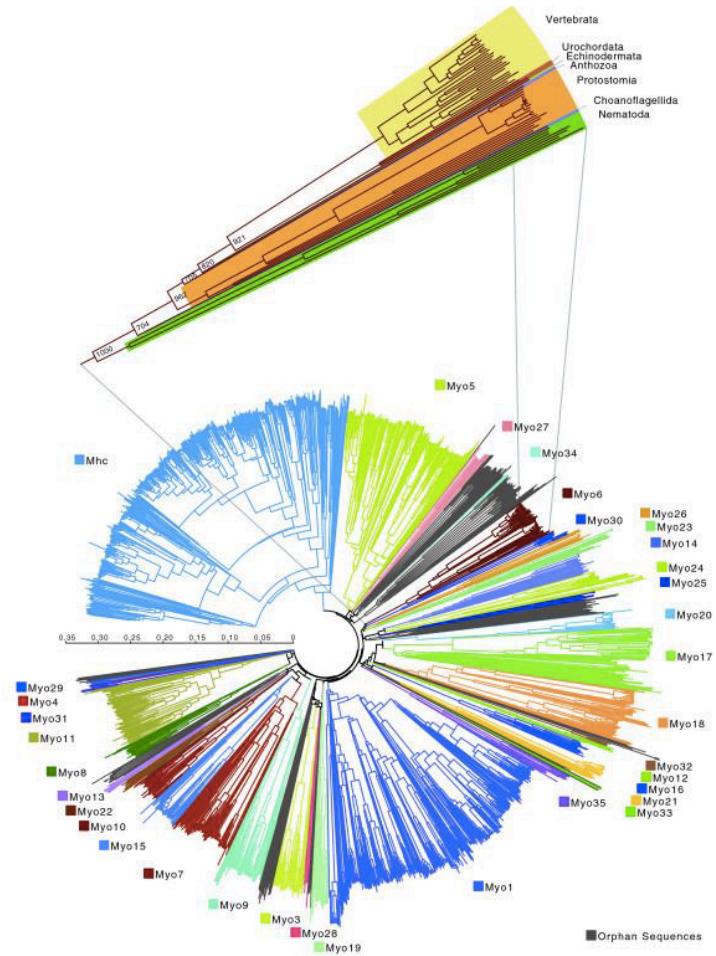


**Figure 1.14. Phylogenetic tree of 1,984 myosin motor domains divided into 35 subgroups. The expanded view shows the sequences of myosin class-VI and distribution within taxa. The scale bar represents estimated amino acid substitutions per site. Figure from (Odriontz and Kollmar 2007).**

Sebe-Pedros and colleagues followed on from this to demonstrate the diversity of myosin proteins in the last eukaryotic common ancestor (LECA) genome (Sebé-Pedrós et al. 2014). They showed that LECA possessed a minimum of six myosin paralog families all encoding different protein domain architectures (summarised in Figure 1.15). The authors also demonstrated that paralogs and domain architectures were continuously generated throughout eukaryote evolution, with a significant expansion of myosin abundance and domain architectural diversity at the stem of Holozoa, predating the origin of animal multicellularity. Their data demonstrated that the myosin gene family underwent multiple large-scale expansions and contractions in paralog families combined with extensive remodelling of domain architectures.

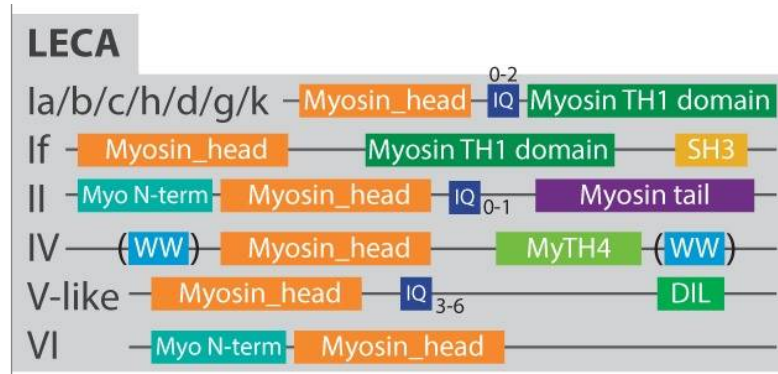


Figure 1.15. The six paralog families found within the LECA genome, and their protein domain structures. Numbers indicate the number of IQ domains found within a myosin class. Figure adapted from (Sebé-Pedrós et al. 2014).

Whilst there is an extensive number of myosin classes, Class I and class II myosins were proposed to be the most ancient (Thompson and Langford 2002). As shown in Figure 1.1 in Chapter 1.1.1, these two classes contain the highest number proteins per class for all 35 sub-groups. Class II contains almost twice as many proteins as class I (617 versus 381, respectively). Whilst there is a high sequence homology between these two classes, a novel glycine residue inserted at position 507 in the *Dictyostelium discoideum* sequence was found to distinguish all class II myosins from other classes (Figure 1.16). This demonstrates the potential significance a single amino acid change can have on diversifying such a complex protein.

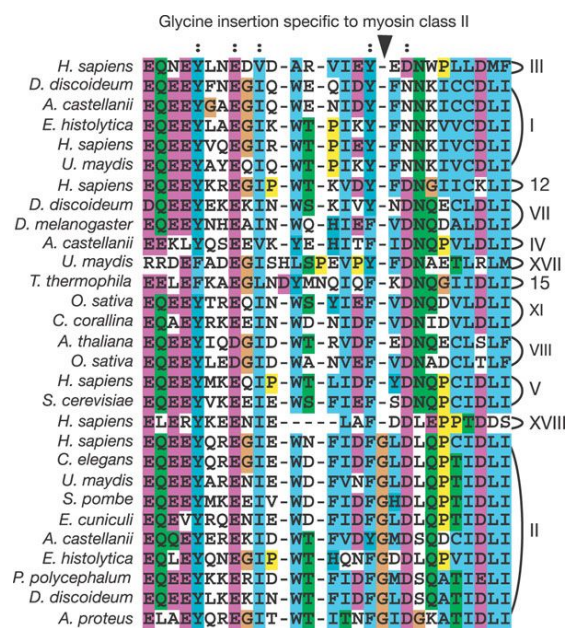


Figure 1.16. Multiple sequence alignment from residues 488 – 517 showing the glycine insertion at residue 507 specific to class II myosins. Figure from (Richards and Cavalier-Smith 2005).

Another interesting aspect of myosin evolution is the branch which generates striated and non-striated muscles. Previous analyses of myosin II proteins in bilaterian animals (animals with bilateral symmetry) have recognised two phylogenetic groups; the first containing genes expressed in smooth muscle cells and in non-muscle cells, while genes of the second group are specifically expressed in skeletal or cardiac muscle cells (Hodge and Cope 2000; Sellers 2000). This suggests a gene duplication event gave rise to these two distinct phylogenetic groups (Goodson and Spudich 2006; Korn 2000; Oota and Saitou 1999).

Steinmetz and colleagues however demonstrated that the gene duplication that generated the two groups occurred much earlier than the origin of muscle cells; they showed that a muscle protein core set, including a type II myosin heavy chain (MyHC) motor protein characteristic of striated muscles in vertebrates, was already present in unicellular organisms before the origin of multicellular animals (Steinmetz et al. 2012). Furthermore, 'striated muscle' and 'non-muscle' myosin orthologues are expressed differentially in two sponges (*Tethya wilhelma* and *Amphimedon queenslandica*), compatible with a functional diversification before the origin of true muscles. Cnidarians and ctenophores possess striated muscle myosin heavy chain orthologues but lack crucial components of bilaterian striated muscles, such as genes that code for titin and the troponin complex, suggesting the convergent evolution of striated muscles (Steinmetz et al. 2012).

### 1.3.2 Adaptation to body mass in mammals

When studying the structure of myosin, it is known where the changes in sequence occur between the different isoforms, but how they alter the behaviour of myosin is harder to define. A defining feature of myosin, the rate of muscle contraction, can be controlled in two ways. The first is by expression of different combinations of myosin isoforms within a whole muscle (Pellegrino et al. 2003). The second process is the adaptation of individual myosin isoforms to change in species size to meet physiological demands. The contraction parameters of a muscle fibre have to adjust to the size of an organism; as size increases, muscle contraction becomes slower to compensate for the greater momentum associated with a larger body mass. An example of this is the decrease in heart rate of species as their body mass increases; heart rate is correlated with basal metabolic rate and inversely related to body size (Savage et al. 2007).

Variations in properties between isoforms are well established, but changes in the properties of the same isoforms in different species is less well defined. McGreig et al

investigated the evolution of myosin class-II isoforms in mammals to identify if the isoforms have adapted to the change in body mass as animals evolved from smaller to larger body masses (McGreig et al. 2019). They analysed 730 sequences from 12 class-II isoforms in 65 mammalian species and found that non-muscle and developmental myosin class II isoforms have not adapted to increased species size. Counter to this, there is strong evidence for adaptation in the MyHC- $\beta$  and two adult fast myosin II isoforms, MyHC-IIa and MyHC-IIb, motor domains whose sequence divergence is correlated with body mass. Figure 1.17 shows this relationship for MyHC-emb, MyHC- $\beta$ , NNM-IIa, MyHC-IIb, NMMHC-IIb, and MyHC-IIa isoforms. To note, mammals from three clades were represented. As seen in Figure 1.17, the relationship between sequence divergence and body mass is not dependent on the clade the species belongs to.

Based on the rate of divergence with body mass, the 12 myosin II isoforms form three distinct groups. The first group contains four of the five main adult sarcomeric isoforms, with the MyHC-IIb and MyHC- $\beta$  isoforms showing the greatest mass related sequence divergence, followed by the MyHC-IIa and MyHC-IIc isoforms. Further, the rate of change at the DNA sequence level for the MyHC- $\beta$  and fast isoforms shows an increase in the number of non-synonymous changes, while the rate of synonymous changes remains relatively stable with increasing body mass. This implies there has been a specific increase in non-synonymous changes. At the other extreme, five of the isoforms (MyHC-7b, MyHC-emb, MyHC-peri, NMMIIa and NMMIIb) exhibit little divergence of sequence with body mass. This result with quite distinct dependence upon mass suggests different selection conditions apply to the two groups. This is compatible with the adult muscle myosins adapting to the requirements of changes in size whilst the cellular myosins were not exposed to this selection pressure. The remaining three isoforms (MyHC- $\alpha$ , MyHC-smooth and MyHC-EO) are intermediate between the two groups with a lower rate of sequence divergence with body mass.

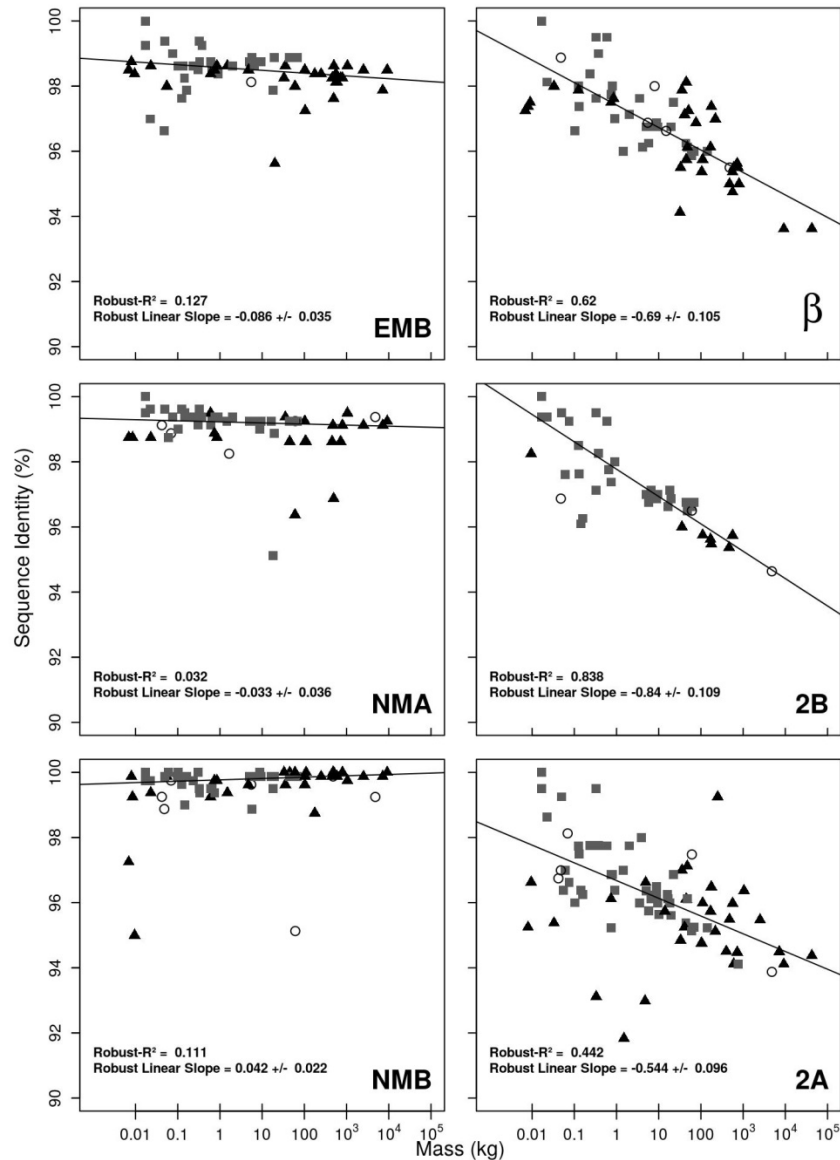


**Figure 1.17. Sequence Identity (%ID) vs Mass (kg) for the motor domains of six myosin II isoforms; MyHC-emb (EMB), non-muscle A (NMA), non-muscle B (NMB), MyHC-β (β), MyHC-IIa (2A) and MyHC-IIb (2B). Symbols indicate the clade that each species belongs to; grey squares (Euarchontoglires), black triangles (Laurasiatheria) and clear circles (Afrotheria and Metatheria). Sequence identity is pairwise to the mouse. Figure from (McGreig et al. 2019).**

Pellegrino et al showed that for a muscle fibre expressing a single myosin heavy chain, the maximum shortening velocity was characteristic of the myosin isoform expressed (Pellegrino et al. 2003). As the myosin motor domain contributes to muscle contraction velocity, it is hypothesised that the changes in velocity can occur via variation in the amino acid sequence of the myosin motor domains for the MyHC-IIa, MyHC-IIb and MyHC-β isoforms. Unlike the ventricle tissue in which MyHC-β is expressed, skeletal muscles in mammals use their muscles and myosin isoforms in many different ways for different purposes. Thus, the selective pressure on a specific myosin isoform in skeletal muscle may



be different in each mammal. However, the heart and slow muscle fibres are relatively similar in function across mammals and the simple relationship between heart rate and size is well established. This makes MyHC- $\beta$  an attractive protein to study to investigate the adaptation of sequence identity to match changes in body mass.

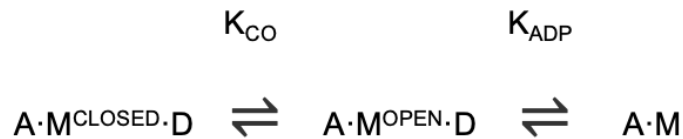
### 1.3.3 Velocity and ADP-release

The mechanical activity a myosin can perform is an inherent characteristic of the motor, and this property varies between myosin types. It was proposed in 2011 by Bloemink and Geeves that myosin motors can be classified into four distinct types; 1) Slow, efficient force holders; 2) fast, powerful movers; 3) strain sensors and 4) processive/signal transducers (Bloemink and Geeves 2011). A defining feature that differs between these types, and hence different isoforms, is how the ADP release step affects the overall cycle. This can include differences in the thermodynamic and kinetic coupling of actin and ADP binding to myosin, different load sensitivity of ADP release step and changes in duty ratio (Nyitrai et al. 2006; Nyitrai and Geeves 2004).

Duty ratio (DR) refers to the fraction of time a myosin motor spends strongly bound to actin during the cross-bridge cycle. Changes in DR facilitate adaptation of a myosin molecule to suit its individual function. For example, fast myosins which work in groups have a DR of 0.05-0.1 (O'Connell, Tyska, and Mooseker 2007), whereas processive myosins have a DR of  $>0.7$ , enabling a single myosin molecule to track along an actin filament and drag a cargo (De La Cruz et al. 1999). Other motors can adjust their DR in response to load, calcium and magnesium concentration, or phosphorylation states (Adamek, Coluccio, and Geeves 2008; Durrwang et al. 2006; Fujita-Becker et al. 2005). The rate constants that define detachment and reattachment of myosin to actin govern the DR; detachment of myosin from actin is controlled by ADP release from an actin.myosin.ADP complex, or by ATP binding to actin.myosin. For fast type myosins, measured ADP-release is typically too fast to limit the shortening velocity, and so the rate of cross-bridge detachment after completion of the powerstroke limits the maximum shortening velocity of the muscle fibre (Iorga, Adamek, and Geeves 2007; Nyitrai et al. 2006). For class III, IV and slow myosins, shortening velocity is limited by ADP release (or the isomerisation leading to ADP release) (Iorga, Adamek, and Geeves 2007; Bloemink et al. 2007).

It has been shown for some isoforms (although it may be true for all) that isomerisation of an actin.myosin.ADP complex is required for ADP release, as described in Scheme 1 (Nyitrai and Geeves 2004). Equilibrium between these two states varies for

different myosins, both between and within classes. After phosphate release and swinging of the myosin lever arm, ADP is retained in the nucleotide pocket which is in a closed conformation. A further rotation of the lever arm in the direction of the load the motor is bearing is required for the nucleotide pocket to open (Batters et al. 2004; Cremo and Geeves 1998; Smith and Geeves 1995). The protein conformational change that drives the nucleotide pocket from a closed to open state is termed  $K_{CO}$ , and is required to facilitate ADP release. The apparent affinity of ADP for actin.myosin and thermodynamic coupling is controlled by  $K_{CO}$  (Bloemink and Geeves 2011). The apparent ADP affinity,  $K_{ADP}$ , is typically weak (of the order of 100  $\mu$ M), meaning that  $K_{CO}$  is the driver of the ADP affinity, and  $k_{+CO}$  is rate-limiting for ADP release. Indeed, this constant varies between different myosin classes (Bloemink and Geeves 2011; Walklate, Ujfalusi, and Geeves 2016).



**Scheme 1. The two-step process of ADP release from an actin.myosin.ADP complex. A = actin, M = myosin, D = ADP.**

Further highlighting this is the relationship between maximum shortening velocity and body mass of a mammal, as seen on a logarithmic plot in Figure 1.18A. The allometric equation was fitted to the data points to determine whether maximum shortening velocity has scaled with changes in body mass. For IIa, IIb and IIc fibres, the allometric coefficients were -0.098, -0.041 and -0.048 respectively (Pellegrino et al. 2003). Slow fibres showed a steeper decrease of maximum shortening velocity with mass, and had an allometric coefficient of -0.175. This suggests that the slow isoform has adapted to changes in body mass.

A well-established relationship of sliding velocity ( $v$ ), the lifetime of a cross-bridge ( $\tau$ ) and the working stroke ( $d$ ) can be defined by  $\tau = d / v$  (Siemankowski and White 1984; Siemankowski, Wiseman, and White 1985).  $\tau$  can be no greater than  $d / v$  without producing drag on moving filaments, so  $1 / \tau$  is the minimum rate constant ( $k_{min}$ ) for any event during the attached part of the cycle, i.e.,  $k_{min} = v / d$ . From this, the rate constant controlling ADP release can be predicted from shortening velocity data, as shown in Figure 1.18B for MyHC- $\beta$ . This shows a very close fit between the measured values and the predicted values; the two parameters show a high correlation with a slope close to 1, which indicates that the rate of ADP release controls velocity. Further, the rate constant controlling ADP release does

vary for different myosins (Weiss et al. 2001), highlighting its importance in tuning the protein for a specific function.

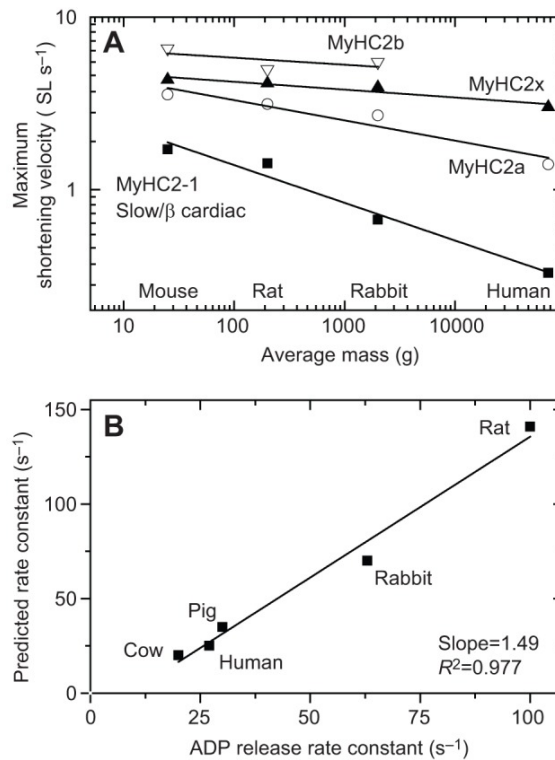


**Figure 1.18. Relationship between myosin isoform, muscle shortening velocity and the rate constant for ADP release. (A) Maximum shortening velocity of muscle fibres expressing a single myosin isoform, plotted against the average mass of the species the muscle came from. (B) Relationship between the measured rate constant for ADP release from the actin.myosin cross-bridge and that predicted from the measured velocity of muscle shortening for MyHC-β. Figure from (J Walklate et al. 2016).**

The relationship between myosin sequence and velocity of contraction remains to be elucidated. How MyHC-β has adapted this ADP release step to generate changes in contraction velocity in mammals will be considered in Chapter 4.

### 1.4 Cardiomyopathies

Myopathies are muscular and neuromuscular disorders, characterised by muscle weakness as a result of dysfunction of the muscle fibre. Myopathies have been reported in five of the nine striated *MYH* class II genes (see table 1.5). As shown in Table 1.5, the highest number of mutations reported in a single *MYH* gene is that of the *MYH7* gene. These mutations have been implicated in a number of myopathies, including Hypertrophic Cardiomyopathy (HCM), Dilated Cardiomyopathy (DCM), left ventricular non-compaction, Laing distal myopathy, Scapuloperineal and limb girdle syndromes. More than 300 of these mutations give rise to HCM (Buvoli et al. 2008; Colegrave and Peckham 2014; Walsh et al. 2010).

**Table 1.5. Summary of myopathies caused by mutations in *MYH* genes. Table adapted from (Marston 2018).**

| Gene        | Protein        | Myopathy   | No. of mutations reported |
|-------------|----------------|--|---------------------------|
| <i>MYH2</i> | MyHC-IIa       | Inclusion body myopathy, distal and proximal myopathy, ophthalmoplegia   | 15                        |
| <i>MYH3</i> | MyHC-emb       | Distal arthrogyrosis types 1, 2A (also known as Freeman-Sheldon syndrome), 2B (also known as Sheldon-Hall Syndrome), 8 | 33                        |
| <i>MYH6</i> | MyHC- $\alpha$ | HCM, DCM atrial-septal defect, other congenital defects  | 33                        |
| <i>MYH7</i> | MyHC- $\beta$  | HCM, DCM, left ventricular non-compaction, Laing distal myopathy, Scapuloperineal and limb girdle syndromes            | >800                      |
| <i>MYH8</i> | MyHC-peri      | Distal arthrogyrosis DA7   | 1                         |

### 1.4.1 Hypertrophic cardiomyopathy

**Cardiomyopathies refer to diseases of cardiac muscle.** The 3 most common types of cardiomyopathy are; dilated cardiomyopathy (DCM), arrhythmogenic right ventricular cardiomyopathy (ARVC), and hypertrophic cardiomyopathy (HCM), which this thesis will focus on. HCM is an inherited form of cardiovascular disease, characterised by hypertrophy of the interventricular septum, which separates the left and right ventricles (Figure 1.19). This hypertrophy impedes the flow of oxygen-rich blood from the heart due a decreased left ventricular chamber volume. Patients often present with impaired diastolic dysfunction, fibrosis and myocyte disarray (Ho et al. 2002, 2010; Varnava et al. 2000) (Figure 1.20). The most common HCM phenotype is also accompanied by non-dilated, hyperdynamic left ventricle ejection fraction of less than 65% (Soler et al. 2018). This can lead to adverse remodelling with progressive dilation and subsequent thinning of the interventricular septum, leading to heart failure which simulates other cardiomyopathies such as restrictive or dilated cardiomyopathies (Olivotto et al. 2012).

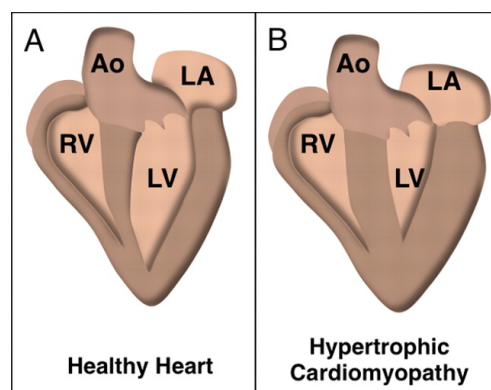


**Figure 1.19. Schematic comparison of a healthy (A) and HCM diseased heart (B). Asymmetric hypertrophy of the interventricular septum as well as the left ventricular posterior wall and apex is present. Figure adapted from (Harvey and Leinwand 2011).**

HCM is a common cause of sudden cardiac death in young adults and athletes. It is currently unclear why the natural history of HCM is so variable; some individuals remain asymptomatic throughout life, and others may develop progressive symptoms with or without heart failure or experience sudden cardiac death (Fatkin and Graham 2002).

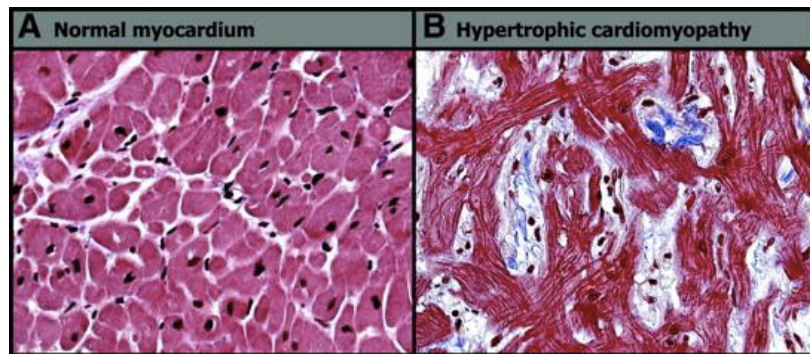


**Figure 1.20.** Examples of histological images of myocardium in A) normal myocardium and B) patient with HCM myofibre disarray and fibrosis. Figure adapted from (Yilmaz et al. 2010).

The first case of HCM was described in 1958 (Teare 1958). HCM has a disease prevalence of 1:500 (Maron et al. 1995), although this figure is now thought to be closer to 1:200 (Semsarian et al. 2015). Over 50% of cases of HCM are inherited, the most common inheritance pattern being an autosomal dominant trait (Poutanen et al. 2006). A large number of genetic studies have established that HCM can be caused by mutations in 10 cardiac sarcomeric proteins (Figure 1.21). Mutations in MyHC- $\beta$  account for 40% of the known mutations (Maron and Maron 2013).

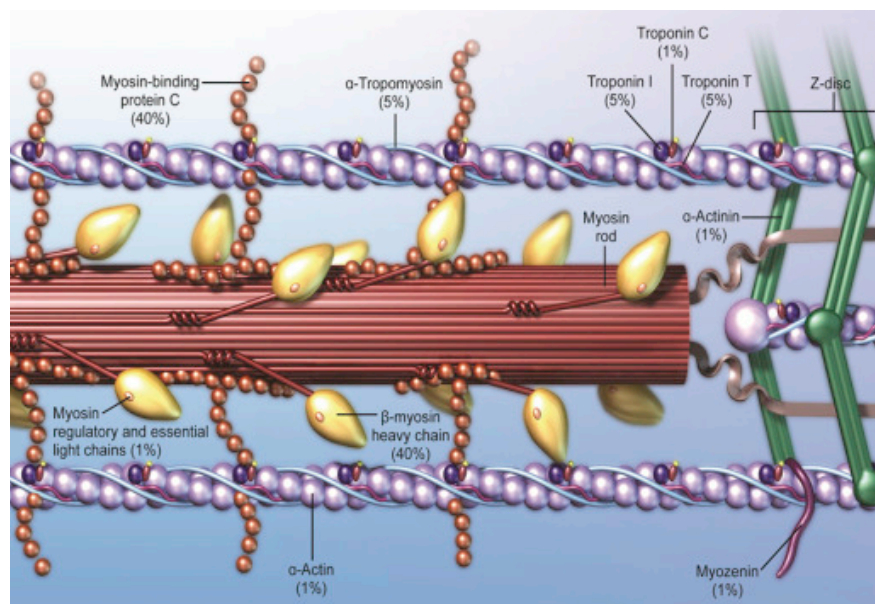


**Figure 1.21.** Schematic representation of the prevalence for each of the 10 known HCM-causing genes in a cardiac sarcomere. Figure from (Maron and Maron 2013).

#### 1.4.2 Early and late onset mutations

The first single point mutation, R403Q, in human MyHC- $\beta$  of heart muscle was identified in 1990 as a cause of a particularly malignant form of familial HCM (Geisterfer-Lowrance et al. 1990). Since then, a further 300 have been identified, ~65% of which occur in the motor domain (Colegrave and Peckham 2014). Offspring of an affected individual have a 50% probability of inheriting a mutation and risk for the disease, although sporadic cases have been reported due to *de novo* mutations (Greber-Platzer et al. 2001).

Genetic causation is very complex because HCM typically shows variable penetrance and expressivity, even within the same family (Cahill, Ashrafian, and Watkins 2013; Ingles et al. 2017). The range of ages at clinical diagnosis of HCM is broad; however, manifestations before 14 years of age are atypical (Maron et al. 2003). The early age at diagnosis and the striking differences between childhood cardiomyopathies from adult-onset cardiomyopathies in terms of morbidity and mortality indicate distinct causes of these pathologic conditions (Maron 2004; Yetman and McCrindle 2005). To investigate this, Morita et al in 2008 assessed family medical histories of 84 children diagnosed with HCM before the age of 15 (Morita et al. 2008). 33 of these children had a family history of cardiomyopathy, 21 of which carried a mutation. 51 children did not have a family history of cardiomyopathy, 25 of which carried a mutation. Sequence analysis of the *MYH7* gene of these children identified nine mutations, five of which were novel. Four of these mutations were found in the motor domain.

A similar study from 2009 (Kaski et al. 2009) investigated causes of HCM in 79 patients diagnosed before or at the age of 13. 42 were found to be mutation positive. Many of these mutations were known mutations in MyHC- $\beta$ , actin, myosin binding protein-C (MyBP-C), myosin light chain, Tnl and TnT. However, six novel mutations in MyHC- $\beta$  were also identified; among these four were found in the motor domain. Prior to these studies, little data was available for the causes of HCM in children, due to the low reporting frequency of the disease in children (Colan et al. 2007).

Over 50 mutations have been identified in the converter domain of the MyHC- $\beta$  motor, which suggests this region is a hot spot for cardiomyopathy mutations (Homburger et al. 2016). Three such mutations are classically linked with adult-onset HCM, and are predicted to be likely-pathogenic - R719W, R723G and G741R (Anan et al. 1994; Enjuto et al. 2000; Fananapazir et al. 1993). At present, it remains unclear as to what drives clinical symptom progression between the early and adult-onset mutations.

It is also important to note what constitutes a disease-causing HCM mutation. A mutation can be considered pathogenic, or likely pathogenic, on the basis that the clinical data meet the following criteria: 1) presentation of a HCM phenotype (i.e., left ventricular hypertrophy) in family members; 2) previously reported or identified as a cause of HCM; 3) absent from unrelated controls; 4) protein structure and function is importantly altered (e.g. frameshift with truncation); and 5) amino acid sequence change in a region of the protein otherwise highly conserved through evolution with virtually no variation observed among species, suggesting its importance to basic cellular function (Tester and Ackerman 2011; Richards et al. 2008). As shown in Tables 1.2 MyHC- $\beta$  is a highly conserved protein, and Table 1.3 demonstrates the high sequence homology between species. The problem with novel mutations is the lack of data to suggest it is disease-causing. Such mutations, when reported in only a single individual, may be assigned as VUS (variants of uncertain significance). This is true for three of the mutations studied in this thesis; the H251N, P710R and V763M mutations.

To address the problem of whether the molecular changes in function of MyHC- $\beta$  is different between early- and late-onset mutations, the work in Chapter 5 aims to elucidate the kinetic properties of the cross-bridge cycle of four early-onset mutations (H251N, D382Y, P710R and V763M) and three late-onset mutations (R719W, R723G and G741R).



## 1.5 Myosin folding

Correct activity and function of myosin is dependent on precise assembly and folding of the protein in the sarcomere. Whilst the components and overall architecture of the sarcomere is well established, less is known about the assembly process (Sanger et al. 2006). Myosin incorporation into thick filaments is one element of this assembly process that is not well understood. So far, it has been shown that folding of the myosin motor domain involves the assistance of the general chaperones Heat Shock Protein 70 (Hsp70) and Heat Shock Protein 90 (Hsp90) (Du et al. 2008; Etard et al. 2007; Gaiser et al. 2011; Hawkins et al. 2008; Srikakulam and Winkelmann 2004) and of UCS-domain-containing proteins that function as myosin-specific chaperones (Barral et al. 2002; Hutagalung et al. 2002; Kachur and Pilgrim 2008; Lord and Pollard 2004; Wesche, Arnold, and Jansen 2003; Yu and Bernstein 2003).

### 1.5.1 UCS family

The UCS (named after **UNC-45** in *Caenorhabditis elegans*, **CRO1** in *Podospora anserina* and **She4p** in *Saccharomyces cerevisiae*) family of proteins encompass chaperones that are required for the folding, assembly and function of myosin (Lee, Melkani, and Bernstein 2014). Homologs of UCS proteins can broadly be divided into animal UCS proteins, generally referred to as UNC-45 proteins which contain an N-terminal tetratricopeptide repeat (TPR) domain (Das, Cohen, and Barford 1998), and fungal UCS proteins which lack this TPR domain. Both of these two sub-classes contain the canonical C-terminal UCS domain that is required for interactions with myosins. The presence of the TPR domain confer different functions of UCS proteins, as demonstrated in Figure 1.22 (Hellerschmied and Clausen 2014). Biochemical studies show that the fungal She4 UCS protein serves as a ligand for a 27-residue epitope of a yeast myosin V motor domain, which is located in close proximity to the nucleotide- and actin-binding sites (Shi and Blobel 2010). This suggests that the She4 dimer may physically link two myosin motor domains to determine the step size of myosin molecules walking along actin filaments. Contrastingly, TPR-containing UCS proteins are able to form multi-chaperone complexes with the chaperones Hsp70 and Hsp90 (Gazda et al. 2013). TPR-containing UCS chaperones form oligomers which can fold myosin and assemble thick filaments (Gazda et al. 2013; Hellerschmied and Clausen 2014).

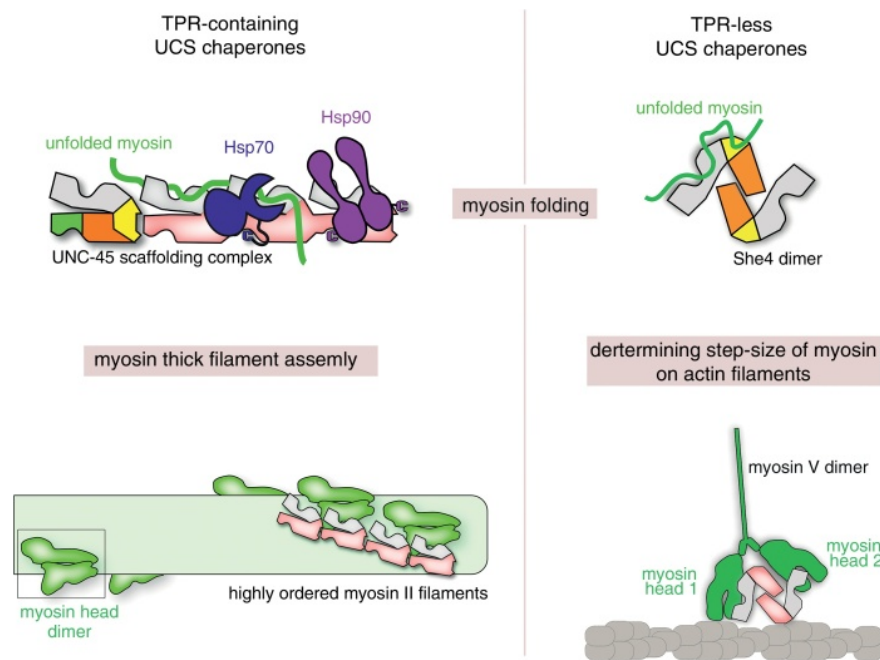


**Figure 1.22. UCS proteins exert their chaperone activity with or without a TPR domain. On the left panel, TPR-containing UCS chaperones form chains to initiate myosin and partner chaperone (Hsp70, Hsp90) interactions and assemble thick filaments by arranging myosin head domains, as shown for myosin class II filaments. On the right panel, UCS chaperones without a TPR domain function as dimers. Interaction with folded myosin can also determine the step-size, as shown for the myosin V dimer. Figure from (Hellerschmied and Clausen 2014).**

UNC-45 (uncoordinated-45) was originally identified as a result of mutations causing structural disruption of thick filaments in body wall muscle in the nematode *Caenorhabditis elegans* (*C. elegans*) (Epstein and Thomson 1974; Venolia and Waterston 1990). The *unc-45* gene is essential in *C. elegans*, but missense mutations result in disorganized and reduced numbers of myosin-containing thick filaments giving rise to a slow-moving, or uncoordinated, phenotype of adult worms (Barral et al. 1998; Ao and Pilgrim 2000). Mutations affecting the UCS domain of *C. elegans* UNC-45 result in paralyzed worms with reduced amounts of thick filaments and severe myofibril disorganization (Barral et al. 1998; Epstein and Thomson 1974; Hoppe et al. 2004; Venolia et al. 1999), indicating that UNC-45 is important for myosin maturation and sarcomere organization (Ao and Pilgrim 2000; Kachur and Pilgrim 2008).

UNC-45 homologs are present throughout metazoans, including worms, flies, frogs, mice and humans (Epstein and Thomson 1974; Etheridge, Diorio, and Sagerström 2002; Price et al. 2002; Geach and Zimmerman 2010; Lee et al. 2011). In vertebrates, two homologs of UNC-45 have been identified, with different expression patterns and functions (Etheridge et al. 2002; Price et al. 2002); one that is expressed in general cell types (UNC-

45a) and another that is specific to striated muscle (UNC-45b). UNC-45a is ubiquitously expressed and has been implicated in a diverse array of activities from chaperoning the progesterone receptor (Chadli et al. 2006; Chadli et al. 2008; Chadli, Felts, and Toft 2008) to cell proliferation and oncogenesis (Bazzaro et al. 2007; Price et al. 2002). In zebrafish and mice, UNC-45b has been implicated in myogenic processes in skeletal and cardiac muscles; when UNC-45b is absent the myosin containing thick filaments in trunk muscles are reduced and disorganized (Etard et al. 2007; Etheridge et al. 2002; Price et al. 2002). In line with this tissue specificity, abnormal UNC-45b function is associated with severe muscle defects resulting in skeletal and cardiac myopathies (Janiesch et al. 2007; Walker 2001).

### 1.5.2 *C. elegans* UNC-45 structure

Gazda et al recently reported the crystallisation of the *C. elegans* UNC-45 protein (Figure 1.23) (Gazda et al. 2013). UNC-45 contains a TPR domain that binds Hsp70/Hsp90 partner chaperones (Barral et al. 2002; Rajani Srikakulam, Liu, and Winkelmann 2008), a central armadillo repeat (ARM) domain of unknown function and a C-terminal UCS domain that interacts with the motor domain of myosin (Barral et al. 1998; Barral et al. 2002; Lee Venolia et al. 1999).

As shown in Figure 1.23, the TPR domain of UNC-45 is assembled by three TPR motifs, each containing two antiparallel  $\alpha$  helices. The helices are packed in a curved, right-handed superhelix featuring a shallow groove at its concave side that is critical to recognize and bind specific peptide ligands and to tether partner chaperones (Scheufler et al. 2000).

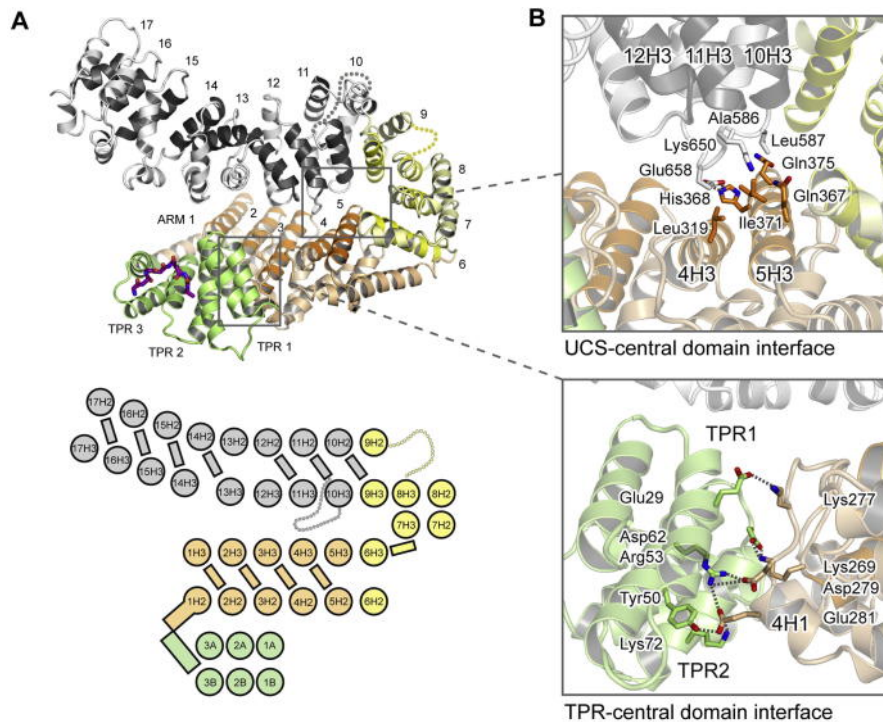


**Figure 1.23. Structure of the *C. elegans* UNC-45 protein. (A) Ribbon model and folding topology of UNC-45 illustrating its domain architecture and the used helix nomenclature (TPR: green; central: orange; neck: yellow; UCS: grey). Each TPR motif is made of two  $\alpha$  helices A and B, whereas the ARM repeats are composed of three helices H1, H2 and H3. (B) The central domain serves as a scaffolding unit that arranges TPR and UCS domain. The two close-up views illustrate the corresponding UNC-45 domain interfaces (polar interactions represented as dotted lines). Upper panel: Interface of the central and UCS domains. Lower panel: Interface of central and TPR domain highlighting several short-distanced salt-bridges formed between Asp62-Lys269, Arg53-Asp279, Lys72-Glu281 and Glu29-Lys277. Figure adapted from (Gazda et al. 2013).**

The central domain is a flat, rectangular protein ribbon that is structured by helices H1, H2, and H3 of ARM repeats 1–5. The consecutive ARM hold the TPR domain in place. Interactions with the second functional domain, the UCS domain, are mediated by residues located on the H3 side of the central domain. Here, helices 4H3 and 5H3 form a flat binding surface to accommodate the loops protruding from ARM repeats. The UCS and central domains are connected by the neck domain. The helix pairs of the neck domain adopt a super-turn structure. In the slightly open UNC-45 fold, the UCS domain protrudes in a 20° angle from the central domain and is situated above the interface of the central and TPR domains. The UCS domain itself forms an almost regular right-handed superhelix. The parallel packed helices of neighbouring repeats assemble a spiralling scaffold with a long shallow groove that is lined by the H3 helices (Figure 1.23A). The UCS domain encompasses an extended loop (residues 602–630) that is inserted after helix 10H3 and represents one of the most conserved signature motifs of UCS proteins.

### 1.5.3 UNC-45 function

In muscle cells, UNC-45 ensures proper folding of myosin to allow its assembly and function in the sarcomere (Ao and Pilgrim 2000; Barral et al. 1998; Etard et al. 2007; Lee et al. 2011; Melkani et al. 2011; Price et al. 2002; Srikakulam and Winkelmann 2004). During normal development, myosin maturation involves chaperones such as TriC/CCT and Hsp70 (Srikakulam and Winkelmann 1999, 2004). Data from zebrafish studies suggest myosin then forms a complex with UNC-45 and Hsp90 in the cytosol (Etard, Roostalu, and Strähle 2008).

The elucidation of UNC-45's crystal structure (Lee et al. 2011; Gazda et al. 2013) suggested that it serves as a scaffold-like protein that can present Hsp90 bound at the TPR domain to myosin bound in the surface groove of the UCS domain, with the myosin possibly held in place by a binding loop (Fratev, Ósk Jónsdóttir, and Pajeva 2013; Gazda et al. 2013). Gazda et al proposed that the UNC-45 multimer establishes a multisite docking platform, which can recruit Hsp70 and Hsp90 partner chaperones to perform their activity in a periodic pattern on the unfolded myosin substrate. This is summarised in Figure 1.24. It is important to note, however, that direct observation of UNC-45 oligomers *in vivo* has not yet been reported.

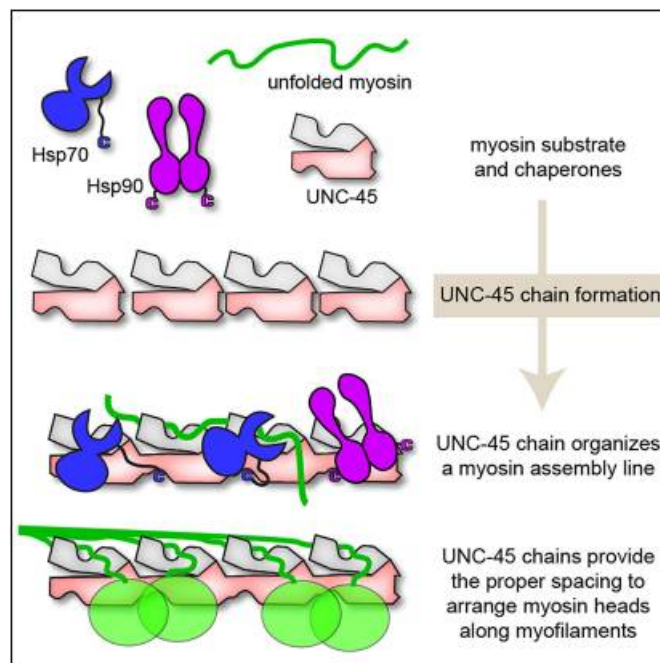


**Figure 1.24. UNC-45 self-assembles a docking platform for multiple chaperone and myosin proteins. Hsp70/90 and myosin bind to specific sites on the TPR and UCS domains of UNC-45. The UNC-45 multimer confers the proper spacing required to simultaneously fold and assembly myosin filaments. Figure from (Gazda et al. 2013).**

UNC-45 may also have a protective role against in stress response (see Figure 1.25). UNC-45 prevents heat-induced aggregation of myosin in vitro (Barral et al. 2002; Melkani et al. 2010). In fact, UNC-45 relocates from the Z-disks to the myosin-containing A-bands during stress in zebrafish muscle (Etard et al. 2008). Once myosin successfully incorporates into thick filaments, UNC-45 and Hsp90 dissociate from myosin and move to the Z-disk for storage. In cases where UNC-45 needs to be cleared, this is accomplished by the ubiquitin/proteasome protein degradation system. UNC-45 associates with various enzymes such as ubiquitin-activating enzyme E1, ubiquitin-conjugating enzyme E2 and ubiquitin ligases E3/E4 (Hoppe et al. 2004). This complex can then transit to the 26S proteasome for degradation (Figure 1.25) (Janiesch et al. 2007).

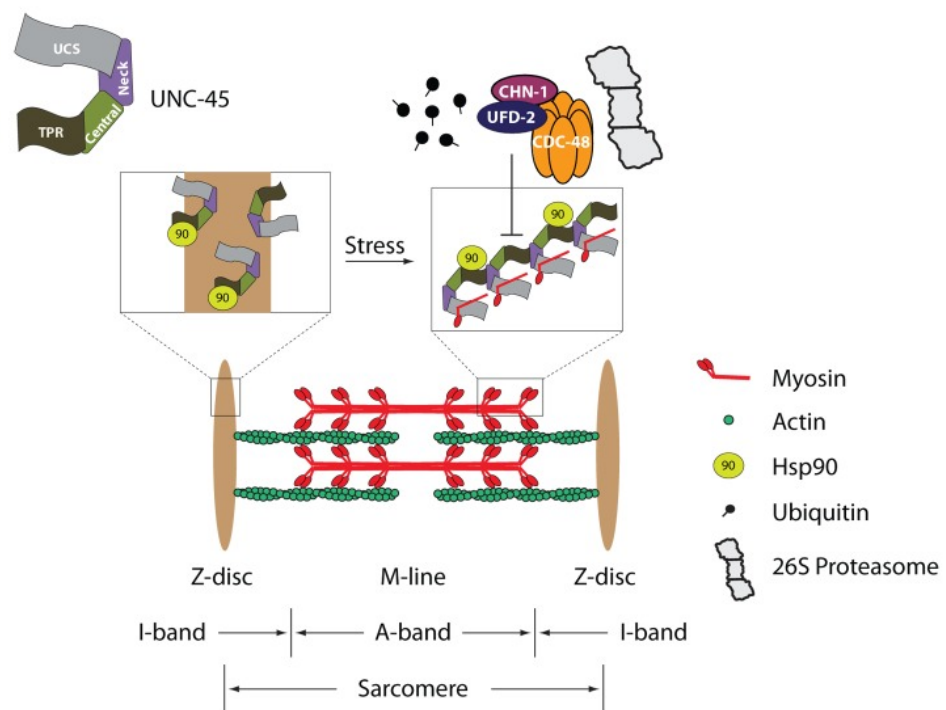


**Figure 1.25. Model of UNC-45 chain formation in muscle maintenance. UNC-45 forms tandem modules that allow the simultaneous binding of Hsp70/Hsp90 and myosin, enabling the folding and assembly of myosin in regular spacing. In the fully developed muscle, monomeric UNC-45 might be stored at the Z-disk, which anchors the thin actin filaments of the I-band. Under stress conditions, UNC-45 is relocated to damaged myosin filaments of the A-band and might assemble into short chaperone chains to maintain the sarcomeric structure. Figure from (Pokrzywa and Hoppe 2013).**

As detailed above, the *C. elegans* UNC-45 has been well studied and characterised. However, the molecular basis for the activity of UNC-45 is not completely understood. In chapter 6, the interaction between the *C. elegans* UNC-45 and the *C. elegans* body wall myosin will be investigated in a cellular context. It will also deal with the question of whether the myosin-folding activity of UNC-45 can be exploited to produce recombinant myosin in a non-muscle environment.

## 1.6 Techniques used to probe functional properties of myosin

The work of this thesis is focused on understanding how the kinetic signatures of myosin class II isoforms allow them to carry out diverse mechanical functions. To do this, stopped-flow spectroscopy and a kinetic modelling approach were used.

### 1.6.1 Stopped-flow spectroscopy

Transient kinetic analysis is a useful tool for deducing the mechanisms of chemical interactions and complements traditional steady-state approaches which determine the overall behaviour of a reaction. Transient kinetics refers to the time course of a reaction before it reaches the steady-state - the concentrations of species change in time according to the Law of Mass action, and hence monitoring the progress of a reaction can lead to determination of the rate constants of the steps that make up a pathway (Bagshaw 2013b). Stopped-flow spectroscopy (hereon in referred to as stopped-flow) is a powerful technique used for studying such transient reaction kinetics. A typical stopped-flow spectrophotometer is shown in Figure 1.25, and consists of two air-driven drive syringes, mixing and observation chambers, a stop-syringe and a recording system.

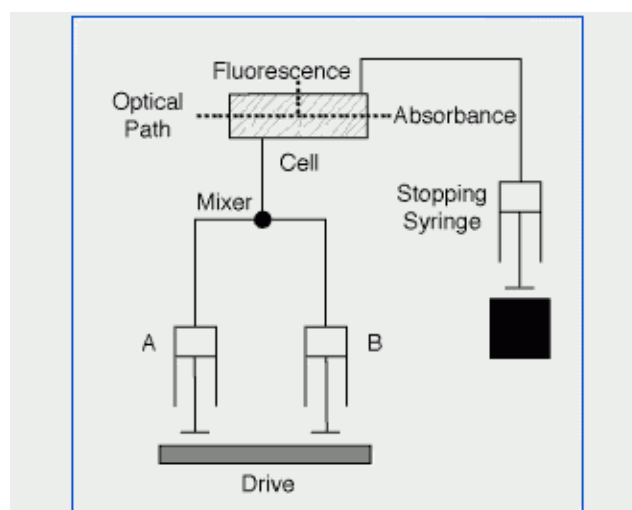
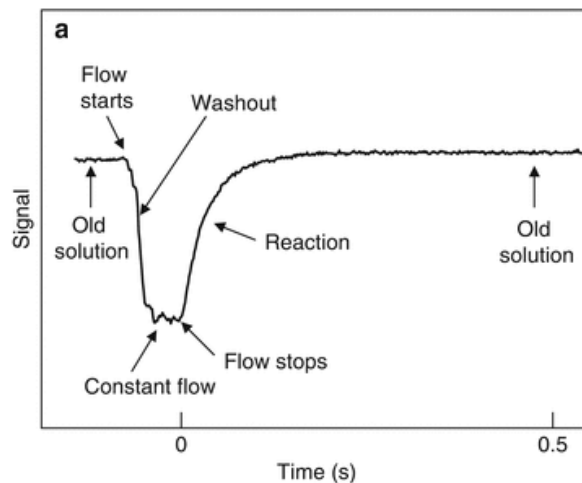


Figure 1.26. Schematic setup of a single mixing stopped-flow apparatus. Figure from (TgK Scientific 2019).

Small volumes (typically 60  $\mu\text{L}$ ) of solutions are rapidly driven from the two syringes (labelled A and B in Figure 1.26) containing the reactants into a mixing chamber. The resultant reaction volume then displaces the previous contents of the observation cell, thus filling it with freshly mixed reagents. The solution entering the observation cell is typically  $\sim$  two milliseconds old. The volume injected is limited by the stop syringe which provides the “stopped-flow”; as the solution fills the stopping syringe, the plunger hits a backstop, causing the flow to be stopped instantaneously and trigger data collection (Figure 1.27). The detectors can measure any optical signal, such as the absorbance or fluorescence of the solution, which is monitored as a function of time. It is important to note that the concentration of the reactants inside the observation cell is half that of the concentration in the drive syringes, as the samples are mixed in a 1:1 ratio in the mixing chamber.



**Figure 1.27.** Three phases can be identified in the progression of the stopped-flow reaction. First, the old solution from the previous reaction is washed out; second, there is a brief continuous-flow phase as new solution passes through the cell; and third, the flow is stopped and the reaction profile is measured, which is when the detector is triggered. Figure adapted from (Bagshaw 2013a).

There are a number of benefits to using stopped-flow to measure rapid kinetics of myosin and the ATP-driven cross-bridge cycle, most notably the kinetic identification of reaction intermediates formed throughout the cycle, and their corresponding lifetimes (De La Cruz and Ostap 2009). Furthermore, many of the experimentally observed rate constants in the cross-bridge cycle occur around the order of several hundred per second, and so data collection with millisecond time resolution is required to measure these rate constants. Therefore, stopped-flow is invaluable for measuring the kinetics of myosin.



### 1.6.2 Kinetic Modelling

The transient kinetic analysis outlined in 1.6.1 and 2.3 can define a number of biochemical events of the actin.myosin ATPase cross-bridge cycle. This cycle is conserved for all myosins classes (De La Cruz and Ostap 2004). Unknown parameters of the cross-bridge cycle that cannot be determined experimentally, be that because of lack of experimental resolution or limited protein sample, can be predicted using kinetic modelling programs. Such programs fit multiple kinetic parameters determined from transient kinetics to steady-state ATPase data. To investigate how such closely related myosin class II isoforms yield such a wide range of physiological properties, a modelling program called MUSICO (Muscle Simulation Code) was developed by Mijailovich and colleagues (Mijailovich et al. 2017). MUSICO simulates ATPase data from experimentally determined cross-bridge kinetics to predict the occupancy of the intermediates of the cross-bridge cycle. Within myosin class II isoforms, changes in the overall cycling speed and the fraction of the cycle spent in intermediate states determine distinct properties of an isoform, tuning it for its specific function (De La Cruz and Ostap 2004; Bloemink and Geeves 2011; Heissler and Sellers 2016). Understanding how each isoform is adapted for its specific role, or how single point mutations can alter the behaviour of the motor, requires the contribution of each step in the cycle to be defined. This will be discussed in Chapters 3 and 5.

The kinetic modelling approach used in this thesis is based upon an 8-state actin.myosin ATPase cycle, as shown in Figure 1.28 (Walklate, Ujfalusi, and Geeves 2016; Mijailovich et al. 2017). This is a more detailed description of the cross-bridge cycle, built on the Lymm-Taylor model shown in Figure 1.11. In the absence of nucleotide, myosin is bound to actin in a rigor complex (A.M). Upon ATP binding to the nucleotide pocket of the myosin motor domain, fast, irreversible detachment of myosin from actin occurs as a result of a conformational change in the myosin head (Sweeney and Houdusse 2010). This is caused by switch 1 closing around the ATP molecule, which pulls the U50 subdomain away from the L50 subdomain, opening the actin-binding cleft and resulting in a weaker affinity to actin. The subsequent release of actin from myosin leaves ATP bound to myosin (M.T), and is followed by switch 2 being brought into close proximity to the bound nucleotide, causing the SH1-SH2 helix to rotate and subsequently the converter domain to rotate by 60 degrees (Geeves and Holmes 2005). This action is termed the recovery stroke, and is necessary to prime the myosin for the power stroke (Muretta et al. 2015). The catalytic activity of myosin will then hydrolyse ATP to form ADP and Pi once switch 1 and 2 are closed. A stable myosin.ADP.Pi complex is formed (M.D.Pi), which has a higher affinity for actin than the M.T complex, meaning that actin is now able to rebind to the L50 subdomain (De La Cruz

and Ostap 2004; Heissler and Sellers 2016). This induces another conformational change; the 7-stranded central beta sheet twists to bring the U50 subdomain close to the L50 subdomain, closing the actin-binding cleft. Next, 2 events occur but the order in which they take place is still under debate (Houdusse and Sweeney 2016; Woody et al. 2019). Switch 2 changes from a closed to open state, which opens the  $\gamma$ -phosphate binding pocket and facilitates phosphate release. Phosphate release coincides with the transition of myosin from a weakly bound to a strongly bound state with actin. The relay helix rotates, generating the power stroke (Sweeney and Houdusse 2010). Movement of the converter domain in the same direction as the working stroke opens the nucleotide binding pocket to facilitate the subsequent release of ADP, forming either the rigor complex in the absence of nucleotide or by displacement with ATP to repeat the cycle.

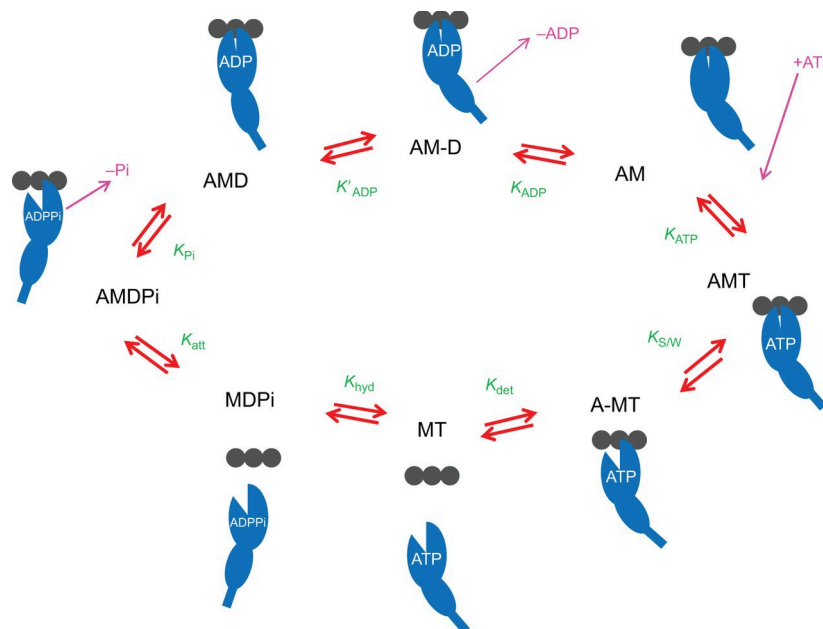


**Figure 1.28. The ATP-driven actin.myosin cross-bridge cycle.** Myosin is shown as 2 ellipses and a rod; the larger ellipse represents the U50 and L50 domains, the smaller ellipse and rod representing the converter domain, lever arm and light-chain binding region. An actin polymer is represented by 3 grey circles. The nucleotide-free complex of actin.myosin (**AM**) can bind to ATP (**AMT**), leading to an isomerisation step (**A-MT**) with subsequent detachment of actin from myosin (**MT**). Hydrolysis of ATP generates a the myosin.ADP.Pi complex (**MDPi**). Actin rebinds to this complex (**AMDPi**), leading to phosphate release and the power-stroke occur (the exact order is still unknown). The actin.myosin now has a weaker affinity for ADP (**AM-D**), leading to ADP release (**AM**), completing the cycle. Figure adapted from (J Walklate et al. 2016).

## **1.7 Themes**

Despite decades of research into myosin, research activity in the field is still as lively, both in terms of basic research and disease-therapy focussed studies. There are still a number of unanswered questions within the field, one of which is how different myosin isoforms meet a wide spectrum of physiological needs whilst having such a high sequence identity. The work presented in chapters 3-6 aims to address this question. To do this, this thesis has four aims:

1. To understand how human sarcomeric myosins from the class II family adapt their mechanochemical ATPase cycle to perform different functions within different muscle types. A combination of kinetic data and computer modelling was used to predict how myosin class II isoforms change the fraction of time spent in different occupancies of the cross-bridge cycle to bring about differences in contractile properties, such as economy of ATP usage, duty ratio and shortening velocity.
2. Having identified some of the differences in contractile properties between myosin isoforms, the MyHC- $\beta$  isoform was then used to further investigate how the sequence of the protein can drive adaptation to changes in body mass. In particular, the sequence changes that drive acceleration in ADP-release rates as body mass increases was explored. The relationship between ADP-release and velocity has been well documented, so we set out to identify if these sequence changes could contribute to the faster heart rates observed in smaller mammals.
3. Having used MyHC- $\beta$  to probe how the protein adapts to selective pressures, attention was then turned to understanding what goes wrong in the mechanochemical ATPase cycle of the same isoform during diseased states. More specifically, a number of mutations have been identified in childhood patients with HCM (early-onset), and it has been hypothesised that the effect of the mutations are more severe than mutations found in adults with HCM (or late-onset mutations). Stopped-flow was used to characterise kinetic parameters of the cross-bridge cycle for four early-onset and three late-onset HCM mutations. The mechanochemical cycle was then further explored using MUSICO, to try to understand the different contractile properties between the two groups of mutations.

4. One of the main problems with studying human cardiac disease, such as HCM, is the lack of available samples to study muscle function in health and disease. Recombinant expression systems currently enable myosin and its associated disease-causing mutations to be produced, but protein yields are limited and the method is very technical. Folding and assembly of myosin is critical for correct functioning of the protein, so using insights into the UNC-45 chaperone that is responsible for myosin folding we attempted to improve the current expression systems to purify sarcomeric myosins.

The overarching theme of this thesis is the aim to understand at a molecular level, how myosin can fine-tune its properties to allow such a diverse range of functions to be achieved, and how this is disrupted during diseased states.

## **2. Materials and Methods**

### **2.1 Materials**

#### 2.1.1. Chemicals, Hardware and Software

All reagents and chemicals were supplied from Melford laboratories, Sigma-Aldrich or Fisher chemicals, except for those listed in Table 2.1.

**Table 2.1 List of chemicals, hardware, software and apparatus used throughout this thesis.**

| <b>Chemical/Hardware/Software/Apparatus</b> | <b>Supplier/Address</b> |
|---|-------------------------|
| Nucleotides (ATP, ADP)                      | Roche                   |
| Pyrene                                      | Molecular Probes        |
| EDTA free protease inhibitor tablets        | Roche                   |
| Stopped-flow SF-61 DX2                      | TgK Scientific, UK      |
| LED light sources                           | Ocean Optics            |
| Optical filters                             | Schott, Germany         |
| Temperature controlled water baths          | K20, Haake, Germany     |
| Cary UV-50 spectrophotometer                | Varian, Germany         |
| Quartz cuvettes                             | Hellma, Germany         |
| Eppendorf 5415R centrifuge                  | Eppendorf, Germany      |
| Beckman J-26 XP centrifuge                  | Beckman, USA            |
| Beckman Optima Ultracentrifuge              | Beckman, USA            |
| AKTA FPLC                                   | GE Healthcare, UK       |
| HisTrap 1 mL columns                        | GE Healthcare, UK       |
| Sepharose 500 ml column                     | GE Healthcare, UK       |
| IX71 Microscope                             | Olympus                 |
| Microscope slides and coverslips            | Thermo Scientific       |
| Weighing scales                             | Sigma-Aldrich           |
| pH meter                                    | Sigma-Aldrich           |
| Pipettes, pipette tips                      | Gilson, USA             |
| Unicorn                                     | GE Healthcare, UK       |
| Cary UV                                     | Varian, Germany         |
| Kinetic Studio                              | TgK Scientific, UK      |
| Origin Studio                               | OriginLab Corporation   |
| Methamorph                                  | Molecular Devices, USA  |
| MUSICO                                      | Mijailovich lab         |

### 2.1.2 Buffers

Buffers used throughout this thesis are described in Table 2.2.

**Table 2.2 List of buffers used in this thesis. All buffers were prepared at room temperature. Where applicable, pH was adjusted using 1 M HCl and 1 M KOH.**

| Buffer                            | Ingredients   | pH  |
|-----------------------------------|---|-----|
| Standard stopped flow             | 25 mM KCl, 5 mM MgCl <sub>2</sub> , 20 mM MOPS, 1 mM NaN <sub>3</sub>   | 7.0 |
| Acetone-actin powder resuspension | 10 mM NaHCO <sub>3</sub> , 10 mM NaCO <sub>3</sub> , and 0.1 mM CaCl <sub>2</sub>                             | 7.5 |
| Actin depolymerisation            | 10 mM Tris, 0.5 mM ATP, 0.2 mM CaCl <sub>2</sub> , 1 mM DTT   | 8.0 |
| F-actin                           | 100 mM KCl, 2 mM MgCl <sub>2</sub> , 10 mM Tris, 1 mM ATP   | 7.5 |
| Lysis Buffer                      | 20 mM Imidazole, 100 mM NaCl, 50 mM Tris, 1 x EDTA free protease inhibitor, 3 mM ATP, 0.5% Tween-20, 1 mM DTT | 7.4 |
| HisTrap Buffer A                  | 50 mM Tris pH 7.0, 500 mM NaCl, 0.05 % Tween-20, 1 mM DTT,  | 7.0 |
| HisTrap Buffer B                  | 50 mM Tris pH 7.0, 500 mM NaCl, 0.05% Tween-20, 1 mM DTT, 1 M Imidazole                                       | 7.0 |
| Guba-Straub                       | 100 mM KH <sub>2</sub> PO <sub>4</sub> , 50 mM K <sub>2</sub> HPO <sub>4</sub> , 300 mM KCl                   | 6.6 |
| S1 digestion buffer               | 125 mM KCl, 10 mM KPi (pH 6.2), 2 mM EDTA, 2 mM DTT   | 6.5 |
| Myosin storage                    | 500 mM KCl, 10 mM KPi, 1 mM DTT, equal volume of glycerol   | 7.0 |
| 5X SDS-PAGE sample buffer         | 10% SDS, 0.05 % Bromophenol Blue (w/v), 10% 2-mercaptoethanol, 40% glycerol (w/v), 0.625 M Tris base          | 6.8 |
| In vitro motility assay buffer    | 25 mM imidazole, 25 mM KCl, 4 mM MgCl <sub>2</sub> , 1 mM EGTA, and 1 mM DTT                                  | 7.0 |

## 2.2 Protein preparation

### 2.2.1 Rabbit *psoas* and rat *soleus* myosin and S1 preparation

The *psoas* muscle was extracted from the back and leg muscles of two rabbits, which were dissected immediately post mortem and stored on ice. After removing all fat and ligaments, the muscle was minced and left to stir in 3 L of Guba-Straub for 30 minutes at 4 °C. This was then centrifuged at 5,000 RPM for 30 minutes. The supernatant was used for the myosin preparation while the pellet was used to purify actin (section 2.2.2).

Rabbit myosin was prepared by the method of Margossian and Lowey (Margossian, Lowey 1982). The supernatant was filtered through a cheese cloth to remove large parts of unhomogenised muscle, and subsequently through homogenised filter paper to remove fat. The filtrate was added rapidly to 30 L of cold water and left overnight at 4 °C to allow the myosin to precipitate. The water was siphoned off and the precipitated myosin centrifuged for 45 minutes at 5,000 RPM. The pellet was re-suspended in 1 L 0.5 M KCl and the overnight precipitation repeated. The precipitated myosin was centrifuged for 20 minutes at 12,000 RPM. Myosin could either be stored in -20 °C by dissolving the pellet in myosin storage buffer and storing in 50% glycerol, or further digested to produce S1 fragments.

Fresh myosin or myosin from a glycerol stock was allowed to precipitate in a large volume of distilled water overnight. The supernatant was siphoned off and the remaining precipitate centrifuged for 45 minutes at 5,000 RPM. The pellets were dissolved in the rabbit S1 digestion buffer. The mixture was warmed to 23 °C and 0.1 mg Chymotrypsin per mL of solution was added and left to stir at 23 °C for 10 minutes. To stop the digestion, 0.5 mM phenylmethylsulfonyl fluoride (PMSF) was added and the solution left to stir for 10 minutes. The digested myosin solution was dialysed against 5 mM KPi pH 6.5 for 12 hours. After dialysis, the solution was centrifuged for 1 hour at 12,000 RPM and the S1 was then purified by anion-exchange chromatography on a DEAE-sephacel column (500 mL gel bed volume), which had been equilibrated with 50 mM Imidazole pH 7.0. A KCl gradient of 0-250 mM KCl was used to elute the S1 which resulted in a peak with an absorbance at 280 nm. The fractions with high S1 content were checked for purity on a 4-12% Bis-Tris SDS-Page gel. UV spectroscopy was used to determine the final concentration of the S1 using the extinction coefficient  $\epsilon^{1\%} = 7.9 \text{ cm}^{-1}$  and a molecular weight of 115 kDa. 3% sucrose (w/v) was added, before the solution was drop frozen in liquid nitrogen, and stored at -20 °C. Once defrosted, the S1 was stable at 4 °C for 4-6 weeks.

Rat *soleus* muscle was purified using the same method as for rabbit *psoas* S1 outlined above, with some modifications. The *soleus* muscle was dissected from the calf muscle of male rats immediately post mortem. Minced muscle was left to stir in 100 ml of Guba-Straub. Myosin was precipitated using 250 ml of cold dH<sub>2</sub>O for 1 hour. Digested myosin was purified using a 20 ml gel bed volume DEAE-Sepharose column. After purification the S1 was stored at 4 °C and used within 5 days.

### 2.2.2 Rabbit actin preparation

The pellet obtained from the first centrifugation from the myosin extraction which contained the actin and thin filament proteins was dissolved in 5 L of buffer containing 4% NaHCO<sub>3</sub> and 0.1 mM CaCl<sub>2</sub>. This was left to stir at 4 °C for 30 minutes. The solution was then filtered through a cheese cloth, and the filtrate discarded. The residue from the filtration step was re-suspended in 1 L of acetone powder resuspension buffer. At room temperature, 10 L of water was added, stirred for 1 minute and the filtration step repeated. The residue was dissolved in 2.5 L cold acetone and left to stir for 20 minutes. This was filtered through cheese cloth and the filtrate discarded; this step was repeated a further three times until the residue became fibrous. The residue was then dried between two pieces of blotting paper for 48 hours and was sieved to form a fine powder, which can be stored at -20 °C.

F-actin preparation was performed as described by Lehrer and Kerwar (Lehrer and Kerwar 1972), with modifications. 3 g of acetone powder was dissolved in 500 mL of cold actin acetone-powder resuspension buffer and left to stir for 30 minutes. Using a double layer of cotton cloth, the mixture was filtered under vacuum. The filtrate, which contained the actin, was centrifuged for 1 hour at 30,000 RPM. In order to polymerise the actin, the concentration of KCl and MgCl<sub>2</sub> were increased to a final concentration of 100 and 2 mM, respectively. This was left to stir for 1 hour, followed by centrifugation for 3 hours at 30,000 RPM. The pellet was dissolved into depolymerising buffer, homogenised, and dialysed for 12 hours against 4 litres of depolymerisation buffer. Centrifuging the actin the next day at 30,000 RPM for 1 hour removed any remaining filamentous actin. Using UV spectroscopy the actin concentration was determined using the extinction coefficient  $\epsilon^{1\%} = 11.04 \text{ cm}^{-1}$  and molecular weight of 42 kDa. This was then either drop-frozen in liquid nitrogen and stored at -80 °C, or used to prepare pyrene-labelled actin.

Preparation of pyrene actin labelling is based on the method by Criddle et al (Criddle, Geeves, and Jeffries 1985). Actin was polymerised at room temperature by increasing the concentration of KCl and MgCl<sub>2</sub> to a final concentration of 100 and 2 mM, respectively, and



was left to stir for 1 hour. The actin was diluted to 1 mg/ml. N-(1-pyrenyl)-iodoacetamide (pyrene; 5 mg/mL dissolved in dimethylformamide) was added stepwise to the F-actin solution while stirring to a final concentration of 1% (w/w) pyrene. The solution was stirred at room temperature for 18 hours in the dark and then centrifuged at 8,000 RPM for 1 hour to remove residual pyrene. The labelled actin was then pelleted by centrifugation at 30,000 RPM for 3 hours. The actin pellet was dissolved, homogenised and dialysed overnight against standard stopped-flow buffer. The labelled actin was assayed by actin content (extinction coefficient  $\epsilon^{1\%} = 11.04 \text{ cm}^{-1}$  and molecular weight of 42 kDa) and pyrene content (extinction coefficient at 280 nm  $\epsilon^{1\%} = 10.59$ ; at 344 nm  $\epsilon^{1\%} = 23.3$ ). The final concentration of labelled actin was usually 100-200  $\mu\text{M}$  and the efficiency of labelling was typically 80-95%.

When the concentration of actin is below 1  $\mu\text{M}$ , F-actin will spontaneously depolymerise. To prevent this in stopped-flow assays, the F-actin was stabilised by the addition of phalloidin (Kurzawa and Geeves 1996). An equimolar stock of 10  $\mu\text{M}$  actin and phalloidin (from *Amanita phalloides*) was incubated over night at 4 °C and remained stable for 4-5 days.

### 2.2.3 C2C12 cell protein expression and purification

Shuttle plasmids containing the coding regions of the human MYH7 gene were constructed upstream of a 6x-Histidine tag. For the rat-human chimera studied in Chapter 4, the coding region was Met1-Ser843. For the HCM mutations studied in Chapter 5, a shorter S1 (sS1) was used, with translation terminating after ELC-binding IQ domain at Arg808. Using the pAdEasy kit (MP Biomedicals), the plasmids were used to construct recombinant replication-deficient adenovirus that expressed MYH7, as described by Resnicow and colleagues (Resnicow et al. 2010).

To generate the rat-human chimera clone, a pUC19 plasmid containing the human  $\beta$ -myosin motor domain gene was digested with NsiI and NgoMIV to excise DNA encoding for residues 310 – 599 of the human  $\beta$ -myosin. This region was replaced with a complementary pair of synthetic oligos encoding for the same region, but with nine amino-acid substitutions (Ala326Ser, Ser343Pro, Leu366Gln, Ile421Ala, Thr424Ile, Ala430Ser, Arg434Lys, Phe553Tyr, Pro573Gln). The HCM mutations were created using site directed mutagenesis to produce the His251Asn, Asp382Tyr, Pro710Arg, Arg719Trp, Arg725Gly, Gly741Arg, and Val763Met mutants. All clones were confirmed by sequencing. HEK293 cells were used to amplify the viral particles, and the cell lysates were clarified using

caesium chloride gradients with the concentrated virus being stored in a glycol buffer at -20 °C.

For the culturing of C2C12 cells, 4-layer Nunc™ cell factory systems (Thermo Fisher) were used to increase culturing capacity. After the cells were seeded into these factories and had reached full confluency, they were differentiated from myoblasts to myotubes by addition of Differentiation Media, containing Dulbecco's Modified Eagle Medium, 2% Horse serum, 1X Pen/Strep and 1X L-Glutamine. The cells were incubated for 3 - 4 days, after which the surface area in the factories were covered in myotubes and ready to infect. The myotubes were infected with  $1 \times 10^6 - 1 \times 10^8$  plaque forming units of adenovirus and incubated for 5 days in infection media containing Dulbecco's Modified Eagle Medium, 5% Fetal Bovine Serum, 1X Pen/Strep and 1X L-Glutamine. The cells were harvested by lifting off the surface with trypsin and collecting in a buffer of 30 mM HEPES, 15 mM KCl, 135 mM NaCl, 2 mM EDTA, 60 mM sucrose, 0.2% Pluronic F-68 (cell membrane stabilizer from Sigma), at pH 7.5 and 4 °C. The cells were then pelleted at 4,000 rpm at 4 °C for 30 min and fast-frozen in liquid N<sub>2</sub>.

S1 or sS1 was purified from cell pellets as described by Resnicow et al and Deacon et al (Resnicow et al. 2010; Deacon et al. 2012). One cell pellet was incubated at 37 °C for 1 minute before addition of 3 mL of lysis buffer. When the pellet was fully defrosted the volume was made up to 18 mL with lysis buffer. The sample was homogenised using a glass homogeniser (Fisher Scientific). The cell lysate was centrifuged at 80,000 RPM for 20 minutes to remove the majority of the cell contents. The supernatant was then filtered through a 5 µm Minisart single use syringe filter (Sartorius Stedim Biotech, Germany), and the volume was increased to 18 mL using lysis buffer. 5 M NaCl was added to the solution to increase the final NaCl concentration to 0.5 M. A HisTrap HP 1 mL nickel column was equilibrated with HisTrap buffer A. The recombinant S1 was then eluted using a 0-1 M stepped imidazole gradient, eluting from the column at around 350 mM Imidazole using His-Trap buffer B. The fractions were run on a 4-12% Bis-Tris SDS gel to identify the fractions with the highest purity, which were collected and pooled. Samples were dialysed overnight into the recombinant S1 stopped-flow buffer. The concentration of the S1 was determined using UV spectroscopy (extinction coefficient  $\epsilon^{1\%} = 7.9 \text{ cm}^{-1}$  and a molecular weight of 115 kDa). Cell pellets weighing approximately 0.6 g derived from 1500-3000 mL would yield between 1-2 mL 2-20 µM active S1. S1 proteins were stored at -20 °C with 3% sucrose (w/v) and stored at -20 °C. When defrosted all protein preparations were used within 3 days.

#### 2.2.4 SDS-PAGE gels

Pre-cast polyacrylamide NuPAGE® 4-12% Bis-Tris Gels (1.0 mm thick, 10 or 15 wells) were used to check protein purity after purification. 5x sample buffer containing 2-mercaptoethanol was added to samples and heated at 90 °C for 10 mins before loading. The gels were run in MOPS buffer (50 mL of 20 x NuPAGE® MOPS running buffer (Life Technologies) mixed with 950 mL dH<sub>2</sub>O) at 200 volts for 45 minutes. The gels were incubated in Coomassie blue staining solution (1 g Coomassie Brilliant Blue dissolved in 1 L of: 50% (v/v) methanol, 10% (v/v) glacial acetic acid, 40% (v/v) dH<sub>2</sub>O). The stained gels were transferred to a de-staining solution (7% (v/v) glacial acetic acid, 25% (v/v) methanol, 68% (v/v) dH<sub>2</sub>O) 3 times to reveal the protein bands. Proteins of interest were identified by comparison with PageRuler™ unstained protein ladder ranging from 10 to 200 kDa (Fermentas Life Sciences).

## **2.3 Kinetic measurements**

### 2.3.1 Stopped-flow and Fluorescence

As described in section 1.6.2, stopped-flow spectroscopy was utilised to characterise kinetic properties of a number of different human isoforms or mutations. To do this, both intrinsic and extrinsic fluorescence was used.

Intrinsic fluorescence is a result of fluorescence from a tryptophan residue at position 508 (residue position in human MyHC- $\beta$  sequence). This residue is found on the end of the relay helix which moves relative to the rest of the motor domain during the ATPase cycle. Upon ATP binding, the conformational change associated with the recovery stroke causes the tryptophan to move, and resulting changes in fluorescence of this residue can be monitored. The intensity of this fluorescence varies between myosin isoforms, but for human cardiac isoforms a fluorescence change of 10% can typically be observed. Intrinsic fluorescence was excited at 290 nm and emission monitored through a WG320 cut off-filter.

Extrinsic fluorescence is the result of a signal change from a fluorophore added to a protein of interest. As described in 2.2.2, pyrene can be chemically linked to polymerised actin, which attaches via a disulphide bond to a cysteine residue at position 374. Pyrene can be excited at 365 nm, but addition of myosin will quench this fluorescence. Fluorescence is restored upon myosin dissociation from actin. Pyrene fluorescence was excited at 365 nm and emission monitored through a KV399 cut-off filter. Human class II myosin isoforms quench pyrene fluorescence by 60 - 65%, and the *C. elegans* MHC-B protein by ~76%.

Stopped-flow experiments were performed to measure transient kinetics of the acto.myosin ATP-driven cross-bridge cycle, which are outlined in 2.3.2. To note, all stopped-flow experiments in this thesis were conducted with the motor domain of myosin proteins (S1), rather than full length myosin.

### 2.3.2 Transient Kinetics

The simplest, unimolecular reaction possible is described in scheme 2.1.



**Scheme 2.1. The rate law of a first order reaction with respect to A, where k is the first order rate constant (s<sup>-1</sup>).**

The Law of Mass Action states that the rate at which B is formed is proportional to the concentration of A. The rate at which A is lost can be expressed as:

$$-\frac{d[A]_t}{dt} = k[A]_t \quad \text{Equation 2.1}$$

Integration gives the integrated first order rate law:

$$-kt = \ln[A]_t - \ln[A]_0 \quad \text{Equation 2.2}$$

where  $[A]_t$  is the concentration of A at time t and  $[A]_0$  is the concentration of A at time 0.

Rearranging the equation gives:

$$[A]_t = [A]_0 e^{-kt} \quad \text{Equation 2.3}$$

This equation can be used to describe the enzymatic reactions measured in stopped flow, which behave either as single or double exponentials. All single exponential transients from stopped-flow measurements were fitted to a single exponential equation:

$$F = A(1 - e^{-kt}) + c \quad \text{Equation 2.4}$$

whilst all double exponential transients were fitted to a double exponential equation:

$$F = A_1(1 - e^{-k_1t}) + A_2(1 - e^{-k_2t}) + c \quad \text{Equation 2.5}$$

where F = fluorescence, A = amplitude, t = time, k = rate constant, c = fluorescence offset.

There are a number of different types of reactions that can be measured with stopped-flow, as summarised in Table 2.3. Each type of reaction is characterised by a number of assumptions or conditions, which then determine the definition of the observed rate constant ( $k_{\text{obs}}$ ) in the assay.

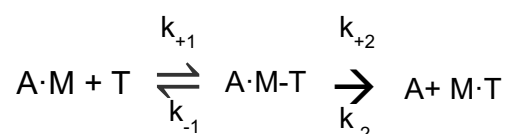
**Table 2.3 Summary of kinetic reactions.**

| Reaction   | Assumptions   | $k_{\text{obs}}$                              |
|--|---|---|
| $A \rightarrow B$                                  | 1 <sup>st</sup> order, irreversible                                       | $k$   |
| $A+B \rightarrow AB$                               | 2 <sup>nd</sup> order, 1-step, irreversible<br>$[B] \gg [A]$              | $[B]k$  |
| $A+B \rightleftharpoons AB$                        | 2 <sup>nd</sup> order, 1-step, reversible<br>$[B] \gg [A]$                | $[B]k_{+1} + k_{-1}$                          |
| $A+B \rightleftharpoons AB \rightleftharpoons A'B$ | 2 <sup>nd</sup> order, 2-step, reversible<br>$[B] \gg [A]$<br>Step 1 fast | $\frac{K_1 k_{+2} [B]}{1 + K_1 [B]} + k_{-2}$ |

2<sup>nd</sup>-order 1-step and 2-step reversible reactions are difficult to analyse because they involve two variables. The experimental conditions are therefore altered in stopped-flow assays to mimic first-order reactions, also known as pseudo-first order. In these conditions, one reactant is used in large excess (a minimum of 5-fold) over the concentration of the second reactant to ensure the concentration of the first reactant remains constant over the time course of the reaction being studied, and so does not become second order. Reactions of this type which have been studied in this thesis are described below.

### 2.3.3 Pseudo-first order reactions

Let us consider a second-order 2 step reversible reaction, as shown below for the ATP induced-dissociation of actin.S1 as an example. In a second-order 2 step reversible reaction, one of the two steps needs to be faster in order to differentiate the two steps. As shown in scheme 2.2, step 1 involves ATP binding to an actin.myosin complex, and the second step is the irreversible step of S1.ATP dissociating from actin.



**Scheme 2.2 – ATP induced dissociation of myosin or S1 from actin. A = actin, M = myosin, T = ATP.**

We can make the assumption that step 1 is very fast compared to step 2, and  $k_{+2}$  is very small. Therefore:

$$\frac{d[MT]}{dt} = [AMT] k_{+2} \quad \text{Equation 2.6}$$

To find the total concentration of AM:

$$[AM]_{TOTAL} = [AM] + [AMT] + [MT] \quad \text{Equation 2.7}$$

Putting AM in terms of AMT and MT:

$$K_1 = \frac{[AMT]}{[AM][T]} \quad \text{which rearranges to} \quad [AM] = \frac{[AMT]}{K_1[T]} \quad \text{Equation 2.8}$$

Inserting equation 2.8 into 2.7:

$$[AM]_{TOTAL} = \frac{[AMT]}{K_1[T]} + [AMT] + [MT] \quad \text{Equation 2.9}$$

Solving for AMT gives:

$$[AMT] = \frac{[AM]_{TOTAL} - [MT]}{1 + \frac{1}{K_1[T]}} \quad \text{Equation 2.10}$$

Inserting into equation 2.6:

$$\frac{d[MT]}{dt} = \left( \frac{[AM]_{TOTAL} - [MT]}{1 + \frac{1}{K_1[T]}} \right) k_{+2} \quad \text{Equation 2.11}$$

This can be simplified to:

$$\frac{d[MT]}{dt} = \frac{[AM]_{TOTAL} K_1 k_{+2} [T]}{K_1 [T] + 1} - [MT] \left( \frac{K_1 k_{+2} [T]}{1 + K_1 [T]} \right) \quad \text{Equation 2.12}$$

Integration of the 2<sup>nd</sup> part of equation 2.12 results in:

$$k_{obs} = \frac{K_1 k_{+2} [T]}{1 + K_1 [T]} + k_{-2} \quad \text{Equation 2.13}$$

Where  $k_{+2}$  defines the maximum rate constant,  $1/K_1$  gives the concentration of T to reach 50%  $k_{max}$  and  $k_{-2}$  is the overall dissociation rate constant. The initial linear part of the hyperbola defines  $K_1 k_{+2}$ .

This hyperbola was used to fit the  $k_{obs}$  values obtained from stopped-flow transients.

#### 2.3.4 S1 affinity for actin

The method for determining the affinity of S1 for actin was described by Kurzawa and Geeves (Kurzawa and Geeves 1996). This is a titration assay in which a fixed concentration of actin is preincubated with increasing concentrations of S1. This can then be rapidly mixed with ATP in the stopped-flow to induce complete dissociation of S1 from actin. With increasing [S1], the amplitude will also increase as more pyrene fluorescence is quenched at the beginning of the reaction. Therefore, the amplitude provides an estimate of the fraction of actin bound to S1 at increasing S1 concentrations. As the affinity value is close to the total protein concentration in the assay, the data cannot be fit with a hyperbola. The amplitude was plotted against [S1] and fitted to the physically significant root of the following quadratic equation:

$$a = \frac{[M] + K_D + [A]_0 - \sqrt{([M] + K_D + [A]_0)^2 - \frac{4}{[M][A]_0}}}{2[A]_0} \quad \text{Equation 2.14}$$

where [M] = concentration of free S1 at equilibrium,  $K_D$  = the actin affinity equilibrium constant,  $[A]_0$  = concentration of total actin at time 0.



## 2.4 Modelling

Figure 1.28 shows the ATP-drive acto.myosin cross-bridge cycle. The cycle is defined by 18 rate and 9 equilibrium constants. Each step  $i$  in the cycle can be defined by:

$$K_i = \frac{k_{+i}}{k_{-i}} \quad \text{Equation 2.15}$$

where  $K_i$  is the equilibrium constant,  $k_{+i}$  is the forward rate constant, and  $k_{-i}$  is the reverse rate constant. Transient kinetics is able to define 13 of these parameters (see Chapter 3). Estimates of the remaining unknown parameters can be obtained by fitting the transient kinetic data to steady-state ATPase data in a process called global fitting.

Global fitting refers to simultaneous curve fitting using numerical integration to simulate kinetic data and calculate the rate of transition between different intermediates in a pathway or cycle. A number of kinetic software packages are available to do this, such as Berkeley Madonna, Dynafit or KinTek, and all work on the same principle. These programs allow numerical solving of differential kinetic equations, to simulate the time course of kinetically complex systems. This yields insights into the time dependence of reactant disappearance or product appearance, as well as the concentration of intermediates in the pathway. It is possible to optimise rate constants for steps in the model using best fit procedures. During the global fitting process, the rate constants are adjusted iteratively to give the best fit to the experimental data. This generates estimates for rate constants that cannot be determined experimentally.

Whilst the ATPase cycle in Figure 1.28 can be modelled using any kinetic modelling program, the work presented in this thesis was modelled using MUSICO, as described by Mijailovich et al (Mijailovich et al. 2017). This programme estimates rate transition constants by the Damped Least-Square method (or Levenberg-Marquardt inversion), as set out in (Mijailovich et al. 2010). The DLS method is based on the iterative minimisation of the mean-square error of the model predictions with respect to experimental observations. This was done by minimising the variance between the predicted steady-state ATPase rates over a range of actin concentrations, to simulate steady-state ATPase experiments. The model parameters are uniquely resolved, and the deviation of the model predictions from the experimental observations is represented by the mean-square error, which is an integral measure of the accuracy of the model-prediction fit to the observations. Minimization of the mean-square function provides the set of parameters that best fit the experimental data

using the iterative procedure. The programme also allows varying any one of the fitted parameters by  $\pm 20\%$  (the minimum precision of the transient kinetic measurements) to estimate the effects on the best fit values of the remaining parameters. This confirms the findings of the sensitivity matrix that the parameters are well defined by the fitting procedure. This will be discussed in more detail in Chapters 3 and 5.

## 2.5 *In vitro motility assay*

To measure the velocity of myosin along actin filaments, an *in vitro* motility assay was performed as described in (Adhikari et al. 2016; Aksel et al. 2015). To ensure no inactive myosin heads were present during the assay, a ten-fold molar excess of F-actin and 2 mM ATP was added to the S1, and incubated for 15 minutes at 4 °C. 50 mM MgCl<sub>2</sub> was added and incubated for a further 5 minutes. Actin and bound, inactive myosin heads were sedimented at 100,000 RPM for 15 minutes at 4 °C. The supernatant, containing active myosin heads, was collected and diluted in assay buffer to a final concentration of 1 μM. All reagents were dissolved in assay buffer containing 0.1 mg/ml bovine serum albumin (ABBSA), unless other stated.

All motility experiments were performed at 20 °C. Glass coverslips were coated with 0.2% nitrocellulose and air-dried before use. Reagents were sequentially flowed through the channels in the following order: 50 μL of 4 μM SNAP-PDZ18 incubated for 3 min; 100 μL of ABBSA to block the surface from nonspecific attachments and incubated for 3 min; 50 μL of 100 nM 8-residue (RGSIDTWV)-tagged S1 and incubated for 3 min; 100 μL of ABBSA to wash any unattached proteins; 50 μL of 30 nM rhodamine-phalloidin-labelled rabbit actin; 100 μL of an oxygen-scavenging system consisting of 5 mg/ml glucose, 0.1 mg/ml glucose oxydase and 0.02 mg/ml catalase; 50 μL 2 mM ATP. Actin filaments were detected using a widefield fluorescence imaging system (as described in Johnson et al (Johnson, East, and Mulvihill 2014)) with UAPON 100XOTIRF NA lens and QuantEM emCCD camera (Cairn, UK). The system was controlled and data analysed using Metamorph software.

### **3. The ATPase cycle of Human Muscle Myosin II isoforms: Adaptation of a single mechanochemical cycle for different physiological roles**

**Chloe A. Johnson**, Jonathan Walklate, Marina Svcevic, Srboljub M. Mijailovich, Carlos Vera, Anastasia Karabina, Leslie A. Leinwand, and Michael A. Geeves

Journal of Biological Chemistry, 2019. 294(39):14267-14278

#### **3.1 Context of research**

The data in this publication is a follow up study from two papers utilising the MUSICO modelling programme to study the ATP-dependent acto.myosin cross-bridge cycle. Mijailovich et al first described the programme, and used it to characterise contractile parameters for rabbit MyHC-IIa, human MyHC- $\alpha$  and MyHC- $\beta$ , and the MyHC- $\beta$  R453C HCM mutation using experimentally defined cross-bridge kinetics (Mijailovich et al. 2017). Ujfalusi et al used the same methodology to predict contractile properties of 5 DCM-causing and 2 HCM-causing mutations (Ujfalusi et al. 2018). They also extended the analysis to predict economy of ATP usage in these mutated motor proteins. Using newly acquired data on MyHC- $\beta$ -peri, and published data on 5 human class II isoforms (MyHC-IIa, MyHC-IIb, MyHC-IIc, MyHC-emb and MyHC-exoc), the same approach was used to investigate functional properties of human class II isoforms. The human MyHC- $\alpha$  and MyHC- $\beta$  was also re-examined to predict ATP economy. This research provides a comprehensive overview of characteristics of the fundamental ATPase cycle for 8 of the 9 striated class II myosins.

#### **3.2 Aims of research**

Muscle myosin II isoforms in mammals, including humans, are adapted for a variety of functions, which when expressed in a muscle fibre confers distinct contraction characteristics to each muscle fibre type. Combinations of different fibre types cooperate to produce contractile activity tuned to the functional demands on the muscle. The isoform of myosin expressed in a muscle fibre therefore plays a central role in determining the contractile properties of muscle fibres. However, the way in which each myosin is tuned for its specific function is not understood, so the aim of the research was to understand how

human sarcomeric myosins adapt their mechanochemical ATPase cycle to perform different functions within different muscle types. Whilst fibres of MyHC- $\beta$  and the skeletal isoforms have been well studied, experimental data on the MyHC-emb, MyHC-peri, MyHC-exoc and MyHC- $\alpha$  is limited. The MUSICO approach allowed experimentally defined solution data of these isoforms to be modelled to the ATPase cross-bridge cycle. This predicts the differences in the fraction of time spent in different occupancies of the cycle. These occupancies were then studied to predict the duty ratio and shortening velocities, ATP economy and load dependence. This analysis was completed for 8 human class II isoforms.

### ***3.3 Contribution to publication***

The initial design of the study arose from discussions between myself and my supervisor, Professor Michael Geeves. The study was initially intended to model the MyHC-emb data as a follow up study to the (Mijailovich et al. 2017) paper, but after I collated all published transient kinetic data on the MyHC-IIa, MyHC-IIb, MyHC-IIc, MyHC-emb and MyHC-exoc isoforms, the study was extended to include these isoforms. I performed kinetic modelling with MUSICO on all isoforms, and performed the analysis on ATP economy. Marina Svcevic and Dr Srboljub Mijailovich assisted me with the error analysis on the modelled data. Dr Jonathan Walklate performed transient kinetic analysis on the MyHC-peri isoform, which was provided by Dr Carlos Vera and Dr Anastasia Karabina from Professor Leslie Leinwand's laboratory. Professor Geeves and I wrote the first draft of the manuscript, which was reviewed by all authors.

### ***3.4 Publication*** - see below.



# The ATPase cycle of human muscle myosin II isoforms: Adaptation of a single mechanochemical cycle for different physiological roles

Received for publication, June 17, 2019, and in revised form, July 28, 2019. Published, Papers in Press, August 6, 2019, DOI 10.1074/jbc.RA119.009825

Chloe A. Johnson<sup>‡</sup>, Jonathan Walklate<sup>‡</sup>, Marina Svicevic<sup>§</sup>, Srboj M. Mijailovich<sup>¶</sup>, Carlos Vera<sup>||</sup>, Anastasia Karabina<sup>||</sup>, Leslie A. Leinwand<sup>||1</sup>, and Michael A. Geeves<sup>‡2</sup>

From the <sup>‡</sup>School of Biosciences, University of Kent, Canterbury CT2 7NJ, United Kingdom, the <sup>§</sup>Faculty of Science, University of Kragujevac, Kragujevac 34000, Serbia, the <sup>¶</sup>Department of Biology, Illinois Institute of Technology, Chicago, Illinois 60616, and the <sup>||</sup>BioFrontiers Institute and Department of Molecular, Cellular, and Developmental Biology, University of Colorado, Boulder, Colorado 80309

Edited by Enrique M. De La Cruz

Striated muscle myosins are encoded by a large gene family in all mammals, including humans. These isoforms define several of the key characteristics of the different striated muscle fiber types, including maximum shortening velocity. We have previously used recombinant isoforms of the motor domains of seven different human myosin isoforms to define the actin-myosin cross-bridge cycle in solution. Here, we present data on an eighth isoform, the perinatal, which has not previously been characterized. The perinatal is distinct from the embryonic isoform, appearing to have features in common with the adult fast-muscle isoforms, including weak affinity of ADP for actin-myosin and fast ADP release. We go on to use a recently developed modeling approach, MUSICO, to explore how well the experimentally defined cross-bridge cycles for each isoform in solution can predict the characteristics of muscle fiber contraction, including duty ratio, shortening velocity, ATP economy, and load dependence of these parameters. The work shows that the parameters of the cross-bridge cycle predict many of the major characteristics of each muscle fiber type and raises the question of what sequence changes are responsible for these characteristics.

Muscle myosin in all mammals consists of a variety of isoforms, each expressed from its own gene (see Table 1 and references therein). There are 10 such genes in the human genome and one pseudogene. All of the striated muscle myosin sequences are very highly conserved, but each has functional

differences, and these differences are required for normal muscle function because myosin isoform-specific null mice can have profound phenotypes (1). Further, disease-causing mutations in six of the 10 genes have been reported (2, 3). The expression of these genes is regulated temporally and spatially and can be affected by physical activity, animal species, and hormonal status. Each myosin isoform confers distinct contractile characteristics to each muscle fiber type (4, 5). These characteristics include maximum shortening velocity, rate of ATP usage, economy of ATP usage, and velocity at which power output is maximal. Other parameters, such as maximal force per cross-bridge or step size, are much less variable (4, 5). How each myosin is tuned for its specific function is not well understood. Also poorly understood is how changes in the amino acid sequence of each myosin bring about the functional changes. As a first step to understand how striated muscle myosin has evolved to have distinct physiological roles, we first needed to understand how the ATP driven cross-bridge cycle varies between the isoforms. Toward that end, we recently published a complete characterization of the kinetics of the ATPase cycle for the motor domains of six adult human muscle myosin isoforms and the embryonic isoform (6–8) (see Table 1). Here, we extend this data set to include the first study of the human perinatal myosin isoform. We show here that the perinatal isoform is quite distinct from the embryonic form and has more in common with adult fast-muscle isoforms.

With this large set of isoform data, it is possible to examine the extent to which differences in the ATPase cycle for each isoform can predict the differences in mechanochemical properties of muscle fibers expressing them. Here, we use the recently developed MUSICO modeling approach (9, 10) to predict the contraction characteristics of each muscle fiber type and compare the predictions with published data for single muscle fibers expressing single myosin isoforms.

Using MUSICO, we recently reexamined the actin myosin-S1 ATPase cycle of fast rabbit muscle using both fast kinetic methods and steady-state ATPase assays to establish the primary parameters of an eight-step actin-myosin cross-bridge cycle (Fig. 1) (9). These parameters were then used with the addition of the overall ATPase parameters for the cycle, the  $k_{cat}$  (or  $V_{max}$ ), and  $K_{app}$  (concentration of actin needed for half-

This work was supported by National Institutes of Health Grants GM29090 (to L. A. L.) and HL117138 (to L. A. L.) and European Union Horizon 2020 Research and Innovation Programme under Grant agreement No. 777204, SILICOFEM (to M. A. G., J. W., and S. M. M.). This article reflects only the author's view. The European Commission is not responsible for any use that may be made of the information it contains. L. A. L. owns stock in MyoKardia, Inc and has received research funding from the company. The authors declare that they have no conflicts of interest with the contents of this article.

This article contains Tables S1–S5 and Figs. S1–S5.

<sup>1</sup> To whom correspondence may be addressed: BioFrontiers Institute and Dept. of Molecular, Cellular, and Developmental Biology, University of Colorado, Boulder, CO 80309. E-mail: leslie.leinwand@colorado.edu.

<sup>2</sup> To whom correspondence may be addressed: School of Biosciences, University of Kent, Canterbury CT2 7NJ, United Kingdom. Tel.: 44-1227827597; E-mail: m.a.geeves@kent.ac.uk.

## Human muscle myosin isoforms

**Table 1**  
Summary of isoforms

| Isoform                                    | Human gene   | Human tissue expression <sup>a</sup>    | Maximum shortening velocity in muscle fiber <sup>b</sup> | Light chains <sup>c</sup> | Expression tags on heavy chain |
|--|--------------|---|--|---------------------------|--------------------------------|
| $\alpha$ -Cardiac ( $\alpha$ )             | <i>MYH6</i>  | Atrial myocardium                       | 0.330 $\pm$ 0.022  | Endogenous mouse          | His <sub>6</sub>               |
| $\beta$ -Cardiac/slow muscle I ( $\beta$ ) | <i>MYH7</i>  | Ventricular myocardium/slow skeletal    |  | Human MYL3                | His <sub>6</sub> on MYL3       |
| Embryonic (Emb)                            | <i>MYH3</i>  | Fetal skeletal and regenerating muscles |  | Endogenous mouse          | His <sub>6</sub>               |
| Perinatal (Peri)                           | <i>MYH8</i>  | Fetal skeletal and regenerating muscles | 1.401 $\pm$ 0.101  | Endogenous mouse          | His <sub>6</sub>               |
| Extraocular (Exoc)                         | <i>MYH13</i> | Extraocular and laryngeal muscles       |  | None                      | e-GFP, His <sub>6</sub>        |
| Ila  | <i>MYH2</i>  | Fast skeletal                           |  | Endogenous mouse          | e-GFP, His <sub>6</sub>        |
| Ilb  | <i>MYH4</i>  | Not expressed                           | 3.022 $\pm$ 0.935  | Endogenous mouse          | e-GFP, His <sub>6</sub>        |
| Ild  | <i>MYH1</i>  | Fast skeletal                           |  | Endogenous mouse          | e-GFP, His <sub>6</sub>        |

<sup>a</sup> Ref. 39.

<sup>b</sup> Ref. 14.

<sup>c</sup> Endogenous mouse light chains are a combination of MLC1A, MLC3F, MLC1F, and MLC2F.

maximum ATPase rates) to model the complete cycle in solution. This allowed the occupancy of each state of the cycle to be predicted as a function of actin concentration. The occupancies calculated were then used to predict the duty ratio (DR;<sup>3</sup> the proportion of the cycle myosin bound to actin), the expected maximal velocity of contraction ( $V_0$ , in a motility assay or muscle sarcomere shortening) as a function of actin concentration, and the effect of a 5-pN load on state occupancies for a single motor. To test this approach, we compared the information obtained for rabbit fast-muscle myosin with two human cardiac myosin isoforms ( $\alpha$  and  $\beta$ ) that we had characterized previously (6). These illustrated how the cycle was altered to define myosins with different velocities and different sensitivities to load. Whereas the duty ratio was largely unchanged among isoforms, the ATPase cycling rates and predicted velocities were altered in line with published experimental data. The effect of load reduced the predicted velocities and ATPase rates but to differing extents. Here, we have added in predictions about the economy of ATP usage during rapid shortening and while holding a 5-pN load.

In the current study, the analysis described above has been extended to four additional adult, fast-skeletal, human isoforms (Ila, Ilb, Ild, and extraocular (ExOc)) together with two developmental isoforms: embryonic (Emb) and perinatal (Peri) myosins. The analysis reveals that the relative velocities predicted for the isoforms vary widely (9-fold). Duty ratios vary over a narrow 2-fold range, whereas the economy of ATP usage varies 4–5-fold. Experimental data for these values are only available for a limited number of isoforms but, where available, are compatible with our predictions. The extent to which these ATPase cycle studies can predict the properties of contracting muscle for both the well-defined and unstudied isoforms (e.g. ExOc and Peri) is discussed.

### Results and discussion

We have modeled, using MUSICO, the complete ATPase cycle for all isoforms listed in Table 1. The modeling used the previously published values for the rate and equilibrium constants (Table S1) that have defined the cycle shown in Fig. 1. The best-fit parameters are listed in Table 2. In all cases, the measured constants were defined with a precision of at least  $\pm 20\%$ . The limitations of this precision on the modeling will be

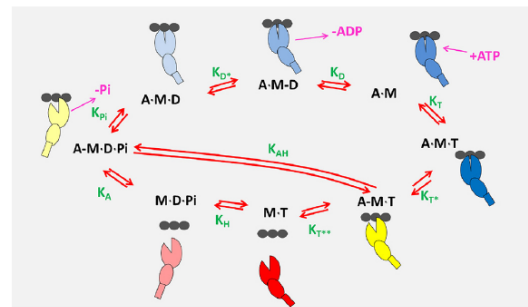


**Figure 1. ATP-driven actomyosin cross-bridge cycle.** The black circles represent an actin filament composed of three actin monomers. Myosin is shown as two ellipses and a rod; the larger ellipse represents the upper and lower 50 k domains, the smaller ellipse and rod representing the converter domain, lever arm, and light-chain binding region. Myosin in a strongly attached, force-holding state is represented in blue, weakly attached in yellow, and detached in red shades. Green characters are the equilibrium constants for each step defined in the direction of ATP hydrolysis (clockwise).

considered below, but in general, varying any of the parameters by  $\pm 20\%$  has a limited effect on the cycle, in most cases altering the occupancy of each state by much less than 20%. One new set of experimental data is presented here, that for the Peri isoform. Data collection was identical to that presented for all other isoforms, with the measured parameters listed in Table S1 and the predicted occupancies in Table S2.

Using a combination of best-fit and measured values for the cycle, the occupancy of each state in the cycle was calculated at three different actin concentrations:  $[\text{actin}] = K_{\text{app}}$  (the actin concentration required for 50% of the  $V_{\text{max}}$  of the ATPase) and  $[\text{actin}] = 3K_{\text{app}}$  and  $20K_{\text{app}}$  (actin concentration required for 75 and 95% of  $V_{\text{max}}$ , respectively). A range of actin concentrations was chosen because it is not known what the appropriate actin concentration is in muscle fibers. Fig. 2 presents the calculated occupancies for each state in the cycle as pie charts for each isoform. The color scheme of the pie charts matches that of the ATPase cycle states shown in Fig. 1, where red shades represent detached states, yellow shades represent weakly attached states, and blue shades represent strongly attached states.

### $\alpha$ - and $\beta$ -cardiac isoforms

For  $\beta$ -cardiac myosin, at low actin concentrations ( $[\text{actin}] = K_{\text{app}}$ ), the detached state M·D·P<sub>i</sub> predominated (pale red shade;  $\sim 45\text{--}50\%$ ), with similar amounts of the detached M·T and the

<sup>3</sup> The abbreviations used are: DR, duty ratio; pN, piconewton(s); ExOc, extraocular; Emb, embryonic; Peri, perinatal.

**Table 2****Fitted rate and equilibrium constants of the ATPase cycle**

Constants are highlighted to show which are fitted (blue), which are measured (red), and which are derived from assumption (black on yellow background) or detailed balance (purple on yellow background). Buffer conditions are as follows: 25 mM KCl, 20 mM MOPS, 5 mM MgCl<sub>2</sub>, and 1 mM NaN<sub>3</sub>. Note that  $k_D$  values in red were measured with an ADP displacement with excess ATP assay. For the other isoforms that have a low affinity of ADP for actin-S1, the ADP release rate will be faster than the maximal rate of ATP-induced actin-S1 dissociation and therefore too fast to be measured by ADP displacement.

**A. Equilibrium Constants**

|              | Units              | <i><math>\alpha</math>-S1</i> | <i><math>\beta</math>-S1</i> | <i>Emb</i> | <i>Peri</i> | <i>ExOc</i> | <i>Ila</i> | <i>Ilb</i> | <i>Ild</i> |
|--------------|--------------------|-------------------------------|------------------------------|------------|-------------|-------------|------------|------------|------------|
| $K_{app}$    | $\mu\text{M}$      | 67.8                          | 39.55                        | 39         | 20.6        | 18.6        | 22.5       | 7          | 7.9        |
| $k_{cat}$    | $\text{s}^{-1}$    | 18                            | 5.94                         | 7          | 29.9        | 29.6        | 26.4       | 43.1       | 32.9       |
| $K_A$        | $\mu\text{M}^{-1}$ | 0.011                         | 0.0107                       | 0.0164     | 0.0241      | 0.035       | 0.0293     | 0.0874     | 0.0913     |
| $K_{pi}$     | mM                 | 100                           | 100                          | 100        | 100         | 100         | 100        | 100        | 100        |
| $K_{D^*}$    |                    | 50                            | 0.167                        | 0.2        | 50          | 50          | 50         | 50         | 50         |
| $K_D$        | $\mu\text{M}$      | 197                           | 36                           | 71.43      | 100         | 100         | 100        | 100        | 100        |
| $K_T$        | $\mu\text{M}^{-1}$ | 0.004                         | 0.003                        | 0.0119     | 0.0068      | 0.00834     | 0.0045     | 0.0042     | 0.005      |
| $K_{T^*}$    |                    | 150                           | 154                          | 77.7       | 85.6        | 138         | 135        | 146        | 122.8      |
| $K_{T^{**}}$ | $\mu\text{M}$      | 1000                          | 1000                         | 1000       | 1000        | 1000        | 1000       | 1000       | 1000       |
| $K_H$        |                    | 4.1                           | 8.9                          | 6.3        | 16.6        | 35.7        | 23.2       | 29.2       | 31.3       |
| $K_{AH}$     |                    | 52.76                         | 63.145                       | 43.6       | 34          | 55          | 47.5       | 30         | 32.5       |

**B. Forward Rate Constants**

|              | Units                           | <i><math>\alpha</math>-S1</i> | <i><math>\beta</math>-S1</i> | <i>Emb</i> | <i>Peri</i> | <i>ExOc</i> | <i>Ila</i> | <i>Ilb</i> | <i>Ild</i> |
|--------------|---------------------------------|-------------------------------|------------------------------|------------|-------------|-------------|------------|------------|------------|
| $k_A$        | $\mu\text{M}^{-1}\text{s}^{-1}$ | 10.68                         | 10.75                        | 16.4       | 24.1        | 3.51        | 2.93       | 8.47       | 9.13       |
| $k_{Pi}$     | $\text{s}^{-1}$                 | 32.14                         | 15.95                        | 13.1       | 69.2        | 50.1        | 44.5       | 86         | 52.3       |
| $k_{D^*}$    | $\text{s}^{-1}$                 | 100                           | 59                           | 22         | 700         | 400         | 400        | 1000       | 1000       |
| $k_D$        | $\text{s}^{-1}$                 | 1970                          | 1000                         | 1000       | 1000        | 1000        | 1000       | 1000       | 1000       |
| $k_T$        | $\mu\text{M}^{-1}\text{s}^{-1}$ | 27.6                          | 10.05                        | 10.13      | 10.67       | 10.27       | 10.37      | 10.1       | 10.9       |
| $k_{T^*}$    | $\text{s}^{-1}$                 | 1800                          | 1543                         | 777        | 856         | 1380        | 1350       | 1460       | 1228       |
| $k_{T^{**}}$ | $\text{s}^{-1}$                 | 1000                          | 1000                         | 1000       | 1000        | 1000        | 1000       | 1000       | 1000       |
| $k_H$        | $\text{s}^{-1}$                 | 77.2                          | 12.5                         | 82.4       | 66.6        | 107.2       | 92.8       | 116.7      | 125.2      |
| $k_{AH}$     | $\text{s}^{-1}$                 | 79.1                          | 12.6                         | 87.2       | 68          | 110         | 95         | 120        | 130        |

**C. Backward Rate Constants**

|               | Units                           | <i><math>\alpha</math>-S1</i> | <i><math>\beta</math>-S1</i> | <i>Emb</i> | <i>Peri</i> | <i>ExOc</i> | <i>Ila</i> | <i>Ilb</i> | <i>Ild</i> |
|---------------|---------------------------------|-------------------------------|------------------------------|------------|-------------|-------------|------------|------------|------------|
| $k_{-A}$      | $\text{s}^{-1}$                 | 1000                          | 1000                         | 1000       | 1000        | 1000        | 1000       | 1000       | 1000       |
| $k_{-Pi}$     | $\text{mM}^{-1}\text{s}^{-1}$   | 0.321                         | 0.159                        | 0.13       | 0.692       | 0.501       | 0.445      | 0.86       | 0.523      |
| $k_{-D^*}$    | $\text{s}^{-1}$                 | 2                             | 354                          | 110        | 14          | 8           | 8          | 20         | 20         |
| $k_{-D}$      | $\mu\text{M}^{-1}\text{s}^{-1}$ | 10                            | 27.8                         | 14         | 10          | 10          | 10         | 10         | 10         |
| $k_{-T}$      | $\text{s}^{-1}$                 | 6597                          | 3349                         | 851.5      | 1569.2      | 1230.9      | 2304.4     | 2396.6     | 2179.3     |
| $k_{-T^*}$    | $\text{s}^{-1}$                 | 12                            | 10                           | 10         | 10          | 10          | 10         | 10         | 10         |
| $k_{-T^{**}}$ | $\mu\text{M}^{-1}\text{s}^{-1}$ | 1                             | 1                            | 1          | 1           | 1           | 1          | 1          | 1          |
| $k_{-H}$      | $\text{s}^{-1}$                 | 19                            | 1.4                          | 13         | 4           | 3           | 4          | 4          | 4          |
| $k_{-AH}$     | $\text{s}^{-1}$                 | 1.5                           | 0.2                          | 2          | 2           | 2           | 2          | 4          | 4          |



## Human muscle myosin isoforms

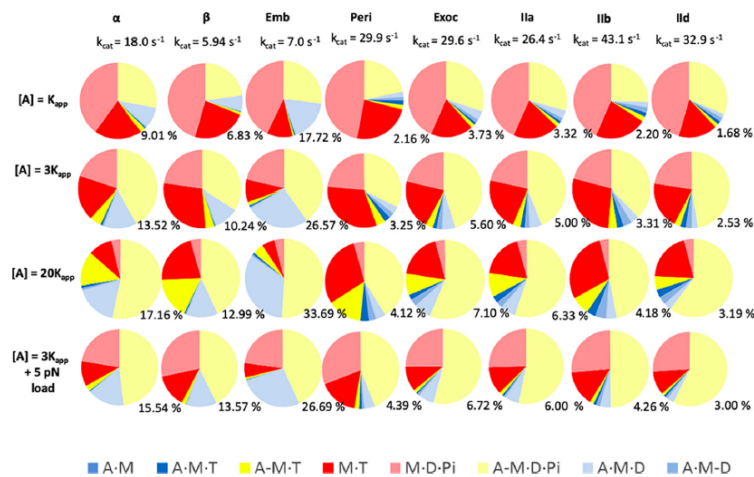


**Figure 2. Fractional occupancies of each state in the ATPase at three different actin concentrations,  $[A] = K_{app}$ ,  $3K_{app}$ , and  $20K_{app}$ , for each isoform and at  $[A] = 3K_{app}$  plus 5-pN load. Colors of the pie chart match those of Fig. 1. The percentage value next to each chart gives the percentage of each cycle spent as the force-holding A-M-D state.**

weakly attached A-M-D-P<sub>i</sub> state (each ~25%). Only 6.8% of the myosin is strongly attached as A-M-D, the predominant force-holding state. All other species in the cycle have very low occupancy in the steady state. As actin concentration increased (to  $3K_{app}/75\% V_{max}$  and  $20K_{app}/95\% V_{max}$ ), the total occupancy of the detached states fell to ~50% and then 25%, and the weakly attached A-M-ATP and A-M-D-P<sub>i</sub> increased from <25 to 35% and then >50% as expected. The strongly attached force-holding states are dominated by the pale blue A-M-D state, which increased from 6.8% at low actin concentrations to 10 and 13.0% as the actin concentration approached saturation. Thus, the DR is dominated by A-M-D and lies between 0.07 and 0.14, depending upon the actin concentration, at the zero load experienced in these solution assays. A similar pattern was observed for the human  $\alpha$ -myosin except for a slightly higher level of the A-M-D state, between 9.0 and 17.6%, depending upon the actin concentration and a DR of 0.1 to 0.19.

Table 2 and Fig. 2 list the measured  $k_{cat}$  values (ATPase cycling rates) for the  $\alpha$ - and  $\beta$ -isoforms. Despite quite similar occupancies of the intermediates in the cycle, the cycling rates are very different;  $\alpha$ -cardiac turns over ATP almost 3 times faster than  $\beta$ -cardiac. The predicted velocities were 2.25-fold faster for the  $\alpha$ - versus the  $\beta$ -isoform (Fig. 3 and Table 3), which is similar to measured values (11). This calculation assumes an average 5-nm step for both. This result has implications for the economy of ATP usage, which will be discussed below (see Fig. 5).

Single-molecule laser trap assays have provided estimates of the load dependence of the ADP release rate constant ( $k_{D^-}$ ) for human  $\beta$ -myosin and indicate that this rate constant slows down by a factor of ~3 for a load of 5 pN (see “Materials and methods” (12, 13)). We argued that a similar load dependence is expected on the force-generating step/P<sub>i</sub> release step ( $k_{P_i}$  in Fig. 1), and for the values used in the cycle, a 3-fold reduction in  $k_{P_i}$  is required to slow the ATPase cycling rate under load, as has

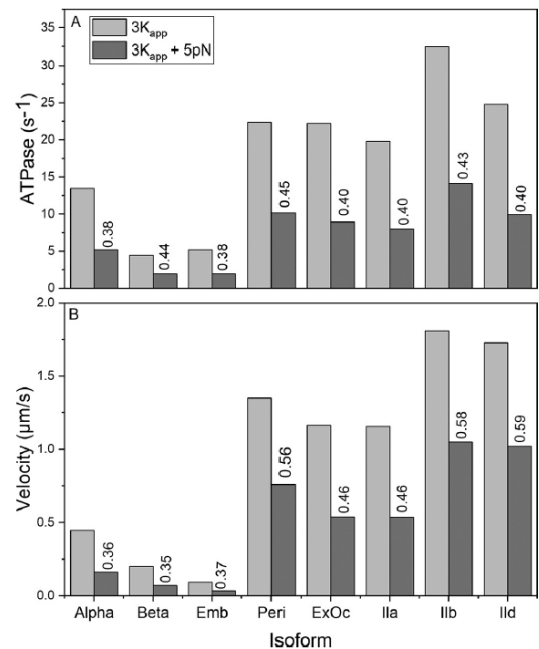


**Figure 3. Plots of the estimated ATPase and  $V_0$  values at  $[actin] = 3K_{app}$  and the effect of a 5-pN load. The numbers give the loaded value as a fraction of the unloaded value.**

been reported for contracting muscle fibers (14, 15). Slowing both rate constants ( $k_{P_i}$  and  $k_{D^-}$ ) down by a factor of 3 allows us to explore how the cycle would change under a 5-pN load, approaching the load that might be expected during isometric contraction of a fiber. The results are illustrated in the *last row* of the pie charts in Fig. 2 for an actin concentration of  $3K_{app}$ ,

**Table 3**

Predicted cross-bridge cycle parameters at three actin concentrations from the modeled ATPase cycle  
Buffer conditions were as for Table 2.

| Isoform     | [Actin]                         | ATPase          | Detached | Weakly attached | Strongly attached | Duty ratio | Velocity             |
|-------------|---------------------------------|-----------------|----------|-----------------|-------------------|------------|----------------------|
|             | $\mu\text{M}$                   | $\text{s}^{-1}$ |          |                 |                   |            | $\mu\text{m s}^{-1}$ |
| $\alpha$    | $K_{\text{app}} = 67.8$         | 9.00            | 0.60     | 0.30            | 0.10              | 0.10       | 0.45                 |
|             | $3K_{\text{app}} = 203.4$       | 13.50           | 0.38     | 0.47            | 0.15              | 0.15       | 0.45                 |
|             | $20K_{\text{app}} = 1356$       | 17.14           | 0.14     | 0.67            | 0.19              | 0.19       | 0.45                 |
| $\beta$     | $3K_{\text{app}} + \text{load}$ | 5.27            | 0.33     | 0.51            | 0.16              | 0.16       | 0.16                 |
|             | $K_{\text{app}} = 39.55$        | 2.97            | 0.73     | 0.20            | 0.073             | 0.073      | 0.20                 |
|             | $3K_{\text{app}} = 75$          | 4.46            | 0.57     | 0.32            | 0.11              | 0.11       | 0.20                 |
| Embryonic   | $20K_{\text{app}} = 500$        | 5.66            | 0.30     | 0.56            | 0.14              | 0.14       | 0.20                 |
|             | $3K_{\text{app}} + \text{load}$ | 1.97            | 0.47     | 0.39            | 0.14              | 0.14       | 0.071                |
|             | $K_{\text{app}} = 39$           | 3.51            | 0.54     | 0.28            | 0.19              | 0.19       | 0.095                |
| Perinatal   | $3K_{\text{app}} = 117$         | 5.27            | 0.30     | 0.42            | 0.28              | 0.28       | 0.095                |
|             | $20K_{\text{app}} = 780$        | 6.68            | 0.093    | 0.55            | 0.35              | 0.35       | 0.095                |
|             | $3K_{\text{app}} + \text{load}$ | 1.89            | 0.29     | 0.44            | 0.27              | 0.27       | 0.035                |
| Extraocular | $K_{\text{app}} = 20.6$         | 14.92           | 0.71     | 0.23            | 0.055             | 0.055      | 1.36                 |
|             | $3K_{\text{app}} = 61.8$        | 22.41           | 0.55     | 0.36            | 0.083             | 0.083      | 1.35                 |
|             | $20K_{\text{app}} = 412$        | 28.44           | 0.34     | 0.55            | 0.11              | 0.11       | 1.34                 |
| IIa         | $3K_{\text{app}} + \text{load}$ | 10.19           | 0.47     | 0.46            | 0.067             | 0.067      | 0.76                 |
|             | $K_{\text{app}} = 18.6$         | 14.82           | 0.62     | 0.312           | 0.064             | 0.064      | 1.17                 |
|             | $3K_{\text{app}} = 55.8$        | 22.24           | 0.43     | 0.47            | 0.095             | 0.095      | 1.17                 |
| IIb         | $20K_{\text{app}} = 372$        | 28.16           | 0.23     | 0.65            | 0.12              | 0.12       | 1.16                 |
|             | $3K_{\text{app}} + \text{load}$ | 8.94            | 0.37     | 0.55            | 0.083             | 0.083      | 0.54                 |
|             | $K_{\text{app}} = 22.5$         | 13.21           | 0.63     | 0.31            | 0.057             | 0.057      | 1.16                 |
| IIc         | $3K_{\text{app}} = 67.5$        | 19.82           | 0.44     | 0.48            | 0.086             | 0.086      | 1.16                 |
|             | $20K_{\text{app}} = 450$        | 25.11           | 0.23     | 0.66            | 0.11              | 0.11       | 1.15                 |
|             | $3K_{\text{app}} + \text{load}$ | 7.98            | 0.37     | 0.55            | 0.074             | 0.074      | 0.54                 |
| IId         | $K_{\text{app}} = 7$            | 21.59           | 0.67     | 0.27            | 0.060             | 0.060      | 1.81                 |
|             | $3K_{\text{app}} = 21$          | 32.47           | 0.5      | 0.41            | 0.090             | 0.090      | 1.81                 |
|             | $20K_{\text{app}} = 140$        | 41.0            | 0.34     | 0.55            | 0.11              | 0.11       | 1.80                 |
| IId         | $3K_{\text{app}} + \text{load}$ | 14.12           | 0.42     | 0.51            | 0.067             | 0.067      | 1.049                |
|             | $K_{\text{app}} = 8$            | 16.47           | 0.62     | 0.33            | 0.048             | 0.048      | 1.73                 |
|             | $3K_{\text{app}} = 24$          | 24.77           | 0.42     | 0.50            | 0.072             | 0.072      | 1.73                 |
| IId         | $20K_{\text{app}} = 160$        | 31.27           | 0.25     | 0.66            | 0.091             | 0.091      | 1.72                 |
|             | $3K_{\text{app}} + \text{load}$ | 9.93            | 0.37     | 0.58            | 0.049             | 0.049      | 1.02                 |

and the predicted effect on the ATPase rates and velocity of shortening are illustrated in Fig. 3. There is no measurement of the load dependence of ADP release for any isoform other than  $\beta$ -cardiac. For the purposes of illustration throughout, we assume a similar load dependence for all isoforms to understand how a load may influence the cycle differently based on the observed differences in the cycle rate constants. The data for the effect of load on the state occupancy, the ATPase rate, and the velocity are presented in Figs. 2 and 3 and Table 3. For both  $\alpha$  and  $\beta$ , the ATPase cycling rates were reduced by approximately a factor of 3, whereas the occupancy of the A·M·D state increased from 10.2 to 13.6% for human  $\beta$  and 13.5 to 15.5% for  $\alpha$ . This implies that for an ensemble of myosins (in a thick filament or sarcomere), the  $\alpha$ -myosin would maintain a higher occupancy of the force-holding states. Note, however, for  $\beta$ -myosin, the occupancy of A·M·D increases by one-third under load, whereas for  $\alpha$ -myosin, the occupancy increases by only about one-seventh.

#### Embryonic isoform

The complete experimental data set for the human Emb isoform was published in 2016 (8), and the published data are reproduced in Table S1. The results of the modeling are presented in Figs. 2–4 in the same format as for the  $\alpha$ - and  $\beta$ -isoforms for ease of comparison.

What is immediately striking in the Emb data set is that, although the  $k_{\text{cat}}$  values for the Emb isoform and  $\beta$ -isoform are similar (7.0 and 5.9  $\text{s}^{-1}$ , respectively), there are marked differences in the occupancy of the force-holding A·M·D state (*pale*

*blue*; Fig. 1). Whereas the detached M·D·P<sub>i</sub> (*pale red*) and A·M·D·P<sub>i</sub> (*pale yellow*) appear similar for  $\beta$  and Emb, the detached M·T (*red*) state was much smaller and the A·M·D state (*pale blue*) was much larger for Emb than for  $\beta$  (e.g. A·M·D = 26.5% for Emb versus 10.24% at [actin] =  $3K_{\text{app}}$ ). This difference was less marked when compared with the  $\alpha$ -isoform. This large difference in A·M·D occupancy and duty ratio are brought about through differences in the contribution of three steps to the overall cycling speed ( $k_{\text{cat}}$ ): the hydrolysis step  $k_{\text{H}}$ , the phosphate release step  $k_{\text{Pi}}$ , and the ADP release step  $k_{\text{D}}$ . For  $\beta$ -myosin,  $k_{\text{H}}$  and  $k_{\text{Pi}}$  are comparable at 2–3-fold  $k_{\text{cat}}$ , whereas  $k_{\text{D}}$  is 10-fold larger than  $k_{\text{cat}}$  (see Table 4). Thus, as seen in Fig. 2 for the  $\beta$ -isoform at high actin concentration ([actin] =  $20K_{\text{app}}$ ), the predominant states are the ATP states M·T and A·M·T (together 45%), the weakly bound A·M·D·P<sub>i</sub> (35%), and A·M·D (12.9%). In the case of Emb,  $k_{\text{cat}}$  is similar to that of  $\beta$ , but the balance of the cycle is quite different:  $k_{\text{H}}$  is  $10k_{\text{cat}}$  and  $k_{\text{Pi}}$  and  $k_{\text{D}}$  are now comparable at 2–3-fold  $k_{\text{cat}}$ . Thus, the ATP states M·T and A·M·T are much smaller than  $k_{\text{D}}$ , whereas the A·M·D·P<sub>i</sub> (51%) and A·M·D (33%) states predominate, and thus a much larger DR is observed for Emb myosin.

The higher occupancy of the force-holding A·M·D state implies that the Emb isoform would be much better at holding loads than either of the two cardiac isoforms discussed so far. Assuming a similar load-holding capacity for each cross-bridge independent of the isoform, then there are almost twice as many cross-bridges present in the steady-state for Emb myosin, which suggests that a fiber expressing Emb myosin would need

## Human muscle myosin isoforms

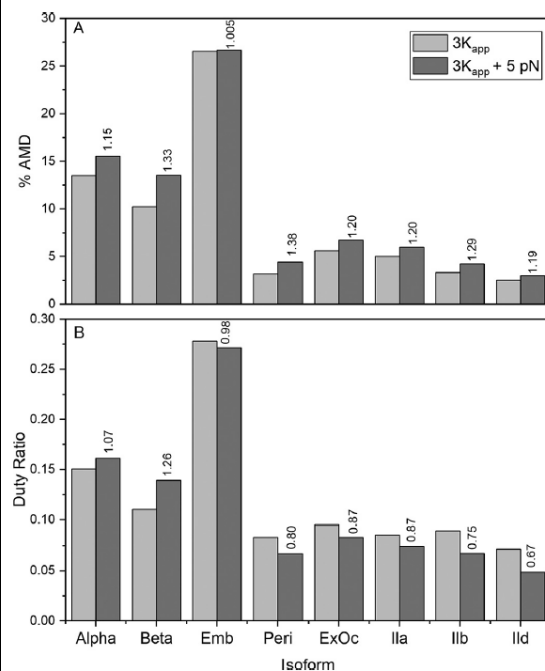


**Figure 4.** The estimated value of the duty ratio and the occupancy of the main force-holding state A·M·D at [actin] = 3K<sub>app</sub> and the effect of a 5-pN load. The numbers with each isoform give the 5-pN loaded value as a fraction of the unloaded value.

**Table 4**

### Balance of significant rate constants around the ATPase cycle

Note that the slowest step (gray background) is, in each case, ~2 times the  $k_{cat}$  value. If this step is largely irreversible (true for  $k_{pi}$ , not always true for  $k_{D-}$ ), then ~50% of the myosin will occupy the state before this slow step ( $k_{cat} = \theta \cdot k$ , where  $\theta$  is the fractional occupancy of that state and  $k$  is the rate constant for the breakdown of that state. The second slowest step in all cases (yellow background) is ~3–4 times  $k_{cat}$ , and because  $\theta = k_{cat}/k$  then  $\theta \sim 0.25$ . The third slowest step in each case (blue background) is ~10 times  $k_{cat}$ , so the occupancy of the relevant state will be approximately 0.1.

| Isoform  | $k_{cat}$ | $k_{pi}/k_{cat}$ | $k_{D-}/k_{cat}$ | $k_{H}/k_{cat}$ |
|----------|-----------|------------------|------------------|-----------------|
| $\alpha$ | 18.00     | 1.78             | 5.56             | 4.28            |
| $\beta$  | 6.00      | 2.67             | 9.83             | 2.07            |
| Emb      | 7.00      | 1.87             | 3.14             | 11.71           |
| Peri     | 29.90     | 2.31             | 23.4             | 2.23            |
| Exoc     | 29.60     | 1.69             | 13.51            | 3.72            |
| Ila      | 26.40     | 1.74             | 15.13            | 3.60            |
| Ilb      | 43.10     | 2.09             | 23.20            | 2.78            |
| Ild      | 32.40     | 1.64             | 30.86            | 4.01            |

to activate half the number of cross-bridges (per sarcomere or per thick filament) to hold the same load as a fiber expressing  $\beta$ -myosin. At the whole-fiber or whole-muscle level, the differences in the packing of the filaments would need to be considered.

In contrast to  $\beta$  or  $\alpha$ , the presence of a 5-pN load on Emb has almost no effect on the occupancy of the force-holding A·M·D state or the duty ratio. This was unexpected, but a closer examination of the effect of load suggests that because  $k_{D-}$  and  $k_{pi}$  are both similar and dominate the ATPase cycling rate, when both are reduced to a similar extent by load, ATPase cycling is

reduced by a factor of 3, but the balance of states around the cycle does not change significantly.

### Perinatal isoform

Like Emb, Peri is found in developing and regenerating muscle (2, 16). No biochemical kinetic study of this isoform has been published. Using the C2C12 expression system, we have expressed the motor domain and completed a kinetic analysis as described previously for the other isoforms. Details of the measurements are given in Figs. S1–S4. The measured values for the steps in the ATPase cycle are listed in Table S1. The data do show distinct differences compared with the both the cardiac and Emb isoforms discussed so far.

As the Peri and Emb myosins are both developmental isoforms, a comparison between these is drawn here. A full comparison can be seen in Table S1. In the absence of actin, the Peri S1 had an almost 3-fold slower second-order rate constant of ATP binding to S1 compared with the Emb isoform ( $4.5 \mu\text{M}^{-1} \text{s}^{-1}$  versus  $12.5 \mu\text{M}^{-1} \text{s}^{-1}$ ). The maximum rate of ATP binding ( $k_H + k_{-H}$ ) is almost 50% slower for the Peri than for the Emb ( $68.7 \text{s}^{-1}$  versus  $130 \text{s}^{-1}$ ). This is assumed to measure the ATP hydrolysis step. The Peri actin·S1 had a maximum rate of dissociation ( $k_{+T}$ ) of  $856 \text{s}^{-1}$  and is similar to the Emb S1 ( $777 \text{s}^{-1}$ ). However, the ATP binding affinity ( $K_T$ ), and hence the second-order rate constant ( $K_T k_{+T}$ ), was almost 2-fold tighter than that of Emb ( $146.5 \mu\text{M}$  versus  $84.3 \mu\text{M}$  Peri and Emb, respectively). The crucial difference between the two developmental isoforms is the ADP release rate ( $k_{+D}$ ), which is considerably faster ( $>700 \text{s}^{-1}$ ) than the Emb isoform ( $22 \text{s}^{-1}$ ). A slow ADP release rate is indicative of a slow-type isoform, such as  $\beta$  and Emb, whereas the Peri is more like the fast skeletal isoforms ( $\alpha$ , Ila, Ilb, Ild, and ExOc). However, as shown in Fig. S2, the rate constant for ADP release ( $k_D = 700 \text{s}^{-1}$ ) is only marginally slower than the maximum rate of actin dissociation by ATP ( $k_{T-} = 856 \text{s}^{-1}$ ). We have assigned this to  $k_{D-}$ , but it could equally be assigned to  $k_D$ .

The ATPase of the Peri isoform is much faster than Emb, with a  $k_{cat}$  of almost  $30 \text{s}^{-1}$ , and the rapid release of ADP from A·M·D suggests a fast-type myosin (17). The results of the modeling are shown in Figs. 2–4.

Modeling the cycle shows a similar pattern to the  $\alpha$ - and  $\beta$ -myosins but with some key differences. The occupancy of the force-holding, pale blue, A·M·D state (pale blue) is much smaller for Peri (~4.1% at [A] =  $20K_{app}$ ) compared with  $\alpha$  (17%) or  $\beta$  (13%), resulting in a smaller DR (0.11) than for  $\beta$  (0.14). The difference in DR could be considered small, but examination of the pie charts in Fig. 2 shows a redistribution among the strongly attached states with the presence of significant amounts of the strongly attached states, A·M·D (~2.8%) and A·M·T (~3.5%) in addition to A·M·D. The presence of other strongly attached states appears to be a feature of the fast-type myosins and will be discussed further when the fast adult myosins are considered.

Similar to the result for the Emb isoform, the change in occupancy observed here for Peri is the result of changes in the balance between  $k_{pi}$ ,  $k_{D-}$ , and  $k_H$  and their contributions to  $k_{cat}$ . Whereas the rate of the hydrolysis step, controlled by  $k_H$ , is much faster for Peri at  $68.7 \text{s}^{-1}$  than for  $\beta$  ( $13.9 \text{s}^{-1}$ ), it is only

twice the value of  $k_{\text{cat}}$ . This means that the M·T and A·M·T states dominate at all actin concentrations considered, even more than is the case for  $\beta$ -myosin.

The estimate of velocity for this isoform is  $1.35 \mu\text{m}\cdot\text{s}^{-1}$ , much faster than for  $\alpha$  ( $0.45 \mu\text{m}\cdot\text{s}^{-1}$ ) or  $\beta$  ( $0.2 \mu\text{m}\cdot\text{s}^{-1}$ ). But this depends upon the assignment of  $k_{\text{D}}$  to  $700 \text{ s}^{-1}$ . If instead this is  $k_{\text{D}}$ , then there would be a missing value of  $k_{\text{D}}$ , which could be much lower than  $700 \text{ s}^{-1}$  and result in a much lower velocity.

#### Fast skeletal isoforms

The adult fast skeletal isoforms, IIa, IIb, and IIc, form a closely related group of myosins, and in humans they have ~92% sequence identity in the motor domain (18). The ExOc is also believed to be a fast-muscle isoform based on contractile velocity of extraocular and pharyngeal muscles (19, 20). However, because it is only found in specialized muscle fibers expressing multiple isoforms, little is known about its biochemical and mechanical properties. It is ~85% identical to the adult fast isoforms. The experimental data for these four isoforms were published in two papers. Resnicow *et al.* (21) published the first ever data on a set of recombinant human isoforms, and Bloemink *et al.* (7) followed this with a more detailed biochemical kinetic study of the same isoforms. The data in Table S1 are a summary of these studies.

Notably, like many larger mammals, humans have not been found to express any IIb protein, although the gene is intact and theoretically capable of expressing protein. The IIb we characterized is thus the only human IIb to have been studied. The fact that its properties appear similar to IIa and IIc suggests that the gene has not degenerated significantly, despite not being expressed.

The  $k_{\text{cat}}$  values for the four isoforms ( $26\text{--}43 \text{ s}^{-1}$ ) are similar to that of Peri ( $29.9 \text{ s}^{-1}$ ) and much faster than those for the cardiac and Emb isoforms. As might have been expected, these four fast isoforms show a very similar pattern of occupancy of the states in the cycle (Fig. 2 and Fig. S2), with IIb being slightly different from the other three isoforms. The IIb isoform has a higher occupancy of the MT state and correspondingly lower A·M·D·P<sub>i</sub> weakly attached state at high actin concentrations. All four have low occupancy of the A·M·D state (<10% in each case) but with significant variation among the four, varying from 2.5 to 5.6% at  $[\text{actin}] = 3K_{\text{app}}$ . As seen for the Peri isoform, the DR is not dominated by the A·M·D state; the other strongly attached states (A·M·D, A·M·T) contribute equally to the DR. We set the fast isomerization steps controlling ADP release and actin dissociation arbitrarily as a fast event at  $1000 \text{ s}^{-1}$ . It is possible that, for these very fast myosins, this value of  $1000 \text{ s}^{-1}$  is too slow and should be considerably faster. We increased these values to 2000 or  $3000 \text{ s}^{-1}$  individually or as a group and repeated the modeling. This made little difference to the overall balance of the cycle (see Table S5 for the data set for myosin IIc and IIb), with only those intermediates closely associated with the modified rate constant changed, if at all. For all other intermediates, the change was very small and always <10% of the initial value. The strongly attached states remained significantly occupied. The presence of these additional strongly attached states has implications for the DR and how sensitive the cycle is to load. This will be considered further below.

Before considering the implications of the modeling for understanding the different mechanochemical cycles and the role for which each isoform has been optimized, we should first consider the limitations of the data sets used. There are limited amounts of the protein available for the assays used to define the ATPase cycle, and for good experimental reasons, all data sets were not collected under identical conditions. The early experiments (all fast isoforms) were done at  $20^\circ\text{C}$  and  $0.1 \text{ M}$  KCl to make a better comparison with physiological conditions. Later, the conditions were changed to  $25 \text{ mM}$  KCl, as this lower salt concentration was required to generate more reliable actin-activated ATPase data. The data presented for  $\beta$ -myosin were collected at  $20^\circ\text{C}$  at both  $100$  and  $25 \text{ mM}$  KCl (6, 22) and allowed us to make corrections between salt conditions for each measured parameter. Similar studies have been published for the rabbit IIa isoform at both salt concentrations, and the corrections required were similar (6, 9). Similarly, there is an extensive collection of temperature dependence data on the  $\beta$ -isoform, from different sources, and for rabbit fast-muscle myosin (23–27). The observation that the corrections are similar for both the fast IIa and the  $\beta$ -cardiac isoforms supports our assumption that the corrections will be similar for each of the closely related isoforms used here; however, this remains an assumption. The measured values are all listed in Table S1, and the corrected values are used in Table 2.

We state under “Materials and methods” that we tested the robustness of our fitting by varying key fitted parameters by  $\pm 20\%$ , and these have been published for the cardiac isoforms (9). The supporting information (Table S4) shows representative data for the Emb isoform where one of  $K_{\text{D}}^*$ ,  $k_{\text{D}}$ ,  $K_{\text{T}}$ ,  $k_{\text{T}}$ ,  $k_{\text{-D}}$ , or  $k_{\text{H}}$  was varied and all others were refitted. Most parameters are changed by very little; those that change by  $>10\%$  are highlighted in Table S4 and are only those values directly linked to the altered parameter.

Having defined the ATPase and cross-bridge cycle for each of the eight isoforms, we will now consider the implications of the different cycles for the contraction of muscle fibers containing each of these isoforms. Specifically, we will explore the maximum shortening velocity, the load dependence of the cycle, and the economy of ATP utilization.

#### Maximum velocity of shortening, load dependence, and economy of ATP usage

The  $V_{\text{max}}$  of shortening ( $V_0$ ; zero load) of a muscle fiber expressing a single isoform can be estimated from the lifetime ( $\tau$ ) of the strongly attached force-holding state (predominantly AMD) and the individual step size of the working stroke,

$$V_0 = d/\tau \quad (\text{Eq. 1})$$

From our modeling,  $\tau$  can be calculated from the equation,  $\tau = \text{DR}/\text{ATPase rate}$ , at any actin concentration. Because DR and ATPase rates have very similar dependence on actin concentrations (both proportional to the fractional saturation of myosin with actin),  $\tau$  and hence  $V_0$  are independent of actin concentration in this model. This means that the ATPase rate and velocity are not directly related except at saturating actin concentrations. The calculation of the  $V_0$  is identical for a con-

## Human muscle myosin isoforms

tracting muscle fiber and velocity of actin movement in a motility assay, often measured in the absence of load. The model is therefore consistent with the observation that  $V_0$  is independent of the degree of activation of a muscle and only a very small number of myosin cross-bridges are required to achieve  $V_0$ . For the purposes of the arguments set out below, we have assumed the working stroke,  $d$ , to be 5 nm for each isoform.

The equation above assumes that the velocity is limited by the lifetime of the strongly attached states, which, in the model used here, is controlled by the rate of cross-bridge detachment after completing the working stroke. This has been demonstrated to be true for the relatively slow  $\beta$ -type myosin, where the ADP release rate constant ( $k_D$ ) is easily measured. The same is true for the slow Emb isoform. For all other isoforms, the ADP release rate constant has not been measured because either the rate constant is too fast for current methods or the relevant A·M·D complex cannot be easily formed by simply mixing ADP with A·M. The equilibrium  $K_D$ , in Fig. 1 lies too far toward the A·M·D complex, and little (<5%) A·M·D is formed. For fast rabbit muscle myosin, the value of  $K_D$  was estimated as  $\sim 50$  (28). Thus, we have good estimates of ADP release from  $\beta$ -cardiac and Emb myosin. For  $\alpha$ , Peri, and all fast-muscle isoforms, we have to estimate the ADP release based upon reasoned argument. If ADP release is too fast, then the lifetime and steady-state occupancy of the force-holding state becomes too small, and a muscle would be unable to hold much force. For example, a 1% occupancy of the force-holding state would mean only three force-holding cross-bridges for a fully activated 300-myosin thick filament. If the rate constant is too slow, the velocity becomes smaller than that observed experimentally. Here, we have set that value for these fast fibers at the minimal possible, compatible with the expected velocities.

As noted above, fast-muscle myosins have a higher predicted occupancy of other strongly attached states (*dark blue*), not just the A·M·D state. When  $k_D$  was doubled, it had little effect on the occupancy of states in the cycle or the overall ATPase rates, but velocity was increased by 15–20%, and there was a 10% decline in the DR because of a  $\sim 10\%$  fall in the A·M·D state. The system does remain, however, a detachment-limited model.

Fig. 3B plots the predicted  $V_0$  values for each isoform and indicates there is an  $\sim 20$ -fold range of velocities from Emb ( $0.09 \mu\text{m}\cdot\text{s}^{-1}$ ) to IId ( $1.66 \mu\text{m}\cdot\text{s}^{-1}$ ). The order of predicted velocities and their values relative to Emb velocity are as follows: Emb, 1;  $\beta$ , 2;  $\alpha$ , 4; Peri, 8; Ila and ExOc, 12; IId and IIb, 20. Thus, our analysis of the cross-bridge cycle predicts Emb to be both the slowest of the isoforms and the one most capable of holding large steady-state loads (*i.e.* longest lifetime of the A·M·D state and the highest occupancy of A·M·D in the steady state). In contrast, IId was the fastest isoform and has the lowest DR and, hence, lowest force-holding capacity.

The assumption of a 3-fold reduction in the rate constants for  $P_i$  and ADP release ( $k_{P_i}$  and  $k_D$ ) induced by a 5-pN load predicts that for each isoform, the different cycle characteristics result in different sensitivities of velocity to load. This effect of the cycle characteristics would remain true even if the measured load sensitivity varied for each isoform. The slower isoforms  $\alpha$ ,  $\beta$ , and Emb have the highest sensitivity, with  $V_0$  being reduced by 2.7–2.8-fold. The velocity of ExOc, Ila, and Peri are

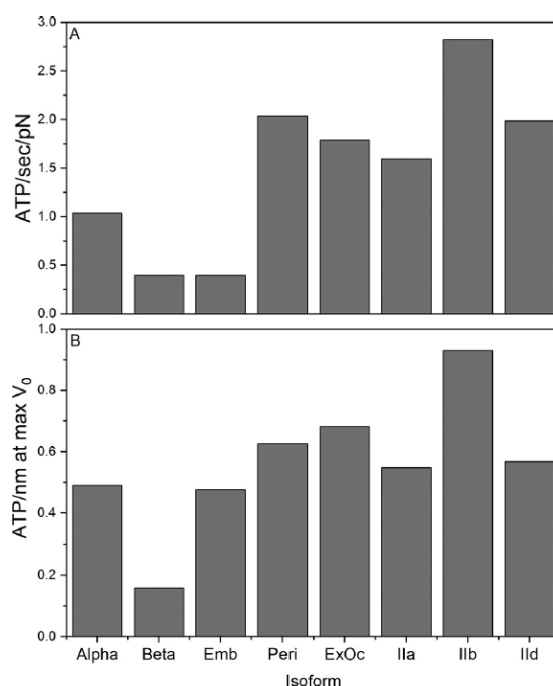


**Figure 5. The economy of ATP usage (per myosin head).** A, when holding a 5-pN load.  $\text{Economy}_L = \text{ATPase (ATP/s)}/5 \text{ (pN)}$  (where ATPase is estimated at  $[\text{actin}] = 3K_{\text{app}}$ , assuming a similar load dependence for each isoform); B, when shortening at  $V_{\text{max}}$  ( $V_0$ ) and  $V_{\text{max}}$  for the ATPase.  $\text{Economy}_V \text{ (ATP/nm)} = V_{\text{max}} \text{ (ATP/s)}/V_0 \text{ (nm/s)}$ .

reduced 2.1-fold, whereas the fastest isoforms IId and IIb show only a 1.6–1.7-fold reduction. This reflects the relative importance of the A·M·D and A·M·T strongly attached states. In the current model, we have assumed that the fast events (rapid ADP release ( $K_D$ ), ATP binding ( $K_T$ ), and the ATP-induced dissociation of actin ( $K_{T^-}$  and  $K_{T^+}$ )) are not directly affected by load.

The difference in load sensitivity of the cycle is reflected in the calculation of the economy of the isoforms shown in Fig. 5, which plot ATP used per second when holding a force of 5 pN (Fig. 5A) and when shortening at  $V_{\text{max}}$  and saturating actin (zero load, Fig. 5B). At a 5-pN load, both  $\beta$  and Emb myosin have a similar economical usage of ATP ( $\sim 0.35$  ATP/s/pN) and are more economical than  $\alpha$  ( $\sim 3$ -fold higher ATP usage) or the fast isoforms, which use 1.5–2-fold more ATP than  $\alpha$ -myosin for the same load. In contrast, Emb is not as efficient in turning ATPase activity into movement as  $\beta$ -myosin (0.2 ATP/nm of travel) but is similar to  $\alpha$ -myosin, which uses just less than 0.5 ATP/nm. Thus, Emb myosin appears to be designed for slow movement but economical force holding. As reported previously, this myosin is also able to continue functioning at much lower ATP concentrations than other myosin isoforms because of tight affinity for ATP ( $K_T$ ) (8). This property is shared with Peri and, to a lesser extent, with ExOc.

To fully understand the mechanical behavior of a muscle fiber, the force–velocity relationship is required, as this can define the power output (force  $\times$  velocity) and the velocity at which the power output of the muscle is maximal. This is often

**Table 5**  
Comparison with human muscle fiber data

Values in parenthesis are relative to the type I fiber/ $\beta$  myosin isoform.

| Fiber/myosin type | $V_0$ 12 °C <sup>a</sup> | $V_0$ 12 °C <sup>b</sup> | $V_0$ 20 °C <sup>b</sup> | Isometric economy 12 °C <sup>b</sup> | Predicted $V_0$ 20 °C | Predicted isometric economy 20 °C |
|-------------------|--------------------------|--------------------------|--------------------------|--------------------------------------|-----------------------|-----------------------------------|
|                   | $\mu\text{m/s/hs}$       | muscle lengths/s         | muscle lengths/s         |                                      |                       |                                   |
| I                 | 0.33 ± 0.02 (1.0)        | 0.37 ± 0.06 (1.0)        | 1.15 ± 0.36 (1.0)        | 1                                    | 0.2 (1.0)             | 0.7 (1.0)                         |
| Ila               | 1.40 ± 0.10 (4.2)        | 0.88 ± 0.12 (2.4)        | 2.37 ± 0.34 (2.06)       | 3.5                                  | 1.16 (5.8)            | 1.7 (2.4)                         |
| IId               | 3.02 ± 0.935 (9.15)      |                          |                          |                                      | 1.73 (8.65)           |                                   |

<sup>a</sup> From Ref. 14.

<sup>b</sup> From Ref. 15.

considered to be the mechanical parameter that defines the optimal operating conditions for a muscle. An equivalent of the force–velocity curve at the single-molecule level has recently been developed, which shows how point mutations and small molecules can alter the relationship (29). Extrapolation between single molecule and whole fiber force–velocity curves is not trivial due to interactions between motors in the ensemble and the elasticity of the sarcomere filament. Thus, our data cannot be used at present to predict the force–velocity relationship. However, the sarcomeric version of the MUSICO program is in principle capable of generating the force–velocity relationship (9). Modeling using this approach is a longer-term project.

Our predictions can be compared, to a limited extent, with the published data on human muscle fibers, where the myosin isoforms present are well-defined. He *et al.* (15) studied the force–velocity and ATPase properties of slow and type Ila human muscle fibers containing only  $\beta$ -myosin and myosin Ila, respectively. Data were collected at 12 and 20 °C, and they calculated the economy of ATPase usage and the optimum velocities for power output. Pellegrino *et al.* (14) additionally reported the velocities of human type I, Ila, and IId/x fibers at 12 °C (and velocities for the same set of fibers from mice, rats, and rabbits). These studies therefore provide detailed muscle fiber data that can be compared with the predictions from our study. That said, there are assumptions built into any extrapolation from solution biochemistry to a muscle fiber that limit direct comparison. These include the number of myosin heads present and fully activated in a muscle fiber, which in turn depends upon the density and packing of filaments in the muscle fiber. The units used to report velocities and ATPases differ due to these corrections. We will therefore limit ourselves to the values of the parameters relative to the values reported for Type I fibers containing  $\beta$ -myosin.

Table 5 lists the relative values of  $V_0$ , ATPase, and ATP economy under isometric conditions, provided by Pellegrino *et al.* (14) and He *et al.* (15). The relative values of  $V_0$  at 12 °C for Type Ila fibers relative to Type I were 4.2 for Pellegrino *et al.* (14) and 2.4 for He *et al.* (15). He *et al.* (15) had a similar ratio at 20 °C of 2.06. Our data give a ratio nearer to that of Pellegrino's 5.8 for type Ila and 8.65 for type IId, compared with Pellegrino's value of 9.15. Given the degree of error in each of these experimental measurements, the values are of the correct order of magnitude. Similarly, He *et al.* measured the economy of ATP usage by type I fibers to be 3.5-fold better than that of type Ila fibers. In contrast, we calculate a 2.4-fold difference for the two types of myosin.

## Overview

Our modeling has revealed distinct characteristics of the ATPase cycle or each of the human isoforms studied. Differences lie in the overall speed of the ATPase cycle ( $k_{\text{cat}}$ ) and the balance of the events in the cycle, which affects how much time the myosin spends at each point of the cycle. There are three significant events in the cycle that define the characteristics of the cycle. 1) the  $P_i$  release step ( $k_{\text{pi}}$ ) controls entry into the strong actin-binding, force-holding states. This event is shown as a single step but probably involves a myosin conformational change before or after the  $P_i$  release itself (30, 31). 2) The ADP release step, controlled by the isomerization ( $k_{\text{D}}$ ), is followed by rapid ADP release, rapid ATP binding, and then actin dissociation. Thus, the ADP-coupled isomerization is linked to detachment of the cross-bridge. 3) Finally, the ATP hydrolysis step limits how long the cross-bridge remains detached before again being available to bind actin as A-M-D- $P_i$ , which then gives access to the  $P_i$  release and force-generating step. All other events are far more rapid, and steps such as nucleotide binding/release and actin binding and release can be treated as rapid equilibration steps. Each of the myosins has a unique relationship between  $k_{\text{cat}}$  and the three events, which is simply illustrated in Table 4 by showing the value of  $k_{\text{cat}}$  for each isoform and the value of each of the other rate constants relative to  $k_{\text{cat}}$ . The values listed give some indication of the contribution of each transition to  $k_{\text{cat}}$ . In all cases, at least one of the three values is  $\sim 2$  times  $k_{\text{cat}}$ , highlighted with a gray background in Table 4. This is  $k_{\text{pi}}$  in most cases, but for  $\beta$  and Peri, the value of  $k_{\text{H}}$  is smaller or comparable with  $k_{\text{pi}}$ . A second value for each myosin is  $\sim 3$ – $5$  times  $k_{\text{cat}}$  (yellow background). This is  $k_{\text{H}}$  for all fast isoforms and  $\alpha$ , whereas it is  $k_{\text{D}}$  for Emb and  $k_{\text{pi}}$  for  $\beta$  and Peri. The third value is  $\sim 10$  times  $k_{\text{cat}}$ , and this is  $k_{\text{D}}$  in most cases except Emb. The value for  $\alpha$  stands out, as this is  $\sim 5$  times  $k_{\text{cat}}$  and similar to the value of  $k_{\text{H}}$ . These different relationships between the three constants define the mechanical properties of the isoforms.

The isometric force of muscle fibers is normally found to be relatively invariant within the limits of the precision of the measurement and proportional to the number of strongly attached cross-bridges, although a contribution of weakly attached bridges cannot be ruled out. If this is true, then  $P_0$  will be a function of the number of active bridges and the DR. If all bridges are active (a function of  $\text{Ca}^{2+}$  activation, force activation, the superrelaxed states, and phosphorylation effects, none of which operates in our pure S1 and actin system), then  $P_0$  is a function of DR. In our hands, the DR is a function of the actin

## Human muscle myosin isoforms

concentration, and the estimate of  $P_0$  will depend on the effective actin concentration present in the fiber. For a truly isometric fiber, the actin concentration may not be the same for every myosin head due to the mismatch of the actin and myosin filament helices in a muscle. For this reason, we presented our data at different actin concentrations.

Our data show that the DR varies between isoforms: 0.05–0.075 for fast isoforms and 0.1–0.15 for slow/cardiac (even higher for Emb). Thus, the expected  $P_0$  values per myosin head will be proportional to these DR values. Of course, in the fiber, the myosins act as an ensemble, and the mechanical coupling between myosin may alter these numbers. In addition, whereas the density of thick filaments in a muscle fiber may be similar for all fast muscles, variations in packing are expected in slow and developing muscle, where cell contents are not so exclusively packed with myofilaments.

The predicted  $V_0$  values vary in a way roughly compatible with expectation; the velocities are expected to be independent of actin concentration and so should be independent of the packing of filaments in the fiber. However, a question remains of whether unloaded shortening truly exists in the muscle fiber, where some internal load may always be present, and therefore measured values will underestimate the true  $V_0$ . Comparison of  $V_0$  muscle fiber values with motility velocities rarely shows exact correspondence for reasons not yet fully explained, although myosin orientation on the surface and the exact make up of actin filaments are thought to play a part in such discrepancies (32).

A limitation of our analysis is the limited data available on the load dependence of myosin isoforms. In the absence of experimental data, we have made the simplifying assumption that the load dependence is the same in each case. Although this assumption may not be true, our modeling does illustrate how differences in the cycle alone can generate different load sensitivities for the isoforms. Force–velocity curves for muscle fibers in principle contain the information on load dependence but are not available for many fibers containing a single myosin isoforms.

The solution data do not currently allow us to generate a force–velocity curve, which would be required to define the optimal velocity for power output for each myosin type. This is believed to be the condition where the muscle is designed to operate.  $V_0$  and  $P_0$  will provide the end points for the force–velocity curve, but the shape of the relationship is distinct for different fibers and may depend on internal muscle elastic elements in addition to the ATPase cycle of different myosin motor domains. Single molecule methods or loaded motility assays could be used to measure the load dependence of individual myosin isoforms. This will reveal whether the myosin motor domain itself defines the shape of the force–velocity curve.

In common with most studies of myosin in solution our data are collected at 20 °C and 25 mM KCl as the reference conditions. These are some way from the physiological conditions of 0.15–0.17 M ionic strength and 37 °C. The conditions stated above are needed to allow accurate measurement of the ATPase and motility data and to allow comparison with muscle fiber mechanics. Extrapolation to physiological conditions is possi-

ble for the well-defined  $\beta$ -cardiac myosin and adult fast-muscle myosin, where there are extensive data on the temperature and salt dependence of many of the parameters. For all other isoforms, no such data currently exist.

Our analysis of the differences in the cross-bridge cycle for each myosin isoform raises the issue of the sequence changes that bring about the adaptations to function. Earlier studies have examined groups of isoforms to identify key sequence changes (18, 33–35). These have often emphasized the variable surface loops in which isoform-specific sequence changes occur. However, the source of the sequence changes required to bring about the changes in the overall balance of the cross-bridge cycle is likely to be more widespread. We show a sequence alignment of the eight human isoforms in Fig. S5 and outline the major areas where changes occur in the legend to the figure. These span several regions: (i) residues 302–339, an area that corresponds to one of the alternate spliced regions in the *Drosophila* muscle myosins; (ii) actin-binding loop 3 (residues 561–579) and loop 4 (residues near 370); and (iii) helix O (residues 425–451) in the upper 50-kDa domain. These areas are of interest because the same areas were highlighted in a study of the sequence variation of the  $\beta$ -cardiac myosin motor domain associated with changes in velocity between mammals (36). Future analyses will include a combination of bioinformatics, modeling, and experimental investigation to define the sequences that generate the different properties of sarcomeric myosins and are responsible for their functional diversity.

## Materials and methods

### Protein expression and purification

Human muscle MyHC-sS1 for the  $\beta$ -isoform and MyHC-S1 for the  $\alpha$ -isoform were expressed and purified as described previously (6). The motor domain of the  $\beta$  heavy chain was co-expressed with the N-terminal His<sub>6</sub>-tagged, human essential light chain MYL3. The motor domain of the Emb myosin isoform was expressed with a His<sub>6</sub> tag on the C terminus (8). The fast-muscle isoforms (Iib, Iid, and Iia), Peri, and ExOc isoforms were expressed with a C-terminally fused enhanced GFP and His<sub>6</sub> tag. All proteins carrying a C-terminal His<sub>6</sub> tag when purified carried the endogenous mouse light chains present in the C2C12 cells (see Table 1) (21). Briefly, replication-incompetent recombinant adenoviruses were produced using the pAdEasy system containing expression cassettes encoding S1 of the human myosins under the transcriptional control of a cytomegalovirus promoter. The adenoviral particles were amplified using HEK293 cells; the viruses were purified using CsCl gradients, and the concentrated virus was stored in a glycerol buffer at –20 °C. These adenoviruses were used to infect C<sub>2</sub>C<sub>12</sub> myotubes in culture, and cells were collected and frozen into cell pellets. Pellets were then homogenized in a low-salt buffer and centrifuged, and the supernatants were purified by affinity chromatography using a HisTrap HP 1-ml column. The proteins were then dialyzed into the low-salt experimental buffer (25 mM KCl, 20 mM MOPS, 5 mM MgCl<sub>2</sub>, 1 mM DTT, pH 7.0).

Actin was prepared from rabbit muscle as described previously (37). The actin was labeled with pyrene at Cys-374 as described previously (38). When used at submicromolar con-

centrations, the actin was stabilized by incubation in a 1:1 mixture with phalloidin.

#### Kinetic measurements

Fast kinetic data for every isoform except for the Peri isoform have been published previously (6–8). All kinetic measurements for the Peri isoform were performed as described previously (6–8). Solutions were buffered with 20 mM MOPS, 5 mM MgCl<sub>2</sub>, 25 mM KCl, 1 mM DTT at pH 7.0, and measurements were conducted at 20 °C on a High-Tech Scientific SF-61 DX2 stopped-flow system. Traces were analyzed in Kinetic Studio (TgK Scientific) and Origin (OriginLab). The experimental data for all isoforms are summarized in Table S1. ATPase data for Peri, ExOc, IIa, IIb, and IIc isoforms were performed at 37 °C (21). To calculate the expected  $k_{\text{cat}}$  values at 20 °C, a  $Q_{10}$  value of 1.5 was used (27).

#### Modeling

The published set of rate and equilibrium constants is summarized in Table S1, together with the  $k_{\text{cat}}$  and  $K_{\text{app}}$  values from steady-state actin-activated ATPase assays. With these data, the eight-state actin-myosin ATPase cycle was modeled using the MUSICO software as described (9, 10). The eight-step scheme of Fig. 1 has a total of 24 rate and equilibrium constants, but not all are independent. For each step,  $i$ ,  $K_i = k_i/k_{-i}$ , and thus only two of the constants need to be defined experimentally for a complete description of the cycle. The free energy of ATP hydrolysis further constrains the overall balance of the cycle. Experiments have defined forward rate constants  $k_{D^*}$ ,  $k_{T^*}$ , and  $k_H$  and the equilibrium constants  $K_T$  and either  $K_D$  or  $K_{D^*}$ , in most cases to a precision of at least 20% (see Table S1). The rate constants  $k_{T^*}$  and  $k_D$  are defined as diffusion-limited. The events  $k_{T^*}$  and  $k_{-A}$  are considered too fast to measure and thus have little effect on the modeling. Fitting the model to the actin-dependent steady-state ATPase data can give estimates for the equilibrium constants for actin binding ( $K_A$ ), ATP hydrolysis ( $K_H$ ), and on-actin hydrolysis step ( $K_{AH}$ ) and the rate constants for phosphate release and ATP dissociation ( $k_{P_i}$  and  $k_T$ , respectively). The  $K_i = k_i/k_{-i}$  detailed balance equation can be used to define  $K_{T^*}$ ,  $k_A$ ,  $k_{-P_i}$ ,  $k_{-D^*}$ ,  $k_{-D}$ ,  $k_{-T}$ ,  $k_{-H}$ , and  $k_{-AH}$ . The initial concentration of ATP was set at 5 mM, and those of ADP and P<sub>i</sub> were set at 0 mM; under steady-state conditions, these are assumed to be zero.

The fraction of myosin in the strongly attached states AMD, AM-D, AM, and AMT in the steady state is defined as the DR. From the DR, an estimate of the maximal velocity,  $V_o$ , can be calculated from Equation 1, where  $d$  is the distance over which myosin can produce force, and  $\tau$  is the lifetime of the strongly attached state. The lifetime of the attached state is equal to DR/ATPase rate; hence,  $V_o = d \cdot \text{ATPase} / \text{DR}$ . The economy, or the amount of ATP used per myosin per nm of travel when the ATPase and the velocity are maximal, can be derived from  $\text{Economy}_V (\text{ATP}/\text{nm}) = V_{\text{max}} (\text{ATP}/\text{s}) / V_o (\text{nm}/\text{s})$ .

In our previous modeling, we used the data from two laboratories that used single-molecule laser trap methods to define the effect of load on the ADP release step of the cycle ( $k_{D^*}$ ) (12, 13). These indicated that for  $\beta$ -cardiac, a 5-pN load on actin-myosin slowed the ADP release by  $\sim 3$ -fold. A similar

effect on the power stroke (coupled to P<sub>i</sub> release in our eight-state model) is also required to slow the ATPase cycling by  $\sim 3$ -fold, as reported for muscle fibers under isometric conditions (15). Here, in the absence of any direct measurements on any other isoform, we make the assumption that all isoforms have a similar load dependence. Whereas this is an oversimplification, it does allow us to illustrate how load affects each isoform differently due to the changed balance of events in the cycle. To estimate the economy of ATP usage per pN of force generated at any actin concentration, the ATPase rate was divided by the load, here 5 pN.

#### Error analysis

The sensitivity matrices shown in Table S3 demonstrate that with the exception of  $k_{-T}$ , the fitted parameters are all well-defined in the modeling program; values in the diagonal of  $>0.8$  indicate well-resolved parameters with little codependence. As reported previously (9), varying one of the fitted parameters ( $k_H$ ,  $k_{-D}$ ,  $K_{D^*}$ ,  $k_{-D^*}$ ,  $k_{-T^*}$ , or  $K_{T^*}$ ) by  $\pm 20\%$  has minimal effect on the best-fit values for the remaining parameters. This observation remained true for the data presented in this study (see Table S4 for analysis of the Emb data), with the remaining parameters varying by much less than 20%, with a few exceptions.

In our previous paper on DCM mutations in  $\beta$ -cardiac myosin, we also explored the effect of a 20% error in the value of  $V_{\text{max}} (k_{\text{cat}})$  or  $K_{\text{app}}$  used in the fitting. These again showed that the data are reasonably robust.  $K_{\text{app}}$  is primarily defined by the value of  $K_A$ , and a 20% change in  $K_{\text{app}}$  has little effect on the cycle apart from a change in  $K_A$ . This is also because we model the data at different actin concentration related to  $K_A$ . Changes in  $V_{\text{max}}$  will change the flux round the cycle.  $V_{\text{max}}$  is largely controlled by a combination of  $k_{P_i}$  and  $k_H$ , depending upon the isoform, and these will adjust as the  $k_H$  changes by 20%. If  $k_{\text{AMD}}$  does not change and we use our measured value, then the occupancy of AMD must change to increase or decrease the flux through this state to match the altered  $V_{\text{max}}$ . Thus, AMD will change by some fraction of 20% but no more than this. A 20% change is within the tolerance we claim for the overall precision of the cycle and will not alter substantially the pattern seen for each isoform.

**Author contributions**—C. A. J., M. A. G., and L. A. L. conceived the study. C. A. J., with M. S. and S. M. M., completed the kinetic modeling. J. W. designed, performed, and analyzed the stopped-flow experiments on the perinatal protein provided by C. D. V. and A. K. All authors contributed to the final version of the manuscript.

#### References

1. Acakpo-Satchivi, L. J. R., Edelman, W., Sartorius, C., Lu, B. D., Wahr, P. A., Watkins, S. C., Metzger, J. M., Leinwand, L., and Kucherlapati, R. (1997) Growth and muscle defects in mice lacking adult myosin heavy chain genes. *J. Cell Biol.* 139, 1219–1229 [CrossRef Medline](#)
2. Oldfors, A. (2007) Hereditary myosin myopathies. *Neuromuscul. Disord.* 17, 355–367 [CrossRef Medline](#)
3. Haraksingh, R. R., Jahanbani, F., Rodriguez-Paris, J., Gelernter, J., Nadeau, K. C., Oghalai, J. S., Schrijver, I., and Snyder, M. P. (2014) Exome sequencing and genome-wide copy number variant mapping reveal novel associ-



## Human muscle myosin isoforms

- ations with sensorineural hereditary hearing loss. *BMC Genomics* 15, 1155 CrossRef Medline
4. Schiaffino, S., and Reggiani, C. (2011) Fiber types in mammalian skeletal muscles. *Physiol. Rev.* 91, 1447–1531 CrossRef Medline
  5. Bottinelli, R., and Reggiani, C. (2000) Human skeletal muscle fibres: molecular and functional diversity. *Prog. Biophys. Mol. Biol.* 73, 195–262 CrossRef Medline
  6. Deacon, J. C., Bloemink, M. J., Rezavandi, H., Geeves, M. A., and Leinwand, L. A. (2012) Erratum to: Identification of functional differences between recombinant human  $\alpha$  and  $\beta$  cardiac myosin motors. *Cell Mol. Life Sci.* 69, 4239–4255 CrossRef Medline
  7. Bloemink, M. J., Deacon, J. C., Resnicow, D. I., Leinwand, L. A., and Geeves, M. A. (2013) The superfast human extraocular myosin is kinetically distinct from the fast skeletal IIa, IIb, and IIc isoforms. *J. Biol. Chem.* 288, 27469–27479 CrossRef Medline
  8. Walklate, J., Vera, C., Bloemink, M. J., Geeves, M. A., and Leinwand, L. (2016) The most prevalent freeman-sheldon syndrome mutations in the embryonic myosin motor share functional defects. *J. Biol. Chem.* 291, 10318–10331 CrossRef Medline
  9. Mijailovich, S. M., Nedic, D., Svicevic, M., Stojanovic, B., Walklate, J., Ujfalusi, Z., and Geeves, M. A. (2017) Modeling the actin.myosin ATPase cross-bridge cycle for skeletal and cardiac muscle myosin isoforms. *Biophys. J.* 112, 984–996 CrossRef Medline
  10. Ujfalusi, Z., Vera, C. D., Mijailovich, S. M., Svicevic, M., Yu, E. C., Kawana, M., Ruppel, K. M., Spudich, J. A., Geeves, M. A., and Leinwand, L. A. (2018) Dilated cardiomyopathy myosin mutants have reduced force-generating capacity. *J. Biol. Chem.* 293, 9017–9029 CrossRef Medline
  11. VanBuren, P., Harris, D. E., Alpert, N. R., and Warshaw, D. M. (1995) Cardiac V1 and V3 myosins differ in their hydrolytic and mechanical activities *in vitro*. *Circ. Res.* 77, 439–444 CrossRef Medline
  12. Greenberg, M. J., Shuman, H., and Ostap, E. M. (2014) Inherent force-dependent properties of  $\beta$ -cardiac myosin contribute to the force-Velocity relationship of cardiac muscle. *Biophys. J.* 107, L41–L44 CrossRef Medline
  13. Sung, J., Nag, S., Mortensen, K. L., Vestergaard, C. L., Sutton, S., Ruppel, K., Flyvbjerg, H., and Spudich, J. A. (2015) Harmonic force spectroscopy measures load-dependent kinetics of individual human  $\beta$ -cardiac myosin molecules. *Nat. Commun.* 6, 7931 CrossRef Medline
  14. Pellegrino, M. A., Canepari, M., Rossi, R., D'Antona, G., Reggiani, C., and Bottinelli, R. (2003) Orthologous myosin isoforms and scaling of shortening velocity with body size in mouse, rat, rabbit and human muscles. *J. Physiol.* 546, 677–689 CrossRef Medline
  15. He, Z. H., Bottinelli, R., Pellegrino, M. A., Ferenczi, M. A., and Reggiani, C. (2000) ATP consumption and efficiency of human single muscle fibers with different myosin isoform composition. *Biophys. J.* 79, 945–961 CrossRef Medline
  16. Schiaffino, S., Rossi, A. C., Smerdu, V., Leinwand, L. A., and Reggiani, C. (2015) Developmental myosins: Expression patterns and functional significance. *Skelet. Muscle* 5, 22 CrossRef Medline
  17. Bloemink, M. J., and Geeves, M. A. (2011) Shaking the myosin family tree: biochemical kinetics defines four types of myosin motor. *Semin. Cell Dev. Biol.* 22, 961–967 CrossRef Medline
  18. Weiss, A., Schiaffino, S., and Leinwand, L. A. (1999) Comparative sequence analysis of the complete human sarcomeric myosin heavy chain family: implications for functional diversity. *J. Mol. Biol.* 290, 61–75 CrossRef Medline
  19. Brueckner, J. K., Itkis, O., and Porter, J. D. (1996) Spatial and temporal patterns of myosin heavy chain expression in developing rat extraocular muscle. *J. Muscle Res. Cell Motil.* 17, 297–312 Medline
  20. Sartore, S., Mascarello, F., Rowleron, A., Gorza, L., Ausoni, S., Vianello, M., and Schiaffino, S. (1987) Fibre types in extraocular muscles: a new myosin isoform in the fast fibres. *J. Muscle Res. Cell Motil.* 8, 161–172 CrossRef Medline
  21. Resnicow, D. I., Deacon, J. C., Warrick, H. M., Spudich, J. A., and Leinwand, L. A. (2010) Functional diversity among a family of human skeletal muscle myosin motors. *Proc. Natl. Acad. Sci. U.S.A.* 107, 1053–1058 CrossRef Medline
  22. Nag, S., Sommese, R. F., Ujfalusi, Z., Combs, A., Langer, S., Sutton, S., Leinwand, L. A., Geeves, M. A., Ruppel, K. M., and Spudich, J. A. (2015) Contractility parameters of human  $\beta$ -cardiac myosin with the hyper-trophic cardiomyopathy mutation R403Q show loss of motor function. *Sci. Adv.* 1, e1500511 CrossRef Medline
  23. Walklate, J., and Geeves, M. (2015) Temperature manifold for a stopped-flow machine to allow measurements from  $-10$  to  $+40$  °C. *Anal. Biochem.* 476, 11–16 CrossRef Medline
  24. Bloemink, M. J., Adamek, N., Reggiani, C., and Geeves, M. A. (2007) Kinetic analysis of the slow skeletal myosin MHC-1 isoform from bovine masseter muscle. *J. Mol. Biol.* 373, 1184–1197 CrossRef Medline
  25. Iorga, B., Adamek, N., and Geeves, M. (2007) The slow skeletal muscle isoform of myosin shows kinetic features common to smooth and non-muscle myosins. *J. Biol. Chem.* 282, 3559–3570 CrossRef Medline
  26. White, H. D., and Taylor, E. W. (1976) Energetics and mechanism of actomyosin adenosine triphosphatase. *Biochemistry* 15, 5818–5826 CrossRef Medline
  27. Siemankowski, R. F., Wiseman, M. O., and White, H. (1985) ADP dissociation from actomyosin subfragment 1 is sufficiently slow to limit the unloaded shortening velocity in vertebrate muscle. *Proc. Natl. Acad. Sci. U.S.A.* 82, 658–662 CrossRef Medline
  28. Sleep, J. A., and Hutton, R. L. (1980) Exchange between inorganic phosphate and adenosine 5'-triphosphate in the medium by actomyosin subfragment 1. *Biochemistry* 19, 1276–1283 CrossRef Medline
  29. Liu, C., Kawana, M., Song, D., Ruppel, K. M., and Spudich, J. A. (2018) Controlling load-dependent kinetics of  $\beta$ -cardiac myosin at the single-molecule level. *Nat. Struct. Mol. Biol.* 25, 505–514 CrossRef Medline
  30. Houdusse, A., and Sweeney, H. L. (2016) How myosin generates force on actin filaments. *Trends Biochem. Sci.* 41, 989–997 CrossRef Medline
  31. Muretta, J. M., Rohde, J. A., Johnsrud, D. O., Cornea, S., and Thomas, D. D. (2015) Direct real-time detection of the structural and biochemical events in the myosin power stroke. *Proc. Natl. Acad. Sci. U.S.A.* 112, 14272–14277 CrossRef Medline
  32. Homsher, E., Wang, F., and Sellers, J. R. (1992) Factors affecting movement of F-actin filaments propelled by skeletal muscle heavy meromyosin. *Am. J. Physiol.* 262, C714–C723 CrossRef Medline
  33. Alpert, N. R., Brosseau, C., Federico, A., Krenz, M., Robbins, J., and Warshaw, D. M. (2002) Molecular mechanics of mouse cardiac myosin isoforms. *Am. J. Physiol. Heart Circ. Physiol.* 283, H1446–H1454 CrossRef Medline
  34. Chikuni, K., Muroya, S., Tanabe, R., and Nakajima, I. (2003) Comparative sequence analysis of four myosin heavy chain isoforms expressed in porcine skeletal muscles: sequencing and characterization of the porcine myosin heavy chain slow isoform. *Anim. Sci. J.* 73, 257–262 CrossRef
  35. Toniolo, L., Patrino, M., Maccatrozzo, L., Pellegrino, M. A., Canepari, M., Rossi, R., D'Antona, G., Bottinelli, R., Reggiani, C., and Mascarello, F. (2004) Fast fibres in a large animal: fibre types, contractile properties and myosin expression in pig skeletal muscles. *J. Exp. Biol.* 207, 1875–1886 CrossRef Medline
  36. Johnson, C. A., Mcgreig, J. E., Vera, C. D., Mulvihill, D. P., Ridout, M., Leinwand, L. A., Wass, M. N., and Geeves, M. A. (2019) Cardiac contraction velocity has evolved to match heart rate with body size through variation in  $\beta$ -cardiac myosin sequence. *bioRxiv* CrossRef
  37. Spudich, J. A., and Watt, S. (1971) The regulation of rabbit skeletal muscle contraction. I. Biochemical studies of the interaction of the tropomyosin-troponin complex with actin and the proteolytic fragments of myosin. *J. Biol. Chem.* 246, 4866–4871 Medline
  38. Criddle, A. H., Geeves, M. A., and Jeffries, T. (1985) The use of actin labelled with *N*-(1-pyrenyl)iodoacetamide to study the interaction of actin with myosin subfragments and troponin/tropomyosin. *Biochem. J.* 232, 343–349 CrossRef Medline

## Supplementary Information

The ATPase cycle of Human Muscle Myosin II Isoforms:  
Adaptation of a single mechanochemical cycle for different physiological roles

**Chloe A. Johnson<sup>1</sup>, Jonathan Walklate<sup>1</sup>, Marina Svcevic<sup>2</sup>, Srboljub M. Mijailovich<sup>3</sup>,  
Carlos Vera<sup>4</sup>, Anastasia Karabina<sup>4</sup>, Leslie A. Leinwand<sup>4,\*</sup> and Michael A. Geeves<sup>1,\*</sup>**

1. School of Biosciences, University of Kent, Canterbury CT2 7NJ, UK
2. Faculty of Science, University of Kragujevac, Serbia;
3. Department of Biology, Illinois Institute of Technology, Chicago IL 60616 USA
4. BioFrontiers Institute and Department of Molecular, Cellular and Developmental Biology, University of Colorado Boulder, Boulder CO 80309 USA

Running title: Human muscle myosin isoforms

\*To whom correspondence should be addressed:

Michael A Geeves  
School of Biosciences,  
University of Kent,  
Canterbury CT2 7NJ, UK  
m.a.geeves@kent.ac.uk  
+44 1227827597

Leslie Leinwand  
BioFrontiers Institute and Department of  
Molecular, Cellular and Developmental  
Biology,  
University of Colorado Boulder, Boulder CO  
80309 USA  
leslie.leinwand@colorado.edu

**Keywords:** developmental myosin, adult skeletal myosin, cardiac myosin, fast muscle, slow muscle, modeling, ATPase, ATP economy

### **List of Figures and Tables:**

Table S1 – Experimentally measured constants for each isoform.

Table S2 – Predicted Occupancy of the states during the ATPase cycle.

Table S3 – Resolution matrices for the embryonic and perinatal isoforms.

Table S4 – Sensitivity analysis; Percentage change of the predicted constants induced by a change of +20% or -20% to one of the six fitted parameters for the embryonic isoform.

Table S5 – The effect of increasing the fast isomerisation forward and backward rate constants by a factor of 2 on the occupancies of states in the cycle.

Figure S1 – ATP induced dissociation of Perinatal S1 from pyrene-labelled actin.

Figure S2 – ADP affinity for perinatal S1 in the presence of actin.

Figure S3 – Tryptophan fluorescence of ATP binding to perinatal S1.

Figure S4 – ADP affinity for Peri S1 in the absence of actin.

Figure S5 – Multiple sequence alignment for the 8 myosin class II sequences analysed in this study.

**Supplementary Tables**

**Table S1. Experimentally measured constants for each isoform.** All measurements were made at 20° C unless otherwise stated.

| Step                             | Constant  | <i>Alpha</i> <sup>1</sup> | <i>Beta</i> <sup>1</sup> | <i>Beta</i> <sup>2</sup> | <i>Embryonic</i> <sup>3</sup> | <i>Perinatal</i> <sup>*</sup> | <i>Extraocula</i> <sup>4</sup> | <i>Iia</i> <sup>4</sup> | <i>Iib</i> <sup>4</sup> | <i>Iid</i> <sup>4</sup> |
|----------------------------------|---|---------------------------|--------------------------|--------------------------|-------------------------------|-------------------------------|--------------------------------|-------------------------|-------------------------|-------------------------|
|                                  |   | 100 mM KCl                | 100 mM KCl               | 25 mM KCl                | 25 mM KCl                     | 25 mM KCl                     | 100 mM KCl                     | 100 mM KCl              | 100 mM KCl              | 100 mM KCl              |
| <i>ATP binding to S1</i>         | Second order rate constant of ATP binding ( $\mu\text{M}^{-1}\text{s}^{-1}$ ) | 2.2 ± 0.1                 | 1.5 ± 0.1                | 5.8 ± 0.4                | 12.5 ± 1.9                    | 4.5 ± 1.0                     | 1.0 ± 0.2                      | 2.5 ± 0.5               | 1.7 ± 0.1               | 3.8 ± 0.2               |
|                                  | $k_H + k_{-H}$ ( $\text{s}^{-1}$ )  | 168 ± 28                  | 14                       | 91.2 ± 1.8               | 130 ± 3.4                     | 68.7 ± 1.9                    | 177 ± 8                        | 141 ± 28                | 169 ± 2                 | 195 ± 11                |
| <i>ATP binding to actin.S1</i>   | $K_T k_{+T^*}$ ( $\mu\text{M}^{-1}\text{s}^{-1}$ )                            | 2.5 ± 0.3                 | 1.6 ± 0.3                | 4.4 ± 0.3                | 9.4 ± 1.0                     | 5.9 ± 0.2                     | 3.2 ± 0.4                      | 1.7 ± 0.1               | 1.7 ± 0.3               | 1.7 ± 0.6               |
|                                  | $K_T$ ( $\mu\text{M}$ )   | 626 ± 143                 | 710 ± 65                 | 327.9 ± 53.3             | 84.3 ± 9.4                    | 146.5 ± 9                     | 360                            | 662                     | 715                     | 602                     |
|                                  | $k_{+T^*}$ ( $\text{s}^{-1}$ )  | 1500 ± 167                | 1081 ± 50                | 1543 ± 100               | 777 ± 17                      | 856 ± 26.9                    | 1152 ± 60                      | 1125 ± 78               | 1216 ± 283              | 1023 ± 215              |
| <i>ADP affinity for actin.S1</i> | $(K_{D^*+1})/K_D K_{D^*}$ ( $\mu\text{M}$ )                                   | 152 ± 25                  | 10 ± 3                   | 6.1 ± 0.7                | 14.3 ± 1.9                    | 69.4 ± 11.2                   | 352 ± 9                        | 80 ± 15                 | 54 ± 11                 | 118 ± 33                |
|                                  | $k_{+D^*}$ ( $\text{s}^{-1}$ )  | >1252                     | 64 ± 3                   | 58.7 ± 3.3               | 22.0 ± 1.8                    | >700                          | >1100                          | >1100                   | >1200                   | >1000                   |
| <i>ATPase (0-10 mM KCl)</i>      | $k_{\text{cat}}$ ( $\text{s}^{-1}$ )  | 18                        |                          | 5.94                     | 7.0 ± 0.105                   | **59.7 ± 4.9                  | **59.2 ± 5.7                   | **52.8 ± 4.4            | **86.1 ± 8.4            | **65.7 ± 2.1            |
|                                  | $K_{\text{app}}$ ( $\mu\text{M}$ )  | 67.8                      |                          | 39.55                    | 38.5 ± 2.4                    | 41.2 ± 3.7                    | 37.2 ± 4.5                     | 44.5 ± 5.6              | 14 ± 3.2                | 15.7 ± 1.3              |

<sup>1</sup> (6)

<sup>2</sup> (16)

<sup>3</sup> (8)

<sup>4</sup> (7)

\* This study

\*\* ATPase measurements conducted at 37 °C and 10 mM KCl (11)

**Table S2. Predicted Occupancy of the states during the ATPase cycle.**

| <i>Isoform</i>    | <i>[Actin]</i>            | <i>A·M</i> | <i>A·M·T</i> | <i>A·M·T</i> | <i>M·T</i> | <i>M·D·Pi</i> | <i>A·M·D·Pi</i> | <i>A·MD</i> | <i>A·M·D</i> |
|-------------------|---------------------------|------------|--------------|--------------|------------|---------------|-----------------|-------------|--------------|
| Alpha             |                           |            |              |              |            |               |                 |             |              |
| $K_{app} = 67.8$  | $K_{app}$                 | 0.0003     | 0.0051       | 0.021        | 0.20       | 0.40          | 0.28            | 0.090       | 0.0046       |
|                   | 3 $K_{app}$               | 0.0005     | 0.0078       | 0.048        | 0.18       | 0.20          | 0.42            | 0.14        | 0.0069       |
|                   | 20 $K_{app}$              | 0.0006     | 0.011        | 0.14         | 0.098      | 0.037         | 0.53            | 0.17        | 0.0087       |
|                   | 3 $K_{app} + \text{Load}$ | 0.0002     | 0.003        | 0.025        | 0.106      | 0.22          | 0.48            | 0.16        | 0.0026       |
| Beta              |                           |            |              |              |            |               |                 |             |              |
| $K_{app} = 39.55$ | $K_{app}$                 | 0.0002     | 0.002        | 0.014        | 0.28       | 0.45          | 0.19            | 0.068       | 0.003        |
|                   | 3 $K_{app}$               | 0.0032     | 0.0032       | 0.044        | 0.34       | 0.22          | 0.28            | 0.10        | 0.0045       |
|                   | 20 $K_{app}$              | 0.0004     | 0.005        | 0.21         | 0.26       | 0.042         | 0.36            | 0.13        | 0.0057       |
|                   | 3 $K_{app} + \text{Load}$ | 0.0001     | 0.0014       | 0.022        | 0.17       | 0.29          | 0.37            | 0.14        | 0.002        |
| Embryonic         |                           |            |              |              |            |               |                 |             |              |
| $K_{app} = 39$    | $K_{app}$                 | 0.00015    | 0.0046       | 0.0076       | 0.11       | 0.43          | 0.27            | 0.18        | 0.0035       |
|                   | 3 $K_{app}$               | 0.00022    | 0.0070       | 0.015        | 0.091      | 0.21          | 0.40            | 0.27        | 0.0053       |
|                   | 20 $K_{app}$              | 0.00029    | 0.0092       | 0.045        | 0.052      | 0.040         | 0.51            | 0.34        | 0.0067       |
|                   | 3 $K_{app} + \text{Load}$ | 0.00008    | 0.0025       | 0.0090       | 0.060      | 0.23          | 0.43            | 0.27        | 0.0019       |
| Perinatal         |                           |            |              |              |            |               |                 |             |              |
| $K_{app} = 20.6$  | $K_{app}$                 | 0.00080    | 0.018        | 0.019        | 0.24       | 0.47          | 0.22            | 0.022       | 0.015        |
|                   | 3 $K_{app}$               | 0.00120    | 0.027        | 0.040        | 0.32       | 0.23          | 0.32            | 0.032       | 0.022        |
|                   | 20 $K_{app}$              | 0.0016     | 0.035        | 0.14         | 0.30       | 0.044         | 0.41            | 0.041       | 0.028        |
|                   | 3 $K_{app} + \text{Load}$ | 0.00055    | 0.012        | 0.020        | 0.16       | 0.31          | 0.44            | 0.044       | 0.010        |
| Extraocular       |                           |            |              |              |            |               |                 |             |              |
| $K_{app} = 18.6$  | $K_{app}$                 | 0.00055    | 0.011        | 0.017        | 0.14       | 0.48          | 0.30            | 0.037       | 0.015        |

|                  |                    |          |        |          |       |       |      |       |        |
|------------------|--------------------|----------|--------|----------|-------|-------|------|-------|--------|
|                  | 3 $K_{app}$        | 0.00083  | 0.016  | 0.030    | 0.19  | 0.24  | 0.44 | 0.056 | 0.022  |
|                  | 20 $K_{app}$       | 0.0011   | 0.021  | 0.087961 | 0.18  | 0.045 | 0.56 | 0.071 | 0.028  |
|                  | 3 $K_{app}$ + Load | 0.000332 | 0.0066 | 0.013    | 0.087 | 0.28  | 0.54 | 0.067 | 0.0089 |
| IIa              |                    |          |        |          |       |       |      |       |        |
| $K_{app} = 22.5$ | $K_{app}$          | 0.0007   | 0.0099 | 0.016    | 0.15  | 0.48  | 0.30 | 0.033 | 0.013  |
|                  | 3 $K_{app}$        | 0.001    | 0.015  | 0.031    | 0.20  | 0.24  | 0.45 | 0.050 | 0.020  |
|                  | 20 $K_{app}$       | 0.0013   | 0.019  | 0.099    | 0.18  | 0.044 | 0.56 | 0.063 | 0.025  |
|                  | 3 $K_{app}$ + Load | 0.00042  | 0.0060 | 0.014    | 0.095 | 0.28  | 0.54 | 0.060 | 0.0080 |
| IIb              |                    |          |        |          |       |       |      |       |        |
| $K_{app} = 7$    | $K_{app}$          | 0.0011   | 0.015  | 0.021    | 0.19  | 0.48  | 0.25 | 0.022 | 0.022  |
|                  | 3 $K_{app}$        | 0.0017   | 0.022  | 0.035    | 0.26  | 0.23  | 0.38 | 0.033 | 0.032  |
|                  | 20 $K_{app}$       | 0.0022   | 0.029  | 0.075    | 0.29  | 0.043 | 0.48 | 0.042 | 0.041  |
|                  | 3 $K_{app}$ + Load | 0.00075  | 0.0098 | 0.017    | 0.13  | 0.29  | 0.49 | 0.043 | 0.014  |
| IIc              |                    |          |        |          |       |       |      |       |        |
| $K_{app} = 8$    | $K_{app}$          | 0.00084  | 0.014  | 0.017    | 0.14  | 0.48  | 0.32 | 0.017 | 0.016  |
|                  | 3 $K_{app}$        | 0.0013   | 0.020  | 0.028    | 0.19  | 0.24  | 0.4  | 0.025 | 0.025  |
|                  | 20 $K_{app}$       | 0.0016   | 0.026  | 0.059    | 0.21  | 0.043 | 0.60 | 0.032 | 0.031  |
|                  | 3 $K_{app}$ + Load | 0.00051  | 0.0082 | 0.013    | 0.093 | 0.28  | 0.57 | 0.030 | 0.0099 |

**Table S3. Resolution matrices for the embryonic and perinatal isoforms.**

| Embryonic | Predicted value          | $K_A$       | $k_{pi}$    | $k_T$            | $K_H$       |
|-----------|--------------------------|-------------|-------------|------------------|-------------|
| $K_A$     | 0.0164                   | <b>0.99</b> | 0.0047      | -0.00024         | -0.0021     |
| $k_{pi}$  | 13.1 (s <sup>-1</sup> )  | 0.0047      | <b>0.98</b> | 0.00025          | 0.081       |
| $k_T$     | 851.5 (s <sup>-1</sup> ) | 0.00024     | 0.00025     | <b>0.0000032</b> | -0.00001    |
| $K_H$     | 6.34                     | 0.0021      | 0.082       | -0.000011        | <b>0.88</b> |
| $K_{AH}$  | 43.6                     | 0.034       | 0.090       | 0.000067         | -0.45       |

| Perinatal | Predicted value          | $K_A$       | $k_{pi}$    | $k_T$            | $K_H$       |
|-----------|--------------------------|-------------|-------------|------------------|-------------|
| $K_A$     | 0.019                    | <b>0.99</b> | 0.000030    | -0.0013          | -0.000014   |
| $k_{pi}$  | 89.9 (s <sup>-1</sup> )  | 0.000030    | <b>0.99</b> | 0.0014           | 0.00011     |
| $k_T$     | 584.7 (s <sup>-1</sup> ) | -0.0013     | 0.0014      | <b>0.0000036</b> | -0.000004   |
| $K_H$     | 15.6                     | -0.000014   | 0.00011     | -0.0000037       | <b>0.99</b> |

**Table S4. Sensitivity analysis; Percentage change of the predicted constants induced by a change of +20% or -20% to one of the six fitted parameters for the embryonic isoform.**

Red numbers indicate the % change imposed in each set, Blue/yellow background colors indicate modelled constants that decrease (blue) or increase (yellow) by > 10% (pale shade) or 20% (dark).

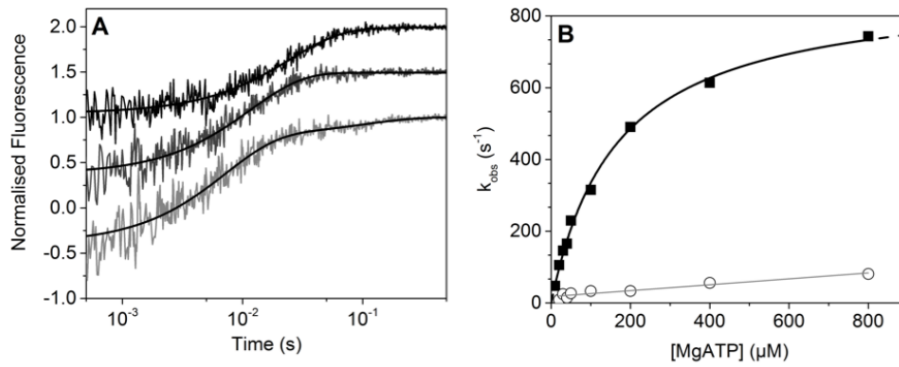
|                                   | Units              | Estimate | $K_{D^*+20\%}$ | $K_{D^*-20\%}$ | $k_{D^*+20\%}$ | $k_{D^*-20\%}$ | $K_{T^*+20\%}$ | $K_{T^*-20\%}$ | $k_{T^*+20\%}$ | $k_{T^*-20\%}$ | $k_{-D+20\%}$ | $k_{-D-20\%}$ | $k_H+20\%$ | $k_H-20\%$ |
|-----------------------------------|--------------------|----------|----------------|----------------|----------------|----------------|----------------|----------------|----------------|----------------|---------------|---------------|------------|------------|
| <b>Equilibrium Rate Constants</b> |                    |          |                |                |                |                |                |                |                |                |               |               |            |            |
| $K_A$                             | $\mu M^{-1}$       | 0.02     | 10.37          | -16.46         | 9.76           | -14.63         | 0.00           | -0.61          | 0.00           | -0.61          | 1.22          | -1.83         | 0.61       | -1.22      |
| $K_{D^*}$                         |                    | 0.20     | 20.00          | -20.00         | 0.00           | 0.00           | 0.00           | 0.00           | 0.00           | 0.00           | 0.00          | 0.00          | 0.00       | 0.00       |
| $K_D$                             | ( $\mu M$ )        | 71.43    | 0.00           | 0.00           | 0.00           | 0.00           | 0.00           | 0.00           | 0.00           | 0.00           | -16.67        | 25.00         | 0.00       | 0.00       |
| $K_{T^*}$                         |                    | 77.70    | 0.00           | 0.00           | 0.00           | 0.00           | 20.00          | -20.00         | 0.00           | 0.00           | 0.00          | 0.00          | 0.00       | 0.00       |
| $K_H$                             |                    | 6.34     | 3.38           | -5.38          | 4.50           | -1.38          | 0.99           | -0.41          | 0.14           | -0.22          | -0.45         | -0.98         | 20.00      | -20.00     |
| $K_{AH}$                          |                    | 43.62    | 3.43           | -5.44          | 4.62           | -1.26          | 1.10           | -0.10          | 0.14           | -0.22          | -0.48         | -1.00         | 21.23      | -20.82     |
| <b>Forward Rate Constant</b>      |                    |          |                |                |                |                |                |                |                |                |               |               |            |            |
| $k_A$                             | $\mu M^{-1}s^{-1}$ | 16.40    | 10.37          | -16.46         | 9.76           | -14.63         | 0.00           | -0.61          | 0.00           | -0.61          | 1.22          | -1.83         | 0.61       | -1.22      |
| $k_{P_i}$                         | $s^{-1}$           | 13.10    | -10.69         | 19.85          | -9.92          | 16.79          | -0.38          | 0.00           | -0.76          | 0.00           | -1.53         | 1.53          | -3.05      | 4.58       |
| $k_{D^*}$                         | $s^{-1}$           | 22.00    | 20.00          | -20.00         | 20.00          | -20.00         | 0.00           | 0.00           | 0.00           | 0.00           | 0.00          | 0.00          | 0.00       | 0.00       |
| $k_T$                             | $\mu M^{-1}s^{-1}$ | 10.13    | -0.04          | -0.01          | -0.02          | -0.08          | 0.02           | -0.01          | 0.00           | 0.00           | -0.01         | -0.01         | -0.10      | -0.04      |
| $k_{T^*}$                         | $s^{-1}$           | 777.00   | 0.00           | 0.00           | 0.00           | 0.00           | 20.00          | -20.00         | 20.00          | -20.00         | 0.00          | 0.00          | 0.00       | 0.00       |
| $k_H$                             | $s^{-1}$           | 82.38    | 3.38           | -5.38          | 4.50           | -1.38          | 0.99           | -0.41          | 0.14           | -0.22          | -0.45         | -0.98         | 20.00      | -20.00     |
| $k_{AH}$                          | $s^{-1}$           | 87.24    | 3.43           | -5.44          | 4.62           | -1.26          | 1.10           | -0.10          | 0.14           | -0.22          | -0.48         | -1.00         | 21.23      | -20.82     |
| <b>Backward Rate Constants</b>    |                    |          |                |                |                |                |                |                |                |                |               |               |            |            |
| $k_{P_i}$                         | $mM^{-1}s^{-1}$    | 0.159    | -10.69         | 19.85          | -9.92          | 16.79          | -0.38          | 0.00           | -0.76          | 0.00           | -1.53         | 1.53          | -3.05      | 4.58       |
| $k_{-D}$                          | $\mu M^{-1}s^{-1}$ | 14.00    | 0.00           | 0.00           | 0.00           | 0.00           | 0.00           | 0.00           | 0.00           | 0.00           | 20.00         | -20.00        | 0.00       | 0.00       |
| $k_{-T}$                          | $s^{-1}$           | 851.50   | -0.04          | -0.01          | -0.02          | -0.08          | 0.02           | -0.01          | 0.00           | 0.00           | -0.01         | -0.01         | -0.10      | -0.04      |
| $k_{-T^*}$                        | $s^{-1}$           | 10.00    | 0.00           | 0.00           | 0.00           | 0.00           | 0.00           | 0.00           | 20.00          | -20.00         | 0.00          | 0.00          | 0.00       | 0.00       |

**Table S5. The effect of increasing the fast isomerisation forward and backward rate constants by a factor of 2 on the occupancies of states in the cycle.**

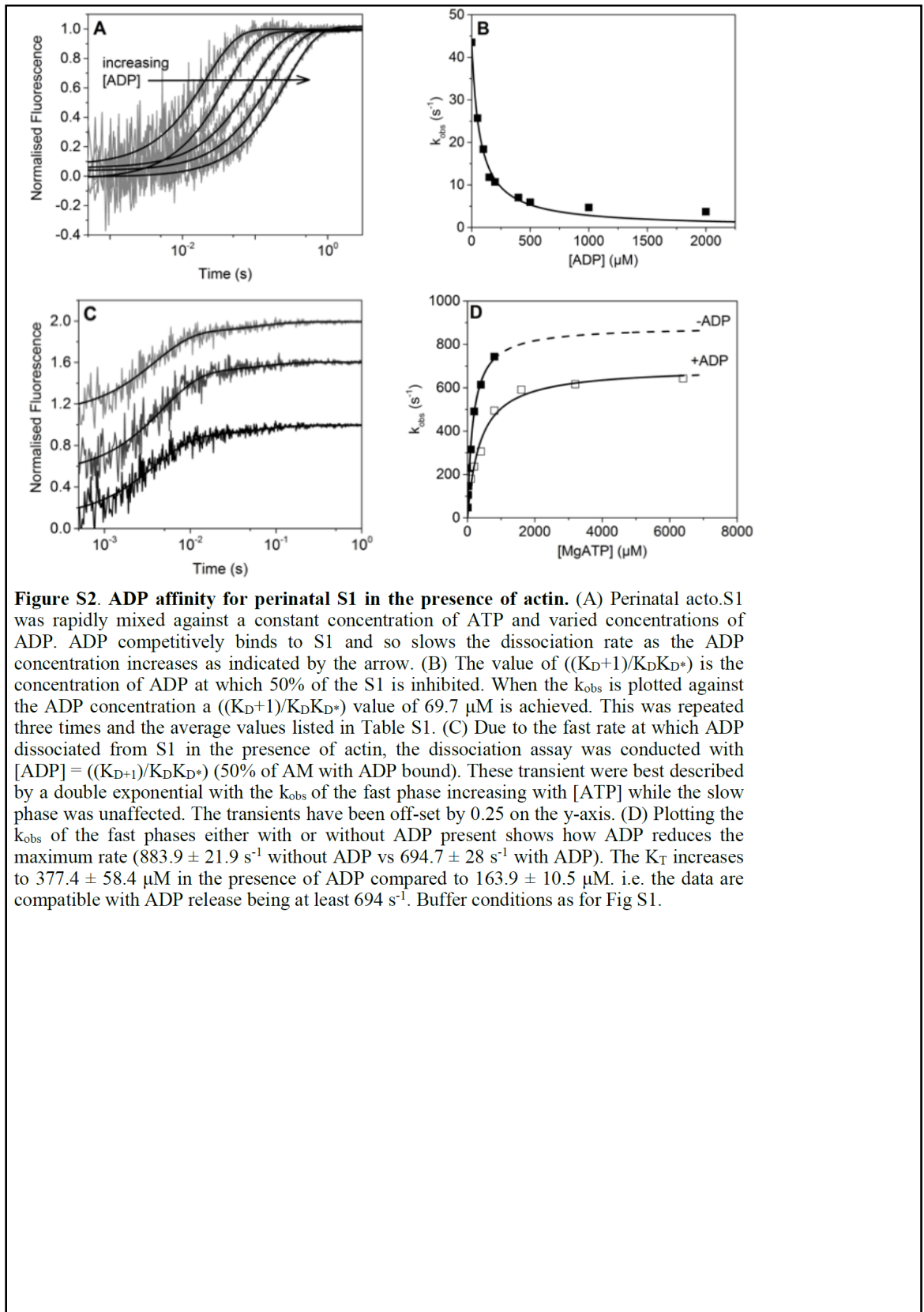
| [Actin]                       | Isoform | Step changed      | M·DPi | A-M·D·Pi | A·M·D   | A·M·D   | A·M     | A·M·T   | A-M·T   | A-M·T  | ATPase (s <sup>-1</sup> ) | Velocity (μm s <sup>-1</sup> ) | Duty Ratio |
|-------------------------------|---------|-------------------|-------|----------|---------|---------|---------|---------|---------|--------|---------------------------|--------------------------------|------------|
| 3K <sub>app</sub>             | IIb     | None              | 0.23  | 0.38     | 0.033   | 0.032   | 0.0017  | 0.022   | 0.035   | 0.26   | 32.47                     | 1.808                          | 0.090      |
|                               |         | 2k <sub>D</sub>   | 0.238 | 0.384    | 0.0033  | 0.0165  | 0.00174 | 0.0229  | 0.0357  | 0.267  | 33.01                     | 2.217                          | 0.074      |
|                               |         | 2k <sub>T**</sub> | 0.235 | 0.377    | 0.0033  | 0.0324  | 0.00171 | 0.0224  | 0.0214  | 0.277  | 32.43                     | 1.81                           | 0.090      |
|                               |         | 2x both           | 0.239 | 0.383    | 0.033   | 0.0164  | 0.00174 | 0.0227  | 0.0217  | 0.282  | 32.98                     | 2.22                           | 0.074      |
| 3K <sub>app</sub> + 5 pN load | IIb     | None              | 0.29  | 0.49     | 0.043   | 0.014   | 0.00075 | 0.0098  | 0.017   | 0.13   | 14.12                     | 1.049                          | 0.067      |
|                               |         | 2k <sub>D</sub>   | 0.295 | 0.496    | 0.00428 | 0.00711 | 0.00033 | 0.00986 | 0.0169  | 0.132  | 14.23                     | 1.183                          | 0.060      |
|                               |         | 2k <sub>T**</sub> | 0.293 | 0.492    | 0.00426 | 0.0141  | 0.00033 | 0.00974 | 0.0102  | 0.137  | 14.11                     | 1.056                          | 0.067      |
|                               |         | 2x both           | 0.295 | 0.496    | 0.0428  | 0.00711 | 0.00033 | 0.00981 | 0.0103  | 0.138  | 14.22                     | 1.184                          | 0.060      |
| 3K <sub>app</sub>             | IIId    | None              | 0.24  | 0.474    | 0.025   | 0.025   | 0.0013  | 0.020   | 0.028   | 0.19   | 24.77                     | 1.728                          | 0.072      |
|                               |         | 2k <sub>D</sub>   | 0.238 | 0.480    | 0.0253  | 0.0125  | 0.00129 | 0.0207  | 0.0279  | 0.194  | 25.09                     | 2.10                           | 0.060      |
|                               |         | 2k <sub>T**</sub> | 0.236 | 0.473    | 0.0252  | 0.0248  | 0.00127 | 0.0203  | 0.0169  | 0.203  | 24.75                     | 1.729                          | 0.072      |
|                               |         | 2x both           | 0.239 | 0.479    | 0.0253  | 0.0125  | 0.00128 | 0.0206  | 0.0171  | 0.205  | 25.07                     | 2.10                           | 0.060      |
| 3K <sub>app</sub> + 5 pN load | IIId    | None              | 0.28  | 0.57     | 0.030   | 0.0099  | 0.00051 | 0.0082  | 0.013   | 0.093  | 9.93                      | 1.021                          | 0.049      |
|                               |         | 2k <sub>D</sub>   | 0.277 | 0.573    | 0.0300  | 0.0050  | 0.00051 | 0.00823 | 0.0128  | 0.0936 | 9.98                      | 1.140                          | 0.044      |
|                               |         | 2k <sub>T**</sub> | 0.276 | 0.570    | 0.0300  | 0.0099  | 0.00051 | 0.00815 | 0.00786 | 0.0982 | 9.93                      | 1.022                          | 0.049      |
|                               |         | 2x both           | 0.277 | 0.573    | 0.0300  | 0.0050  | 0.00051 | 0.00819 | 0.00790 | 0.0987 | 9.98                      | 1.141                          | 0.044      |

Grey background highlights any value that changes by > 10%. Note these are all very low occupancy states that have little consequence for the overall ATPase rates or on the occupancy of most other states. Increases in k<sub>D</sub> do cause a ~15-20% increase in V<sub>0</sub> and a ~10% decrease in DR.





**Figure S1. ATP induced dissociation of Perinatal S1 from pyrene-labelled actin.** (A) Example transients of ATP induced dissociation of S1 from pyrene-labelled actin. Transients have been off-set on the y-axis for clarity. The concentration of S1.pyrene-labelled actin complex was kept constant at 50 nM while the ATP concentration was increased. The example transients here show 10, 20 and 30 μM ATP. At ATP concentrations above 10 μM the transients were best described by a double exponential. The  $k_{obs}$  of both phases of the transient were plotted in B. (B) When the  $k_{obs}$  is plotted against the ATP concentration the fast phase had a hyperbolic dependence giving a maximum  $k_{obs} = k_{+T^*}$  of  $883.9 \pm 21.9 \text{ s}^{-1}$ , the concentration for half-maximum  $k_{obs} = K_T$  of  $163.9 \pm 10.5 \text{ μM}$ , and the second-order rate constant  $K_T k_{T^*}$  of  $5.4 \pm 0.24 \text{ μM}$ . These were repeated three times and the average is summarised in Table S1. Measurements were conducted with 25 mM KCl, 5 mM MgCl<sub>2</sub>, 20 mM MOPS, pH 7.0 at 20 °C.



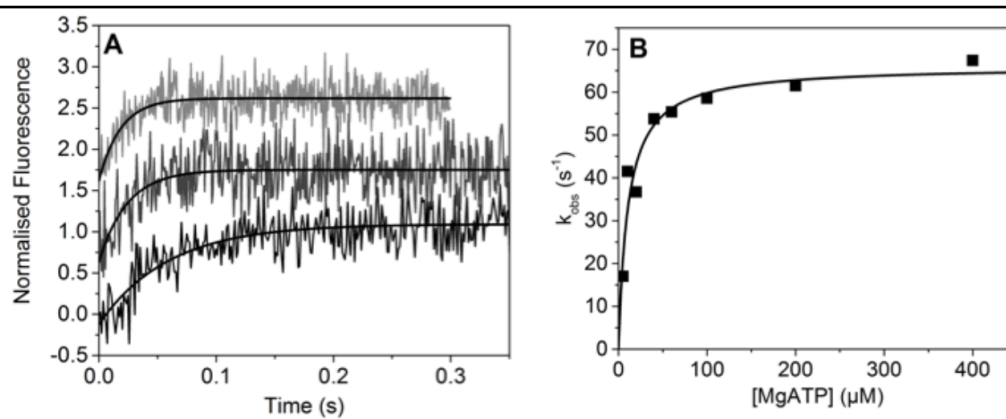


**Figure S3. Tryptophan fluorescence of ATP binding to perinatal S1.** (A) Example transients of the increase in intrinsic tryptophan fluorescence upon the binding of ATP to perinatal S1. This gave a relatively small  $\Delta f$  (2.5% - 4%) and were best described by a single exponential. (B) When the  $k_{obs}$  is plotted against the ATP concentration the data can be best described by a hyperbola which yields a maximum rate  $k_{obs} = k_H + k_{-H}$  of  $66.1 \pm 3.4 \text{ s}^{-1}$ , the concentration of half-maximum  $k_{obs} = K_{50\%}$  of  $10.6 \pm 2.6 \text{ } \mu\text{M}$ , and the second-order rate constant rate constant of  $6.2 \pm 1.3 \text{ } \mu\text{M}^{-1} \text{ s}^{-1}$ . Buffer conditions as for Fig S1.

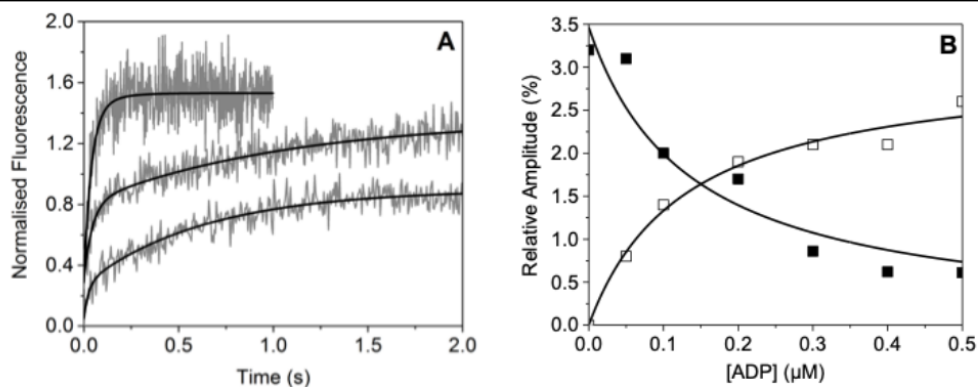


**Figure S4. ADP affinity for Peri S1 in the absence of actin.** (A) S1 was incubated with varied concentrations of ADP (0-0.5  $\mu\text{M}$  after mixing) and rapidly mixed with ATP. In the absence of ADP the transient was best described by a single exponential, whereas when ADP was added the transients could be described by a double exponential. The  $k_{\text{obs}}$  of these phases did not change as the [ADP] was varied however the fluorescence amplitudes did. (B) Relative amplitudes of the fast phase (closed squares) and slow phase (open squares) when plotted against the [ADP] shows two hyperbolic dependencies. The half-maximum fluorescence change = 0.15  $\mu\text{M}$  and 0.06  $\mu\text{M}$  for the fast and slow phase respectively. This gave an average ADP affinity of  $0.105 \pm 0.045 \mu\text{M}$ . The  $k_{\text{obs}}$  of the slow phase represents the ADP release rate constant from S1 =  $1.17 \pm 0.1 \text{ s}^{-1}$ . The averages of three repeats are summarised in Table S1. Buffer conditions as for Fig S1.



## **4. Cardiac/slow muscle contraction velocity has evolved to match heart rate with body size through variation in $\beta$ -cardiac myosin sequence.**

**Chloe A. Johnson\***, Jake E. McGreig\*, Carlos D. Vera, Daniel P. Mulvihill, Martin Ridout, Leslie A. Leinwand, Mark N. Wass, Michael A. Geeves

\* Contributed equally

E-life, under review

### **4.1 Context of research**

Whilst the work in Chapter 3 identified how myosin class II isoforms adapt their mechanochemical cycle for different functions, it is still not fully understood how these differences arise from the sequence changes of the isoforms. As shown in Table 1.2, the isoforms have a high sequence homology. To explore how sequence changes in myosin can contribute to different properties of the muscle in which it is found, McGreig et al investigated the relationship between muscle contraction and body mass (McGreig et al. 2019). This is a well-documented relationship; the larger the species, the slower muscle contraction. If velocity of contraction is matched to body mass in mammals, then there may exist changes in the sequence of myosin to tune its properties to the species size and thus give rise to alterations to the physiology of the muscle. The sequences of 12 myosin class II isoforms from 65 mammals (ranging from 0.006 – 10,000 kg) were examined, and the authors proposed that MyHC- $\beta$ , MyHC-IIa and MyHC-IIb have adapted to changes in body mass. The data in the following manuscript continues this work to focus on the MyHC- $\beta$  isoform, to investigate the relationship between sequence and velocity of contraction.

### **4.2 Aims of research**

For the MyHC- $\beta$  isoform, the rate of ADP release from an actin.myosin complex is predicted to limit contraction velocity (as described in Chapter 1.3.3). We therefore set out to identify if the sequence changes found within the motor domain of MyHC- $\beta$  could contribute to the slower contraction observed in larger mammals by a slowing of ADP release, and hence

velocity. Using a combination of bioinformatics analysis and biochemical characterisation, we set out to identify the sequence changes that drive a change in the rate of ADP-release. We identified 14 amino acid changes in the  $\beta$ -myosin motor domain with a strong association with species size. Of these 14 sequence changes, 9 differ between the well-characterised human and rat MyHC- $\beta$ . We introduced these 9 amino acid changes into the human MyHC- $\beta$ , and used stopped-flow spectroscopy and *In vitro* motility assays to experimentally test the computational predictions. This approach aims to address how small sequence variations, as seen between myosin class II isoforms, can alter protein function. This has wider implications for our understanding of evolution and the role of genetic variation.

#### **4.3 Contribution to publication**

Jake McGreig, with supervision from Dr Mark Wass, performed computational research and bioinformatics analysis with suggestions from Professor Michael Geeves and myself. Professor Geeves and I designed an initial outline for a study which biochemically tests the predictions from the computational analysis. When visiting Professor Leslie Leinwand's laboratory to gain experience in producing recombinant myosin, I held extensive discussions with both Leslie and members of her lab to gain their support in producing a chimera protein using the C2C12 system Leslie's lab specialises in. With the help of Professor Daniel Mulvihill, I planned and performed the cloning strategy of the chimera. With Dr Stephen Langers in Professor Leslie Leinwand's group, I produced the adenovirus containing the chimera gene for transfecting C2C12 cells. Dr Carlos Vera grew the transfected C2C12 cells expressing both MyHC- $\beta$  and the chimera protein, and sent to me for purification. I purified the two recombinant proteins, as well as the endogenous rat soleus MyHC- $\beta$ . I then designed, performed and analysed the biochemical characterisation of all of the proteins. Professor Geeves, Jake McGreig, Dr Wass and myself wrote the first draft of the manuscript, which was reviewed by all authors.

**4.4 Publication.** The manuscript in the format submitted to E-Life is below.

Cardiac/slow muscle contraction velocity is matched to heart rate and body size through variation in  $\beta$ -myosin sequence.

**Chloe A. Johnson<sup>1\*</sup>, Jake E. McGreig<sup>1\*</sup>, Carlos D. Vera<sup>2</sup>, Daniel P. Mulvihill<sup>1</sup>, Martin Ridout<sup>3</sup>, Leslie A. Leinwand<sup>2</sup>, Mark N. Wass<sup>1</sup>, Michael A. Geeves<sup>1</sup>**

<sup>1</sup>School of Biosciences, University of Kent, Canterbury, UK

<sup>2</sup>BioFrontiers Institute and Department of Molecular, Cellular and Developmental Biology, University of Colorado Boulder, Colorado, USA

<sup>3</sup>School of Mathematics, Statistics and Actuarial Science, University of Kent, Canterbury, UK

\* Contributed equally to this work.

Key words: evolution, motility, muscle

Address for correspondence:

Prof M.A.Geeves

School of Biosciences,

University of Kent,

Canterbury

CT1 7NJ

UK

[m.a.geeves@kent.ac.uk](mailto:m.a.geeves@kent.ac.uk)

tel 44 1227827597

Dr M.N. Wass

School of Biosciences

University of Kent,

Canterbury

CT1 7NJ

UK

[m.n.wass@kent.ac.uk](mailto:m.n.wass@kent.ac.uk)

tel 44 1227 827626

Prof L.A. Leinwand

BioFrontiers Institute and

Department of Molecular, Cellular

and Developmental Biology,

University of Colorado Boulder,

Boulder CO 80309 USA

[leslie.leinwand@colorado.edu](mailto:leslie.leinwand@colorado.edu)



## **Abstract**

Heart rate and the maximum velocity of contraction of striated muscle are inversely related to species size. As mammals evolve to different sizes, adaptations are required such as slower contracting heart and skeletal muscles. Analysis of the motor domain of  $\beta$ -myosin from 67 mammals from two clades identifies 14 sites, out of 800, strongly associated with body mass ( $p < 0.01$ ) but not with the clade ( $p > 0.05$ ). Nine of these sites were mutated in the human  $\beta$ -myosin to make it resemble the rat sequence. Biochemical analysis revealed that the rat-human  $\beta$ -myosin chimera functioned like the native rat myosin with a two fold increase in both motility and in the rate of ADP release from the actin-myosin cross-bridge (the step that limits contraction velocity). Both clades use the same small set of amino acids to adjust contraction velocity, suggesting a limited number of ways in which velocity can be manipulated.

## **Introduction**

Proteins adapt and evolve over long time periods tuning their function to the specific needs of the organisms in which they are expressed. Understanding how proteins adapt to different physiology is one of the challenges of current molecular and structural biology. One approach is to consider a protein expressed as different isoforms within a species (paralogues) or in different species (orthologues) where adaptation has taken place. Such a study is easier if a close link can be established between different phenotypes in the organism for which a specific protein function is needed. Striated-muscle myosin motors represent a protein family where such evolutionary relationships can be explored. The maximum contraction velocity of a muscle,  $V_0$ , is a key attribute of muscle contraction<sup>1,2</sup>. It is a parameter which contributes to the Force-Velocity relationship of a muscle, the power output (force x velocity) and the velocity at which power and efficiency are maximum. These properties can be expected to be under selective pressure. The maximum shortening velocity of a muscle is a property of the myosin isoform expressed in the muscle<sup>3</sup>. The maximum shortening velocity varies more than-ten fold among both paralogues and orthologues of myosin. In contrast, the maximum force a myosin can generate varies little between myosin isoforms. Maximum velocity is therefore a central parameter that defines both the Force-Velocity relationship, power output and the efficiency of muscle contraction. Note larger forces can be generated by increasing muscle mass (e.g. through exercise) but maximum velocity is an intrinsic property of the muscle and the myosin isoform present.

In mammals, there are 10 different striated muscle myosins, each expressed from a different gene; many of which have been shown to have distinct biochemical and mechanical properties<sup>3-6</sup>. Larger mammals tend to have slower contracting muscles than

small mammals where the movement of a larger mass results in slower velocity. This phenomenon is well-established in heart muscle where heart rate is inversely related to body mass for a wide range of species<sup>7</sup>. Since velocity of contraction is matched to the size of the animal expressing the myosin, then there should be changes in the myosin sequence to tune the myosin properties to the species size and correspondingly, to the physiology of the muscle. In a recent study we tested the hypothesis that muscle myosin-II isoforms from mammals would have adaptations in protein sequence associated with mean body mass<sup>8</sup>. In this study, of ~730 sequences from 12 myosin-II isoforms from an average of 65 mammalian species, there was a strong correlation of the number of sequence changes with differences in species mass. The correlation was strongest in adult striated muscle myosins IIa and IIb and  $\beta$ .  $\beta$ -myosin is found in the heart and in slow Type I muscle fibers. Here we examine in greater detail the sequence differences within the mammalian  $\beta$ -myosin to establish the relationship between sequence and velocity of contraction.

The contractile properties of mammalian muscles have been widely studied but detailed mechanical and biochemical studies have been completed on only a few species and myosin isoforms. Such data are available for Type 1/ $\beta$ -cardiac/slow muscle fibres from four species (see Fig 1). Each of these muscles expresses only the  $\beta$ -myosin isoform (MYH7), and each species has a characteristic contraction velocity that varies approximately five-fold across the set of four muscles. Moreover, it is well established for the  $\beta$ -myosin isoform that the contraction velocity is limited by how fast ADP escapes from the actin.myosin cross-bridge after the working stroke is completed<sup>9</sup>. Data in Fig 1 show that like velocity, the ADP release rate constant differs 4-5 fold across the set of four myosins. Furthermore, the measured rate constant for ADP release from the actin.myosin complex, measured using the purified  $\beta$ -myosin isoform, is exactly that predicted to limit the contraction velocity (based on the detachment limited model of contraction (see Fig 1 legend)<sup>9-11</sup>. It is therefore expected that this set of myosins will have changes in the amino acid sequence that alter the ADP release rate and hence contraction velocity.

Examining the sequences of the 800 amino acid motor domains of the four  $\beta$ -myosins in Fig 1 show them to be 96% identical which means there are 49 sequence differences among the four, with 34 differences between rat and human. These differences in sequence are scattered throughout the motor domain (see Fig 2 and alignment in Fig S1). It seems likely that groups of amino acids and not a single amino acid change determine the functional differences between the  $\beta$ -myosins. If the correlation between body size and contraction velocity is a general phenomenon amongst mammals, as is seen for resting

heart rates<sup>7</sup>, then a bioinformatics study of  $\beta$ -myosin sequences would be a way to identify which sequence changes correlate with size. We hypothesised that the variation of  $\beta$ -myosin contraction velocity (and rate of ADP release from the cross bridge) with the size of the mammal is due to a subset of the sequence changes observed for different mammals, and that these tune myosin velocity to that appropriate for the size of species. Here, we examine a set of 67 mammalian  $\beta$ -myosin sequences<sup>8</sup> using a bioinformatics approach to identify a group of 12 amino acids which have the strongest association with the size of the mammal. Of these 12 amino acids, nine differ between human and rat  $\beta$ -myosin and we test our hypothesis through the construction and subsequent biochemical characterisation of a rat-human  $\beta$ -myosin chimera (hereafter referred to as chimera).

## Results

The alignment of the  $\beta$ -myosin sequences from four mammals (Fig 2 & Fig S1) demonstrates that while the sequences are highly conserved, the 49 sites of variation among the species are scattered throughout the motor domain. High levels of variation are found in the N-terminal domain (1-60) and near the surface loops, Loop 1 (near residue 210) and Loop 2 (near 630). These loops are known to be hypervariable across the larger myosin family<sup>23</sup>. The broad distribution of the sequence variants means that an experimental approach to define which residue changes are linked to the change in ADP release (and hence velocity of contraction) is too complex to consider. Instead, we used a bioinformatics-based approach to identify the residues most likely to be linked to the change in velocity of contraction.

### *Distinguishing between variation due to clade and body mass:*

We analysed 67 complete sequences of the  $\beta$ -myosin motor domains from species ranging in size from 7g (Brandt's bat, *Myotis brandtii*) to 42,000 kg (sperm whale, *Physeter catodon*). Of these, about half were Euarchontoglires (32, e.g. rodents and primates) and half were Laurasiatheria (30, e.g. bats, ungulates, cetaceans). We used this set of sequences to distinguish between sequence changes that were primarily associated with the clade versus those that correlated with the size of the animal (see Methods). A total of 171 sites were identified where a sequence change occurred. At the majority of these positions, variation occurred in a small number of species and is unlikely to be associated with changes in function relevant to body mass, so 119 positions where a sequence change was present in less than 10% of the species were excluded. This included 84 sites where

a change occurred in only one species, while changes in two species occurred at 20 sites and in three species at four sites.

The remaining 52 sites of variation were analysed to distinguish between changes that correlated with clade and those that correlated with body mass (as illustrated in Fig 3 for four sites with the remaining plots in Supp Info – Fig S2). In most cases, only two residues were observed at each specific site; in the small number of cases (11 of 52) with multiple amino acids, only the two most frequent residues were considered. The identity of the two most frequent amino acids were coded as 0 and 1 and a logistic regression model was fitted with  $\log(\text{mass})$  as the explanatory variable (Fig 3, Fig S2; see methods) to model the transition between residues. Data for four sites are presented in Fig 3 and of the sites shown, two had a strong correlation with species body mass (the amino acid common in small mammals is given first P343S, I349P;  $p_{\text{adj}} \leq 0.01$ . Note the adjusted one percent significance threshold is  $p = 9.50 \times 10^{-4}$  and the 5% significance threshold is  $p = 9.62 \times 10^{-4}$ .  $p_{\text{adj}}$  will be used to indicate the adjusted significance threshold). Each of the positions has a distinct midpoint mass for the transition between the two amino acids (see below). In contrast, I125V has a low association with mass ( $p = 0.03$ ) and M77L has an intermediate association ( $p = 9.50 \times 10^{-4}$ ), however both M77L and V125I have a strong association with the clade (Fig 4); L77 and I125 are found almost exclusively in *Laurasiatheria*.

Overall, only 12 sites had a very strong association with clade ( $p_{\text{adj}} \leq 0.01$ ) and a further two were significant at the five percent level ( $p_{\text{adj}} \leq 0.05$ ; Fig 4A). Some of these residues occur in two groups; one group of four in the N terminal region below residue 135 (4, 11, 52, 77, 110, 125) and four residues near surface loop 2 (610, 616, 627, 629). The remaining four are at D208E, E509T, T585I and I684M. Twenty positions were strongly associated ( $p_{\text{adj}} \leq 0.01$ ) with body mass and a further four were significantly associated at  $p_{\text{adj}} \leq 0.05$  (Fig 4B). Nine positions were associated with both clade and body mass (Fig 3C), which is likely to represent that the very largest mammals (body mass > 500 kg) in the data set are all *Laurasiatheria* (Fig S5).

Twelve of the 24 sites associated with body mass occur in the known hypervariable regions, four in the N terminal region (11, 15, 52, 65, bold **residues** also occur in the clade list), one in loop 1 (D208E), and a further six occur in or near loop 2 (607, 610, 616, 627, 629, 631) and one at I684M. The remaining 12 sites (Table 2) group into three sets of four; most with  $p_{\text{adj}} \leq 0.01$  (coloured in Fig 4 & 5). Comparing the strength of association between clade and body mass, these 12 sites, are strongly associated with body mass but not with clade (Fig 4C). Hence, we propose that these 12 positions are likely to be important in

determining the  $\beta$ -myosin velocity of contraction. At eight of the twelve positions only two amino acids are observed, one position contains three amino acids, although the third is only present once (residue 366). Multiple amino acids (4-7) were observed at the remaining three positions. For two of the positions, 421 and 424, this reflects a subset of the species from one clade having an alternate amino acid in some of the larger species (see Sup Fig S4).

The first group of residues is in a region 331-371 (Orange in Fig 4 and 5) adjacent to the exon 7 region of *Drosophila* myosin II (and the “linker region”). This region is equivalent to one of the four exons in the single myosin II gene of *Drosophila* which are alternately spliced to generate all isoforms of myosin II in *Drosophila* <sup>24</sup>. We have previously shown <sup>25</sup> that the alternatively spliced forms of this region alter ADP release in the *Drosophila* myosin. The second set (426-439; Magenta in Fig 4 and Fig 5) is in a long helix (Helix-O) in the upper 50 kDa domain that links an actin binding site (the myopathy loop) to the nucleotide binding pocket (via switch 2). The third region (560 - 587; Red in Fig 4 and Fig 5) is in the lower 50 kDa domain and lies close to loop 3, an actin binding site in the lower 50kDa domain.

*Experimental testing of the computational predictions:*

We have previously expressed the motor domain of human  $\beta$ -myosin in mouse C<sub>2</sub>C<sub>12</sub> muscle cells and isolated the protein using His tags attached to the co-expressed human light chain. This is currently the only way to express mammalian striated muscle myosin motors but is complex and time consuming and yields just a few mg of protein <sup>6,26,27</sup>. To test the hypothesis that the highlighted group of 12 residues are responsible for a significant part of the adjustment of ADP release rate constant, we generated a chimeric human-rat  $\beta$ -myosin motor domain where the nine positions (of the 12) that vary between human and rat were replaced with the amino acid present in rat (A326S, S343P, L366Q, I421A, T424I, A430S, R434K, F553Y, P573Q – human residue number and amino acid listed first). The other three positions are the same in rat and human (354, 576 & 587). At residue 421 we replaced Ile with Ala as present in rat, although Ser is present in most of the smallest mammals (See Fig 6).

As shown in Fig 1, the velocity of contraction for  $\beta$  cardiac/Type I slow muscle fibres in rat and humans differ by a factor of ~4. Given that these residues have a range of transition masses (see Fig 5 & 6) the hypothesis is that each of these nine residues will contribute a fraction of the difference between the rat and human  $\beta$ -myosin ADP release rate constant

and hence, velocity. With all nine residues changed, our prediction is that the differences in the rate constant should be large enough to be easily detectable.

The S1 fragment of human  $\beta$ -myosin and the chimera were expressed in C<sub>2</sub>C<sub>12</sub> cells and purified with the human essential light chain attached. Few details of the kinetic characterisation of the rat  $\beta$ -myosin S1 have been published<sup>28</sup>. The rat  $\beta$ -myosin S1 was therefore purified from rat soleus muscle to use as a comparator for the chimera. The supplementary data include the SDS PAGE of all three proteins used in this study and demonstrates that all three proteins are pure and contain the appropriate light chains (Fig S5).

As a test of the behaviour of the chimeric protein, the ATP-induced dissociation of the chimera from pyrene labelled actin was monitored and compared to the recombinant human and the native rat S1. A typical transient is presented inset in Fig 7B and the observed amplitude of the signal change was the same for all three proteins. The similarity of observed amplitudes of the pyrene signal changes for the chimera, human and native rat proteins indicates that the chimera binds actin and releases it on ATP binding as for the human and rat S1. This is consistent with the chimera being a fully folded and active protein. A plot of the observed rate constant ( $k_{obs}$ ) vs [ATP] gives a straight line which defines the apparent 2<sup>nd</sup> order rate constant for the reaction (Fig 7B) and appears the same for all three proteins. The observed rate constant of this reaction has been defined for many myosins and has two components,  $k_{obs} = [ATP] K'_1 k'_{+2}$ . The reaction is sensitive to both the affinity of ATP for the complex ( $K'_1$ ) and the efficiency with which ATP induced a major conformational change in the myosin ( $k'_{+2}$ ). This involves the closure of switches 1 and 2 onto the ATP and the opening of the major cleft in the actin binding site of myosin. The absence of any change in  $K'_1 k'_{+2}$  is consistent with a well preserved nucleotide pocket and a preserved communication pathway between the ATP binding pocket and the actin binding site.

The affinity of ADP for actin.S1 was measured in a competition assay with ATP (Fig 7C) and the affinity of ADP for the rat actin.S1 complex (14  $\mu$ M) was 2.3 fold weaker than for the human WT protein (6.3  $\mu$ M). These values are consistent with published values<sup>29</sup>. The chimera was distinct from the human S1 and indistinguishable from the rat S1. To confirm this result the ADP release rate constant was measured directly by displacing ADP from actin.S1.ADP through addition of an excess of ATP. The results (Fig 7D) for human and rat S1 are again consistent with published values with ADP leaving the rat complex at ~ 2X the rate of the human complex (107 vs 59 s<sup>-1</sup>). The chimera was indistinguishable from

the rat S1. As predicted, the amino acids introduced into the human  $\beta$ -myosin motor domain weaken ADP affinity for actin.myosin by accelerating ADP release to make the human  $\beta$ -myosin S1 behave like the rat  $\beta$ -myosin S1.

Footnote to the inset shown in Fig 7D; a complication of the ADP displacement measurement is that ADP displacement from human  $\beta$ -myosin occurs in two phases (fast and slow). The fast phase corresponds with ADP released at the end of the normal ATPase cycle while the slow phase is a trapped ADP which is released much slower and at a much slower rate than the overall cycling. This is therefore a dead-end side branch of the pathway commonly seen in slow muscle & non muscle myosins<sup>14,28,30</sup>. The fraction of ADP trapped in this way is characteristic of each myosin. The rat  $\beta$ -myosin S1 has no apparent slow phase, the human has ~10% of ADP released in the slow phase while the chimera has a larger fraction (~40%) of the total ADP released in the slow phase. The role of the substituted amino acids in the slow phase requires further study, but the reader is referred to the literature for a broader study of this phenomena<sup>14,28,30</sup>.

Motor activity of the recombinant human  $\beta$ -myosin S1 and the chimera protein was measured using an *in vitro* motility assay (Fig 7A, Supplementary movie 1). This assay determines the myosin-mediated velocities of fluorescent actin-filaments moving on a nitrocellulose-coated slide surface. The human WT  $\beta$ -myosin moved actin at a velocity of  $0.49 \mu\text{m}\cdot\text{s}^{-1}$  at  $20^\circ\text{C}$ . Introduction of the nine rat amino acids into the WT protein increased the mean filament velocity by almost 2-fold, from  $0.49 \mu\text{m}\cdot\text{s}^{-1}$  to  $0.9 \mu\text{m}\cdot\text{s}^{-1}$  for the chimera, which is consistent with the ~ 2 fold increase in ADP release-rate data. Our human S1 velocity was similar to the  $0.612 \mu\text{m}\cdot\text{s}^{-1}$  value reported by Ujfalusi et al, which was measured at  $23^\circ\text{C}$ <sup>31</sup>. A similar velocity of  $0.378 \mu\text{m}\cdot\text{s}^{-1}$  was reported for full length human- $\beta$  myosin at  $25^\circ\text{C}$ <sup>3</sup> and a velocity of  $0.624 \mu\text{m}\cdot\text{s}^{-1}$  for the rat. This gives a rat/human ratio of 1.65, very similar to our chimera/human ratio (1.84). Note this data from motility assays gives a different ratio of velocities from that taken from muscle fiber contraction velocity data quoted in Fig 1. The motility assay was not performed for the rat S1 as we do not have an expression system for the protein. The native rat S1 has only a single light chain and lacks a tag to attach the protein to the surface. The rat protein will not therefore give a valid comparable measurement. However, it is known from the literature (Table in Fig 1 & references therein) that the rat protein moves 3-5 times faster than the human protein, depending upon the exact measurement conditions.

## Discussion

Our analysis confirmed our hypothesis that there is a set of sequence changes in the  $\beta$ -myosin, among mammals, that have a high probability of association with species mass. In the 67 species examined, for 52 sites in the motor domain the residue present varied in more than six species. Of these 52 sites a set of 24 sequence changes had the strongest association with mass ( $p_{\text{adj}} < 0.05$ ) and little association with clade ( $p_{\text{adj}} > 0.05$ ). These sites were found throughout the motor domain but we noticed three clusters of four residues (Fig 4) within the group that would allow a cloning approach to test if these residues do play a role in adjusting the velocity of muscle contraction. Of these 12 residues, nine differ between the rat and human  $\beta$ -myosin. We have an expression system for the human myosin motor domain and therefore made a human/rat chimera by exchanging these nine residues.

The chimera displayed a two-fold weakening of ADP binding to actin.myosin due to a two-fold acceleration of the rate constant controlling ADP release from the complex. The two fold faster ADP release rate constant, since it is believed to limit contraction velocity, predicts a two-fold acceleration of the velocity of muscle contraction and a two-fold acceleration of the speed at which actin would move over a bed of myosin. The motility assay confirmed this prediction. The mutations could have caused a generalised loss of nucleotide binding to the protein but a control examining the ability of ATP to bind to actin.myosin and displace actin was indistinguishable among the three proteins (Fig 7B).

Thus our bioinformatics approach has successfully identified nine residues with a role in modulating the velocity of muscle contraction which have been selected over time to adjust the velocity to that required for the slower contraction in human vs rat hearts.

Before considering the sites in the motor domain of myosin where these changes occur we should consider the role of the remaining 40 sites. As shown in Fig 4C, 21 sites have no apparent association with clade or mass and therefore the functional significance of these residue changes remains undefined. Eight sites have a strong association with clade but no or only modest association with mass. A further four sites had a strong association with both clade and mass. Each of these four sites that have strong association with both mass and clade along with the four sites with a strong association with mass, which were not made in the chimera, may contribute to the changes in contraction velocity between mammals. Our approach here was to establish the principle of the effect rather than



delineate the contribution of every sequence change. Thus we focussed on three groups of amino acids.

As stated in the introduction making single point mutations in the motor domain is unlikely to give sufficient experimental resolution to define the contribution of each residue to the 2-3 fold changes we were expecting between rat and human. However, groups of changes could possibly define the relative contributions of each of the three groups of residues. At the moment the complexity and expense of expressing the protein in mouse cell lines prohibits a larger scale study.

What was unexpected was the finding that a set of 12 residues with the highest correlation with mass are predicted to have a narrow mass range over which each sequence change is found (Fig 5 & 6). Additionally, each of the residues has its own distinct midpoint for the transition. This implies that as mass increases, there is a limited number of ways in which the ADP release can be modified step-wise and mammals from distinct clades utilise the same set and order of sequence changes. This is illustrated for seven mammals in Fig 6 where the amino acid present at each of the 12 sites is listed in the order of the mass at which the switch occurs between the amino acid for small vs large mammals. The plot shows the gradual shift between the two sets of amino acids. Note that the small and large Laurasiatheria (bat and cow) differ at every one of the 12 sites as do the small and large Euarchontoglires, mouse and human. In contrast, the mouse sequence is identical to the bat, and human sequence is the same as cow at nine of the twelve sites. A similar plot for all 67 mammals is include in the supplementary materials (Fig S3) and, in addition to demonstrating the same relationships for the larger group of mammals, shows that the small number of Metatheria, and Afrotheria fit into the same pattern. This is consistent with the same set of amino acids being selected for, at each site, in each clade. This is an example of convergent evolution.

None of the mutated residues are in direct contact with the nucleotide binding pocket (Fig 5), thus suggesting that the mutations have allosteric effects. Four of the changes occur in helix-O, a long helix in the upper 50 kDa domain that links the actin binding site (cardiomyopathy loop) with switch 2 in the nucleotide binding site. It is therefore in a position to influence the communication between these two important functional sites. However, the available crystal structures published from a variety of myosins show this helix to move with the whole of the upper 50 kDa domain (e.g. see Fig 7 in M. Bloemink et al., 2014). The other two groups of changes (three residues in the upper 50 kDa domain and two in the lower 50 kDa domain) are not close to each other in space. Understanding how the changes (for the most part conservative substitutions) in these regions alter the behaviour

of the myosin will require a detailed molecular dynamics study. Seven of the twelve positions include amino acid changes that introduce or remove side chains that are capable of forming hydrogen bonds, thus it is possible that the sequence changes result in minor changes to hydrogen bonding networks in the protein. None of these sites appear in the ClinVar web site as sites of mutations in human  $\beta$ -myosin associated with cardiomyopathies or the Genome Aggregation Database (GnomAD) of sites of polymorphisms in humans. This means there are three distinct sets of sites of variation in  $\beta$  myosin, the benign (changes have no known effect on function) the pathological (where there is a relative mild loss of function since the patients typically live into adulthood) and those associated with species adaptation which can induce a more significant change in function.

The results presented here show how a direct link between an organism's physiology and a specific protein sequence allows the exploration of how selection may have adapted protein function to match the physiological requirements. The observation that the same set of amino acids have independently changed in two clades suggests constraints on the way a protein sequence can adapt whilst maintaining function. A wider study of muscle myosin sequences may show if different isoforms use the same or distinct sets of amino acids to adapt to the same selective pressure.

## **Methods**

### *Sequence Analyses:*

Amino acid sequences for the  $\beta$ -myosin motor from 67 different mammalian species were aligned using Clustal Omega<sup>12</sup> comprising organisms from the clades Euarchontoglires (32), Laurasiatheria (30), Metatheria (4) and Afrotheria (1). The start and end points of the motors in *Homo sapiens* were considered to be residues 1 and 800 (based on UniProtKB – P12883).

### *Statistical analysis:*

For each position in the alignment that had more than one amino acid present, species masses were compared between the two highest frequency amino acids at that position using the Mann-Whitney U test, a nonparametric two-sample test. Multiple testing was accounted for by applying the Bonferroni correction. To avoid very imbalanced comparisons, the analysis was not run if the frequency of the second amino acid was less than 10% of the frequency of the most frequent one. Where more than two amino acids were present at an alignment position, only the two most frequent amino acids were considered. See Fig S3 for details of sites with more than 2 amino acids.

Alignment positions were divided into three groups: those with an adjusted p-value ( $p_{adj}$ ) less than 0.01 (with Bonferroni correction applied this is equivalent to a p-value of  $p=9.50 \times 10^{-04}$ ), those with  $0.01 < p_{adj} < 0.05$  (5% significance threshold equivalent to  $p=9.62 \times 10^{-4}$ ), and those with a  $p_{adj} > 0.05$ . In addition, the two highest frequency amino acids were coded as 0 and 1 and a logistic regression model was fitted with  $\log(\text{mass})$  as the explanatory variable (Fig 3 & Supplementary Fig 2). In order to overlay these residue plots, as the coding of the amino acids as 0 and 1 was arbitrary, it was done in such a way that the slope of the fitted logistic regression line was positive (Fig 3). The value of mass at which the two amino acids were predicted to be equally likely to occur was estimated from the regression line.

For each alignment position, a 2x2 table was constructed classifying the species by amino acids present (most frequent and second most frequent) and clade. Fisher's exact test was used to test whether these two factors were associated. The residue and  $-\log_{10}$  of the P-value from the Fisher's exact test were plotted to identify residues for which the amino acid variation was likely to have resulted from clade associated changes. The residue and  $-\log_{10}$  of the p-value from the Mann-Whitney U test were also plotted to determine when residue variation was likely attributed to mass changes. Finally, the  $-\log_{10}$  p-values obtained from

both tests were plotted against each other. For each of these plots, lines at positions of the Bonferroni adjusted p-values 0.01, and 0.05 were added to assess the confidence in each residues association with mass or clade.

All statistical analyses were run in R<sup>13</sup>.

*Molecular Biology of the chimera:*

A pUC19 plasmid containing the human  $\beta$ -myosin motor domain gene was digested with NsiI and NgoMIV to excise DNA encoding for residues 310 – 599 of the human  $\beta$ -myosin. This region was replaced with a complementary pair of synthetic oligos encoding for the same region, but with the nine amino-acid substitutions listed (Ala326Ser, Ser343Pro, Leu366Gln, Ile421Ala, Thr424Ile, Ala430Ser, Arg434Lys, Phe553Tyr, Pro573Gln). The subsequent clone was confirmed by sequencing. This chimera gene was cloned into a pShuttle CMV vector to allow recombinant replication-deficient adenovirus production, as previously described (Deacon et al 2012).

*Protein purification:*

The chimera and the human  $\beta$ -myosin motor domains (known as subfragment 1 or S1) were expressed and purified as described previously<sup>14</sup>. Briefly, the adenoviruses were used to infect C<sub>2</sub>C<sub>12</sub> myotubes in culture and resulted in overexpression of recombinant myosin proteins. The heavy chains (residues 1-842) were co-expressed in C<sub>2</sub>C<sub>12</sub> myotubes with His-tagged human ventricular essential light chain. The recombinant proteins also carried the endogenous mouse regulatory light chain (MLC3). This is homologous to subfragment 1, S1, generated by proteolytic digestion of myosin. For motility assays the heavy chain was additionally tagged with an eight residue (RGSIDTWV) C-terminal extension. Cell pellets were homogenized in a low salt buffer and centrifuged, and the supernatants were purified by affinity chromatography using a HisTrap HP 1 ml column. The proteins were then dialyzed into the low salt experimental buffer (25 mM KCl, 20 mM MOPS, 5 mM MgCl<sub>2</sub>, 1mM DTT, pH 7.0).

The SNAP-PDZ18 affinity tag used for *in vitro* motility measurements were purified as described in<sup>15,16</sup>. SNAP-PDZ18 was expressed through a pHFT2 expression vector, and the plasmid transformed into *E. coli* BL21 DE3 cells. The protein was purified using nickel-affinity chromatography, and dialyzed in PBS.

Actin was prepared from rabbit muscle as described by <sup>17</sup>. The actin was labelled with pyrene at Cys-374 as described in <sup>18</sup>. When used at sub-micromolar concentrations the actin was stabilized by incubation in a 1:1 mixture with phalloidin.

Rat  $\beta$ -myosin S1 was prepared from soleus muscle which was dissected immediately post mortem and stored on ice. The muscle was homogenised into Guba-Straub buffer and left to stir for 30 minutes. After centrifugation at 4600 RPM for 30 minutes at 4 °C, the supernatant was subject to myosin precipitation as described in <sup>19</sup>. The resulting myosin was digested with 0.1 mg chymotrypsin per ml of solution and left to stir for 10 mins exactly, at room temperature. To stop the digestion, 0.5 mM phenylmethylsulfonyl fluoride (PMSF) was added and the solution left to stir for 10 minutes. The digested myosin solution was dialysed into the low salt experimental buffer overnight (25 mM KCl, 20 mM MOPS, 5 mM MgCl<sub>2</sub>, 1mM DTT, pH 7.0). Precipitated myosin and light meromyosin was pelleted and removed via centrifugation at 12,000 RPM for 10 minutes, with the supernatant containing the purified soleus S1. SDS-Gels of the purified protein were run and compared to the expressed human  $\beta$ -myosin and chimera S1.

#### *Stopped flow:*

Kinetic measurements for S1 of chimera, human  $\beta$ -myosin and rat soleus myosin were performed as described previously <sup>5,14,20</sup>. Solutions were buffered with 25 mM KCl, 20 mM MOPS, 5 mM MgCl<sub>2</sub>, 1 mM DTT at pH 7.0, and measurements were conducted at 20 °C on a High-Tech Scientific SF-61 DX2 stopped-flow system. Traces were analysed in Kinetic Studio (TgK Scientific) and Origin.

#### *In vitro motility assay:*

Motility assays were performed essentially as described previously <sup>16,21</sup>. Briefly, flow chambers were constructed with coverslips coated with nitrocellulose mounted on glass slides. Reagents were loaded in the following order: 1) SNAP-PDZ18 affinity tag; 2) BSA to block the surface from non-specific binding; 3) S1 of human  $\beta$ -myosin or the chimera with an eight amino acid C-terminal affinity clamp; 4) BSA to wash the chamber; 5) rhodamine-phalloidin-labelled rabbit actin; 6) an oxygen-scavenging system consisting of 5 mg/ml glucose, 0.1 mg/ml glucose oxydase and 0.02 mg/ml catalase 7; 2 mM ATP. Partially inactivated myosin heads in S1 preparations were removed by incubating with a 10-fold molar excess of actin and 2 mM ATP for 15 minutes, then sedimentation at 100,000 RPM for 15 minutes. Supernatant was collected containing active myosin heads. All solutions were diluted into 25 mM imidazole, 25 mM KCl, 4 mM MgCl<sub>2</sub>, 1 mM EGTA, 1 mM DTT, pH 7.5. Actin filaments were detected using a widefield fluorescence imaging system (described in <sup>22</sup>) with UAPON 100XOTIRF NA lens (Olympus) and QuantEM emCCD

camera (Photometrics). The system was controlled and data analysed using Metamorph software (Molecular Devices, Sunnyvale, USA). Assays were performed at 20 °C and were repeated with three fresh protein preparations, with at least three movies of 30 second duration, recorded at a rate of 0.46 sec per frame. Individual velocities were determined from motile filaments that demonstrated a smooth consistent movement over 10 frames (4.6 sec). 100 individual measured velocities were used to calculate the mean velocity for each recombinant myosin.

### **Acknowledgements**

NIH GM29090 to LAL; NIH HL117138 to LAL. MNW was supported by a Royal Society research grant. JM was supported by an EPSRC PhD studentship.

### **Author Contributions**

MAG, MNW, LAL and MR devised the study and supervised the research. JEM performed computational research. CAJ and DM planned the cloning strategy of the chimera. CAJ and CDV produced the chimera protein. CAJ performed biochemical characterisation of the proteins. CAJ and DM performed the motility assays. All authors contributed to the writing of the paper.

## References

1. Bottinelli, R. & Reggiani, C. Human skeletal muscle fibres: molecular and functional diversity. *Prog. Biophys. Mol. Biol.* **73**, 195–262 (2000).
2. Schiaffino, S. & Reggiani, C. Fiber Types in Mammalian Skeletal Muscles. *Physiol. Rev.* **91**, 1447–1531 (2011).
3. Pellegrino, M. A. *et al.* Orthologous myosin isoforms and scaling of shortening velocity with body size in mouse, rat, rabbit and human muscles. *J. Physiol.* **546**, 677–89 (2003).
4. He, Z. H., Bottinelli, R., Pellegrino, M. A., Ferenczi, M. A. & Reggiani, C. ATP consumption and efficiency of human single muscle fibers with different myosin isoform composition. *Biophys. J.* **79**, 945–61 (2000).
5. Bloemink, M. J., Deacon, J. C., Resnicow, D. I., Leinwand, L. A. & Geeves, M. A. The superfast human extraocular myosin is kinetically distinct from the fast skeletal Ila, IIb, and IId isoforms. *J. Biol. Chem.* **288**, 27469–79 (2013).
6. Resnicow, D. I., Deacon, J. C., Warrick, H. M., Spudich, J. A. & Leinwand, L. A. Functional diversity among a family of human skeletal muscle myosin motors. *Proc. Natl. Acad. Sci. U. S. A.* **107**, 1053–8 (2010).
7. Savage, V. M. *et al.* Scaling of number, size, and metabolic rate of cells with body size in mammals. *Proc. Natl. Acad. Sci.* **104**, 4718–4723 (2007).
8. Mcgreig, J. E. *et al.* Adaptation of mammalian myosin II sequences to body mass. 1–25 (2019). doi:<https://doi.org/10.1101/055434>
9. Walklate, J., Ujfalusi, Z. & Geeves, M. A. Myosin isoforms and the mechanochemical cross-bridge cycle. *J. Exp. Biol.* **219**, 168–174 (2016).
10. Siemankowski, R. F., Wiseman, M. O. & White, H. ADP dissociation from actomyosin subfragment 1 is sufficiently slow to limit the unloaded shortening velocity in vertebrate muscle. *Proc. Natl. Academy Sci. United States Am.* **82**, 658–662 (1985).
11. Homsher E, Wang F, S. J. Factors affecting movement of F-actin filaments propelled by skeletal muscle heavy meromyosin. *Am. J. Physiol.* **263**, 741–23 (1992).
12. Sievers, F. *et al.* Fast, scalable generation of high-quality protein multiple sequence alignments using Clustal Omega. *Mol. Syst. Biol.* **7**, (2011).
13. R Core team. R: A language and environment for statistical computing. R Foundation for Statistical Computing, Vienna, Austria. URL <https://www.R-project.org/>. *R: A Language and Environment for Statistical Computing. R Foundation for Statistical Computing, Vienna, Austria. ISBN 3-900051-07-0, URL <http://www.R-project.org/>.* (2018). doi:10.2788/95827
14. Deacon, J. C., Bloemink, M. J., Rezavandi, H., Geeves, M. A. & Leinwand, L. A. Erratum to: Identification of functional differences between recombinant human  $\alpha$  and  $\beta$  cardiac myosin motors. *Cell. Mol. Life Sci.* **69**, 4239–55 (2012).
15. Huang, Jin. Nagy, Stanislav. Koide, Akiko. Rock, Ronald. Koide, S. A peptide tag system for facile purification and single-molecule immobilization. *Biochemistry* **48**, 11834–11836 (2009).
16. Aksel, T., ChoeYu, E., Sutton, S., Ruppel, K. M. & Spudich, J. A. Ensemble Force Changes that Result from Human Cardiac Myosin Mutations and a Small-Molecule Effector. *Cell Rep.* **11**, 910–920 (2015).
17. Spudich, J. A. & Watt, S. The regulation of rabbit skeletal muscle contraction. I. Biochemical studies of the interaction of the tropomyosin-troponin complex with actin and the proteolytic fragments of myosin. *J. Biol. Chem.* **246**, 4866–71 (1971).

18. Criddle, A. H., Geeves, M. A. & Jeffries, T. The use of actin labelled with N-(1-pyrenyl)iodoacetamide to study the interaction of actin with myosin subfragments and troponin/tropomyosin. *Biochem. J.* **232**, 343–9 (1985).
19. Margossian, S.S. Lowey, S. Preparation of myosin and its subfragments from rabbit skeletal muscle. *Methods Enzymol.* **85**, 55–71 (1982).
20. Walklate, J., Vera, C., Bloemink, M. J., Geeves, M. A. & Leinwand, L. The most prevalent freeman-sheldon syndrome mutations in the embryonic myosin motor share functional defects. *J. Biol. Chem.* **291**, (2016).
21. Adhikari, A. S. *et al.* Early-Onset Hypertrophic Cardiomyopathy Mutations Significantly Increase the Velocity, Force, and Actin-Activated ATPase Activity of Human  $\beta$ -Cardiac Myosin. *Cell Rep.* **17**, 2857–2864 (2016).
22. Johnson, M., East, D. A. & Mulvihill, D. P. Formins determine the functional properties of actin filaments in yeast. *Curr. Biol.* **24**, 1525–1530 (2014).
23. Spudich, J. How molecular motors work. *Nature* **372**, 515–518 (1994).
24. Bernstein, S. I. & Milligan, R. A. Fine Tuning a Molecular Motor : The Location of Alternative Domains in the Drosophila Myosin Head. *J. Mol. Biol.* **271**, 1–6 (1997).
25. Miller, B., Bloemink, M. J., Geeves, M., Nyitrai, M. & Bernstein, S. A Variable Domain Near the ATP Binding Site in Drosophila Muscle Myosin is Part of the Communication Pathway between the Nucleotide and Actin-Binding Sites. *J. Mol. Biol.* **368**, 1051–1066 (2007).
26. Qun Wang Carole L. Moncman and Donald A. Winkelmann. Mutations in the motor domain modulate myosin activity and myofibril organization. *J. Cell Sci.* **116**, 4227–4238 (2003).
27. Rajani Srikakulam and Donald A. Winkelmann. Chaperone-mediated folding and assembly of myosin in striated muscle. *J. Cell Sci.* **117**, 641–652 (2004).
28. Bloemink, M. J., Adamek, N., Reggiani, C. & Geeves, M. A. Kinetic Analysis of the Slow Skeletal Myosin MHC-1 Isoform from Bovine Masseter Muscle. *J. Mol. Biol.* **373**, 1184–1197 (2007).
29. Nag, S. *et al.* Contractility parameters of human  $\beta$ -cardiac myosin with the hypertrophic cardiomyopathy mutation R403Q show loss of motor function. *Sci. Adv.* **1**, e1500511 (2015).
30. Nyitrai, M. & Geeves, M. Adenosine diphosphate and strain sensitivity in myosin motors. *Philos. Trans. R. Soc. B Biol. Sci.* **359**, 1867–77 (2004).
31. Ujfalusi, Z. *et al.* Dilated cardiomyopathy myosin mutants have reduced force-generating capacity. *J. Biol. Chem.* **293**, 9017–9029 (2018).
32. Bloemink, M. *et al.* The hypertrophic cardiomyopathy myosin mutation R453C alters ATP binding and hydrolysis of human cardiac  $\beta$ -myosin. *J. Biol. Chem.* **289**, 5158–5167 (2014).
33. Pereira, J. S. A. *et al.* Kinetic Differences in Cardiac Myosins with Identical Loop 1 Sequences. *J. Biol. Chem.* **276**, 4409–4415 (2001).
34. Toniolo, L. *et al.* Expression of eight distinct MHC isoforms in bovine striated muscles: evidence for MHC-2B presence only in extraocular muscles. *J. Exp. Biol.* **208**, 4243–4253 (2005).



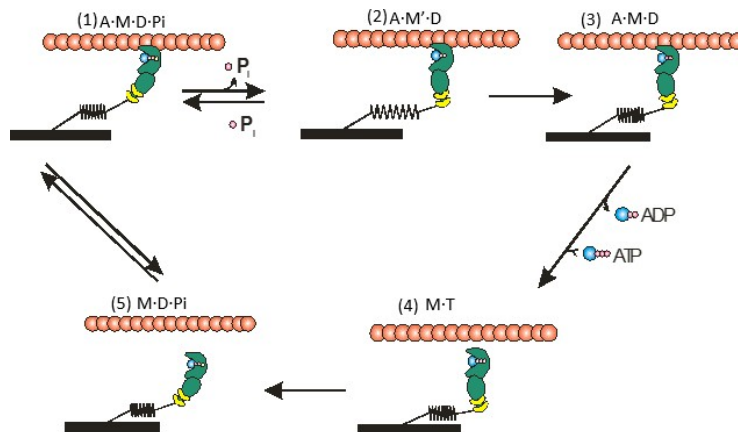
## **Tables**

**Table 1.** Comparison of ATP and ADP binding parameters of native rat S1, and the C<sub>2</sub>C<sub>12</sub> cell expressed human  $\beta$ -myosin and chimera S1. Errors reported are SEM, except for motility which is the HWHM of the normal distribution.

|   | <b>Rat<br/>native<br/>S1</b> | <b>Chimera S1</b> | <b>Human S1</b>     | <b>Chimera/Rat<br/>ratio</b> | <b>Chimera/Human<br/>ratio</b> |
|---|------------------------------|-------------------|---------------------|------------------------------|--------------------------------|
| <b>ATP binding<br/>to A.S1<br/>(<math>\mu\text{M}^{-1}\text{s}^{-1}</math>)</b> | 5 $\pm$ 0.16                 | 4.5 $\pm$ 0.2     | 4.4 $\pm$ 0.3       | 0.9                          | 1.02                           |
| <b>ADP affinity<br/>to A.S1<br/>(<math>\mu\text{M}</math>)</b>                  | 14 $\pm$ 0.09                | 14 $\pm$ 0.14     | 6.1 $\pm$ 0.7       | 1                            | 2.3                            |
| <b>ADP release<br/>from<br/>A.S1.ADP<br/>(<math>\text{s}^{-1}</math>)</b>       | 107.2 $\pm$<br>7.3           | 100.7 $\pm$ 4.2   | 59 $\pm$ 3.3        | 0.94                         | 1.71                           |
| <b>Motility<br/>(<math>\mu\text{m}.\text{s}^{-1}</math>)</b>                    | NA                           | 0.90 $\pm$ 0.221  | 0.49 $\pm$<br>0.129 | NA                           | 1.84                           |

Data are from three separate preparation of protein from either different cell pellets (expressed protein) or different soleus muscles from the rat. Experimental conditions were 25 mM KCl, 20°C.

**Figures:**



| slow/ $\beta$ myosin | Measured                              |  | Predicted $\tau$ (sec)                      |                       |                             |
|----------------------|---------------------------------------|--|---|-----------------------|-----------------------------|
|                      | $k_{\text{-ADP}}$ ( $\text{s}^{-1}$ ) | $V_0$ ( $\mu\text{m}/\text{sec}/\text{half sarcomere}$ ) | $T_{\text{ADP}} = 1/k_{\text{-ADP}}$ (msec) | $TV_0 = d/V_0$ (msec) | Ratio $T_{\text{ADP}}/TV_0$ |
| <b>Rat</b>           | 119                                   | 1.42   | 8.4   | 7.04                  | 1.19                        |
| <b>Rabbit</b>        | 63                                    | 0.67   | 15.9  | 14.9                  | 1.06                        |
| <b>Human</b>         | 30*                                   | 0.33   | 33  | 30.3                  | 1.08                        |
| <b>Cow</b>           | 27                                    | 0.27   | 37  | 37.0                  | 1.00                        |

Experimental data was collected at 100 mM KCl and 12 °C.

$k_{\text{-ADP}}$  values for bovine, rabbit and human are from Deacon et al <sup>14</sup>, the rat from this study. NB the value for human  $k_{\text{-ADP}}$  at 12 °C was estimated from an Arrhenius plot of values between 20 and 10 °C <sup>32</sup>. These values are consistent with rat and porcine  $\beta$ -HMM data carried out at 100 mM KCl and 15 °C <sup>33</sup>.  $V_0$  data for rat, rabbit & human are from Pellegrino et al <sup>3</sup>, bovine from Toniolo et al <sup>34</sup>.

**Figure 1. The relationship between the predicted and measured parameters for four slow/beta cardiac myosin isoforms.** Figure adapted from (Nyitrai & Geeves, 2004). In terms of the actin myosin cross bridge cycle the dominant model proposes that the maximum velocity ( $V_0$ ) is limited by the lifetime of the strongly attached force holding state ( $\tau$ ) the “detachment limited model” ( $V_0 = d/\tau$  where  $d$  is the working stroke of the cross bridge; assumed here to be 5 nm (Siemankowski, Wiseman, & White, 1985). For the mammalian,  $\beta$ -cardiac/slow-muscle myosin isoform, it is well established that  $\tau$  is defined by the rate constant controlling ADP release  $k_{\text{-ADP}} = 1/\tau$  (see table below). Thus, values of  $k_{\text{-ADP}}$  measured using myosin motor domains isolated from  $\beta$ -cardiac/slow muscle of a mammal, predict remarkably accurately the maximum shortening velocity of a muscle fibre taken from the same tissues.

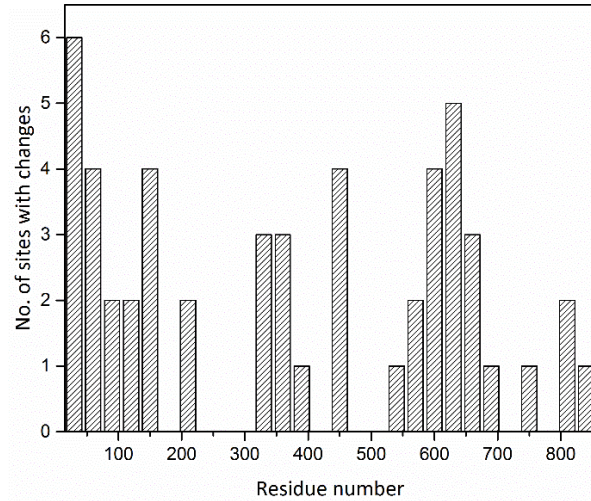


**Figure 2. Distribution of sequence variations for the  $\beta$ -myosin sequences listed in Figure 1.** The sequence which is ~96% conserved was divided into blocks of 30 residues and the number of sites within that group showing a change is plotted. The maximum number is six residues in region 1-30 reflecting the high degree of identity among the four sequences.

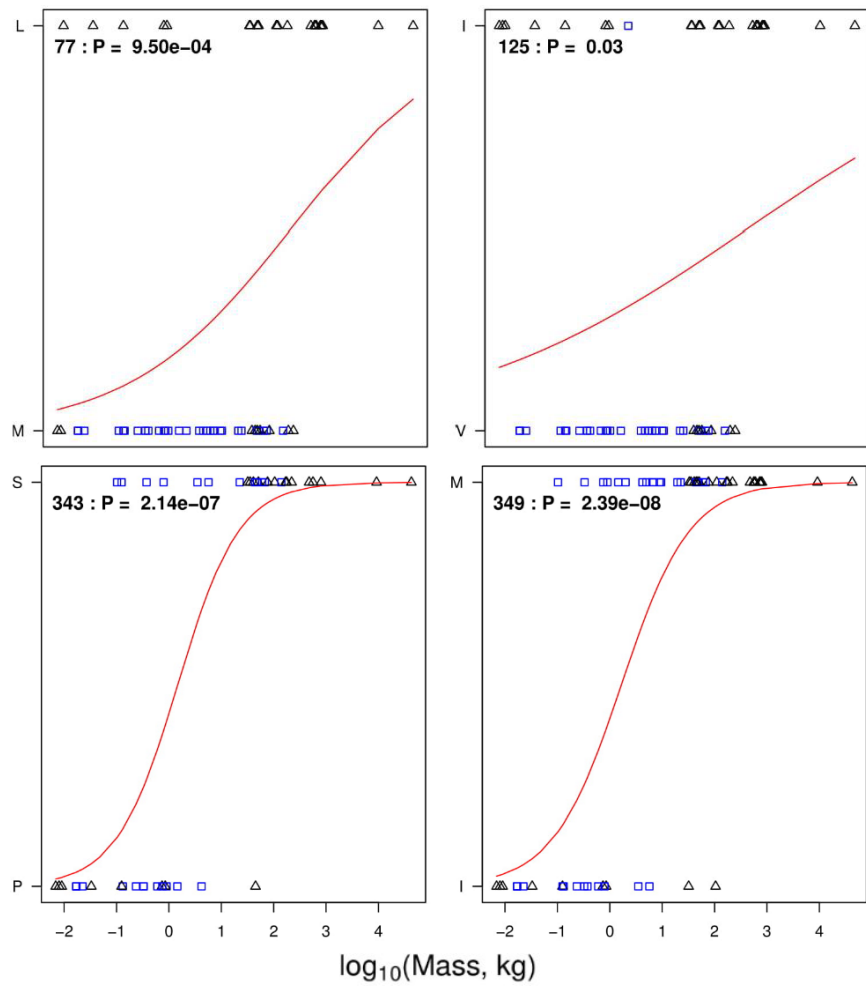


**Figure 3. Residue-mass transition plots.** Binomial regression mapping the transition of the most frequent amino acid at positions in the motor region of  $\beta$ -myosin to the second most frequent amino acid at that position. The residue numbering is that of the human  $\beta$ -cardiac myosin, as oppose to the alignment position. The blue squares are Euarchontoglires, and the triangles are Laurasiatheria. The P-value with each plot arises from a test of the null hypothesis that amino acid type is unrelated to mass.

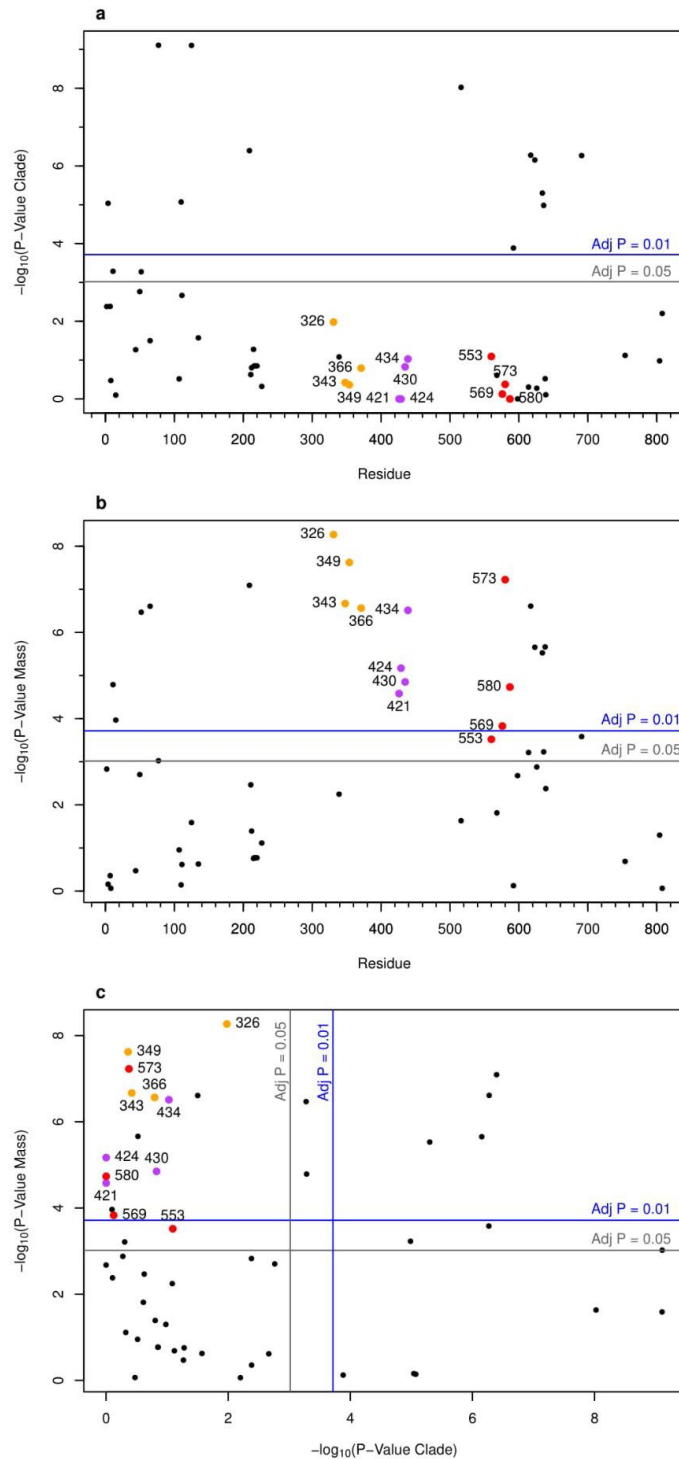


**Figure 4. Residue mass change association with mass, clade, and each other.** The association of each residue with clade (A), mass (B), and the association of the P-values of clade vs mass (C) are plotted. The significance of the P-values is shown with the Bonferroni adjusted lines drawn onto the plots (blue and grey). The three groups of residues investigated are highlighted in orange, purple and red, and labelled with the human residue numbering in each plot.

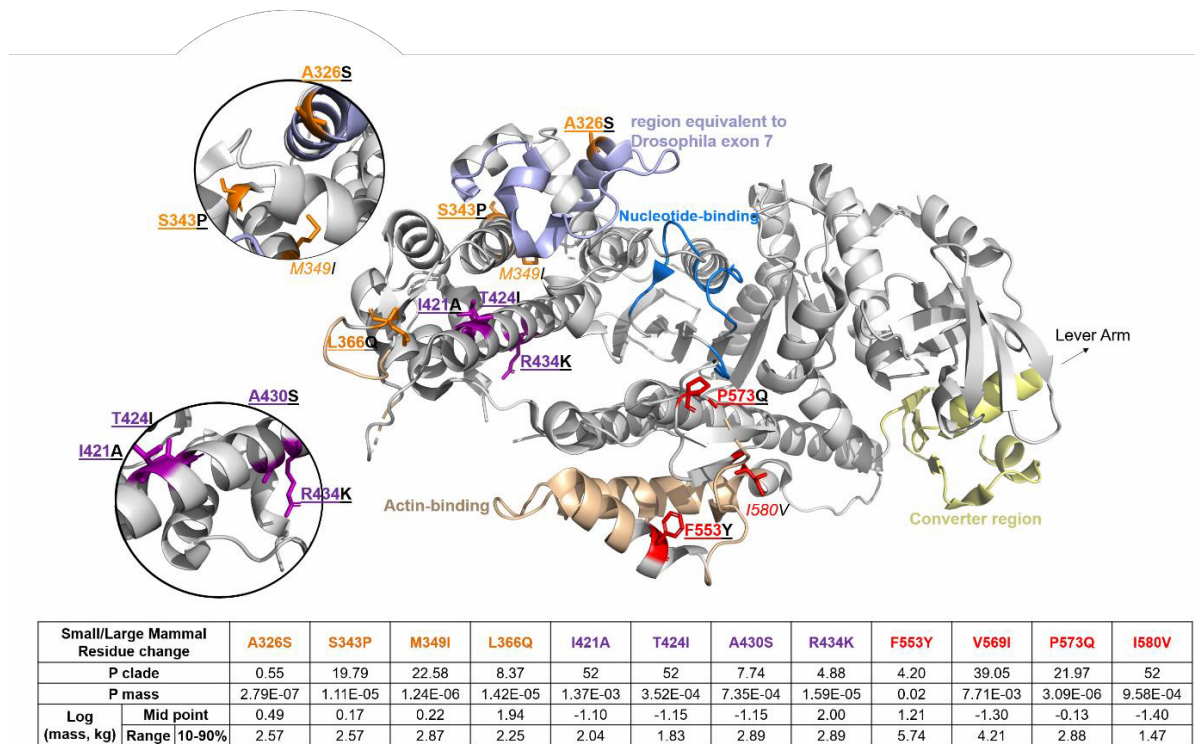
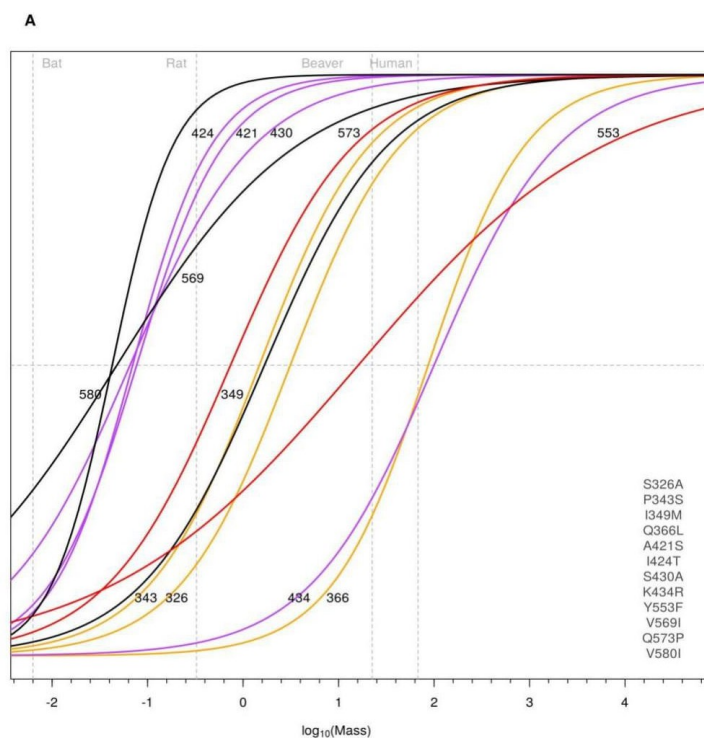


**Figure 5. Location of residues switched in the chimera.** Structure of human  $\beta$ -myosin (PDB:ID 4DB1). The actin-binding site is highlighted in brown, exon 7 in blue, the nucleotide binding site in marine blue, and the converter region in yellow. The three groups of residues investigated are highlighted and labelled in orange (326, 343, 349, 366), purple (421, 424, 430, 434), and red (553, 569, 573, 580) in each plot, and those that were switched are in bold and underlined.



| Species | Mass (kg) | 434 | 366 | 553 | 326 | 349 | 343 | 573 | 421 | 424 | 430 | 569 | 580 |
|---------|-----------|-----|-----|-----|-----|-----|-----|-----|-----|-----|-----|-----|-----|
| Bat     | 0.0069    | K   | Q   | Y   | S   | I   | P   | Q   | S   | I   | S   | V   | V   |
| Mouse   | 0.017     | K   | Q   | Y   | S   | I   | P   | Q   | S   | I   | S   | V   | V   |
| Rat     | 0.325     | K   | Q   | Y   | S   | I   | P   | Q   | A   | I   | S   | I   | I   |
| Rabbit  | 2         | K   | Q   | Y   | S   | M   | L   | P   | A   | T   | A   | I   | I   |
| Beaver  | 22.5      | K   | Q   | F   | S   | M   | S   | P   | A   | T   | A   | I   | I   |
| Human   | 68        | R   | L   | F   | A   | M   | S   | P   | I   | T   | A   | I   | I   |
| Cow     | 755       | R   | L   | F   | A   | M   | T   | P   | V   | K   | A   | I   | I   |

**Figure 6. Residue mass transition plots.** Overlapping binomial regression mapping the transition of the most frequent amino acid at positions in the motor region of  $\beta$ -myosin to the second most frequent amino acid at that position. The amino acids (AA) that occur most frequently and second most frequently are at the extremes of the y-axis. The groups of residues investigated are highlighted and labelled in orange (326, 343, 366), purple (421, 424, 430, 434), red (553, 573), and black (349, 569, 580) which show the three groupings of the nine residues changed in the chimera, and the three additional residues predicted to transition as a result of mass changes respectively. The table below shows the residues in seven species across each of the twelve positions, sorted by the mid-point of the transition. The related table for all 67 species is provided in Table S3.

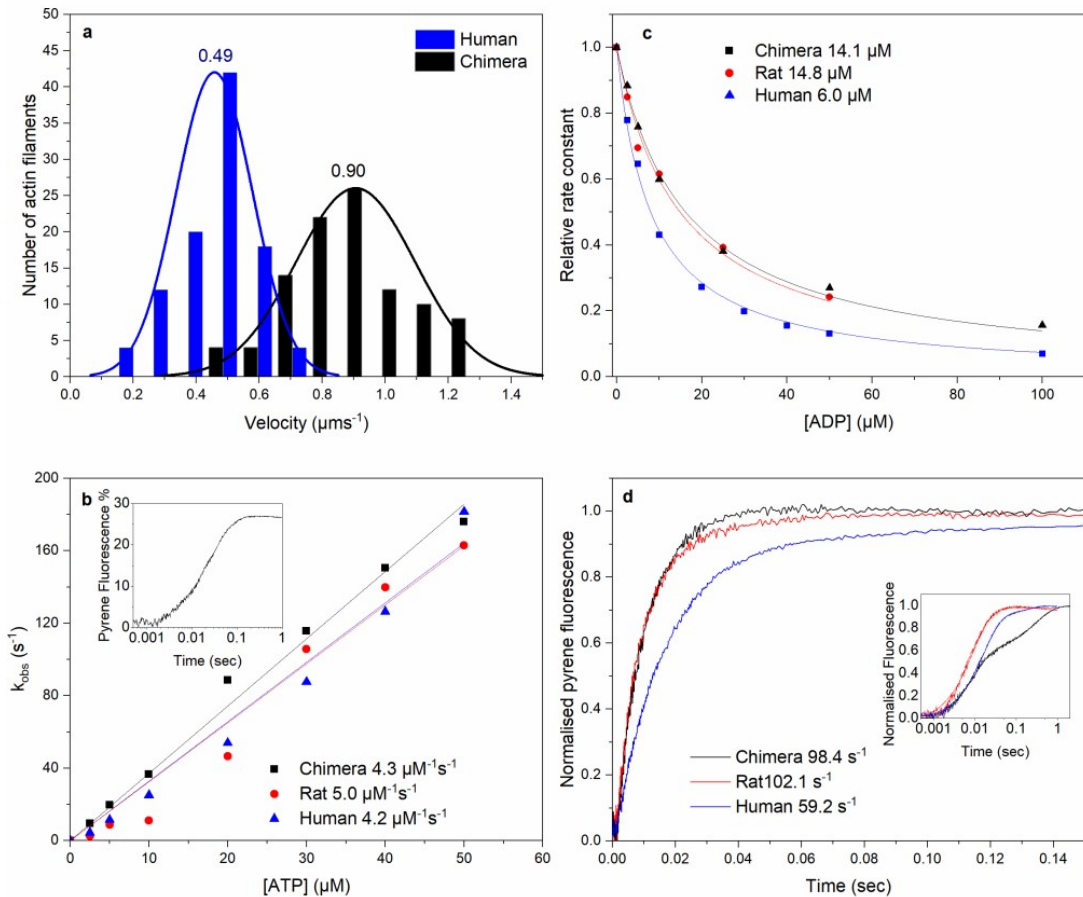


**Figure 7. Stopped-flow analysis of the chimera, rat and human  $\beta$ -S1 proteins.** A. Histogram of *in vitro* velocity of 100 rhodamine-labelled-phalloidin actin filaments moving over human  $\beta$ -S1 or chimera S1. The solid line shows the data fitted to a single Gaussian curve. The mean velocity for the human  $\beta$ -S1 was  $0.49 \pm 0.028 \mu\text{m s}^{-1}$  and for the chimera  $0.90 \pm 0.015 \mu\text{m s}^{-1}$ . B. The effect of ATP concentration on  $k_{\text{obs}}$  for ATP-induced dissociation of pyrene-actin.S1. The gradient generates a second order rate constant of ATP binding; the values for the 3 proteins are highlighted next to the plot. Inset shows an example transient of 50 nM pyrene actin-chimera S1 mixed with 20  $\mu\text{M}$  ATP, resulting in a fluorescence change of 26 %. C. Plot of  $k_{\text{obs}}$  dependence on [ADP] for the ATP induced dissociation of pyrene-actin.S1. 50 nM pyrene-actin.S1 was mixed with 10  $\mu\text{M}$  ATP and varying [ADP] (0-100  $\mu\text{M}$ ). Numbers indicate the values of ADP affinity for acto.S1,  $k_{\text{ADP}}$ , for the 3 proteins. D. To measure  $k_{+\text{ADP}}$ , ADP is displaced from pyrene-actin.S1.ADP complex by an excess of ATP. 2 mM ATP was mixed with 250 nM S1 which was pre-incubated with 500 nM pyrene-actin and 100  $\mu\text{M}$  ADP.  $k_{+\text{ADP}}$  values for the 3 proteins are given 7D. Inset showing data on a longer log time scale showing the slow phase components of the transients. The average values from 3 independent measurements for experiments shown in B, C and D are summarised in table 1.



## Supplementary Information

Cardiac/slow muscle contraction velocity is matched to heart rate and body size through variation in  $\beta$ -myosin sequence.

**Chloe A. Johnson<sup>1\*</sup>, Jake E. McGreig<sup>1\*</sup>, Carlos D. Vera<sup>2</sup>, Daniel P. Mulvihill<sup>1</sup>, Martin Ridout<sup>3</sup>, Leslie A. Leinwand<sup>2</sup>, Mark N. Wass<sup>1</sup>, Michael A. Geeves<sup>1</sup>**

### CONTENT:

Figure S1. Multiple sequence alignment of rat, rabbit, human and bovine  $\beta$ -cardiac myosin.

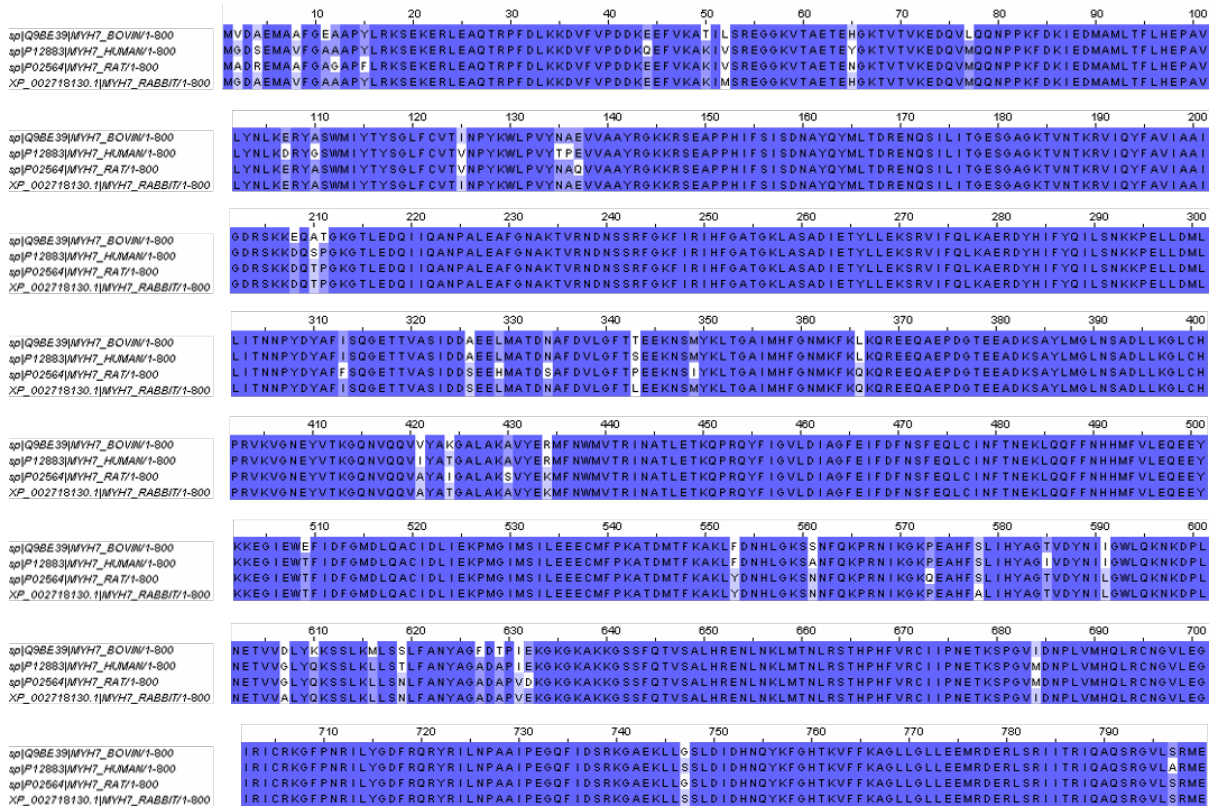
Figure S2. Residue-mass transition plots.

Figure S3. Distribution of amino acids at twelve positions

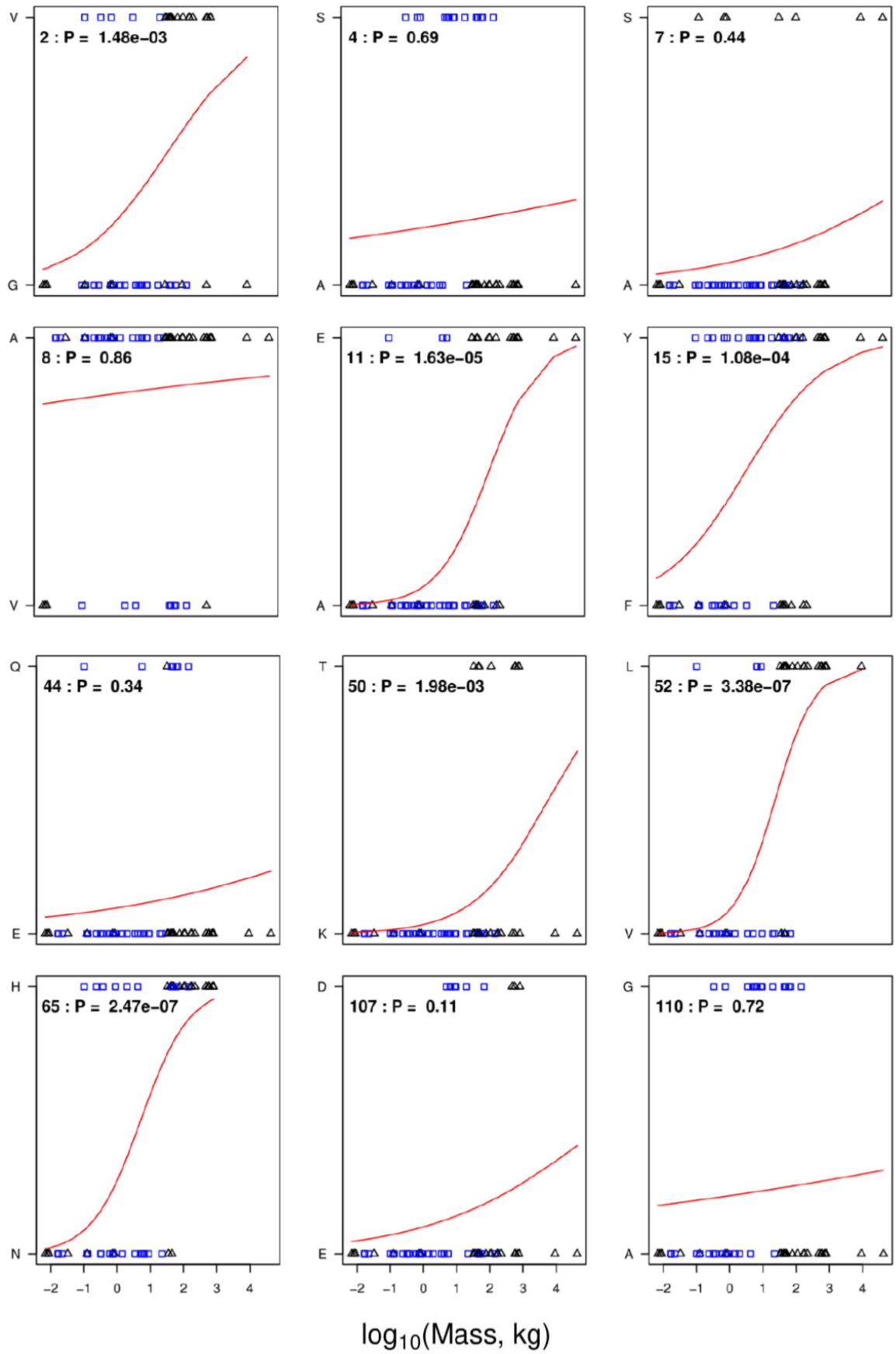
Figure S4. Highly variable residue mass vs amino acid frequencies.

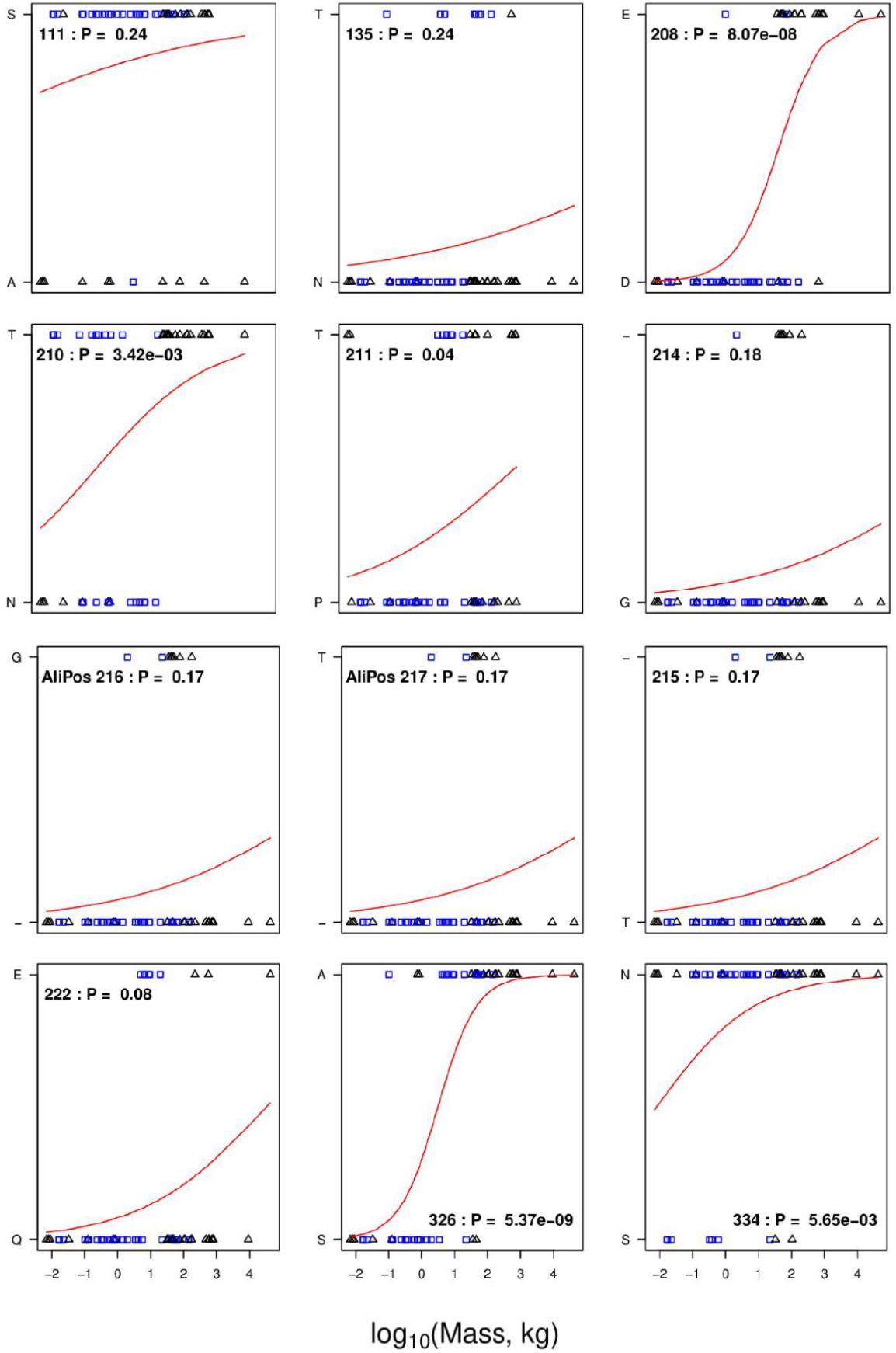
Figure S5. SDS-PAGE of the three protein preparations.

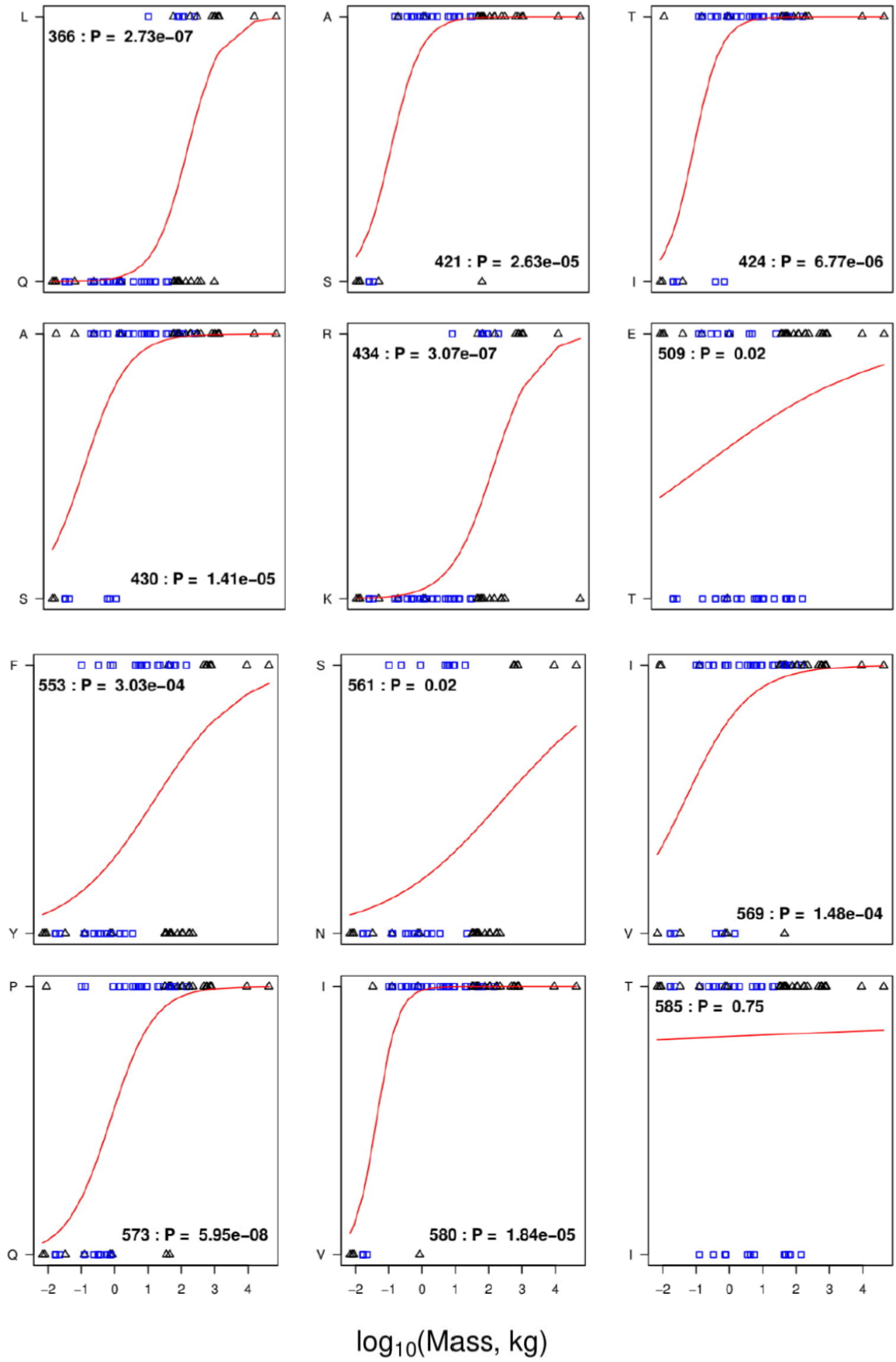
Figure S6. Frequency of organisms at different mass levels.

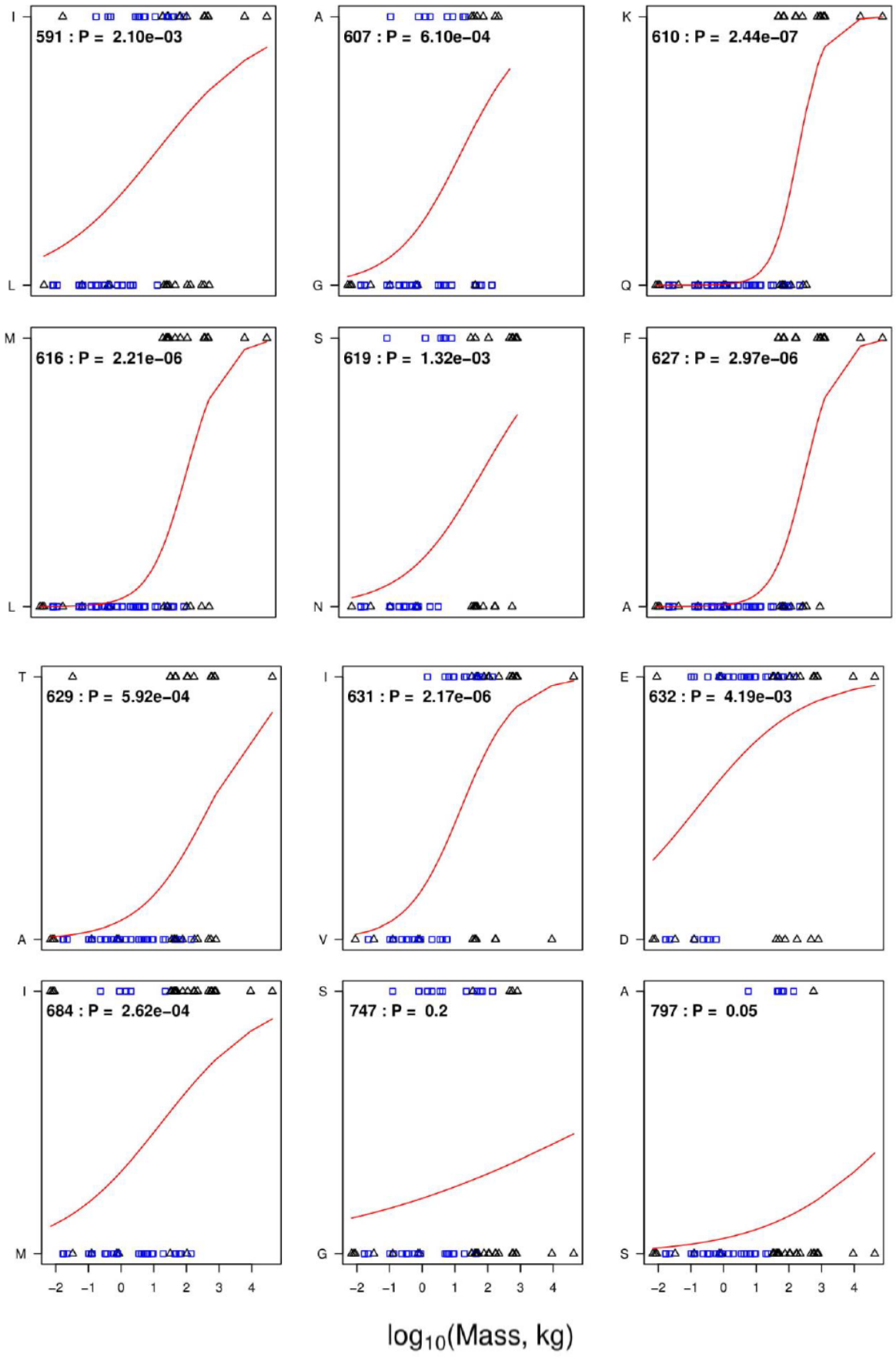


**Supplementary Figure 1. Multiple sequence alignment of rat, rabbit, human and bovine  $\beta$ -cardiac myosin.**







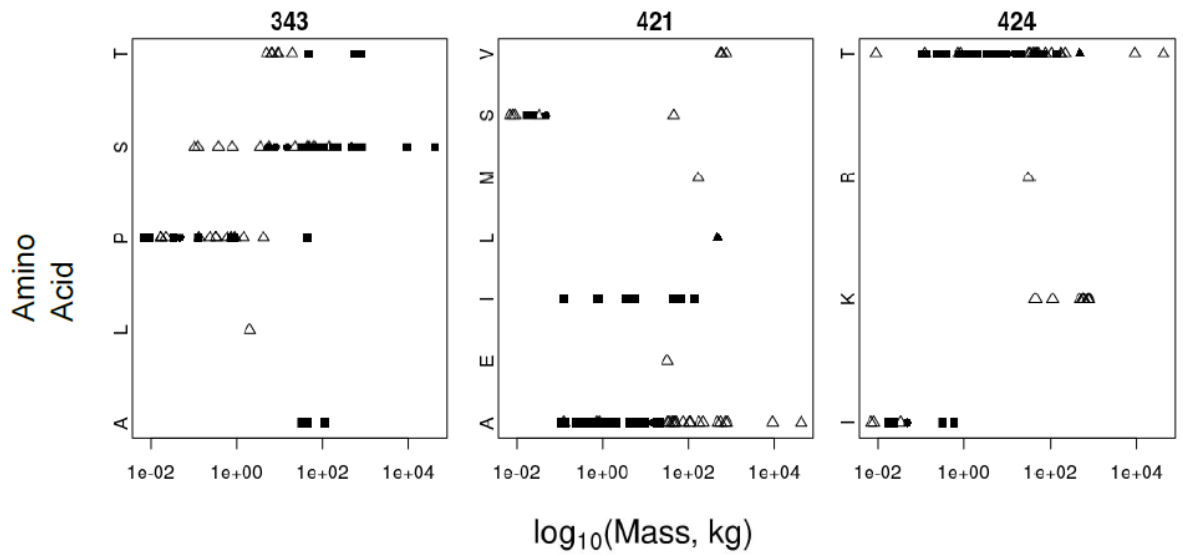


**Supplementary Figure 2. Residue-mass transition plots.** Binomial regression mapping the transition of the most frequent amino acid at positions in the motor region of  $\beta$ -myosin to the second most frequent amino acid at that position. The residue numbering is that of the human  $\beta$ -myosin, as oppose to the alignment position. The black squares are Euarchontoglires, and the triangles are Laurasiatheria. The P-value with each plot indicate the probability that the transition of the amino acids is not a result of change in mass.

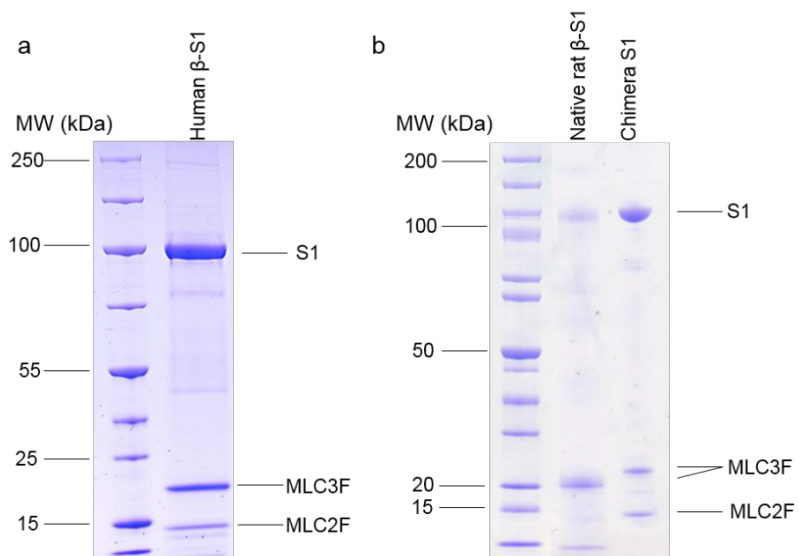
| Species                                   | Mass   | Clade | 366 | 434 | 326 | 553 | 343 | 349 | 573 | 421 | 424 | 430 | 589 | 590 |
|---|--------|-------|-----|-----|-----|-----|-----|-----|-----|-----|-----|-----|-----|-----|
| Myotis_brandtii                           | 0.0069 | L     | Q   | K   | S   | Y   | P   | I   | Q   | S   | I   | S   | V   | V   |
| Myotis_lucifugus                          | 0.008  | L     | Q   | K   | S   | Y   | P   | I   | Q   | S   | I   | S   | I   | V   |
| Hipposideros_armiger                      | 0.009  | L     | Q   | K   | S   | Y   | P   | I   | P   | S   | T   | A   | I   | V   |
| Mus_musculus                              | 0.017  | E     | Q   | K   | S   | Y   | P   | I   | Q   | S   | I   | S   | V   | V   |
| Mus_pahari                                | 0.017  | E     | Q   | K   | S   | Y   | P   | I   | Q   | S   | I   | S   | V   | V   |
| Peromyscus_maniculatus_bairdii            | 0.017  | E     | Q   | K   | S   | Y   | P   | I   | Q   | S   | I   | S   | V   | V   |
| Cricetulus_griseus                        | 0.0224 | E     | Q   | K   | S   | Y   | P   | I   | Q   | S   | I   | S   | V   | V   |
| Desmodus_rotundus                         | 0.033  | L     | Q   | K   | S   | Y   | P   | I   | Q   | S   | I   | A   | V   | I   |
| Monodelphis_domestica                     | 0.048  | M     | Q   | K   | S   | Y   | P   | I   | Q   | S   | I   | S   | I   | I   |
| Otolemur_garnettii                        | 0.1025 | E     | Q   | K   | A   | F   | S   | M   | P   | A   | T   | A   | I   | I   |
| Ictidomys_tridecemlineatus                | 0.125  | E     | Q   | K   | S   | Y   | S   | I   | Q   | I   | T   | A   | I   | I   |
| Rousettus_aegyptiacus                     | 0.125  | L     | Q   | K   | S   | Y   | P   | I   | Q   | A   | T   | A   | I   | I   |
| Tarsius_syrichta                          | 0.1315 | E     | Q   | K   | S   | Y   | P   | I   | P   | A   | T   | A   | I   | I   |
| Octodon_degus                             | 0.235  | E     | Q   | K   | S   | Y   | P   | I   | Q   | A   | T   | A   | I   | I   |
| Rattus_norvegicus                         | 0.325  | E     | Q   | K   | S   | Y   | P   | I   | Q   | A   | I   | S   | I   | I   |
| Callithrix_jacchus                        | 0.33   | E     | Q   | K   | S   | F   | P   | M   | Q   | A   | T   | A   | I   | I   |
| Nannospalax_galili                        | 0.375  | E     | Q   | K   | S   | Y   | S   | I   | Q   | A   | T   | S   | V   | I   |
| Jaculus_jaculus                           | 0.6    | E     | Q   | K   | S   | Y   | P   | I   | Q   | A   | I   | S   | V   | I   |
| Pteropus_alecto                           | 0.74   | L     | Q   | K   | A   | Y   | P   | I   | Q   | A   | T   | A   | V   | I   |
| Aotus_nancymaeae                          | 0.75   | E     | Q   | K   | S   | F   | P   | M   | Q   | A   | T   | A   | I   | I   |
| Urocyon_vulpinus                          | 0.791  | E     | Q   | K   | S   | Y   | S   | I   | Q   | I   | T   | A   | I   | I   |
| Pteropus_vampyrus                         | 0.85   | L     | Q   | K   | A   | Y   | P   | I   | Q   | A   | T   | A   | V   | V   |
| Cavia_porcellus                           | 0.9    | E     | Q   | K   | S   | F   | P   | M   | P   | A   | T   | A   | I   | I   |
| Galeopterus_variegatus                    | 1.45   | E     | M   | K   | S   | Y   | P   | M   | P   | A   | T   | A   | V   | I   |
| Oryctolagus_cuniculus                     | 2      | E     | Q   | K   | S   | Y   | L   | M   | P   | A   | T   | A   | I   | I   |
| Marmota_marmota_marmota                   | 3.5    | E     | Q   | K   | S   | Y   | S   | I   | P   | I   | T   | A   | I   | I   |
| Propithecus_coquereli                     | 4.2    | E     | Q   | K   | A   | F   | P   | M   | P   | A   | T   | A   | I   | I   |
| Chlorocebus_sabaeus                       | 5      | E     | Q   | K   | A   | F   | T   | M   | P   | A   | T   | A   | I   | I   |
| Dasyprocta_noveboracensis                 | 5.5    | M     | Q   | K   | A   | Y   | S   | I   | P   | A   | T   | A   | I   | I   |
| Nomascus_leucogenys                       | 5.7    | E     | L   | R   | A   | F   | S   | I   | P   | I   | T   | A   | I   | I   |
| Macaca_fascicularis                       | 6.55   | E     | Q   | K   | A   | F   | T   | M   | P   | A   | T   | A   | I   | I   |
| Macaca_nemestrina                         | 6.55   | E     | Q   | K   | A   | F   | T   | M   | P   | A   | T   | A   | I   | I   |
| Macaca_fascicularis                       | 6.55   | E     | Q   | K   | A   | F   | T   | M   | P   | A   | T   | A   | I   | I   |
| Macaca_nemestrina                         | 6.55   | E     | Q   | K   | A   | F   | T   | M   | P   | A   | T   | A   | I   | I   |
| Sarcophilus_harrisii                      | 8      | M     | Q   | K   | S   | Y   | S   | M   | P   | A   | T   | S   | I   | I   |
| Colobus_angolensis_palliatu               | 8.9    | E     | Q   | K   | A   | F   | T   | M   | P   | A   | T   | A   | I   | I   |
| Cercopithecus_atys                        | 9.5    | E     | Q   | K   | A   | F   | T   | M   | P   | A   | T   | A   | I   | I   |
| Phascogalea_cinerea                       | 15     | M     | L   | K   | S   | F   | S   | I   | P   | A   | T   | A   | I   | I   |
| Papio_anubis                              | 19.5   | E     | Q   | K   | S   | F   | S   | M   | P   | A   | T   | A   | I   | I   |
| Castor canadensis                         | 22.5   | E     | Q   | K   | S   | F   | S   | M   | P   | A   | T   | A   | I   | I   |
| Neophocaena_asiaorientalis_asiaorientalis | 32     | L     | L   | K   | A   | Y   | S   | I   | P   | E   | R   | A   | I   | I   |
| Panthera_tigris                           | 33     | L     | Q   | R   | A   | Y   | A   | M   | P   | A   | T   | A   | I   | I   |
| Canis_lupus_familiaris                    | 35.5   | L     | Q   | K   | S   | Y   | S   | M   | Q   | A   | T   | A   | I   | I   |
| Panthera_pardus                           | 41     | L     | Q   | K   | A   | F   | S   | M   | P   | A   | T   | A   | I   | I   |
| Pan_paniscus                              | 44     | E     | L   | R   | A   | F   | S   | M   | P   | I   | T   | A   | I   | I   |
| Capra_hircus                              | 45     | L     | Q   | R   | A   | Y   | A   | M   | P   | A   | K   | A   | I   | I   |
| Enhydra_lutris_kenyonii                   | 45     | L     | Q   | K   | S   | Y   | P   | M   | Q   | S   | T   | A   | V   | I   |
| Odocoileus_virginianus_texanus            | 47.6   | L     | Q   | R   | A   | Y   | T   | M   | P   | A   | T   | A   | I   | I   |
| Pan_troglodytes                           | 48     | E     | L   | R   | A   | F   | S   | M   | P   | I   | T   | A   | I   | I   |
| Acinonyx_jubatus                          | 51     | L     | Q   | K   | A   | Y   | S   | M   | P   | A   | T   | A   | I   | I   |
| Pongo_abelii                              | 60     | E     | L   | R   | A   | F   | S   | M   | P   | I   | T   | A   | I   | I   |
| Homo_sapiens                              | 68     | E     | L   | R   | A   | F   | S   | M   | P   | I   | T   | A   | I   | I   |
| Puma_concolor                             | 76.5   | L     | Q   | K   | A   | Y   | S   | M   | P   | A   | T   | A   | I   | I   |
| Lipotes_vexillifer                        | 104.5  | L     | L   | K   | A   | Y   | S   | I   | P   | A   | T   | A   | I   | I   |
| Ovis_aries                                | 110    | L     | Q   | R   | A   | Y   | A   | M   | P   | A   | K   | A   | I   | I   |
| Gorilla_gorilla_gorilla                   | 140    | E     | L   | R   | A   | F   | S   | M   | P   | I   | T   | A   | I   | I   |
| Sus_scrofa                                | 169    | L     | L   | K   | A   | Y   | S   | M   | P   | M   | T   | A   | I   | I   |
| Panthera_tigris_altaica                   | 176.4  | L     | Q   | K   | A   | Y   | S   | M   | P   | A   | T   | A   | I   | I   |
| Neomonachus_schauinslandi                 | 220    | L     | Q   | K   | A   | Y   | S   | M   | P   | A   | T   | A   | I   | I   |
| Camelus_bactrianus                        | 475    | L     | L   | R   | A   | F   | S   | M   | P   | A   | K   | A   | I   | I   |
| Trichechus_manatus_latirostris            | 480    | A     | L   | R   | A   | F   | S   | M   | P   | L   | T   | A   | I   | I   |
| Bos_mutus                                 | 562.5  | L     | L   | R   | A   | F   | T   | M   | P   | V   | K   | A   | I   | I   |
| Equus_caballus                            | 563.5  | L     | Q   | R   | A   | F   | S   | M   | P   | A   | K   | A   | I   | I   |
| Bison_bison_bison                         | 600    | L     | L   | R   | A   | F   | T   | M   | P   | V   | K   | A   | I   | I   |
| Bubalus_bubalis                           | 725    | L     | L   | R   | A   | F   | T   | M   | P   | A   | K   | A   | I   | I   |
| Bos_taurus                                | 755    | L     | L   | R   | A   | F   | T   | M   | P   | V   | K   | A   | I   | I   |
| Camelus_ferus                             | 800    | L     | L   | R   | A   | F   | S   | M   | P   | A   | K   | A   | I   | I   |
| Balaenoptera_acutorostrata_scammoni       | 9200   | L     | L   | R   | A   | F   | S   | M   | P   | A   | T   | A   | I   | I   |
| Physeter_catodon                          | 42500  | L     | L   | K   | A   | F   | S   | M   | P   | A   | T   | A   | I   | I   |



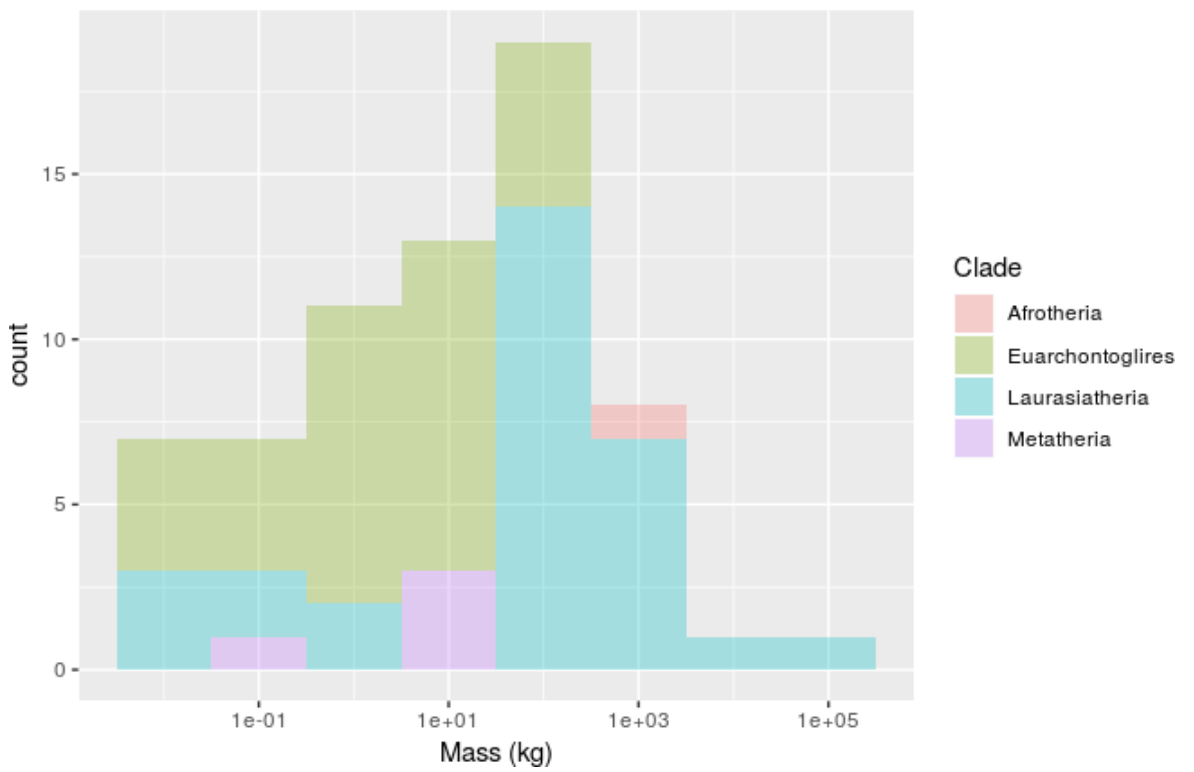
**Supplementary Figure 3. Distribution of amino acids at twelve positions.** This table shows the amino acids that occurs in each of the twelve residues, those predicted to be associated with mass and that are of interest, in each species, sorted by mass. Yellow background is the predominant amino acid in small mammals. Blue background is the predominant amino acid in large mammals. The clades Laurasiatheria, Euarchontoglires, Metatheria, and Afrotheria are represented by the letter L, E, M and A respectively.



**Supplementary Figure 4.** Highly variable residue mass vs amino acid frequencies. Residues which had more than two sites of variation, with the third most frequent amino acid being close in frequency to the second most common amino acid. The black squares are Euarchontoglires, and the triangles are Laurasiatheria. The residue numbering is that of human  $\beta$ -cardiac myosin.



**Supplementary Figure 5. SDS-PAGE of the three protein preparations.** A. Recombinant human  $\beta$ -S1 with 2 light chains. B. Native rat  $\beta$ -S1 and recombinant chimera S1 with 2 light chains.



**Supplementary Figure 6. Frequency of organisms at different mass levels.** Plot to show the counts for organisms from each clade at different mass levels. Pink, dark, yellow, blue and purple shows organisms from the clades Afrotheria, Euarchontoglires, Laurasiatheria, and Metatheria clades.

## **5. Myosin motor domains carrying mutations implicated in early or late onset hypertrophic cardiomyopathy have similar properties**

Carlos D. Vera\*, **Chloe A. Johnson\***, Jonathan Walklate, Arjun Adhikari, Marina Svcevic, Srboljub M. Mijailovich, Ariana C. Combs, Stephen J. Langer, Kathleen M. Ruppel, James A. Spudich, Leslie A. Leinwand, and Michael A. Geeves

\* Contributed equally

Journal of Biological Chemistry, 2019. *In press.*

### **5.1 Context of research**

As described in section 1.4, research into HCM has been extensive since the first identification of a single point mutation in MyHC- $\beta$  (Geisterfer-Lowrance et al. 1990). The collaboration between University of Colorado and University of Kent has contributed to the effort in understanding the molecular basis of the disease. The expertise of the Leinwand laboratory in recombinant myosin production has been coupled with the experience of the Geeves laboratory in rapid kinetic techniques, who are able to measure kinetic properties of myosin to a high precision using limited quantities of protein. Two well-known HCM-causing mutations, R453C and R403Q, were investigated in Bloemink et al and Nag et al, respectively (Bloemink et al. 2014; Nag et al. 2015). The development of MUISCO in 2017 led to the kinetic characterisation using stopped-flow spectroscopy being complemented by kinetic modelling. This was conducted for 5 DCM-causing mutations in the MyHC- $\beta$  motor domain (Ujfalusi et al. 2018). This is a follow up study, using the same approach to investigate the functional effects of seven HCM-causing mutations.

## **5.2 Aims of research**

Single point mutations have been identified in the MyHC- $\beta$  motor domain in both adolescent (early-onset) and adult (late-onset) patients with HCM. We hypothesised that the effect of mutations is more severe in patients with early-onset HCM compared to late-onset HCM. Why disease progression is triggered earlier in life in the early-onset patients has yet to be elucidated. Stopped-flow spectroscopy was used to characterise kinetic parameters of the cross-bridge cycle for four early-onset and three late-onset HCM mutations. The mechanochemical cycle was then further explored using MUSICO, with the aim of understanding if the mutations have altered contractile properties (such as duty ratio, ATP economy, load dependence or shortening velocity) that may give rise to pathology.

## **5.3 Contribution to publication**

Dr Carlos Vera, Dr. Stephen Langers, and Ariana Combs from Professor Leslie Leinwand's laboratory cloned the sequences of all seven mutations, grew the viruses, transfected and grew the C2C12 cells. C2C12 cell pellets were shipped to Dr Jonathan Walklate and myself for purification. I designed, performed and analysed stopped-flow experiments for six of the seven mutations (all except H251N, which was characterised by Dr Walklate). Dr Vera made two trips to the University of Kent to assist with stopped-flow experiments and learn the technique; I supervised and mentored him during his training. I performed kinetic modelling of the transient kinetic data using MUSICO, with assistance from Marina Svcevic and Srboj Mijailovich on the error analysis. Dr Arjun Adhikari, Dr Kathleen Ruppel and Professor James Spudich kindly provided motility and ATPase data. Dr Vera, Professor Leinwand, Professor Michael Geeves and myself wrote the first draft of the manuscript, which was reviewed by all authors.

**5.4 Publication** – see below.



# Myosin motor domains carrying mutations implicated in early or late onset hypertrophic cardiomyopathy have similar properties

Received for publication, August 14, 2019, and in revised form, September 18, 2019. Published, Papers in Press, October 3, 2019, DOI 10.1074/jbc.RA119.010563

Carlos D. Vera<sup>†1</sup>, Chloe A. Johnson<sup>§1</sup>, Jonathan Walklate<sup>§</sup>, Arjun Adhikari<sup>¶</sup>, Marina Svicevic<sup>||</sup>, Srboj M. Mijailovich<sup>\*\*</sup>, Ariana C. Combs<sup>‡</sup>, Stephen J. Langer<sup>‡</sup>, Kathleen M. Ruppel<sup>¶</sup>, James A. Spudich<sup>¶</sup>, Michael A. Geeves<sup>§2</sup>, and Leslie A. Leinwand<sup>‡3</sup>

From the <sup>†</sup>BioFrontiers Institute and Department of Molecular, Cellular and Developmental Biology, University of Colorado Boulder, Boulder, Colorado 80309, the <sup>§</sup>School of Biosciences, University of Kent, Canterbury CT2 7NJ, United Kingdom, the <sup>||</sup>Faculty of Science, University of Kragujevac, Serbia, the <sup>\*\*</sup>Department of Biology, Illinois Institute of Technology, Chicago, Illinois 60616, and the <sup>¶</sup>Department of Biochemistry, Stanford University School of Medicine, Stanford, California 94305

Edited by Enrique M. De La Cruz

Hypertrophic cardiomyopathy (HCM) is a common genetic disorder characterized by left ventricular hypertrophy and cardiac hyper-contractility. Mutations in the  $\beta$ -cardiac myosin heavy chain gene ( $\beta$ -MyHC) are a major cause of HCM, but the specific mechanistic changes to myosin function that lead to this disease remain incompletely understood. Predicting the severity of any  $\beta$ -MyHC mutation is hindered by a lack of detailed examinations at the molecular level. Moreover, because HCM can take  $\geq 20$  years to develop, the severity of the mutations must be somewhat subtle. We hypothesized that mutations that result in early onset disease would have more severe changes in function than do later onset mutations. Here, we performed steady-state and transient kinetic analyses of myosins carrying one of seven missense mutations in the motor domain. Of these seven, four were previously identified in early onset cardiomyopathy screens. We used the parameters derived from these analyses to model the ATP-driven cross-bridge cycle. Contrary to our hypothesis, the results indicated no clear differences between early and late onset HCM mutations. Despite the lack of distinction between early and late onset HCM, the predicted occupancy of the force-holding actin-myosin-ADP complex at  $[\text{Actin}] = 3 K_{\text{app}}$  along with the closely related duty ratio (the fraction of myosin in strongly attached force-holding states), and the measured ATPases all changed in parallel (in both sign and degree of change) compared with wildtype (WT) values. Six of

the seven HCM mutations were clearly distinct from a set of previously characterized DCM mutations.

The most common inherited cardiovascular disease is hypertrophic cardiomyopathy (HCM)<sup>†</sup> with a disease prevalence of 1:250–500 (1, 2). Excluding those with a history of hypertension, aortic stenosis, other pre-existing systemic diseases, or being a world-class athlete, HCM is diagnosed as unexplained left ventricular hypertrophy and is typically accompanied by diastolic dysfunction (3). The first gene identified to contain a mutation leading to HCM was *MYH7* for the  $\beta$ -cardiac myosin heavy chain and was reported almost 30 years ago (4, 5). There are now thousands of mutations in genes that encode proteins of the cardiac sarcomere, and these account for 60–70% of HCM cases (6). There are 8 major sarcomeric proteins that are implicated in the majority of HCM index cases and their families, with 60–70% found in either  $\beta$ -cardiac myosin or myosin-binding protein C (*MyBPC*). This suggests that myosin is an important target for therapeutic intervention (7, 8).

We consider here the difference between myosin mutations causing early onset *versus* late onset HCM. We hypothesized that  $\beta$ -cardiac myosin mutations associated with early onset HCM would be more severe than those mutations seen more typically in individuals who are diagnosed later in life. Analysis of the biochemical and biophysical properties of these 2 classes of myosins should reveal the severity of the mutational changes. We compared the properties of known adult pathogenic HCM mutations (R719W, R723G, and G741R) with novel sporadic mutations that had appeared in recent cardiomyopathy screens as specific to early onset patients (H251N, D382Y, P710R, and V763M) (9, 10).

The locations of the 7 residues in the  $\beta$ -MyHC protein under consideration here are shown in Fig. 1A. The high degree of conservation at those positions underscores the importance of

This work was supported by the Children's Cardiomyopathy Foundation (to L. A. L.), National Institutes of Health Grants 2R01GM029090 (to M. A. G., L. A. L., C. D. V.), 3R01GM029090–3151 and 1F31GM111058–01A1 (to C. D. V.), and 2R01HL117138–05 (to L. A. L., J. A. S., and C. D. V.), and European Union's Horizon 2020 Research and Innovation Programme Grant 777204 SILCOFCM (to M. A. G., S. M. M., M. S., and J. W.). J. A. S. is a co-founder of Cytokinetics and MyoKardia. L. A. L. is a co-founder of MyoKardia. J. A. S., L. A. L., and K. M. R. are members of the scientific advisory board for MyoKardia. The content is solely the responsibility of the authors and does not necessarily represent the official views of the National Institutes of Health.

This article contains Tables S1–S7 and Figs. S1–S6.

<sup>1</sup> Both authors contributed equally to the results of this work.

<sup>2</sup> To whom correspondence may be addressed. E-mail: m.a.geeves@kent.ac.uk.

<sup>3</sup> To whom correspondence may be addressed. E-mail: leslie.leinwand@colorado.edu.

<sup>4</sup> The abbreviations used are: HCM, hypertrophic cardiomyopathy; MyBPC, myosin-binding protein C; sS1, short subfragment 1; ELC, essential light chain; AB, assay buffer; DCM, Dilated cardiomyopathy; eGFP, enhanced green fluorescent protein; pN, piconewton; DR, —.

## Early and late onset HCM causing mutations in MYH7

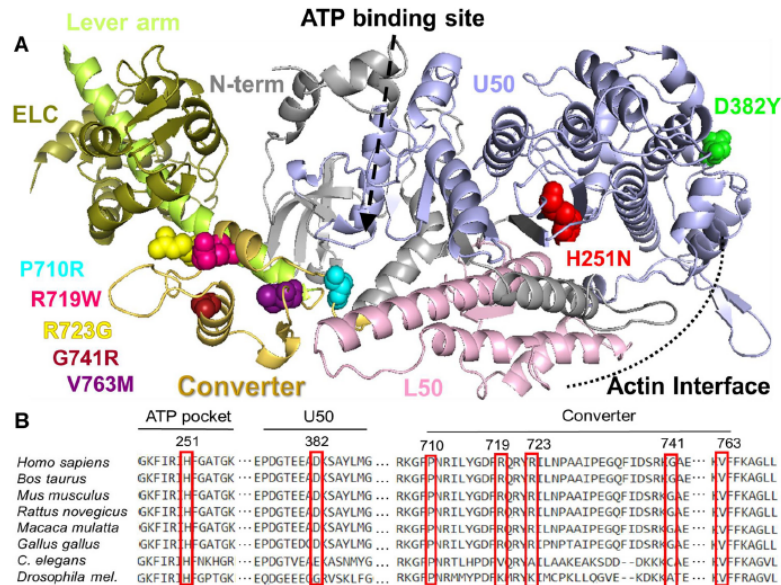


**Figure 1. Structural location of HCM mutations.** A, structural model of the catalytic domain of  $\beta$ -MyHC (based on Protein Data Bank code 4P7H). The heavy chain is shown as a ribbon diagram with the major subdomains and HCM mutations color-coded. The mutations sites are shown in space filling form in individual colors. The same colors are used throughout the figures and tables. Color code: red, H251N; green, D382Y; light blue, P710R; purple, V763M; pink, R719W; yellow, R723G; maroon, G741R. The lever arm and the essential light chain (ELC) are shown in two different shades of green on the left. B, alignment of conserved MYH7 residues where mutations discussed throughout this study can be found.

these sites (Fig. 1B). Myosin is very vulnerable to mutations and there are now >400 different mutations described in MYH7 (11, 12). A number of disease-causing MYH7 mutations have been studied in the context of recombinant human  $\beta$ -MyHC motors (13–17). R403Q, R453C, R719W, R723G, G741R, and D239N are mutations that are widely recognized as pathogenic and have been seen in multiple families (18). Less prevalent sporadic mutations like H251N, D382Y, P710R, and V763M appeared in genetic screens of early onset HCM patients (<15 years old) and their pathogenicity has not yet been clearly established (9, 18, 19).

H251N is in the central  $\beta$ -sheet (Fig. 1A) that undergoes strain-induced twisting upon ATP-binding and communicates to the upper 50,000 domain to open and release actin. H251N was identified in a screen of 79 pre-adolescent children and later characterized biophysically (10, 17). Adhikari *et al.* (17) found that this early onset mutation resulted in higher  $k_{cat}$ , actin-gliding velocity, and intrinsic force. Located close to the cardiomyopathy loop of the actin-binding domain, D382Y has been categorized as a variant of unknown (or uncertain) significance (VUS) (10, 18). Close to this residue is the well-studied pathogenic R403Q mutation that exhibits subtle biophysical changes compared with WT (14). Pro-710, a residue on the border between the SH1 helix and the converter, has been reported to be mutated to an arginine, leucine, or a histidine (10, 20). Unlike the arginine mutation, P710H and P710L have been seen multiple times, but the histidine is considered pathogenic, whereas the leucine and arginine mutations are rare and of unknown severity (10, 18, 20).

The myosin converter is well-known to be enriched for HCM-causing mutations with a range of adverse effects (21, 22). Converter mutations studied here include the late onset mutations R719W, R723G, and G741R and the early onset mutation, V763M. Muscle biopsy and skinned fiber studies have shown the converter domain late onset mutations have increased fiber stiffness with subtle changes in cross-bridge kinetics (23–25). The steady-state  $k_{cat}$ , the actin-gliding velocities, and the intrinsic force measurements of the myosin motor domain for these late onset pathogenic HCM mutations did not vary much when compared with WT (15). V763M has been reported in an early onset HCM screen and in a separate HCM cohort (19, 26). Both pathogenicity and age of symptom emergence are unclear for V763M (18).

Here, for the early and late onset HCM mutations, we show that the kinetic parameters of mutations also do not have a “unifying” disruption of the cycle. Contrary to our hypothesis, we did not detect any strong differences in kinetic parameters between mutations seen in late onset *versus* early onset patients, or among mutations in the different structural domains of the motor that account for the difference in the timing of pathological manifestation.

## Results

We produced recombinant mutant and WT human myosin motors in differentiated C2C12 muscle cells, performed extensive kinetic analysis, and evaluated the severity of these mutations based on alterations to the cross-bridge cycle. We specifically focused on the cross-bridge kinetics of the motor domain



Early and late onset HCM causing mutations in MYH7

**Table 1**  
Kinetic parameters for  $\beta$ -WT and 8 HCM mutations

The color code described in the smaller table indicates degree of difference from WT. Experimental conditions for stopped-flow: 25 mM KCl, 5 mM MgCl<sub>2</sub>, 20 mM MOPS, pH 7.0, 20 °C. Data are the mean  $\pm$  S.E. values from 3–5 independent measurements with 4–6 technical replicates. Values without S.E. are either ratios calculated with other values or parameters with one measurement. Bottom of the table contains the ATPase values used for modeling: \*ATPase values from (17), \*\*ATPase values from (15), \*\*\*Unpublished ATPase values.

|   | $\beta$ -WT      | Early onset     |                    |                   |                    | Late onset       |                   |                  |
|---|------------------|-----------------|--------------------|-------------------|--------------------|------------------|-------------------|------------------|
|   |                  | H251N           | D382Y              | P710R             | V763M              | R719W            | R723G             | G741R            |
| <b>ATP binding to S1</b>  |                  |                 |                    |                   |                    |                  |                   |                  |
| Second order rate constant of ATP binding ( $\mu\text{M}^{-1}\text{s}^{-1}$ ) | 5.8 $\pm$ 0.4    | 6.4 $\pm$ 0.6   | 3.3 $\pm$ 0.6      | 0.6 $\pm$ 0.07    | 3.1 $\pm$ 0.9      | 5.3 $\pm$ 1.7    | 4.1 $\pm$ 0.3     | 3.4 $\pm$ 0.7    |
| K <sub>50%</sub> ( $\mu\text{M}$ )  | 15.9 $\pm$ 2.2   | 20.3 $\pm$ 3.4  | 27.6 $\pm$ 4.1     | 35.7 $\pm$ 0.9    | 20.9 $\pm$ 3.2     | 14.1 $\pm$ 4.8   | 21.3 $\pm$ 2.5    | 37.8 $\pm$ 14.2  |
| K <sub>off</sub> +k <sub>off</sub> ( $\text{s}^{-1}$ )                        | 91.2 $\pm$ 1.8   | 125.7 $\pm$ 9.3 | 88.6 $\pm$ 2.0     | 69.1 $\pm$ 7.1    | 63.3 $\pm$ 8.6     | 58.2 $\pm$ 3.5   | 86.5 $\pm$ 4.2    | 106.5 $\pm$ 15.6 |
| <b>ADP binding to S1</b>  |                  |                 |                    |                   |                    |                  |                   |                  |
| ADP affinity ( $\mu\text{M}$ )  | 0.53 $\pm$ 0.06  | 0.19 $\pm$ 0.01 | 0.220 $\pm$ 0.034  | 3.1 $\pm$ 1.0     | 0.312              | 0.241            | 0.259             | 0.18 $\pm$ 0.03  |
| Rate constant of ADP release ( $\text{s}^{-1}$ )                              | 0.63 $\pm$ 0.03  | 1.0 $\pm$ 0.2   | 0.51 $\pm$ 0.06    | 0.14 $\pm$ 0.005  | 1.2                | 0.9 $\pm$ 0      | 0.98              | 0.71 $\pm$ 0.02  |
| <b>ATP binding to acto.S1</b>   |                  |                 |                    |                   |                    |                  |                   |                  |
| K <sub>T</sub> k <sub>off</sub> ( $\mu\text{M}^{-1}\text{s}^{-1}$ ) 20°C      | 4.4 $\pm$ 0.3    | 5.1 $\pm$ 0.4   | 4.5 $\pm$ 0        | 7.1 $\pm$ 0.7     | 4.4 $\pm$ 0.5      | 6.0 $\pm$ 1.0    | 5.0 $\pm$ 0.5     | 4.9 $\pm$ 0.8    |
| K <sub>T</sub> ( $\mu\text{M}$ ) 20°C   | 327.9 $\pm$ 53.3 | 131 $\pm$ 19    | 289.7 $\pm$ 65.3   | 161.0 $\pm$ 18.3  | 270.0 $\pm$ 78.8   | 125.6 $\pm$ 75.3 | 202.9 $\pm$ 60.4  | 178.4 $\pm$ 11.8 |
| k <sub>off</sub> ( $\text{s}^{-1}$ ) 20°C                                     | 1543 $\pm$ 100   | 666 $\pm$ 58    | 1300.7 $\pm$ 297.1 | 1106.5 $\pm$ 73.2 | 1175.8 $\pm$ 283.0 | 676 $\pm$ 145.9  | 556.1 $\pm$ 235.2 | 940.3 $\pm$ 336  |
| K <sub>T</sub> k <sub>off</sub> ( $\mu\text{M}^{-1}\text{s}^{-1}$ ) 10°C      | 2.7 $\pm$ 0.09   | 3.2             | 3.1 $\pm$ 0.2      | 3.9 $\pm$ 0.9     | 3.3 $\pm$ 0.5      | 3.2 $\pm$ 0.3    | 2.9 $\pm$ 0.2     | 2.7 $\pm$ 0.2    |
| K <sub>T</sub> ( $\mu\text{M}$ ) 10°C   | 365.7 $\pm$ 17.7 | 187             | 239.5 $\pm$ 21.1   | 251.5 $\pm$ 108.9 | 214.0 $\pm$ 23.3   | 184.9 $\pm$ 25.5 | 211.4 $\pm$ 41.0  | 224.0 $\pm$ 22.9 |
| k <sub>off</sub> ( $\text{s}^{-1}$ ) 10°C                                     | 991 $\pm$ 18.2   | 592             | 741.2 $\pm$ 28.4   | 814.1 $\pm$ 134.7 | 699.6 $\pm$ 62.5   | 573.2 $\pm$ 25.3 | 638.6 $\pm$ 56.0  | 639.8 $\pm$ 68.4 |
| <b>ADP affinity for acto.S1</b>   |                  |                 |                    |                   |                    |                  |                   |                  |
| ((K <sub>D</sub> +1)/K <sub>D</sub> K <sub>D</sub> ) ( $\mu\text{M}$ )        | 6.1 $\pm$ 0.7    | 20.8 $\pm$ 3.6  | 17.6 $\pm$ 2.7     | 14.6 $\pm$ 3.0    | 18.6 $\pm$ 8.4     | 15.9 $\pm$ 2.7   | 6.5 $\pm$ 0.7     | 10.1 $\pm$ 3.0   |
| k <sub>off</sub> ( $\text{s}^{-1}$ )  | 58.7 $\pm$ 3.3   | 56.7 $\pm$ 2.9  | 64.3 $\pm$ 2.4     | 69.1 $\pm$ 0.6    | 68.1 $\pm$ 10.5    | 96.8 $\pm$ 0.5   | 106.8 $\pm$ 0.3   | 71.1 $\pm$ 4.8   |
| K <sub>D</sub> K <sub>D</sub> ( $\mu\text{M}^{-1}\text{s}^{-1}$ )             | 9.6              | 2.7             | 3.7                | 4.7               | 3.8                | 5.9              | 16.4              | 7.0              |
| <b>S1 affinity for actin</b>  |                  |                 |                    |                   |                    |                  |                   |                  |
| K <sub>A</sub> (nM)   | 10 $\pm$ 1.8     | 8.7 $\pm$ 1.5   | 4.6                | <10               | 6.5 $\pm$ 3.8      | 1.6 $\pm$ 0.1    | 13.6              | 8.7 $\pm$ 4.7    |
| K <sub>DA</sub> (nM)  | 109.3 $\pm$ 13.8 | 56.3 $\pm$ 9.3  | not determined     | 12.2 $\pm$ 6.3    | 24.6               | 35 $\pm$ 8.2     | 48.4              | 23.1             |
| K <sub>DA</sub> /K <sub>A</sub>   | 10.9             | 6.5             | not determined     | 1.2               | 4.1                | 21.9             | 3.6               | 2.7              |
| <b>ATPase</b>   |                  |                 |                    |                   |                    |                  |                   |                  |
| k <sub>cat</sub> ( $\text{s}^{-1}$ )  | 4.1 $\pm$ 0.4*   | 5.1 $\pm$ 0.5*  | 4.9 $\pm$ 0.2***   | 2.5 $\pm$ 0.1***  | 4.0 $\pm$ 0.2***   | 3.9* $\pm$ 0.4** | 4.0 $\pm$ 0.2**   | 3.7 $\pm$ 0.3**  |
| K <sub>app</sub> ( $\mu\text{M}$ )  | 33 $\pm$ 6*      | 34 $\pm$ 10*    | 52 $\pm$ 5***      | 14 $\pm$ 1***     | 18 $\pm$ 4***      | 33 $\pm$ 4**     | 43 $\pm$ 5**      | 29 $\pm$ 3**     |
| k <sub>cat</sub> /K <sub>app</sub> ( $\text{s}^{-1}\mu\text{M}^{-1}$ )        | 0.124            | 0.150           | 0.094              | 0.171             | 0.222              | 0.118            | 0.093             | 0.128            |

No (significant) change from WT

>30% slower/weaker

>2 fold slower/weaker

>30% faster/tighter

>2 fold faster/stronger

region utilizing the short subfragment 1 (sS1, corresponding to residues 1–808, Fig. S1).

**ATPase activity**

Steady-state ATPase data for 4 of the mutations examined here H251N, R719W, R723G, and G741R, have already been

published (15, 17). These are listed in Table 1 together with the k<sub>cat</sub> values for the remaining 4 mutations. The error on these measurements is of the order of 10% and 3 of the mutations, the early onset V763M and the late onset R719W and R723G, differ from WT by less than 5%. The k<sub>cat</sub> for G741R is less than 10% lower than WT. Three other mutations, H251N, D382Y, and

## Early and late onset HCM causing mutations in MYH7

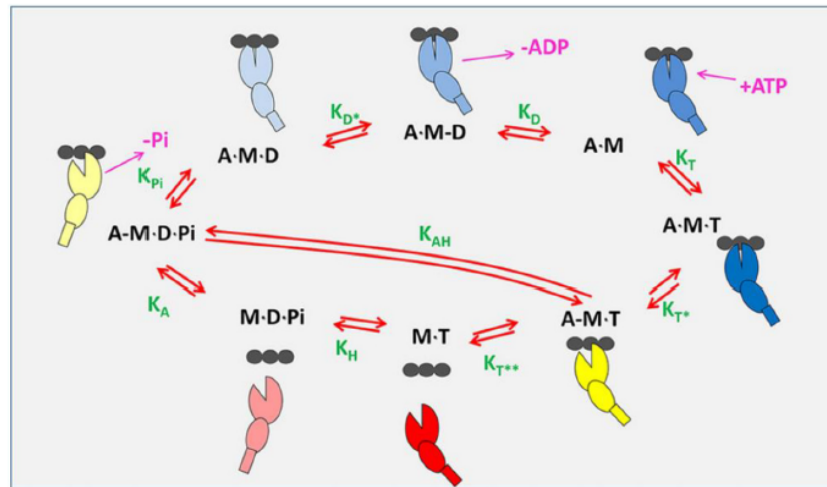


**Figure 2. Actin-myosin ATPase-driven cross-bridge cycle.** As discussed (28) the basic ATPase cycle for myosin can be described in 8 steps: ATP binding to acto-myosin, ATP-induced conformational change that weakens actin affinity, ATP-induced dissociation from actin, ATP hydrolysis, actin re-attachment,  $-P_i$  release + power stroke, conformational change in the transducer region coordinating ADP for release, and ending with ADP release. The myosin is a composite of a large ellipse (motor domain), a smaller ellipse (converter), and a small rectangle (lever arm) binding to an actin filament depicted as three black ellipses. A blue-shaded myosin is strongly-attached to actin (closed ellipse) and is progressively darker as it approaches the rigor state. The myosins with an open cleft are shown in yellow (weakly-attached) and red (detached). Nucleotide and  $P_i$  release are shown in cerise. Equilibrium constants for each step are shown in green and defined in the clockwise direction.

P710R, differ significantly from WT. The early onset H251N and D382Y are higher than WT by 24 and 20%, respectively, whereas P710R is 39% lower than WT. Thus, there is no common pattern of change in the  $k_{cat}$  values for these HCM mutations and no difference in pattern between early and late onset groups. This lack of common patterns led us to focus on the transient kinetic analysis that can reveal more detail about how mutations change the ATPase cycle.

### Transient kinetics data summary

Considerable amounts of pre-steady-state kinetic data have been collected for a number of DCM and HCM mutations in the  $\beta$ -MyHC motor domain. The descriptions of methods, analysis tools, model assumptions, data quality, and details of the measurements have been presented in our earlier works (13, 14, 27–29). We have taken the same approach to understand the impact of this set of HCM mutations and to compare with the results of previous studies. Details of individual measurements and the evaluation of data quality are presented in the supporting information (Fig. S2–S6). Here we focus on what effect each mutation has on the behavior of the cycle. For every mutant, each measurement was made at least 3 times with a minimum of 2 independent protein preparations. In general, all parameters were measured to a precision of better than 20% and in most cases better than 10%. Given this level of sensitivity, we assume any change of less than 20% is not significant.

The data are interpreted in terms of the 8-step ATP-driven cross-bridge cycle that we have used previously (Fig. 2). Red shades indicate detached cross-bridges, yellow shades are weakly-attached, and blue shades represent strongly-attached force-holding cross-bridges. Table 1 shows the mean values and errors of the actin and nucleotide-binding experiments for the steps in the cycle that are accessible, together with the

ATPase parameters. To make the overall pattern of the induced changes clearer, the percent changes relative to WT are color coded in Table 1. The data are also summarized in Fig. 3, where the percentage differences in each parameter relative to WT are plotted.

### Interaction of sS1 with nucleotide in the absence of actin

Even though the reactions are not part of the normal cycle, nucleotide binding to the motor in the absence of actin is measured to understand how the nucleotide-binding pocket and the weakly-attached actin states might be affected by mutations. This process can be important to understand the cycle of the second myosin head, whereas the other can be attached to actin. The affinity of ATP for sS1 is weakened >2-fold for 2 mutations (P710R and G741R). All other mutations were 27–73% weaker except R719W, which was indistinguishable from WT. In contrast, most mutants bound ADP >2-fold tighter, with the exception of V763M (just less than 2-fold tighter) and P710R (6-fold weaker). Thus, no simple pattern of behavior was apparent for the sS1 in the absence of actin, but most mutations significantly affected nucleotide binding.

### Interaction of sS1 with nucleotide in the presence of actin

The darker color coding of the data in Table 1 shows the parameters that change >2-fold (dark blue decrease, dark orange increase) and indicate that a large number of parameters have been affected, and at least one parameter for each mutant. Thus, the changes observed are not minor, despite relatively small changes in the value of the steady-state  $k_{cat}$ .

Fig. 3A shows that in general, the value of  $K_T$  (the affinity of ATP for acto-sS1) measured at 10 °C where it is well-defined,  $K_A$  (the affinity of actin for sS1), and  $K_{DA}$  (the affinity of actin for sS1·ADP) have tighter binding. For  $K_T$  this is >20% tighter, but

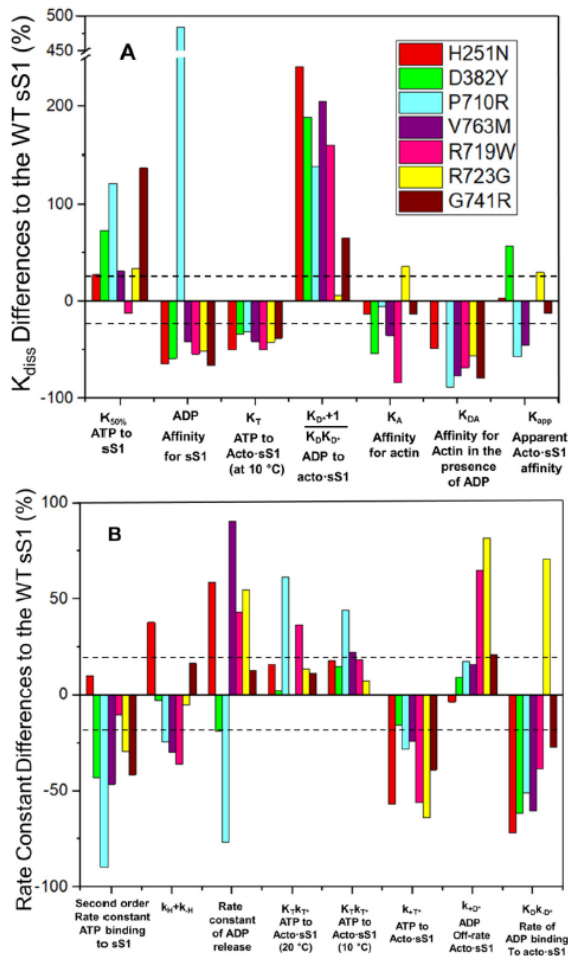


**Figure 3. Summary of percentage differences in kinetic parameters of HCM mutations relative to WT.** A, % change for measured dissociation or equilibrium constants. Also included is the  $K_{app}$  value from ATPase analysis. B, % change of several measured rate constants. Color-coded to match the parameter to each HCM mutation. The dashed lines represent  $\pm 20\%$  change in the parameter considered to be the precision of each measurement.

none is as much as 2-fold tighter. For  $K_{DA}$  the affinities are mostly  $>2$ -fold tighter with V763M, G741R, and P710R  $>4$ -fold tighter, whereas the data for  $K_A$  is much more variable. The affinity of ADP for acto-sS1 is  $>2$ -fold weaker in 5 cases. R723G is an exception for both the  $K_A$  and ADP affinity for acto-sS1 parameters, but there is a general pattern.

Fig. 3B shows changes in measured rate constants. There is some consistent behavior, but it is not uniform for all mutations. The maximum rate constant for sS1 detachment from actin upon binding ATP ( $k_{+1}$ ) is generally slower (20–70%) and the rate constant for ADP binding to acto-sS1 is also generally slower (30–70%) with the exception of R723G, which is increased by 70%. All other rate constants had variable changes or none at all. This highly variable pattern was also seen for the set of DCM mutations we previously reported (27).

**Modeling the ATPase cycle of HCM mutant motors**

We modeled the complete cycle using all of our kinetic data following the approach outlined in recent papers comparing different myosin isoforms and different DCM-causing mutations in MYH7 (27, 29). The transient kinetics data provide definition for 6 of the 8 steps of the cycle with a precision generally of  $\pm 20\%$ . When combined with ATPase data ( $k_{cat}$  and  $K_{app}$ ), the full cycle allows us to predict acto-sS1 occupancy of states (Fig. 4; Table S3), along with key properties of the cycle: DR, shortening velocity, steady-state force (Fig. 5; Table S2), and ATP economy (Fig. 7). Under isometric conditions in a muscle fiber, because of the mismatch of the thick and thin filament helicity, some myosin heads have readily accessible actin, whereas others do not. We therefore modeled a range of actin concentrations ( $[A] = K_{app}, 3 K_{app},$  and  $20 K_{app}$ , where the ATPase rate is 50, 75, and 98% of  $k_{cat}$  values, respectively) to facilitate comparison between the different mutant constructs under conditions that may match those of a contracting sarcomere. In addition, we modeled contraction under load as described previously (29), by assuming both ADP and  $P_i$  release steps were inhibited 3-fold under a 5-pN load for all mutations (see “Discussion”).

The predicted occupancies are shown in Fig. 4. Note that the color schemes are the same in Figs. 2 and 4; red shades indicate detached cross-bridges, yellow shades are weakly-attached, and blue shades represent strongly-attached force-holding cross-bridges. The numbers above each pie chart represent the percentage of the force-holding A·M·D state (pale blue). The WT data predict at low actin concentration ( $[A] = K_{app}$ ), almost 75% of cross-bridges are detached with just 4.7% in the force-holding blue states, dominated by the A·M·D state. As actin concentration increases, the detached-states (red) decrease, the weakly-attached states (yellow) increase, and the strongly-attached A·M·D state increases to 9.0% at  $20 K_{app}$ . The application of a 5-pN load at  $[A] = 3 K_{app}$  did not change the A·M·D state from 7.0% and increased the weakly-attached states (mainly A·M·D·P) at the expense of the detached M·T state. Note the occupancy values here are slightly lower than in Ref. 27 because of a slightly lower WT  $k_{cat}$  value used within this consistent data set.

Examining pie charts in Fig. 4 for the mutations shows that the general distribution of states is very similar between WT and H251N although the force-holding A·M·D state was higher ( $\sim 25\%$ ) for H251N at all actin concentrations. This distribution was marginally larger (by about 10%) for D382Y. However, for P710R, V763M, R719W, R723G, and G741R, the force-holding A·M·D states were smaller (by  $>20\%$ ), whereas the detached M·T states (deep red) were larger. These comparisons are easier to assess in Fig. 5 where the predicted A·M·D occupancy for  $[A] = 3 K_{app}$  with and without load are plotted along with the closely related DR and the calculated ATPases. All 3 parameters change in parallel (in both sign and degree of change) compared with the WT values.

The predicted velocity of shortening was estimated from the equation  $V_o = d \cdot \text{ATPase} / \text{DR}$ , where  $d$  is the step size (assumed to be invariant at 5 nm).  $V_o$  shows little variation among the 7 mutants with 5 mutations varying by  $\sim 10\%$  and only R719W

## Early and late onset HCM causing mutations in MYH7

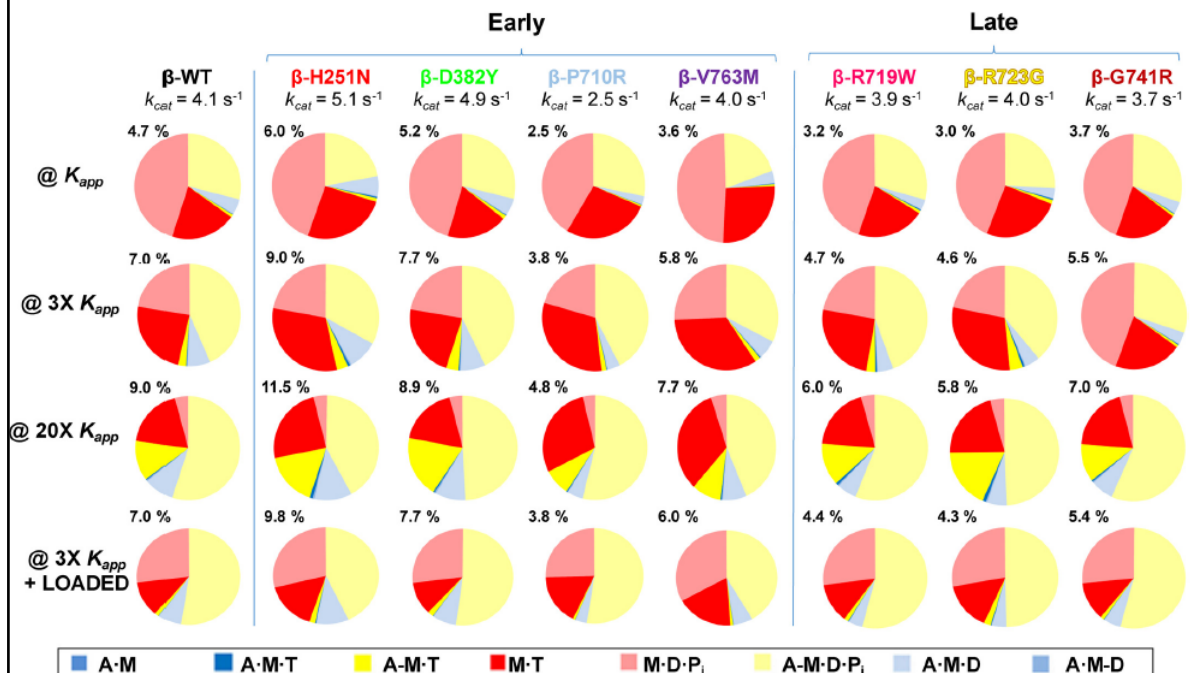


**Figure 4.** The occupancy of each intermediates from the 8-step ATPase cycle. The occupancy is shown at four actin-activated conditions; where  $[A] = K_{app}$ ,  $3K_{app}$ ,  $20K_{app}$ , and  $3K_{app} + 5 \text{ pN}$  load. This figure is color-coded to match the scheme from Fig. 2 and the color legend shown below. Percentages at the upper left of each pie chart represents the percentage of time per cycle spent in the AMD state.

and R723G increase velocity by >30% (Fig. 5). *In vitro* motility measurements of human recombinant cardiac sS1 have been published for several HCM mutations (15, 17). Additional motility data of HCM mutations (D382Y, P710R, and V763M) were collected here to consolidate with the kinetics data (Fig. 6, Table S7). Fig. 6 shows the mean velocity of the top 5% of smoothly moving filaments, normalized to the WT values, compared with our predictions. The normalization to the WT values allows comparison between the data sets different experimental conditions used. For 5 of the 7 mutations, the predicted velocities are in good agreement with those measured. There are large discrepancies for H251N (~50% higher than predicted) and P710R (>60% lower than predicted). We consider this discrepancy under "Discussion."

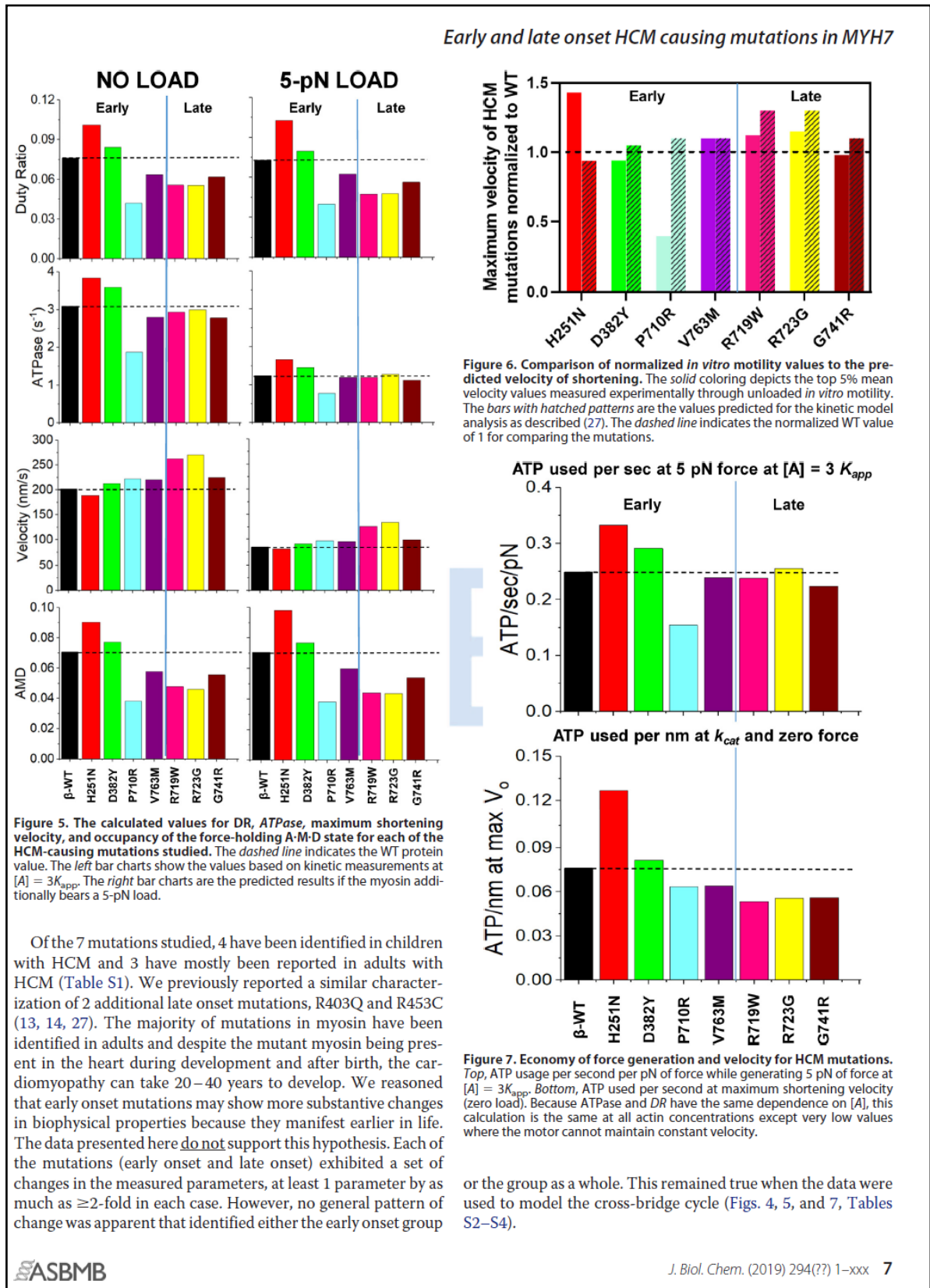
The modeling data also allow an estimate of the economy of ATP usage, another parameter that could be involved in the development of HCM (30) if it results in a metabolic imbalance in the muscle. The predicted rates of ATP usage are shown in Fig. 7 for both a muscle fiber holding a 5-pN load (ATP used per pN) and when shortening at the  $V_{max}$  with ATP being turned over at  $k_{cat}$  (ATP/nm moved). Once more, the changes in economy for each mutation under both conditions reflected the changes in the ATPase rates relative to WT.

### Discussion

We have presented here a detailed evaluation of the human  $\beta$ -cardiac myosin motor domain carrying 7 different HCM missense mutations. Before considering the implications of our data it is pertinent to point out the precision with which we can

evaluate the data. All measured constants are defined to within an error of at least 20%, and in many cases better than 10%, using independent preparations of protein. The fitting of the data to the model uses all of the data to define the 5 missing constants in the 8-state cross-bridge cycle (Fig. 2). In our previous studies of DCM mutations (27) and the  $\alpha$ - and  $\beta$ -cardiac isoforms (29), we showed the fitting was quite robust and that a  $\pm 20\%$  change in any of the constants had minimal effect on the overall balance of the cycle except for the intermediate most directly affected by the varied constant. A similar analysis was carried out here (Tables S5 and S6), so we are confident in the analysis of the cross-bridge cycles presented.

We compared our predictions of velocity with the measured velocities in *in vitro* motility assays using relative values of velocities (Fig. 6). Absolute values of velocity can be difficult to compare because these vary (see Table S7) between laboratories and within a single laboratory. Reference velocities are normally measured at the same time as novel measurements to allow comparisons. A similar problem can occur with  $k_{cat}$  measurements that depend critically on the equality of the protein preparation. Despite these difficulties our predictions are in good agreement with relative measured values for 5 of the 7 HCM mutations. The exceptions are H251N (which has a high  $k_{cat}$  and a high  $DR$  compared with WT) and P710R (which has low values of  $k_{cat}$  and  $DR$ ). We noted previously for the DCM mutations that estimates of velocity can become problematic if the  $DR$  values are very low because higher myosin densities may be required to achieve the true maximum velocities.



## Early and late onset HCM causing mutations in MYH7

We previously identified common traits among myosins carrying 1 of 5 mutations associated with DCM (27). Most of the mutations were found to have a reduced  $k_{\text{cat}}$ , lower occupancy of the force holding AMD state, a lower  $DR$ , and a more economical use of ATP for both rapid movement and force generation. Collectively, the DCM mutant myosins had an impaired capacity to generate or maintain force when working as an ensemble. Curiously, 1 of the mutations examined here shares these properties: the early onset P710R, suggesting some overlap between the groupings. Intersection of molecular phenotypes among different cardiomyopathies has been observed in studies of thin filament mutations and experiments performed in *Drosophila* (31, 32).

The remaining 6 mutations show mostly modest changes in properties as was previously observed for the R403Q and R453C HCM mutations. The  $k_{\text{cat}}$ , economy of ATP usage, and  $DR$ 's were similar to WT for D382Y, V763M, R719W, R723G, and G741R, whereas all 3 parameters were increased for H251N. Thus, for 6 of the 7 HCM mutations, the functional distinctions between HCM and DCM mutations that we previously reported remain valid. There are 3 perspectives that explain the molecular basis of HCM, including: 1) functional parameter changes; 2) increased number of available myosin heads; and 3) and changes in load dependence of contractility (33). A combination of these subtle differences that are detected experimentally could help distinguish HCM severity among the different mutations.

There is considerable interest in the role of the interactions between the 2 motors of myosin in forming a down-regulated form of myosin: the interacting head motif (34, 35). Such motors are likely to be further stabilized by interactions with both the backbone of the thick filament and *MyBPC* (34–36). Myosin mutations that destabilize an off-state would make more heads available and lead to a hyper-contractile state, hypothesized to be the precursor to HCM (33–35, 37). The interaction between the off- and on-states of myosin is postulated to be regulated by phosphorylation of the regulatory light chain or *MyBPC*, mechanical strain on the thick filament, and possibly calcium (36, 38–41). Destabilization of the off-state could occur by reducing motor-motor, motor-backbone, or motor-MyBPC interactions. Any effect on the interacting heads could override the modest effects we report here on the cross-bridge cycle for most of the HCM mutations. This seems less likely to be the case for P710R, which appears similar to the DCM mutations where the large reduction in  $k_{\text{cat}}$  (30–40%) and  $DR$  (40–50%) will have a significant effect on the working cardiac muscle. Any effect on the interacting heads would need to be large enough to compensate for the loss of force-holding cross-bridges in the steady-state caused by these changes in the  $DR$ .

A recent study used the latest crystal structures docked into lower resolution EM images of the interacting motors to identify regions of the motor directly involved with the interaction. This work was combined with a molecular dynamics study to suggest how mutations might affect myosin function (42). HCM mutants were predicted to affect interacting heads, the stability of the M-D-P<sub>i</sub> state required to form the interacting heads, the motor function, the stability of the motor, or some

combination of the effects. From the Robert-Paganin *et al.* (42) study, our mutations H251N, R719W, R723G, and G741R were predicted to affect motor function, which is consistent with our results, and to destabilize the sequestered state due to effects on interacting head motif contacts, which is consistent with other experimental results (for a review, see Ref. 33). P710R was predicted to alter motor function and destabilize the sequestered state by affecting the stability of the pre-power-stroke conformation, whereas V763M was predicted to affect mostly protein stability. Furthermore, studies of converter mutations have concluded that perhaps biochemical and motility data are not the directly involved parameters, but instead it is force generation or how the force-velocity curve is influenced (23, 43).

The question of what distinguishes mutations associated with early onset remains a valid question, but we need to address whether the diagnosis of early onset is a distinct group. It seems likely that factors such as genetic modifiers in addition to the myosin mutation contribute to many aspects of the disease, including age at which symptoms manifest (44, 45). In addition, the assays performed here are purely *in vitro* with single motor domains and other *in vitro* assays may shed further light on mechanisms of pathogenesis (33). Although beyond the scope of this study, the assumption that the step size is unaffected could be tested using a single-molecule laser trap assay. Also, detailed direct biophysical measurements of the load dependence of the strongly-bound state are possible using harmonic force spectroscopy (46) as well as measurements of the extent of sequestering of heads into a super-relaxed state (47). Furthermore, significant differences may be found using regulated thin filaments rather than purified actin in the ATPase measurements (14). In addition to these further *in vitro* studies, the mutant myosins may need a cellular or tissue environment to manifest their full pathological consequences.

At the outset of this series of studies, we began with the expectation that there would be common molecular pathways for HCM *versus* DCM mutations. The work has defined more sharply the ranges of effects mutations can have on the myosin motor and still have a functioning heart. To understand the way in which the mutations lead to myopathies, there is a need for more complex *in vitro* assays as well as assays that include cells and/or engineered 3D tissues to integrate the signals in the muscle that converge to cause disease. This includes the role of a heterogeneous mixture of WT and mutant myosins in tissue.

## Experimental procedures

### Expression and purification of proteins

Producing recombinant  $\beta$ -cardiac myosin in C2C12 cells in several iterations, isoforms, and mutants has been described previously in Refs. 13, 14, 27, 28, 48, and 49). The sS1 (residues 1–808) was followed by a flexible GSG (Gly-Ser-Gly) linker and either a C-terminal 8-residue (RGSIDTWV) PDZ-binding peptide or a C-terminal eGFP. The late onset mutations studied in Ref. 15 had an eGFP molecule at the C terminus of the sS1 followed by the PDZ-binding peptide. The early onset mutations lacked the eGFP molecule. Human ventricular essential light chain (MYL3 or ELC) with either an N-terminal His<sub>6</sub> or a FLAG tag was co-expressed with the heavy chain. Over the

course of the different experiments, a combination of affinity and ion exchange chromatography were used as in our previous studies (*i.e.* His or FLAG + Q column). The fast kinetics experiments in this study were done with protein purified with double affinity, a His-nitrilotriacetic acid resin and the PDZ-C-tag affinity system described in Ref. 50. WT-erbin PDZ was prepared as described in Refs. 50 and 51 and cross-linked to the Sulfolink Coupling Resin (Thermo Fisher) using the manufacturer's protocol. After the myosin was eluted from the His column, the sample was dialyzed into  $1\times$  TBS to remove the imidazole. The PDZ system uses 20–50  $\mu\text{M}$  "elution peptide" ( $\text{NH}_2$ -WETWV-COOH from GenScript). After the second column, the myosin samples were buffer exchanged and frozen in the appropriate assay buffer. Actin preparations were made from bovine left ventricle with protocols adapted from Refs. 52 and 53. The protocol for preparing pyrene-labeled actin is based on the methods described in Ref. 54.

#### Steady-state actin-activated ATPase assays

All ATPase experiments were performed at 23 °C room temperature in a buffer containing 10 mM imidazole, 3 mM  $\text{MgCl}_2$ , 5 mM KCl, and 1 mM DTT, pH 7.5. A colorimetric assay was used to measure  $\text{P}_i$  production at various time points and actin concentrations ranging 0 to 100  $\mu\text{M}$  (55). The rates of phosphate production were plotted and fitted to the Michaelis-Menten equation using Origin (OriginPro) and/or GraphPad Prism to obtain the  $k_{\text{cat}}$  and  $K_{\text{app}}$ . These assays were carried out with a  $\beta$ -WT control.

#### Transient kinetics

All stopped-flow measurements were performed at 20 °C in 20 mM MOPS, 25 mM KCl, 5 mM  $\text{MgCl}_2$ , 1 mM  $\text{NaN}_3$ , pH 7.0, unless indicated otherwise. Rapid-mixing experiments using 2–5 biological replicates, with 4–6 technical replicates, over a wide range of experimental substrates were performed in a High-Tec Scientific SF-61 DX2 stopped-flow system. Transient kinetic traces were initially fitted with TgK Scientific (Kinetic Studios) and subsequently plotted with Origin (OriginPro). For experiments probing the actin-myosin interaction with ATP and ADP we utilized the fluorescence signal for the pyrene-labeled actin, which has an excitation wavelength at 365 nm and the emission was detected after passing through a KV389-nm cut-off filter. In the absence of actin, we relied on the intrinsic tryptophan fluorescence post-nucleotide binding where a tryptophan on the relay helix can be excited at 295 nm and the emission is detected with WG-320 filter.  $\beta$ -WT and rabbit S1 were constantly used as internal controls for data comparison and assay validation. In all figure legends the concentration of reactants refers to those after mixing.

#### Modeling analysis

The parameters estimated experimentally by the transient kinetics analysis can be utilized to model the cross-bridge cycle by having a good estimate of the  $k_{\text{cat}}$  and  $K_{\text{app}}$  values obtained from the ATPase experiments and using the in-house MUSICO software (29). We previously reported a kinetic modeling analysis of 5 DCM mutations using this approach (27). This can be employed to predict the transient occupancy of the states in the

myosin ATPase cycle, across a wide range of actin concentrations assuming initially a state where  $[\text{ADP}] = [\text{P}_i] = 0$ , and the system proceeds to steady-state activity (29). Because the different steps of the cycle have interdependence to each other it is important that the experimental data provide a uniquely resolved set of modeling parameters to properly fit the rate and equilibrium constant of the cycle (56). Consistent with our previous modeling work, the fitted parameters are defined to a precision of  $\sim 20\%$ . Other well-defined assumptions and estimates applied to this mechano-chemical cycle model for  $\beta$ -MyHC are the isoform-specific constraint effect and the effect of load on the motor (57, 58). For a muscle fiber under isometric tension an approximate 5-pN load with a 3-fold reduction in the ADP release rate constant are suggested as good estimates. This reduction of the ADP-release rate has little effect on the ATP flux, because this step is significantly faster than the overall  $k_{\text{cat}}$ . Additionally, the rate of entry into the force-generating state is expected to be inhibited by load via the Fenn effect (59). Therefore, a 3-fold inhibition of the ATPase flux is applied to the model by reducing the entry rate into the force-holding state (A·M·D), which is  $k_{\text{pi}}$  in our model (19). This assumes that a load will impact the  $\text{P}_i$  and ADP release steps similarly.

#### Analysis of errors in the modeling

We have set out in our previous work the approach to defining the errors in the modeling (27, 29). The parameters that go into the model are all assumed to be defined to a precision of  $\sim 20\%$  based on the estimate of errors of the measurements (see Table 1). Fitting the model to the ATPase data then produces definition of the remaining unmeasured parameters ( $K_A$ , actin affinity to M·ADP·Pi;  $K_{\text{HP}}$ , ATP hydrolysis;  $K_{\text{AH}}$ , ATP hydrolysis while attached to actin;  $k_{\text{pi}}$ , the rate constant of  $\text{P}_i$  release/force generating step; and the  $k_{-T}$ , rate of reverse ATP dissociation). The diagonals of resolution matrices (Fig. S3) demonstrate that the values are defined relatively independently of each other with the exception of  $k_{-T}$ , which is codependent of the other values.

As previously, to assess the quality of the fits we varied each of the values in Table S3 by  $\pm 20\%$  and refitted the data to assess the effect on the overall fitting. These have only a small effect on the other fitted parameters usually by much less than 20%. This can be seen in the analysis of the WT data in our previous publication (29). The results for the mutations used here were similar. Here, as we did for a set DCM mutations (27) we additionally varied  $k_{\text{cat}}$ , the rate constant of the step limiting ADP release ( $k_{\text{D}}$ ) and the hydrolysis step ( $k_{\text{H}}$ ) and as an illustration the data are shown for P710R and R723G in Table S6. In general, the test shows the fitting to be quite robust; a change in a parameter of 20% alters only those events most directly affected and to a similar extent as the 20% change imposed. The data are discussed under "Results" and "Discussion."

#### In vitro motility

All the experiments were performed at 23 °C. Glass coverslips (VWR micro-coverglass) were coated with a mixture of 0.2% nitrocellulose (Ernest Fullam Inc.) and 0.2% collodion (Electron Microscopy Sciences) dissolved in amyl acetate

## Early and late onset HCM causing mutations in MYH7

(Sigma) and air-dried before use. A permanent double-sided tape (Scotch) was used to construct 4 channels on each slide, and 4 different experiments were performed on the same slide. Partially inactivated myosin heads in sS1 preparations were removed by the “dead-heading” process before performing the motility assay. The process of dead-heading had the following steps: a 10-fold molar excess of F-actin was added to myosin in the presence of 2 mM ATP; the mixture was incubated for 15 min in an ice bucket; 50 mM MgCl<sub>2</sub> was added to form F-actin Mg<sup>2+</sup>-paracrystals and incubated for 5 min; the paracrystals were sedimented at 350,000 × *g* for 15 min; the supernatant was collected and the sS1 concentration was measured using the Bradford reagent (Bio-Rad). Before any experiments, dead-headed sS1 was diluted in 10% AB-BSA (assay buffer (AB): 25 mM imidazole, pH 7.5, 25 mM KCl, 4 mM MgCl<sub>2</sub>, 1 mM EGTA, and 1 mM DTT) with bovine serum albumin (BSA, 0.1 mg/ml) diluted in AB, unless otherwise stated.

For motility experiments using pure actin, reagents were sequentially flowed through the channels in the following order: 10 μl of 4 μM SNAP-PDZ18 diluted in AB and incubated for 3 min; 20 μl of AB-BSA to block the surface from nonspecific attachments and incubated for 2 min; 10 μl of a mixture of 8-residue (RGSIDTWV) tagged human β-cardiac sS1 (~0.05 to 0.1 mg/ml) and incubated for 3 min; 20 μl of AB to wash any unattached proteins; and finally, 10 μl of the GO solution (5 to 10 nM tetramethylrhodamine-phalloidin (Invitrogen)-labeled bovine actin, 2 mM ATP (Calbiochem), an oxygen-scavenging system consisting of 0.2% glucose, glucose oxidase (0.11 mg/ml; Calbiochem), and catalase (0.018 mg/ml; Calbiochem)), and an ATP regeneration system consisting of 1 mM phosphocreatine (Calbiochem) and creatine phosphokinase (0.1 mg/ml; Calbiochem) in AB-BSA. A β-WT control was present for all mutant measurements.

**Author contributions**—C. D. V., J. A. S., M. A. G., and L. A. L. conceptualization; C. D. V., J. A. S., M. A. G., and L. A. L. resources; C. D. V., J. A. S., M. A. G., and L. A. L. supervision; C. D. V., J. A. S., M. A. G., and L. A. L. funding acquisition; C. D. V., C. A. J., J. W., A. A., M. S., K. M. R., and J. A. S. investigation; C. D. V. and C. A. J. visualization; C. D. V., C. A. J., A. C. C., S. J. L., K. M. R., and J. A. S. methodology; C. D. V. and C. A. J. writing-original draft; C. D. V., J. A. S., M. A. G., and L. A. L. project administration; C. D. V., K. M. R., J. A. S., M. A. G., and L. A. L. writing-review and editing; C. A. J., J. W., M. S., and S. M. M. data curation; C. A. J., J. W., M. S., S. M. M., and A. C. C. formal analysis; M. S., S. M. M., and A. C. C. software; M. S. and S. M. M. validation.

**Acknowledgment**—We thank Sam Lynn for technical assistance.

### References

- Harris, K. M., Spirito, P., Maron, M. S., Zenovich, A. G., Formisano, F., Lesser, J. R., Mackey-Bojack, S., Manning, W. J., Udelson, J. E., and Maron, B. J. (2006) Prevalence, clinical profile, and significance of left ventricular remodeling in the end-stage phase of hypertrophic cardiomyopathy. *Circulation* 114, 216–225 CrossRef Medline
- Hershberger, R. E., Hedges, D. J., and Morales, A. (2013) Dilated cardiomyopathy: the complexity of a diverse genetic architecture. *Nat. Rev. Cardiol.* 10, 531–547 CrossRef Medline
- Stewart, B., Mason, D. T., and Braunwald, E. (1968) Impaired rate of left ventricular filling in idiopathic hypertrophic subaortic stenosis and valvular aortic stenosis. *Circulation* 37, 8–14 CrossRef Medline
- Jarcho, J. A., McKenna, W., Pare, J. A., Solomon, S. D., Holcombe, R. F., Dickie, S., Levi, T., Donis-Keller, H., Seidman, J. G., and Seidman, C. E. (1989) Mapping a gene for familial hypertrophic cardiomyopathy to chromosome 14q1. *N. Engl. J. Med.* 321, 1372–1378 CrossRef Medline
- Geisterfer-Lowrance, A. A., Kass, S., Tanigawa, G., Vosberg, H. P., McKenna, W., Seidman, C. E., and Seidman, J. G. (1990) A molecular basis for familial hypertrophic cardiomyopathy: a β cardiac myosin heavy chain gene missense mutation. *Cell* 62, 999–1006 CrossRef Medline
- Teekakirikul, P., Kelly, M. A., Rehm, H. L., Lakdawala, N. K., and Funke, B. H. (2013) Inherited cardiomyopathies: molecular genetics and clinical genetic testing in the postgenomic era. *J. Mol. Diagn.* 15, 158–170 CrossRef Medline
- Green, E. M., Wakimoto, H., Anderson, R. L., Evanchik, M. J., Gorham, J. M., Harrison, B. C., Henze, M., Kawas, R., Oslob, J. D., Rodriguez, H. M., Song, Y., Wan, W., Leinwand, L. A., Spudich, J. A., McDowell, R. S., Seidman, J. G., and Seidman, C. E. (2016) Heart disease: a small-molecule inhibitor of sarcomere contractility suppresses hypertrophic cardiomyopathy in mice. *Science* 351, 617–621 CrossRef Medline
- Ashrafian, H., McKenna, W. J., and Watkins, H. (2011) Disease pathways and novel therapeutic targets in hypertrophic cardiomyopathy. *Circ. Res.* 109, 86–96 CrossRef Medline
- Morita, H., Rehm, H. L., Menesses, A., McDonough, B., Roberts, A. E., Kucherlapati, R., Towbin, J. A., Seidman, J. G., and Seidman, C. E. (2008) Shared genetic causes of cardiac hypertrophy in children and adults. *N. Engl. J. Med.* 358, 1899–1908 CrossRef Medline
- Kaski, J. P., Syrris, P., Esteban, M. T., Jenkins, S., Pantazis, A., Deanfield, J. E., McKenna, W. J., and Elliott, P. M. (2009) Prevalence of sarcomere protein gene mutations in preadolescent children with hypertrophic cardiomyopathy. *Circ. Cardiovasc. Genet.* 2, 436–441 CrossRef Medline
- Hamady, M., Buvoli, M., Leinwand, L. A., and Knight, R. (2010) Estimate of the abundance of cardiomyopathic mutations in the β-myosin gene. *Int. J. Cardiol.* 144, 124–126 CrossRef Medline
- Colegrave, M., and Peckham, M. (2014) Structural implications of β-cardiac myosin heavy chain mutations in human disease. *Anat. Rec.* 297, 1670–1680 CrossRef
- Bloemink, M., Deacon, J., Langer, S., Vera, C., Combs, A., Leinwand, L., and Geeves, M. A. (2014) The hypertrophic cardiomyopathy myosin mutation R453C alters ATP binding and hydrolysis of human cardiac β-myosin. *J. Biol. Chem.* 289, 5158–5167 CrossRef Medline
- Nag, S., Sommese, R. F., Ujfalusi, Z., Combs, A., Langer, S., Sutton, S., Leinwand, L. A., Geeves, M. A., Ruppel, K. M., and Spudich, J. A. (2015) Contractility parameters of human β-cardiac myosin with the hypertrophic cardiomyopathy mutation R403Q show loss of motor function. *Sci. Adv.* 1, e1500511 CrossRef Medline
- Kawana, M., Sarkar, S. S., Sutton, S., Ruppel, K. M., and Spudich, J. A. (2017) Biophysical properties of human β-cardiac myosin with converter mutations that cause hypertrophic cardiomyopathy. *Sci. Adv.* 3, e1601959 Medline
- Sommese, R. F., Sung, J., Nag, S., Sutton, S., Deacon, J. C., Choe, E., Leinwand, L. A., Ruppel, K., and Spudich, J. A. (2013) Molecular consequences of the R453C hypertrophic cardiomyopathy mutation on human β-cardiac myosin motor function. *Proc. Natl. Acad. Sci.* 110, 12607–12612 CrossRef Medline
- Adhikari, A. S., Kooiker, K. B., Sarkar, S. S., Liu, C., Bernstein, D., Spudich, J. A., and Ruppel, K. M. (2016) Early-onset hypertrophic cardiomyopathy mutations significantly increase the velocity, force, and actin-activated ATPase activity of human β-cardiac myosin. *Cell Rep.* 17, 2857–2864 CrossRef Medline
- Landrum, M. J., Lee, J. M., Benson, M., Brown, G. R., Chao, C., Chitipiralla, S., Gu, B., Hart, J., Hoffman, D., Jang, W., Karapetyan, K., Katz, K., Liu, C., Maddipatla, Z., Malheiro, A., et al. (2018) ClinVar: improving access to variant interpretations and supporting evidence. *Nucleic Acids Res.* 46, D1062–D1067 CrossRef Medline



19. Smith, D. A. (2014) A new mechanokinetic model for muscle contraction, where force and movement are triggered by phosphate release. *J. Muscle Res. Cell Motil.* **35**, 295–306 CrossRef Medline
20. Kindel, S. J., Miller, E. M., Gupta, R., Cripe, L. H., Hinton, R. B., Spicer, R. L., Towbin, J. A., and Ware, S. M. (2012) Pediatric cardiomyopathy: importance of genetic and metabolic evaluation. *J. Card. Fail.* **18**, 396–403 Medline
21. García-Giustiniani, D., Arad, M., Ortíz-Genga, M., Barriales-Villa, R., Fernández, X., Rodríguez-García, I., Mazzanti, A., Veira, E., Maneiro, E., Reboló, P., Lesende, I., Cazón, L., Freimark, D., Gimeno-Blanes, J. R., et al. (2015) Phenotype and prognostic correlations of the converter region mutations affecting the  $\beta$  myosin heavy chain. *Heart* **101**, 1047–1053 CrossRef Medline
22. Homburger, J. R., Green, E. M., Caleshu, C., Sunitha, M. S., Taylor, R. E., Ruppel, K. M., Metpally, R. P., Colan, S. D., Michels, M., Day, S. M., Olivotto, I., Bustamante, C. D., Dewey, F. E., Ho, C. Y., Spudich, J. A., and Ashley, E. A. (2016) Multidimensional structure-function relationships in human  $\beta$ -cardiac myosin from population-scale genetic variation. *Proc. Natl. Acad. Sci.* **113**, 6701–6706 CrossRef Medline
23. Köhler, J., Winkler, G., Schulte, I., Scholz, T., McKenna, W., Brenner, B., and Kraft, T. (2002) Mutation of the myosin converter domain alters cross-bridge elasticity. *Proc. Natl. Acad. Sci. U.S.A.* **99**, 3557–3562 CrossRef Medline
24. Fananapazir, L., Dalakas, M. C., Cyran, F., Cohn, G., and Epstein, N. D. (1993) Missense mutations in the  $\beta$ -myosin heavy-chain gene cause central core disease in hypertrophic cardiomyopathy. *Proc. Natl. Acad. Sci. U.S.A.* **90**, 3993–3997 CrossRef Medline
25. Seebom, B., Matinmehr, F., Köhler, J., Francino, A., Navarro-Lopéz, F., Perrot, A., Ozcelik, C., McKenna, W. J., Brenner, B., and Kraft, T. (2009) Cardiomyopathy mutations reveal variable region of myosin converter as major element of cross-bridge compliance. *Biophys. J.* **97**, 806–824 CrossRef Medline
26. Mohiddin, S. A., Begley, D. A., McLam, E., Cardoso, J. P., Winkler, J. B., Sellers, J. R., and Fananapazir, L. (2003) Utility of genetic screening in hypertrophic cardiomyopathy: prevalence and significance of novel and double (homozygous and heterozygous)  $\beta$ -myosin mutations. *Genet. Test.* **7**, 21–27 CrossRef Medline
27. Ujfalusi, Z., Vera, C. D., Mijailovich, S. M., Svicevic, M., Yu, E. C., Kawana, M., Ruppel, K. M., Spudich, J. A., Geeves, M. A., and Leinwand, L. A. (2018) Dilated cardiomyopathy myosin mutants have reduced force-generating capacity. *J. Biol. Chem.* **293**, 9017–9029 CrossRef Medline
28. Deacon, J. C., Bloemink, M. J., Rezavandi, H., Geeves, M. A., and Leinwand, L. A. (2012) Identification of functional differences between recombinant human  $\alpha$  and  $\beta$  cardiac myosin motors. *Cell. Mol. Life Sci.* **69**, 2261–2277 CrossRef Medline
29. Mijailovich, S. M., Nedic, D., Svicevic, M., Stojanovic, B., Walklate, J., Ujfalusi, Z., and Geeves, M. A. (2017) Modeling the actin-myosin ATPase cross-bridge cycle for skeletal and cardiac muscle myosin isoforms. *Biophys. J.* **112**, 984–996 CrossRef Medline
30. Neubauer, S. (2007) The failing heart: an engine out of fuel. *N. Engl. J. Med.* **356**, 1140–1151 CrossRef Medline
31. Bell, K. M., Kronert, W. A., Huang, A., Bernstein, S. I., and Swank, D. M. (2019) The R249Q hypertrophic cardiomyopathy myosin mutation decreases contractility in *Drosophila* by impeding force production. *J. Physiol.* **597**, 2403–2420 CrossRef Medline
32. Marston, S. (2018) The molecular mechanisms of mutations in actin and myosin that cause inherited myopathy. *Int. J. Mol. Sci.* **19**, pii: E2020 Medline
33. Spudich, J. A. (2019) Three perspectives on the molecular basis of hypercontractility caused by hypertrophic cardiomyopathy mutations. *Pflugers Arch.* **471**, 701–717 CrossRef Medline
34. Alamo, L., Ware, J. S., Pinto, A., Gillilan, R. E., Seidman, J. G., Seidman, C. E., and Padrón, R. (2017) Effects of myosin variants on interacting-heads motif explain distinct hypertrophic and dilated cardiomyopathy phenotypes. *Elife* **6**, 1–31 Medline
35. Trivedi, D. V., Adhikari, A. S., Sarkar, S. S., Ruppel, K. M., and Spudich, J. A. (2018) Hypertrophic cardiomyopathy and the myosin mesa: viewing an old disease in a new light. *Biophys. Rev.* **10**, 27–48 Medline
36. Nag, S., Trivedi, D. V., Sarkar, S. S., Adhikari, A. S., Sunitha, M. S., Sutton, S., Ruppel, K. M., and Spudich, J. A. (2017) The myosin mesa and the basis of hypercontractility caused by hypertrophic cardiomyopathy mutations. *Nat. Struct. Mol. Biol.* **24**, 525–533 CrossRef Medline
37. Spudich, J. A. (2015) The myosin mesa and a possible unifying hypothesis for the molecular basis of human hypertrophic cardiomyopathy. *Biochem. Soc. Trans.* **43**, 64–72 CrossRef Medline
38. Previs, M. J., Mun, J. Y., Michalek, A. J., Previs, S. B., Gulick, J., Robbins, J., Warsaw, D. M., and Craig, R. (2016) Phosphorylation and calcium antagonistically tune myosin-binding protein C's structure and function. *Proc. Natl. Acad. Sci. U.S.A.* **113**, 3239–3244 CrossRef Medline
39. Linari, M., Brunello, E., Reconditi, M., Fusi, L., Caremani, M., Narayanan, T., Piazzesi, G., Lombardi, V., and Irving, M. (2015) Force generation by skeletal muscle is controlled by mechanosensing in myosin filaments. *Nature* **528**, 276–279 CrossRef Medline
40. Toepfer, C., Caorsi, V., Kampourakis, T., Sikkil, M. B., West, T. G., Leung, M. C., Al-Saud, S. A., MacLeod, K. T., Lyon, A. R., Marston, S. B., Sellers, J. R., and Ferenczi, M. A. (2013) Myosin regulatory light chain (RLC) phosphorylation change as a modulator of cardiac muscle contraction in disease. *J. Biol. Chem.* **288**, 13446–13454 CrossRef Medline
41. Mohamed, A. S., Dignam, J. D., and Schlender, K. K. (1998) Cardiac myosin-binding protein C (MyBP-C): identification of protein kinase A and protein kinase C phosphorylation sites. *Arch. Biochem. Biophys.* **358**, 313–319 CrossRef Medline
42. Robert-Paganin, J., Auguin, D., and Houdusse, A. (2018) Hypertrophic cardiomyopathy disease results from disparate impairments of cardiac myosin function and auto-inhibition. *Nat. Commun.* **9**, 4019 CrossRef Medline
43. Newhard, C. S., Walcott, S., and Swank, D. M. (2019) The load dependence of muscle's force-velocity curve is modulated by alternative myosin converter domains. *Am. J. Physiol. Cell Physiol.* **316**, C844–C861 CrossRef Medline
44. Sabater-Molina, M., Pérez-Sánchez, I., Hernández Del Rincón, J. P., and Gimeno, J. R. (2018) Genetics of hypertrophic cardiomyopathy: a review of current state. *Clin. Genet.* **93**, 3–14 CrossRef Medline
45. Perkins, M. J., Van Driest, S. L., Ellsworth, E. G., Will, M. L., Gersh, B. J., Ommen, S. R., and Ackerman, M. J. (2005) Gene-specific modifying effects of pro-LVH polymorphisms involving the renin-angiotensin-aldosterone system among 389 unrelated patients with hypertrophic cardiomyopathy. *Eur. Heart J.* **26**, 2457–2462 CrossRef Medline
46. Liu, C., Kawana, M., Song, D., Ruppel, K. M., and Spudich, J. A. (2018) Controlling load-dependent contractility of the heart at the single molecule level. *Nat. Struct. Mol. Biol.* **25**, 505–514 CrossRef
47. Anderson, R. L., Trivedi, D. V., Sarkar, S. S., Henze, M., Ma, W., Gong, H., Rogers, C. S., Gorham, J. M., Wong, F. L., Morck, M. M., Seidman, J. G., Ruppel, K. M., Irving, T. C., Cooke, R., Green, E. M., and Spudich, J. A. (2018) Mavacamten stabilizes a folded-back sequestered super-relaxed state of  $\beta$ -cardiac myosin. *Proc. Natl. Acad. Sci. U.S.A.* **115**, E8143–E8152 CrossRef Medline
48. Resnicow, D. I., Deacon, J. C., Warrick, H. M., Spudich, J. A., and Leinwand, L. (2010) A functional diversity among a family of human skeletal muscle myosin motors. *Proc. Natl. Acad. Sci. U.S.A.* **107**, 1053–1058 CrossRef Medline
49. Walklate, J., Vera, C., Bloemink, M. J., Geeves, M. A., and Leinwand, L. (2016) The most prevalent Freeman-Sheldon syndrome mutations in the embryonic myosin motor share functional defects. *J. Biol. Chem.* **291**, 10318–10331 CrossRef Medline
50. Huang, J., Nagy, S. S., Koide, A., Rock, R. S., and Koide, S. (2009) A peptide tag system for facile purification and single-molecule immobilization. *Biochemistry* **48**, 11834–11836 CrossRef Medline
51. Huang, J., Koide, A., Makabe, K., and Koide, S. (2008) Design of protein function leaps by directed domain interface evolution. *Proc. Natl. Acad. Sci. U.S.A.* **105**, 6578–6583 CrossRef Medline
52. Spudich, J. A., and Watt, S. (1971) The regulation of rabbit skeletal muscle contraction. *J. Biol. Chem.* **246**, 4866–4871 Medline
53. Zot, H. G., and Potter, J. D. (1981) Purification of actin from cardiac muscle. *Prep. Biochem.* **11**, 381–395 Medline

### Early and late onset HCM causing mutations in MYH7

54. Criddle, A. H., Geeves, M. A., and Jeffries, T. (1985) The use of actin labelled with *N*-(1-pyrenyl)iodoacetamide to study the interaction of actin with myosin subfragments and troponin/tropomyosin. *Biochem. J.* **232**, 343–349 CrossRef Medline
55. Trybus, K. M. (2000) Biochemical studies of myosin. *Methods* **22**, 327–335 CrossRef Medline
56. Mijailovich, S. M., Li, X., del Alamo, J. C., Griffiths, R. H., Kecman, V., and Geeves, M. A. (2010) Resolution and uniqueness of estimated parameters of a model of thin filament regulation in solution. *Comput. Biol. Chem.* **34**, 19–33 CrossRef Medline
57. Smith, D. A., and Geeves, M. A. (1995) Strain-dependent cross-bridge cycle for muscle: II. steady-state behavior. *Biophys. J.* **69**, 538–552 CrossRef Medline
58. Greenberg, M. J., Shuman, H., and Ostap, E. M. (2014) Inherent force-dependent properties of  $\beta$ -cardiac myosin contribute to the force-velocity relationship of cardiac muscle. *Biophys. J.* **107**, L41–L44 CrossRef Medline
59. Fenn, W. O. (1923) A quantitative comparison between the energy liberated and the work performed by the isolated sartorius muscle of the frog. *J. Physiol.* **58**, 175–203 CrossRef Medline



## Supplementary Information

# Myosin motor domains carrying mutations implicated in early or late onset HCM have similar properties

Carlos D. Vera<sup>1,#</sup>, Chloe A. Johnson<sup>2,#</sup>, Jonathan Walklate<sup>2</sup>, Arjun Adhikari<sup>5</sup>, Marina Svcevic<sup>3</sup>, Srboljub M. Mijailovich<sup>4</sup>, Ariana C. Combs<sup>1</sup>, Stephen J. Langer<sup>1</sup>, Kathleen M. Ruppel<sup>5</sup>, James A. Spudich<sup>5</sup>, Michael A. Geeves<sup>2,\*</sup>, and Leslie A. Leinwand<sup>1,\*</sup>

From the <sup>1</sup>BioFrontiers Institute and Department of Molecular, Cellular and Developmental Biology, University of Colorado Boulder, Boulder CO 80309 USA; <sup>2</sup>School of Biosciences, University of Kent, Canterbury UK, CT2 7NJ; <sup>3</sup>Faculty of Science, University of Kragujevac, Serbia; <sup>4</sup>Department of Biology, Illinois Institute of Technology, Chicago IL 60616 USA; <sup>5</sup>Stanford University School of Medicine, Department of Biochemistry, Stanford CA 94305 USA.

Running title: Early and late onset HCM causing mutations in MYH7

\*To whom correspondence should be addressed: Michael A. Geeves School of Biosciences, University of Kent, Canterbury, UK, CT2 7NJ [m.a.geeves@kent.ac.uk](mailto:m.a.geeves@kent.ac.uk); Leslie A. Leinwand BioFrontiers Institute and/or Department of Molecular, Cellular and Developmental Biology, University of Colorado, Boulder CO 80309 [leslie.leinwand@colorado.edu](mailto:leslie.leinwand@colorado.edu)

**Table S1.** This table describes a set of queries regarding the clinical frequency of HCM linked or associated mutations in MYH7 assessed using the NCBI tool ClinVar and the Variant Effect Predictor (VEP) tool for Ensembl (1, 2). The VEP provides a pathogenicity or severity score for three predictive algorithms: PolyPhen, SIFT and Condel. H251N, P710R, P710L and V763M are predicted to have physico-chemical effects and possibly be disease-causing because those residues are highly conserved, but due to rarity it is not enough to be considered pathogenic, hence being categorized "Deleterious, VUS".

| MYH7 Mutation | ClinVar Variation ID | Has the mutation been described in more than one person? | Has the mutation been seen in multiple families? | Has the mutation affected associated family members of the patient? | Is it predicted to be pathogenic?<br>PolyPhen - A<br>SIFT - B<br>Condel - C | Is it present in large population databases? | Identified as early onset? (<15 y.o.) |
|---------------|----------------------|--|--|---|---|--|---------------------------------------|
| H251N         | n/a                  | No   | No   | No  | Deleterious, VUS  | No   | Yes                                   |
| D382Y         | 237432               | Yes  | No   | No  | A: ✓ B: ✓ C: ✓  | No   | Yes                                   |
| R403Q         | 14087                | Yes  | Yes  | Yes   | A: ✓ B: ✓ C: ✓  | No   | No                                    |
| R453C         | 14089                | Yes  | Yes  | Yes   | A: ✓ B: ✓ C: ✓  | No   | No                                    |
| P710R         | n/a                  | No   | No   | No  | Deleterious, VUS  | No   | Yes                                   |
| P710H*        | 177734               | Yes  | No   | No  | A: ✓ B: ✓ C: ✓  | No   | No                                    |
| P710L*        | 177673               | Yes  | No   | No  | Deleterious, VUS  | No   | No                                    |
| R719W         | 14104                | Yes  | Yes  | Yes   | A: ✓ B: ✓ C: ✓  | No   | No                                    |
| R723G         | 42885                | Yes  | Yes  | Yes   | A: ✓ B: ✓ C: ✓  | No   | No                                    |
| G741R         | 42890                | Yes  | Yes  | Yes   | A: ✓ B: ✓ C: ✓  | No   | No                                    |
| V763M         | 177642               | Yes  | No   | n.d.  | Deleterious, VUS  | No   | Yes                                   |

\* = Reported mutations on residue P710, however these were not characterized in this work.

✓ = Algorithm predicts pathogenic and/or "likely-pathogenic".

**Table S2. Fitted Rate and Equilibrium Constants of the ATPase cycle.** Highlighted to show which parameters were fitted & which were measured, and which derived from our previously described assumptions or detailed balance (3).

A. Equilibrium Constants

|              | <i>Units</i>       | <i><math>\beta</math>-WT</i> | <i>H251N</i> | <i>D382Y</i> | <i>P710R</i> | <i>V763M</i> | <i>R719W</i> | <i>R723G</i> | <i>G741R</i> |
|--------------|--------------------|------------------------------|--------------|--------------|--------------|--------------|--------------|--------------|--------------|
| $K_{app}$    | $\mu\text{M}$      | 33                           | 34           | 52           | 14           | 18           | 33           | 43           | 29           |
| $k_{cat}$    | $\text{s}^{-1}$    | 4.1                          | 5.1          | 4.9          | 2.5          | 4            | 3.9          | 4            | 3.7          |
| $K_A$        | $\mu\text{M}^{-1}$ | 0.0199                       | 0.0148       | 0.0124       | 0.0501       | 0.0306       | 0.0204       | 0.014        | 0.0235       |
| $K_{pi}$     | mM                 | 100                          | 100          | 100          | 100          | 100          | 100          | 100          | 100          |
| $K_{D^*}$    |                    | 0.167                        | 0.167        | 0.167        | 0.167        | 0.167        | 0.167        | 0.167        | 0.167        |
| $K_D$        | $\mu\text{M}$      | 36                           | 36           | 36           | 36           | 36           | 36           | 36           | 36           |
| $K_T$        | $\mu\text{M}^{-1}$ | 0.0036                       | 0.00763      | 0.00345      | 0.0062       | 0.0037       | 0.00796      | 0.0049       | 0.0056       |
| $K_{T^*}$    |                    | 154                          | 66.6         | 130          | 110.65       | 117.58       | 67.6         | 55.6         | 94           |
| $K_{T^{**}}$ | $\mu\text{M}$      | 1000                         | 1000         | 1000         | 1000         | 1000         | 1000         | 1000         | 1000         |
| $K_H$        |                    | 9.4                          | 8.6          | 11.7         | 4.9          | 6.5          | 8.5          | 7.2          | 8.4          |
| $K_{AH}$     |                    | 66.6                         | 61.8         | 35.5         | 34.7         | 46.5         | 60.7         | 51.4         | 60.1         |

B. Forward Rate Constants

|              | <i>Units</i>                    | <i>β-WT</i> | <i>H251N</i> | <i>D382Y</i> | <i>P710R</i> | <i>V763M</i> | <i>R719W</i> | <i>R723G</i> | <i>G741R</i> |
|--------------|---------------------------------|-------------|--------------|--------------|--------------|--------------|--------------|--------------|--------------|
| $k_A$        | $\mu\text{M}^{-1}\text{s}^{-1}$ | 19.9        | 14.8         | 12.4         | 50.1         | 30.6         | 20.4         | 14           | 23.5         |
| $k_{Pi}$     | $\text{s}^{-1}$                 | 7.1         | 11.6         | 8.4          | 4.4          | 8.6          | 6.6          | 7.7          | 6.2          |
| $k_{D^*}$    | $\text{s}^{-1}$                 | 59          | 56.7         | 64.3         | 69           | 68           | 96.8         | 106.8        | 71.1         |
| $k_D$        | $\text{s}^{-1}$                 | 1000        | 1000         | 1000         | 1000         | 1000         | 1000         | 1000         | 1000         |
| $k_T$        | $\mu\text{M}^{-1}\text{s}^{-1}$ | 10.17       | 10.07        | 10.32        | 10.25        | 10.15        | 10.03        | 10.07        | 10.02        |
| $k_{T^*}$    | $\text{s}^{-1}$                 | 1540        | 666          | 1300         | 1106.5       | 1175.8       | 676          | 556          | 940          |
| $k_{T^{**}}$ | $\text{s}^{-1}$                 | 1000        | 1000         | 1000         | 1000         | 1000         | 1000         | 1000         | 1000         |
| $k_H$        | $\text{s}^{-1}$                 | 13.1        | 12.1         | 16.4         | 6.8          | 9.1          | 11.9         | 10.0         | 11.8         |
| $k_{AH}$     | $\text{s}^{-1}$                 | 13.3        | 12.35        | 7.1          | 6.9          | 9.3          | 12.1         | 10.3         | 12.0         |

C. Backward Rate Constants

|                        | <b>Units</b>                          | <b><math>\beta</math>-WT</b> | <b>H251N</b> | <b>D382Y</b> | <b>P710R</b> | <b>V763M</b> | <b>R719W</b> | <b>R723G</b> | <b>G741R</b> |
|------------------------|---------------------------------------|------------------------------|--------------|--------------|--------------|--------------|--------------|--------------|--------------|
| <b>k<sub>A</sub></b>   | s <sup>-1</sup>                       | 1000                         | 1000         | 1000         | 1000         | 1000         | 1000         | 1000         | 1000         |
| <b>k<sub>PI</sub></b>  | mM <sup>-1</sup> s <sup>-1</sup>      | 0.071                        | 0.116        | 0.084        | 0.044        | 0.086        | 0.066        | 0.077        | 0.062        |
| <b>k<sub>D'</sub></b>  | s <sup>-1</sup>                       | 353.29                       | 339.52       | 385.03       | 413.17       | 407.19       | 579.64       | 639.52       | 425.75       |
| <b>k<sub>D</sub></b>   | $\mu$ M <sup>-1</sup> s <sup>-1</sup> | 27.78                        | 27.78        | 27.78        | 27.78        | 27.78        | 27.78        | 27.78        | 27.78        |
| <b>k<sub>T</sub></b>   | s <sup>-1</sup>                       | 2824.1                       | 1319.4       | 2989.9       | 1653.5       | 2743.5       | 1260.2       | 2054.3       | 1789.8       |
| <b>k<sub>T'</sub></b>  | s <sup>-1</sup>                       | 10                           | 10           | 10           | 10           | 10           | 10           | 10           | 10           |
| <b>k<sub>T''</sub></b> | $\mu$ M <sup>-1</sup> s <sup>-1</sup> | 1                            | 1            | 1            | 1            | 1            | 1            | 1            | 1            |
| <b>k<sub>H</sub></b>   | s <sup>-1</sup>                       | 1.4                          | 1.4          | 1.4          | 1.4          | 1.4          | 1.4          | 1.4          | 1.4          |
| <b>k<sub>AH</sub></b>  | s <sup>-1</sup>                       | 0.2                          | 0.2          | 0.2          | 0.2          | 0.2          | 0.2          | 0.2          | 0.2          |

**Table S3. Predicted cross-bridge cycle parameters at three actin concentrations and one under loaded conditions from the modelled ATPase cycle.**

| <i>Isoform</i> | <i>[Actin] (μM)</i>        | <i>ATPase (s<sup>-1</sup>)</i> | <i>Detached</i> | <i>Weakly attached</i> | <i>Strongly attached</i> | <i>Duty Ratio</i> | <i>Velocity (μm/s)</i> |
|----------------|----------------------------|--------------------------------|-----------------|------------------------|--------------------------|-------------------|------------------------|
| <b>β-WT</b>    |                            |                                |                 |                        |                          |                   |                        |
|                | K <sub>app</sub> = 33      | 2.06                           | 0.65            | 0.30                   | 0.05                     | 0.05              | 0.20                   |
|                | 3 K <sub>app</sub> = 99    | 3.09                           | 0.46            | 0.46                   | 0.08                     | 0.08              | 0.20                   |
|                | 20 K <sub>app</sub> = 660  | 3.91                           | 0.23            | 0.68                   | 0.10                     | 0.10              | 0.20                   |
|                | 3 K <sub>app</sub> + Load  | 1.25                           | 0.39            | 0.54                   | 0.07                     | 0.07              | 0.09                   |
| <b>H251N</b>   |                            |                                |                 |                        |                          |                   |                        |
|                | K <sub>app</sub> = 34      | 2.56                           | 0.70            | 0.23                   | 0.07                     | 0.07              | 0.19                   |
|                | 3 K <sub>app</sub> = 102   | 3.83                           | 0.53            | 0.37                   | 0.10                     | 0.10              | 0.19                   |
|                | 20 K <sub>app</sub> = 680  | 4.87                           | 0.28            | 0.59                   | 0.13                     | 0.13              | 0.19                   |
|                | 3 K <sub>app</sub> + Load  | 1.67                           | 0.45            | 0.45                   | 0.10                     | 0.10              | 0.08                   |
| <b>D382Y</b>   |                            |                                |                 |                        |                          |                   |                        |
|                | K <sub>app</sub> = 52      | 2.43                           | 0.64            | 0.30                   | 0.06                     | 0.06              | 0.21                   |
|                | 3 K <sub>app</sub> = 156   | 3.59                           | 0.45            | 0.47                   | 0.08                     | 0.08              | 0.21                   |
|                | 20 K <sub>app</sub> = 1040 | 4.14                           | 0.22            | 0.68                   | 0.10                     | 0.10              | 0.21                   |
|                | 3 K <sub>app</sub> + Load  | 1.46                           | 0.38            | 0.54                   | 0.08                     | 0.08              | 0.09                   |
| <b>P710R</b>   |                            |                                |                 |                        |                          |                   |                        |
|                | K <sub>app</sub> = 14      | 1.24                           | 0.68            | 0.29                   | 0.03                     | 0.03              | 0.22                   |
|                | 3 K <sub>app</sub> = 42    | 1.87                           | 0.52            | 0.44                   | 0.04                     | 0.04              | 0.22                   |
|                | 20 K <sub>app</sub> = 280  | 2.36                           | 0.33            | 0.62                   | 0.05                     | 0.05              | 0.22                   |
|                | 3 K <sub>app</sub> + Load  | 0.77                           | 0.43            | 0.53                   | 0.04                     | 0.04              | 0.10                   |



| <b>V763M</b> |                           |      |      |      |      |      |      |
|--------------|---------------------------|------|------|------|------|------|------|
|              | K <sub>app</sub> = 18     | 1.75 | 0.75 | 0.21 | 0.04 | 0.04 | 0.22 |
|              | 3 K <sub>app</sub> = 54   | 2.80 | 0.59 | 0.34 | 0.06 | 0.06 | 0.22 |
|              | 20 K <sub>app</sub> = 360 | 3.75 | 0.38 | 0.53 | 0.09 | 0.09 | 0.22 |
|              | 3 K <sub>app</sub> + Load | 1.20 | 0.51 | 0.43 | 0.06 | 0.06 | 0.10 |
| <b>R719W</b> |                           |      |      |      |      |      |      |
|              | K <sub>app</sub> = 33     | 1.95 | 0.66 | 0.30 | 0.04 | 0.04 | 0.26 |
|              | 3 K <sub>app</sub> = 99   | 2.93 | 0.47 | 0.47 | 0.06 | 0.06 | 0.26 |
|              | 20 K <sub>app</sub> = 660 | 3.71 | 0.24 | 0.69 | 0.07 | 0.07 | 0.26 |
|              | 3 K <sub>app</sub> + Load | 1.19 | 0.56 | 0.40 | 0.05 | 0.05 | 0.13 |
| <b>R723G</b> |                           |      |      |      |      |      |      |
|              | K <sub>app</sub> = 43     | 2.00 | 0.69 | 0.27 | 0.04 | 0.04 | 0.27 |
|              | 3 K <sub>app</sub> = 129  | 3.00 | 0.51 | 0.43 | 0.06 | 0.06 | 0.27 |
|              | 20 K <sub>app</sub> = 860 | 3.81 | 0.25 | 0.68 | 0.07 | 0.07 | 0.26 |
|              | 3 K <sub>app</sub> + Load | 1.28 | 0.43 | 0.52 | 0.05 | 0.05 | 0.13 |
| <b>G741R</b> |                           |      |      |      |      |      |      |
|              | K <sub>app</sub> = 29     | 1.85 | 0.65 | 0.31 | 0.04 | 0.04 | 0.23 |
|              | 3 K <sub>app</sub> = 87   | 2.78 | 0.47 | 0.47 | 0.06 | 0.06 | 0.22 |
|              | 20 K <sub>app</sub> = 580 | 3.52 | 0.24 | 0.68 | 0.08 | 0.08 | 0.22 |
|              | 3 K <sub>app</sub> + Load | 1.12 | 0.39 | 0.55 | 0.06 | 0.06 | 0.10 |

**Table S4. Predicted Occupancy of the 8 states during the ATPase cycle at three actin concentrations and one under loaded conditions.**

| <b>Isoform</b>               | <b>[Actin] (<math>\mu\text{M}</math>)</b> | <b><i>A</i>·<i>M</i></b> | <b><i>A</i>·<i>M</i>·<i>T</i></b> | <b><i>A</i>·<i>M</i>·<i>T</i></b> | <b><i>M</i>·<i>T</i></b> | <b><i>M</i>·<i>D</i>·<i>Pi</i></b> | <b><i>A</i>·<i>M</i>·<i>D</i>·<i>Pi</i></b> | <b><i>A</i>·<i>MD</i></b> | <b><i>A</i>·<i>M</i>·<i>D</i></b> |
|------------------------------|---|--------------------------|-----------------------------------|-----------------------------------|--------------------------|------------------------------------|---|---------------------------|-----------------------------------|
| <b><math>\beta</math>-WT</b> |   |                          |                                   |                                   |                          |                                    |   |                           |                                   |
|                              | $K_{\text{app}} = 33$                     | 0.00012                  | 0.0014                            | 0.0086                            | 0.20                     | 0.45                               | 0.29  | 0.047                     | 0.0021                            |
|                              | 3 $K_{\text{app}} = 99$                   | 0.00018                  | 0.0022                            | 0.026                             | 0.24                     | 0.22                               | 0.43  | 0.071                     | 0.0031                            |
|                              | 20 $K_{\text{app}} = 660$                 | 0.00026                  | 0.0033                            | 0.12                              | 0.19                     | 0.042                              | 0.55  | 0.090                     | 0.0039                            |
|                              | 3 $K_{\text{app}} + \text{Load}$          | 0.000074                 | 0.0009                            | 0.013                             | 0.12                     | 0.27                               | 0.53  | 0.071                     | 0.0012                            |
| <b>H251N</b>                 |   |                          |                                   |                                   |                          |                                    |   |                           |                                   |
|                              | $K_{\text{app}} = 34$                     | 0.00016                  | 0.0040                            | 0.011                             | 0.26                     | 0.45                               | 0.22  | 0.060                     | 0.0026                            |
|                              | 3 $K_{\text{app}} = 102$                  | 0.00024                  | 0.0063                            | 0.035                             | 0.31                     | 0.22                               | 0.33  | 0.091                     | 0.0038                            |
|                              | 20 $K_{\text{app}} = 680$                 | 0.00035                  | 0.0098                            | 0.17                              | 0.24                     | 0.042                              | 0.42  | 0.11                      | 0.0049                            |
|                              | 3 $K_{\text{app}} + \text{Load}$          | 0.00011                  | 0.0028                            | 0.018                             | 0.16                     | 0.29                               | 0.43  | 0.098                     | 0.0017                            |
| <b>D382Y</b>                 |   |                          |                                   |                                   |                          |                                    |   |                           |                                   |
|                              | $K_{\text{app}} = 52$                     | 0.00016                  | 0.0020                            | 0.012                             | 0.19                     | 0.46                               | 0.29  | 0.052                     | 0.0024                            |
|                              | 3 $K_{\text{app}} = 156$                  | 0.00025                  | 0.0031                            | 0.039                             | 0.23                     | 0.22                               | 0.43  | 0.077                     | 0.0036                            |
|                              | 20 $K_{\text{app}} = 1040$                | 0.00035                  | 0.0047                            | 0.19                              | 0.18                     | 0.039                              | 0.49  | 0.089                     | 0.0041                            |
|                              | 3 $K_{\text{app}} + \text{Load}$          | 0.00010                  | 0.0013                            | 0.019                             | 0.11                     | 0.27                               | 0.52  | 0.077                     | 0.0015                            |
| <b>P710R</b>                 |   |                          |                                   |                                   |                          |                                    |   |                           |                                   |
|                              | $K_{\text{app}} = 14$                     | 0.000062                 | 0.0012                            | 0.0050                            | 0.27                     | 0.41                               | 0.28  | 0.025                     | 0.0012                            |
|                              | 3 $K_{\text{app}} = 42$                   | 0.000095                 | 0.0018                            | 0.015                             | 0.31                     | 0.20                               | 0.42  | 0.038                     | 0.0019                            |
|                              | 20 $K_{\text{app}} = 280$                 | 0.00014                  | 0.0029                            | 0.082                             | 0.29                     | 0.039                              | 0.54  | 0.048                     | 0.0024                            |
|                              | 3 $K_{\text{app}} + \text{Load}$          | 0.00004                  | 0.00077                           | 0.0080                            | 0.17                     | 0.25                               | 0.53  | 0.038                     | 0.00077                           |

| <b>V763M</b> |                           |          |        |        |      |       |      |       |        |
|--------------|---------------------------|----------|--------|--------|------|-------|------|-------|--------|
|              | K <sub>app</sub> = 18     | 0.00012  | 0.0015 | 0.0054 | 0.27 | 0.49  | 0.20 | 0.036 | 0.0017 |
|              | 3 K <sub>app</sub> = 54   | 0.00019  | 0.0025 | 0.017  | 0.34 | 0.26  | 0.33 | 0.058 | 0.0028 |
|              | 20 K <sub>app</sub> = 360 | 0.00029  | 0.0040 | 0.096  | 0.33 | 0.051 | 0.44 | 0.078 | 0.0037 |
|              | 3 K <sub>app</sub> + Load | 0.000083 | 0.0011 | 0.0088 | 0.18 | 0.33  | 0.42 | 0.060 | 0.0012 |
| <b>R719W</b> |                           |          |        |        |      |       |      |       |        |
|              | K <sub>app</sub> = 33     | 0.00012  | 0.0030 | 0.0088 | 0.21 | 0.45  | 0.30 | 0.032 | 0.0020 |
|              | 3 K <sub>app</sub> = 99   | 0.00018  | 0.0047 | 0.027  | 0.25 | 0.22  | 0.44 | 0.048 | 0.0029 |
|              | 20 K <sub>app</sub> = 660 | 0.00026  | 0.0074 | 0.130  | 0.19 | 0.042 | 0.56 | 0.061 | 0.0037 |
|              | 3 K <sub>app</sub> + Load | 0.000073 | 0.0020 | 0.014  | 0.13 | 0.27  | 0.54 | 0.044 | 0.0012 |
| <b>R723G</b> |                           |          |        |        |      |       |      |       |        |
|              | K <sub>app</sub> = 43     | 0.00020  | 0.0038 | 0.013  | 0.25 | 0.44  | 0.26 | 0.031 | 0.0020 |
|              | 3 K <sub>app</sub> = 129  | 0.00031  | 0.0061 | 0.041  | 0.30 | 0.22  | 0.39 | 0.046 | 0.0030 |
|              | 20 K <sub>app</sub> = 860 | 0.00049  | 0.010  | 0.18   | 0.21 | 0.041 | 0.49 | 0.058 | 0.0038 |
|              | 3 K <sub>app</sub> + Load | 0.00014  | 0.0027 | 0.021  | 0.16 | 0.28  | 0.50 | 0.044 | 0.0013 |
| <b>G741R</b> |                           |          |        |        |      |       |      |       |        |
|              | K <sub>app</sub> = 29     | 0.00011  | 0.0021 | 0.0077 | 0.21 | 0.45  | 0.30 | 0.037 | 0.0019 |
|              | 3 K <sub>app</sub> = 87   | 0.00017  | 0.0032 | 0.024  | 0.24 | 0.22  | 0.45 | 0.056 | 0.0028 |
|              | 20 K <sub>app</sub> = 580 | 0.00025  | 0.0050 | 0.12   | 0.20 | 0.042 | 0.57 | 0.071 | 0.0035 |
|              | 3 K <sub>app</sub> + Load | 0.000069 | 0.0013 | 0.012  | 0.12 | 0.27  | 0.54 | 0.054 | 0.0011 |

**Table S5. Resolution matrices.**

| <b><i>β</i>-WT</b>    | <b>K<sub>A</sub></b> | <b>k<sub>pi</sub></b> | <b>k-τ</b> | <b>K<sub>H</sub></b> | <b>K<sub>AH</sub></b> |
|-----------------------|----------------------|-----------------------|------------|----------------------|-----------------------|
| <b>K<sub>A</sub></b>  | 0.91                 | 0.10                  | 0.00       | -0.17                | -0.19                 |
| <b>k<sub>pi</sub></b> | 0.10                 | 0.88                  | 0.00       | 0.22                 | 0.22                  |
| <b>k-τ</b>            | 0.00                 | 0.00                  | 0.00       | 0.00                 | 0.00                  |
| <b>K<sub>H</sub></b>  | -0.17                | 0.22                  | 0.00       | 0.59                 | -0.39                 |
| <b>K<sub>AH</sub></b> | -0.19                | 0.22                  | 0.00       | -0.39                | 0.59                  |

| <b>H251N</b>          | <b>K<sub>A</sub></b> | <b>k<sub>pi</sub></b> | <b>k-τ</b> | <b>K<sub>H</sub></b> | <b>K<sub>AH</sub></b> |
|-----------------------|----------------------|-----------------------|------------|----------------------|-----------------------|
| <b>K<sub>A</sub></b>  | 0.79                 | 0.22                  | 0.00       | -0.23                | -0.24                 |
| <b>k<sub>pi</sub></b> | 0.22                 | 0.75                  | 0.00       | 0.26                 | 0.26                  |
| <b>k-τ</b>            | 0.00                 | 0.00                  | 0.00       | 0.00                 | 0.00                  |
| <b>K<sub>H</sub></b>  | -0.23                | 0.26                  | 0.00       | 0.72                 | -0.27                 |
| <b>K<sub>AH</sub></b> | -0.24                | 0.26                  | 0.00       | -0.27                | 0.72                  |

| <b>D382Y</b>          | <b>K<sub>A</sub></b> | <b>k<sub>pi</sub></b> | <b>k-τ</b> | <b>K<sub>H</sub></b> | <b>K<sub>AH</sub></b> |
|-----------------------|----------------------|-----------------------|------------|----------------------|-----------------------|
| <b>K<sub>A</sub></b>  | 0.91                 | 0.09                  | 0.00       | -0.17                | -0.18                 |
| <b>k<sub>pi</sub></b> | 0.09                 | 0.89                  | 0.00       | 0.21                 | 0.21                  |
| <b>k-τ</b>            | 0.00                 | 0.00                  | 0.00       | 0.00                 | 0.00                  |
| <b>K<sub>H</sub></b>  | -0.17                | 0.21                  | 0.00       | 0.58                 | -0.40                 |
| <b>K<sub>AH</sub></b> | -0.18                | 0.21                  | 0.00       | -0.40                | 0.58                  |

| <b>P710R</b>          | <b>K<sub>A</sub></b> | <b>k<sub>pi</sub></b> | <b>k<sub>-T</sub></b> | <b>K<sub>H</sub></b> | <b>K<sub>AH</sub></b> |
|-----------------------|----------------------|-----------------------|-----------------------|----------------------|-----------------------|
| <b>K<sub>A</sub></b>  | 0.88                 | 0.12                  | 0.00                  | -0.17                | -0.19                 |
| <b>k<sub>pi</sub></b> | 0.12                 | 0.84                  | 0.00                  | 0.24                 | 0.25                  |
| <b>k<sub>-T</sub></b> | 0.00                 | 0.00                  | 0.00                  | 0.00                 | 0.00                  |
| <b>K<sub>H</sub></b>  | -0.17                | 0.24                  | 0.00                  | 0.62                 | -0.36                 |
| <b>K<sub>AH</sub></b> | -0.19                | 0.25                  | 0.00                  | -0.36                | 0.62                  |

| <b>V763M</b>          | <b>K<sub>A</sub></b> | <b>k<sub>pi</sub></b> | <b>k<sub>-T</sub></b> | <b>K<sub>H</sub></b> | <b>K<sub>AH</sub></b> |
|-----------------------|----------------------|-----------------------|-----------------------|----------------------|-----------------------|
| <b>K<sub>A</sub></b>  | 0.81                 | 0.21                  | 0.00                  | -0.22                | -0.23                 |
| <b>k<sub>pi</sub></b> | 0.21                 | 0.75                  | 0.00                  | 0.26                 | 0.27                  |
| <b>k<sub>-T</sub></b> | 0.00                 | 0.00                  | 0.00                  | 0.00                 | 0.00                  |
| <b>K<sub>H</sub></b>  | -0.22                | 0.26                  | 0.00                  | 0.72                 | -0.28                 |
| <b>K<sub>AH</sub></b> | -0.23                | 0.27                  | 0.00                  | -0.28                | 0.71                  |

| <b>R719W</b>          | <b>K<sub>A</sub></b> | <b>k<sub>pi</sub></b> | <b>k<sub>-T</sub></b> | <b>K<sub>H</sub></b> | <b>K<sub>AH</sub></b> |
|-----------------------|----------------------|-----------------------|-----------------------|----------------------|-----------------------|
| <b>K<sub>A</sub></b>  | 0.90                 | 0.10                  | 0.00                  | -0.17                | -0.19                 |
| <b>k<sub>pi</sub></b> | 0.10                 | 0.87                  | 0.00                  | 0.22                 | 0.22                  |
| <b>k<sub>-T</sub></b> | 0.00                 | 0.00                  | 0.00                  | 0.00                 | 0.00                  |
| <b>K<sub>H</sub></b>  | -0.17                | 0.22                  | 0.00                  | 0.60                 | -0.39                 |
| <b>K<sub>AH</sub></b> | -0.19                | 0.22                  | 0.00                  | -0.39                | 0.59                  |

| <b>R723G</b>          | <b>K<sub>A</sub></b> | <b>k<sub>pi</sub></b> | <b>k-τ</b> | <b>K<sub>H</sub></b> | <b>K<sub>AH</sub></b> |
|-----------------------|----------------------|-----------------------|------------|----------------------|-----------------------|
| <b>K<sub>A</sub></b>  | 0.60                 | 0.42                  | 0.00       | -0.16                | -0.17                 |
| <b>k<sub>pi</sub></b> | 0.42                 | 0.56                  | 0.00       | 0.18                 | 0.18                  |
| <b>k-τ</b>            | 0.00                 | 0.00                  | 0.00       | 0.00                 | 0.00                  |
| <b>K<sub>H</sub></b>  | -0.16                | 0.18                  | 0.00       | 0.93                 | -0.07                 |
| <b>K<sub>AH</sub></b> | -0.17                | 0.18                  | 0.00       | -0.07                | 0.92                  |

| <b>G741R</b>          | <b>K<sub>A</sub></b> | <b>k<sub>pi</sub></b> | <b>k-τ</b> | <b>K<sub>H</sub></b> | <b>K<sub>AH</sub></b> |
|-----------------------|----------------------|-----------------------|------------|----------------------|-----------------------|
| <b>K<sub>A</sub></b>  | 0.91                 | 0.09                  | 0.00       | -0.16                | -0.18                 |
| <b>k<sub>pi</sub></b> | 0.09                 | 0.89                  | 0.00       | 0.21                 | 0.22                  |
| <b>k-τ</b>            | 0.00                 | 0.00                  | 0.00       | 0.00                 | 0.00                  |
| <b>K<sub>H</sub></b>  | -0.16                | 0.21                  | 0.00       | 0.59                 | -0.40                 |
| <b>K<sub>AH</sub></b> | -0.18                | 0.22                  | 0.00       | -0.40                | 0.58                  |

**Table S6. Sensitivity analysis; Percentage change of the six fitted parameters induced by a change of +20% or -20% to one fitted parameters for the P710R and R723G mutations.**

To test how robust our fitted parameters are we varied the parameters for  $V_{max}$ , ADP release ( $K_{D^*}$ ) and the hydrolysis step ( $K_H$ ) by plus or minus 20% and repeated the fitting procedure. This illustrates the co-dependence the other fitted values within the 20% limit we believe we have for the measured parameters. The values highlighted in red are the parameters that were changed by 20% in each case. Values highlighted in grey background with bold figures are the only values that change by more than 10% while 0.0 means the value did not change by more than 1% when refitted. The majority of value show no change.

| <b>Equilibrium Rate Constants</b> | <b>Units</b>       | <b><math>\beta</math>-R723G</b> | <b><math>V_{max}+20\%</math></b> | <b><math>V_{max} -20\%</math></b> | <b><math>K_{D^*} +20\%</math></b> | <b><math>K_{D^*} -20\%</math></b> | <b><math>K_H +20\%</math></b> | <b><math>K_H -20\%</math></b> |
|-----------------------------------|--------------------|---------------------------------|----------------------------------|-----------------------------------|-----------------------------------|-----------------------------------|-------------------------------|-------------------------------|
| $K_m$                             | ( $\mu M$ )        | 43                              | 0.0                              | 0.0                               | 0.0                               | 0.0                               | 0.0                           | 0.0                           |
| $V_{max}$                         | $s^{-1}$           | 4                               | 20.0                             | -20.0                             | 0.0                               | 0.0                               | 0.0                           | 0.0                           |
| $K_A$                             | $\mu M^{-1}$       | 0.014                           | 1.4                              | 14.3                              | 2.1                               | -2.1                              | 10.7                          | -16.4                         |
| $K_{pi}$                          | mM                 | 100                             | 0.0                              | 0.0                               | 0.0                               | 0.0                               | 0.0                           | 0.0                           |
| $K_{D^*}$                         |                    | 0.167                           | 0.0                              | 0.0                               | 20.0                              | -20.0                             | 0.0                           | 0.0                           |
| $K_D$                             | ( $\mu M$ )        | 36                              | 0.0                              | 0.0                               | 0.0                               | 0.0                               | 0.0                           | 0.0                           |
| $K_T$                             | $\mu M^{-1}$       | 0.0049                          | 0.0                              | 0.0                               | 0.0                               | 0.0                               | 0.0                           | 0.0                           |
| $K_{T^*}$                         |                    | 55.6                            | 0.0                              | 0.0                               | 0.0                               | 0.0                               | 0.0                           | 0.0                           |
| $K_{T^{**}}$                      | $\mu M$            | 1000                            | 0.0                              | 0.0                               | 0.0                               | 0.0                               | 0.0                           | 0.0                           |
| $K_H$                             |                    | 7.2                             | 30.5                             | -7.2                              | -0.2                              | 0.3                               | 20.0                          | -20.0                         |
| $K_{AH}$                          |                    | 51.4                            | 30.6                             | -7.1                              | -0.2                              | 0.3                               | 20.2                          | -20.1                         |
| <b>Forward Rate Constants</b>     |                    |                                 |                                  |                                   |                                   |                                   |                               |                               |
| $k_A$                             | $\mu M^{-1}s^{-1}$ | 14                              | 1.4                              | 14.3                              | 2.1                               | -2.1                              | 10.7                          | -16.4                         |
| $k_{Pi}$                          | $s^{-1}$           | 7.7                             | 15.6                             | -29.9                             | -1.3                              | 2.6                               | -11.7                         | 23.4                          |
| $k_{D^*}$                         | $s^{-1}$           | 106.8                           | 0.0                              | 0.0                               | 20.0                              | -20.0                             | 0.0                           | 0.0                           |
| $k_D$                             | $s^{-1}$           | 1000                            | 0.0                              | 0.0                               | 0.0                               | 0.0                               | 0.0                           | 0.0                           |
| $k_T$                             | $\mu M^{-1}s^{-1}$ | 10.07                           | 0.0                              | 0.0                               | 0.0                               | 0.0                               | 0.2                           | -0.1                          |

|                                |                    |        |      |       |      |     |       |       |
|--------------------------------|--------------------|--------|------|-------|------|-----|-------|-------|
| $k_T$                          | $s^{-1}$           | 556    | 0.0  | 0.0   | 0.0  | 0.0 | 0.0   | 0.0   |
| $k_{T^{**}}$                   | $s^{-1}$           | 1000   | 0.0  | 0.0   | 0.0  | 0.0 | 0.0   | 0.0   |
| $k_H$                          | $s^{-1}$           | 10.0   | 30.5 | -7.2  | -0.2 | 0.3 | 20.0  | -20.0 |
| $k_{AH}$                       | $s^{-1}$           | 10.3   | 30.6 | -7.1  | -0.2 | 0.3 | 20.2  | -20.1 |
| <b>Backward Rate Constants</b> |                    |        |      |       |      |     |       |       |
| $k_{-A}$                       | $s^{-1}$           | 1000   | 0.0  | 0.0   | 0.0  | 0.0 | 0.0   | 0.0   |
| $k_{-Pi}$                      | $mM^{-1}s^{-1}$    | 0.077  | 15.6 | -29.9 | -1.3 | 2.6 | -11.7 | 23.4  |
| $k_{-D^*}$                     | $s^{-1}$           | 639.52 | 0.0  | 0.0   | 0.0  | 0.0 | 0.0   | 0.0   |
| $k_{-D}$                       | $\mu M^{-1}s^{-1}$ | 27.78  | 0.0  | 0.0   | 0.0  | 0.0 | 0.0   | 0.0   |
| $k_{-T}$                       | $s^{-1}$           | 2054.3 | 0.0  | 0.0   | 0.0  | 0.0 | 0.2   | -0.1  |
| $k_{-T^*}$                     | $s^{-1}$           | 10     | 0.0  | 0.0   | 0.0  | 0.0 | 0.0   | 0.0   |
| $k_{-T^{**}}$                  | $\mu M^{-1}s^{-1}$ | 1      | 0.0  | 0.0   | 0.0  | 0.0 | 0.0   | 0.0   |
| $k_{-H}$                       | $s^{-1}$           | 1.4    | 0.0  | 0.0   | 0.0  | 0.0 | 0.0   | 0.0   |
| $k_{-AH}$                      | $s^{-1}$           | 0.2    | 0.0  | 0.0   | 0.0  | 0.0 | 0.0   | 0.0   |

B.

| <b>Equilibrium Rate Constants</b> | <b>Units</b> | <b>P710R</b> | <b><math>V_{max}+20\%</math></b> | <b><math>V_{max}-20\%</math></b> | <b><math>K_{D^*}+20\%</math></b> | <b><math>K_{D^*}-20\%</math></b> | <b><math>K_H+20\%</math></b> | <b><math>K_H-20\%</math></b> |
|-----------------------------------|--------------|--------------|----------------------------------|----------------------------------|----------------------------------|----------------------------------|------------------------------|------------------------------|
| $K_m$                             | ( $\mu M$ )  | 14           | 0.0                              | 0.0                              | 0.0                              | 0.0                              | 0.0                          | 0.0                          |
| $V_{max}$                         | $s^{-1}$     | 2.5          | 20.0                             | -20.0                            | 0.0                              | 0.0                              | 0.0                          | 0.0                          |
| $K_A$                             | $\mu M^{-1}$ | 0.0501       | -7.0                             | 6.6                              | 1.4                              | -0.6                             | 8.2                          | -13.2                        |
| $K_{pi}$                          | mM           | 100          | 0.0                              | 0.0                              | 0.0                              | 0.0                              | 0.0                          | 0.0                          |
| $K_{D^*}$                         |              | 0.167        | 0.0                              | 0.0                              | 20.0                             | -20.0                            | 0.0                          | 0.0                          |
| $K_D$                             | ( $\mu M$ )  | 36           | 0.0                              | 0.0                              | 0.0                              | 0.0                              | 0.0                          | 0.0                          |
| $K_T$                             | $\mu M^{-1}$ | 0.0062       | 0.0                              | 0.0                              | 0.0                              | 0.0                              | 0.0                          | 0.0                          |
| $K_{T^*}$                         |              | 110.65       | 0.0                              | 0.0                              | 0.0                              | 0.0                              | 0.0                          | 0.0                          |



|                                |                                  |        |      |       |      |       |      |       |
|--------------------------------|----------------------------------|--------|------|-------|------|-------|------|-------|
| K <sub>T**</sub>               | μM                               | 1000   | 0.0  | 0.0   | 0.0  | 0.0   | 0.0  | 0.0   |
| K <sub>H</sub>                 |                                  | 4.9    | 13.6 | -18.2 | -0.2 | 4.0   | 20.0 | -20.0 |
| K <sub>AH</sub>                |                                  | 34.7   | 13.6 | -18.2 | -0.2 | 4.1   | 20.4 | -20.3 |
| <b>Forward Rate Constants</b>  |                                  |        |      |       |      |       |      |       |
| K <sub>A</sub>                 | μM <sup>-1</sup> s <sup>-1</sup> | 50.1   | -7.0 | 6.6   | 1.4  | -0.6  | 8.2  | -13.2 |
| k <sub>PI</sub>                | s <sup>-1</sup>                  | 4.4    | 27.3 | -20.5 | 0.0  | 1.1   | -9.1 | 20.5  |
| k <sub>D*</sub>                | s <sup>-1</sup>                  | 69     | 0.0  | 0.0   | 20.0 | -20.0 | 0.0  | 0.0   |
| k <sub>D</sub>                 | s <sup>-1</sup>                  | 1000   | 0.0  | 0.0   | 0.0  | 0.0   | 0.0  | 0.0   |
| k <sub>T</sub>                 | μM <sup>-1</sup> s <sup>-1</sup> | 10.25  | 0.0  | 0.0   | 0.1  | -0.3  | 0.1  | -1.8  |
| k <sub>T*</sub>                | s <sup>-1</sup>                  | 1106.5 | 0.0  | 0.0   | 0.0  | 0.0   | 0.0  | 0.0   |
| k <sub>T**</sub>               | s <sup>-1</sup>                  | 1000   | 0.0  | 0.0   | 0.0  | 0.0   | 0.0  | 0.0   |
| k <sub>H</sub>                 | s <sup>-1</sup>                  | 6.8    | 13.6 | -18.2 | -0.2 | 4.0   | 20.0 | -20.0 |
| k <sub>AH</sub>                | s <sup>-1</sup>                  | 6.9    | 13.6 | -18.2 | -0.2 | 4.1   | 20.4 | -20.3 |
| <b>Backward Rate Constants</b> |                                  |        |      |       |      |       |      |       |
| k <sub>-A</sub>                | s <sup>-1</sup>                  | 1000   | 0.0  | 0.0   | 0.0  | 0.0   | 0.0  | 0.0   |
| k <sub>-PI</sub>               | mM <sup>-1</sup> s <sup>-1</sup> | 0.044  | 27.3 | -20.5 | 0.0  | 1.1   | -9.1 | 20.5  |
| k <sub>-D*</sub>               | s <sup>-1</sup>                  | 413.17 | 0.0  | 0.0   | 0.0  | 0.0   | 0.0  | 0.0   |
| k <sub>-D</sub>                | μM <sup>-1</sup> s <sup>-1</sup> | 27.78  | 0.0  | 0.0   | 0.0  | 0.0   | 0.0  | 0.0   |
| k <sub>-T</sub>                | s <sup>-1</sup>                  | 1653.5 | 0.0  | 0.0   | 0.1  | -0.3  | 0.1  | -1.8  |
| k <sub>-T*</sub>               | s <sup>-1</sup>                  | 10     | 0.0  | 0.0   | 0.0  | 0.0   | 0.0  | 0.0   |
| k <sub>-T**</sub>              | μM <sup>-1</sup> s <sup>-1</sup> | 1      | 0.0  | 0.0   | 0.0  | 0.0   | 0.0  | 0.0   |
| k <sub>-H</sub>                | s <sup>-1</sup>                  | 1.4    | 0.0  | 0.0   | 0.0  | 0.0   | 0.0  | 0.0   |
| k <sub>-AH</sub>               | s <sup>-1</sup>                  | 0.2    | 0.0  | 0.0   | 0.0  | 0.0   | 0.0  | 0.0   |

**Table S7. Comparison of velocity data for wild-type and HCM mutant  $\beta$ -cardiac sS1 at 23 °C.**


| Property     | WT        | H251N <sup>#</sup> | D382Y <sup>**</sup> | P710R <sup>**</sup> | V763M <sup>**</sup> | WT       | R719W <sup>*</sup> | WT       | R723G <sup>*</sup> | WT       | G741R <sup>*</sup> |
|--------------|-----------|--------------------|---------------------|---------------------|---------------------|----------|--------------------|----------|--------------------|----------|--------------------|
| MVIS (nm/s)  | 858 ± 11  | 1195 ± 16          | 769 ± 14            | 275 ± 15            | Not Defined         | 596 ± 21 | 606 ± 22           | 646 ± 25 | 686 ± 26           | 579 ± 48 | 589 ± 49           |
| TOP5% (nm/s) | 1213 ± 15 | 1729 ± 34          | 1143 ± 23           | 468 ± 27            | 1363 ± 24           | 893 ± 26 | 1019 ± 28          | 958 ± 32 | 1068 ± 37          | 905 ± 63 | 885 ± 65           |
| Rel. MVIS    | 1         | 1.3927             | 0.8962              | 0.3205              | Not Defined         | 1        | 1.0167             | 1        | 1.0619             | 0.8962   | 0.9117             |
| Rel. Top 5%  | 1         | 1.4254             | 0.9423              | 0.3858              | 1.1236              | 1        | 1.1410             | 1        | 1.1148             | 0.9446   | 0.9238             |

Mean ± SEM from the number of motor preparations.

MVIS is the mean velocity including stuck filaments.

TOP 5% is the mean of top 5% of all the velocity data.

Relative values are also tabulated to highlight the difference.

 = means those mutations were compared side-by-side to WT proteins that were cultured simultaneously and tested on the same flow chamber.

<sup>#</sup> = Published in (4)    <sup>\*</sup> = Published in (5)    <sup>\*\*</sup> = Unpublished data

Filaments that are tracked longer than 10 frames are included in the analysis. A 20% tolerance filter is applied to eliminate intermittently moving filaments with a velocity dispersion higher than 20% of their mean within a 5-frame window. Each velocity point in the analysis is the average velocity over 5 frames. At least four replicate movies from the indicated number of different preparations of sS1 were analysed.

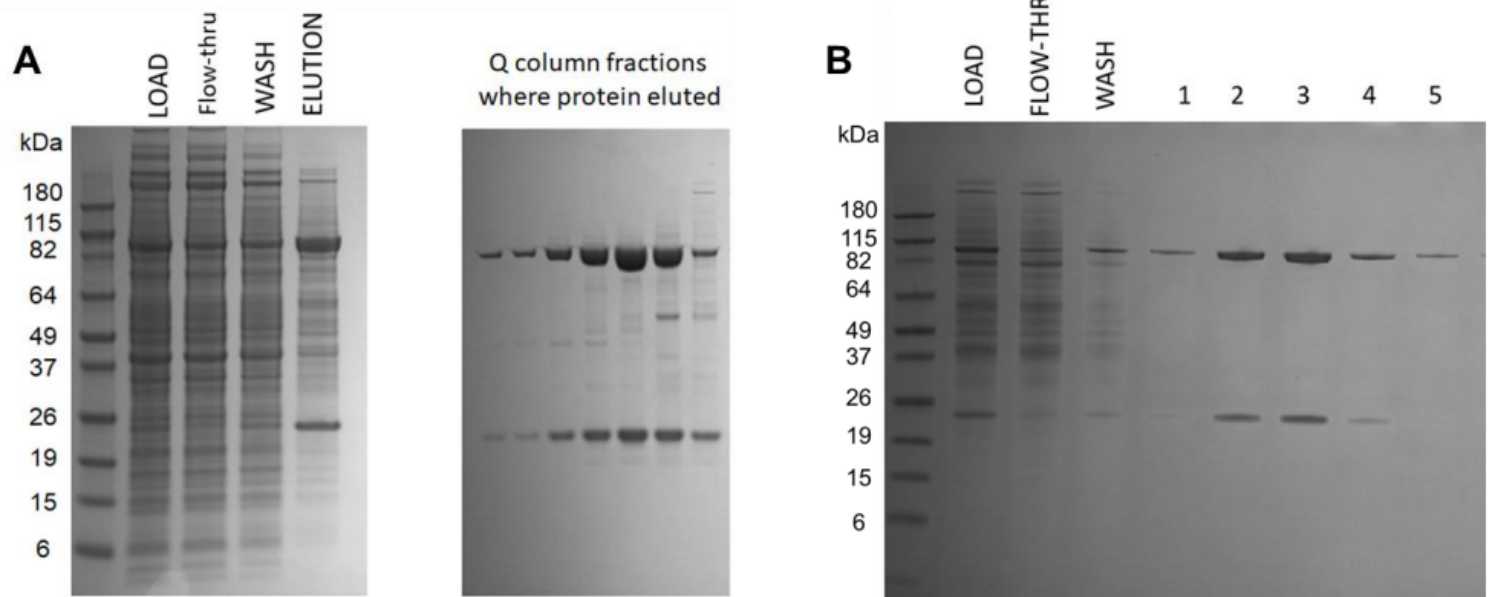


**Figure S1.** (A) Representative gels from a purification of  $\beta$ -R719W. Left is a His-NTA column by gravity flow starting with the lysate and ending with the imidazole eluted sS1. On the right is part of a gel with the sS1 containing fractions. (B) is a representative gel from a purification of  $\beta$ -V763M. After a gravity His column, the solution was loaded on a PDZ column, where the collected fractions also resulted in clean sS1 (sS1: 93 kDa, MYL3: 25 kDa).

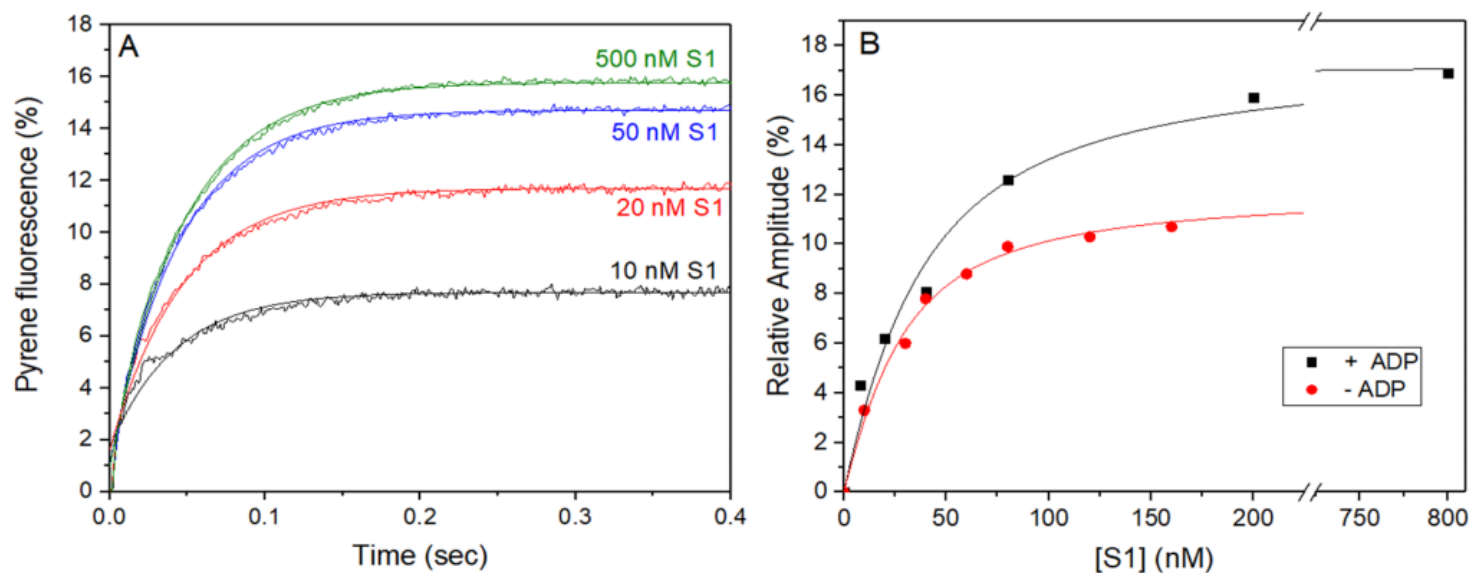


**Figure S2. H251N sS1 affinity for actin in the presence and absence of ADP.** (A) Example traces of the increase in pyrene fluorescence when 15 nM pyr-actin that has been preincubated with 200  $\mu$ M ADP and varying concentrations of sS1 (10-500 nM) was mixed with 10  $\mu$ M ATP. The pyr-actin was treated with hexokinase and  $A_p_5A$  to ensure no ATP was present in the protein before mixing in the stopped-flow. (B) Fluorescence amplitude plotted as a function of sS1 concentration can be described by a quadratic fit resulting in a  $K_{DA}$  of  $65.6 \pm 13$  nM in the presence of ADP, and a  $K_A$  of  $11.5 \pm 1.8$  nM when in the absence of ADP. The average values from 3 independent measurements are given in Table 1.

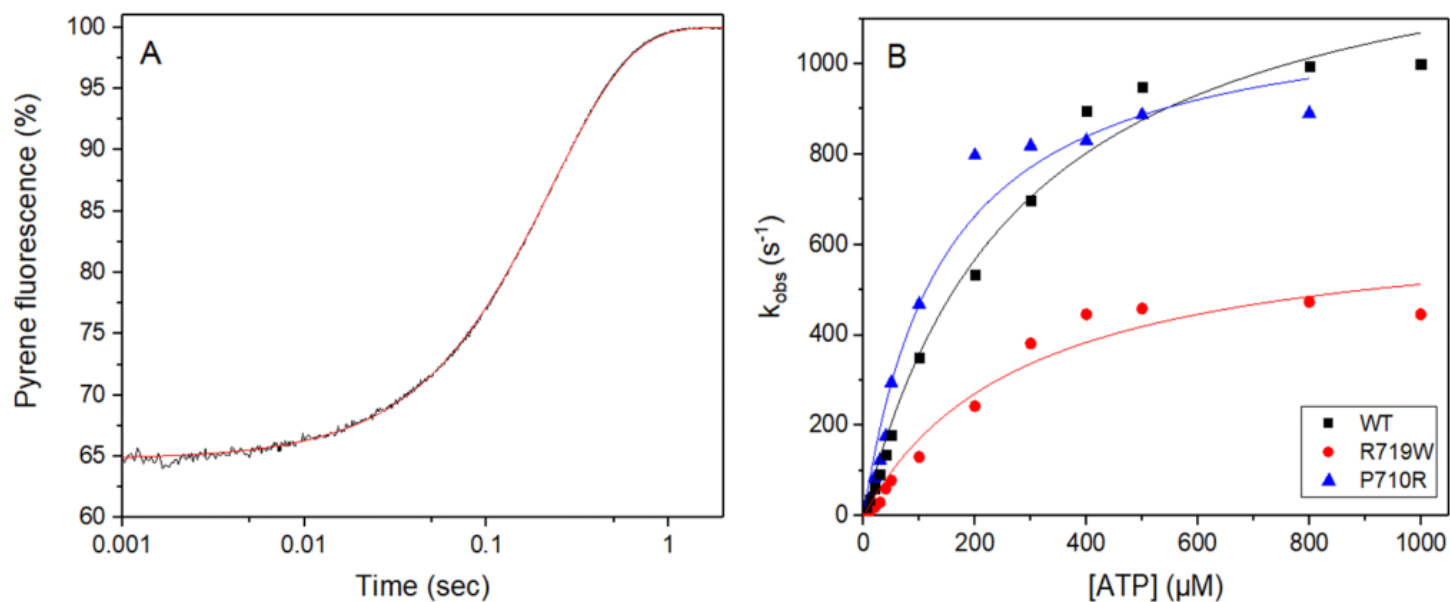


**Figure S3. ATP induced-dissociation of acto.sS1.** (A) Example stopped-flow trace showing the increase in pyrene fluorescence upon ATP-induced dissociation of pyr-actin from the WT sS1. 10  $\mu M$  ATP was mixed with 50 nM pyr-actin.sS1, and the increase in pyrene fluorescence was measured. The experiment was repeated for all constructs and the observed amplitude of the fluorescence changes were similar (within 30%) in each case. (B) The effect of ATP concentration on  $k$  for ATP-induced dissociation of pyr-actin.sS1 for 3 proteins; WT, R719W and P710R sS1. The gradient of the initial slope generates a second order rate constant of ATP binding,  $K_{TK+T^*}$ . The best fit to the hyperbola also yields a maximum  $k = k_{+T^*}$  and the ATP concentration required for half maximum  $k = K_T$ . Best fit values for 3 independent measurements of all constructs are in Table 1.

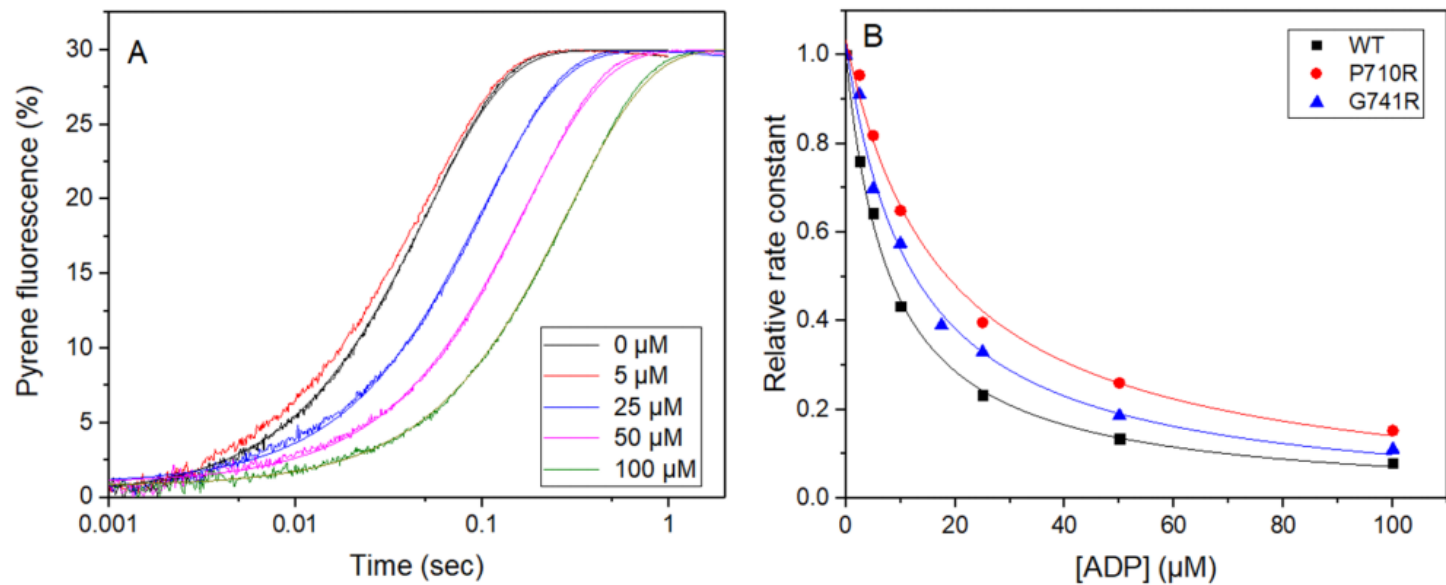


**Figure S4. ADP affinity for acto.sS1.** (A) Example stopped-flow transients showing an increase in pyrene fluorescence when 100 nM pyr-actin.WT sS1 is mixed with 10  $\mu\text{M}$  ATP that has been preincubated with varying concentrations of ADP (0-100  $\mu\text{M}$ ). (B)  $k$  plotted as a function of ADP concentration for WT, P710R and G741R sS1 proteins, showing hyperbolic dependence. The value of  $((K_D+1)/K_DK_D^*)$  is given by the ADP concentration at 50% inhibition.

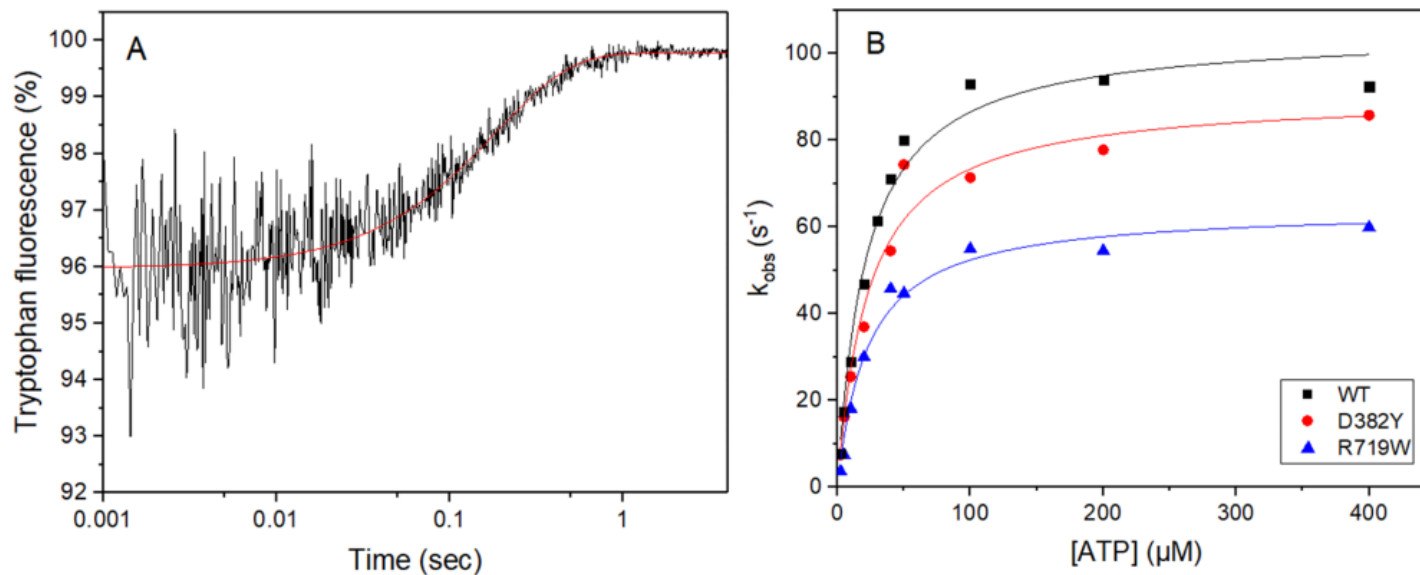


**Figure S5. ATP binding to sS1.** (A) Example stopped-flow trace to measure ATP binding to WT sS1. 10  $\mu\text{M}$  ATP was mixed with 200 nM sS1, and the increase in tryptophan fluorescence was measured. The sS1 was pre-treated with apyrase to ensure no nucleotide was present before mixing in the stopped-flow. Least squares best fit to a single exponential is shown in red with  $k_{\text{obs}} = 22 \text{ s}^{-1}$  and a 4% increase in pyrene fluorescence. (B) The hyperbolic dependence of ATP concentration on  $k_{\text{obs}}$ . The best fit to a hyperbola yields  $\text{max } k = k_{+\text{H}} + k_{-\text{H}}$ , and the ATP concentration required for half maximum  $k = K_{50\%}$ . The initial slope defines the second order rate constant of ATP binding to sS1. Best fit values for 3 independent measurements of all constructs are in Table 1.

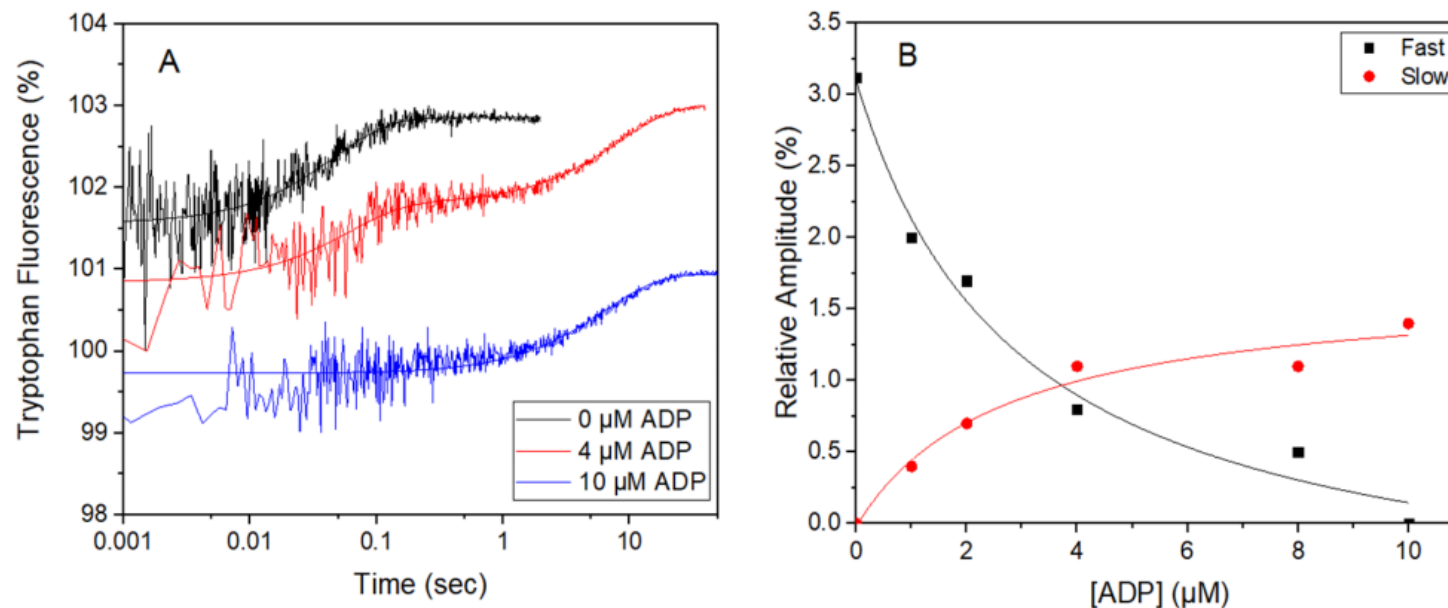


**Figure S6. ADP affinity for P710R sS1.** (A) Example traces of the increase in tryptophan fluorescence when 200 nM sS1 preincubated with ADP (0-10  $\mu\text{M}$  was mixed with 50  $\mu\text{M}$  ATP. The black trace contains no ADP, and results in a transient best described by a single exponential fit. In the presence of 4  $\mu\text{M}$  ADP, the amplitude of the fast phase decreased as the concentration of free sS1 decreases, and a second slow phase is observed representing the release of ADP from sS1. The transient is best described by a double exponential. At high ADP concentration, the amplitude of the fast phase is lost, and the amplitude of the slow phase can be best described by a single exponential. (B) The relative amplitudes of the fast and slow phases plotted against ADP concentration, which has a hyperbolic dependence. Table 1 lists averages for 3 independent measurements for all constructs.



## References

1. Landrum, M. J., Lee, J. M., Benson, M., Brown, G. R., Chao, C., Chitipiralla, S., Gu, B., Hart, J., Hoffman, D., Jang, W., Karapetyan, K., Katz, K., Liu, C., Maddipatla, Z., Malheiro, A., McDaniel, K., Ovetsky, M., Riley, G., Zhou, G., Holmes, J. B., Kattman, B. L., and Maglott, D. R. (2018) ClinVar: Improving access to variant interpretations and supporting evidence. *Nucleic Acids Res.* **46**, D1062–D1067
2. Zerbino, D. R., Achuthan, P., Akanni, W., Amode, M. R., Barrell, D., Bhai, J., Billis, K., Cummins, C., Gall, A., Girón, C. G., Gil, L., Gordon, L., Haggerty, L., Haskell, E., Hourlier, T., Izuogu, O. G., Janacek, S. H., Juettemann, T., To, J. K., Laird, M. R., Lavidas, I., Liu, Z., Loveland, J. E., Maurel, T., McLaren, W., Moore, B., Mudge, J., Murphy, D. N., Newman, V., Nuhn, M., Ogeh, D., Ong, C. K., Parker, A., Patricio, M., Riat, H. S., Schuilenburg, H., Sheppard, D., Sparrow, H., Taylor, K., Thormann, A., Vullo, A., Walts, B., Zadissa, A., Frankish, A., Hunt, S. E., Kostadima, M., Langridge, N., Martin, F. J., Muffato, M., Perry, E., Ruffier, M., Staines, D. M., Trevanion, S. J., Aken, B. L., Cunningham, F., Yates, A., and Flicek, P. (2018) Ensembl 2018. *Nucleic Acids Res.* **46**, D754–D761
3. Mijailovich, S. M., Nedic, D., Svicevic, M., Stojanovic, B., Walklate, J., Ujfalusi, Z., and Geeves, M. A. (2017) Modeling the Actin.myosin ATPase Cross-Bridge Cycle for Skeletal and Cardiac Muscle Myosin Isoforms. *Biophys. J.* **112**, 984–996
4. Adhikari, A. S., Kooiker, K. B., Sarkar, S. S., Liu, C., Bernstein, D., Spudich, J. A., and Ruppel, K. M. (2016) Early-Onset Hypertrophic Cardiomyopathy Mutations Significantly Increase the Velocity, Force, and Actin-Activated ATPase Activity of Human  $\beta$ -Cardiac Myosin. *Cell Rep.* **17**, 2857–2864
5. Kawana, M., Sarkar, S. S., Sutton, S., Ruppel, K. M., and Spudich, J. (2016) Biophysical properties of human  $\beta$ -cardiac myosin with converter mutations that cause hypertrophic cardiomyopathy. *Sci. Adv.* **3**, e1601959

## **6. Molecular features of the UNC-45 chaperone critical for binding and folding muscle myosin.**

Doris Hellerschmied, Anita Lehner, Nina Franicevic, Renato Arnese, **Chloe Johnson**, Antonia Vogel, Anton Meinhart, Robert Kurzbauer, Luiza Deszcz, Linn Gazda, Michael Geeves, Tim Clausen

Nature Communications, 2019. *In press.*

### **6.1 Context of research**

The Clausen lab at the Institute for Molecular Pathology are a structural biology laboratory, with expertise in protein folding. The extensive knowledge and experience of myosin biochemistry in the Geeves lab fostered the collaboration between the two groups.

The folding and assembly of the striated muscle myosin relies on the specific chaperone UNC-45. The study presented in the following manuscript continues the work of Gazda et al, who resolved the crystal structure of the *C. elegans* UNC-45 protein and identified the organisation of UNC-45 in tandem oligomers to facilitate thick filament formation and stability (Gazda et al. 2013). Their work also described the mechanism of UNC-45's interaction with the co-chaperones Hsp90 and Hsp70. The following paper describes the expression of a *C. elegans* skeletal myosin (UNC-54, or MHC-B) in insect cells when co-expressed with the *C. elegans* chaperone UNC-45. This work makes possible the probing of the role of UNC45 and other co-chaperones in myosin folding.

### **6.2 Aims of research**

The aim of this research was 2-fold. Firstly, to produce sarcomeric myosin using baculovirus vectors and insect cells (High Five cells). The reason for this being that protein yields are currently limited by the C2C12 expression and purification system which was used to produce recombinant myosins described in Chapters 3-5. This worked aimed to investigate if recombinant myosin could be produced and folded in a non-muscle environment if co-expressed with the UNC-45 chaperone. The second aim of the research was to show the direct

effect of the temperature sensitive-mutations on the myosin folding activity of UNC-45. Using the insect cell/baculoviral system, a mutational analysis of UNC-45 was conducted. Crystal structures of the temperature sensitive mutations were generated to uncover the molecular basis of the temperature-sensitivity, with a focus on the flexible myosin-binding UCS domain. This could advance the understanding of the folding mechanism of this chaperone.

### **6.3 Contribution to publication**

My contribution to this manuscript was with regards to aim 1. I worked closely with Renato Arnese from the Clausen lab when he visited the University of Kent. Together, we conducted the initial biochemical activity of the purified MHC-B. We did this through single turnover experiments and F-actin co-sedimentation assays. The manuscript was received by Nature Communications, who recommended a more thorough biochemical characterisation of the purified MHC-B protein to confirm that the protein is active. I then completed this through stopped-flow spectroscopy. I designed, performed and analysed the stopped-flow characterisation of the MHC-B protein. For this publication I provided figure 3d, supplementary figure 3, and supplementary table 1. These were added to the following revised manuscript.

**6.4 Publication** – See below for the revised manuscript which was accepted by Nature Communications.

ARTICLE

<https://doi.org/10.1038/s41467-019-12667-8>

OPEN

# Molecular features of the UNC-45 chaperone critical for binding and folding muscle myosin

Doris Hellerschmied<sup>1,5,6\*</sup>, Anita Lehner<sup>2,6</sup>, Nina Franicevic<sup>1,6</sup>, Renato Arnese<sup>1</sup>, Chloe Johnson<sup>3</sup>,  
Antonia Vogel<sup>1</sup>, Anton Meinhart<sup>1</sup>, Robert Kurzbauer<sup>1</sup>, Luiza Deszcz<sup>1</sup>, Linn Gazda<sup>1</sup>, Michael Geeves<sup>3</sup> &  
Tim Clausen<sup>1,4\*</sup>

Myosin is a motor protein that is essential for a variety of processes ranging from intracellular transport to muscle contraction. Folding and assembly of myosin relies on a specific chaperone, UNC-45. To address its substrate-targeting mechanism, we reconstitute the interplay between *Caenorhabditis elegans* UNC-45 and muscle myosin MHC-B in insect cells. In addition to providing a cellular chaperone assay, the established system enabled us to produce large amounts of functional muscle myosin, as evidenced by a biochemical and structural characterization, and to directly monitor substrate binding to UNC-45. Data from in vitro and cellular chaperone assays, together with crystal structures of binding-deficient UNC-45 mutants, highlight the importance of utilizing a flexible myosin-binding domain. This so-called UCS domain can adopt discrete conformations to efficiently bind and fold substrate. Moreover, our data uncover the molecular basis of *temperature-sensitive* UNC-45 mutations underlying one of the most prominent motility defects in *C. elegans*.

<sup>1</sup>Research Institute of Molecular Pathology, Vienna BioCenter, Vienna, Austria. <sup>2</sup>Vienna BioCenter Facilities, Vienna, Austria. <sup>3</sup>School of Biosciences, University of Kent, Canterbury, UK. <sup>4</sup>Medical University Vienna, Vienna, Austria. <sup>5</sup>Present address: Faculty of Biology, Center of Medical Biotechnology, University Duisburg-Essen, Essen, Germany. <sup>6</sup>These authors contributed equally: Doris Hellerschmied, Anita Lehner, Nina Franicevic. \*email: [doris.hellerschmied@uni-due.de](mailto:doris.hellerschmied@uni-due.de); [tim.clausen@imp.ac.at](mailto:tim.clausen@imp.ac.at)

**M**yosins are cytoskeletal, molecular motors promoting a variety of mechano-chemical processes in the cell<sup>1</sup>. The myosin superfamily contains about 35 subtypes, among which the class II muscle proteins (myosin II) are the arguably most prominent member driving muscle contraction<sup>2</sup>. Myosin II molecules found in skeletal and cardiac muscles dimerize via their C-terminal coiled-coil domain and associate with essential and regulatory light-chains to yield the basic hexameric myosin complex. These hexamers further assemble into myosin thick filaments, from where the N-terminal myosin ATPase domains project to interact with the adjacent actin (thin) filaments. Establishing and maintaining the intricate myosin-actin interplay, occurring at the interface of the two differently organized muscle filaments, is a great challenge for the cellular chaperone machinery. Therefore, muscle cells express a vast number of specialized folding and assembly factors that control the expression, folding, assembly and interplay of actin and myosin molecules<sup>3–7</sup>. Failure of muscle filament assembly or maintenance leads to severe myopathies<sup>8,9</sup>.

Among the chaperones expressed in muscle cells, UNC-45 appears to be the key component of the myosin assembly machinery. The UNC-45 protein was initially identified in *C. elegans*, where site-specific *temperature-sensitive* (*ts*) mutants revealed the importance of the chaperone for myosin function<sup>10–13</sup>. Subsequent studies in *C. elegans*, *Xenopus*, *Zebrafish*, and *Drosophila* confirmed the role of UNC-45 as a myosin-specific chaperone, promoting the folding of the myosin ATPase domain as well as coordinating the assembly of thick filaments during muscle development<sup>14–19</sup>. In higher organisms, UNC-45 is particularly important for the maturation of myosin II in muscle cells<sup>20–22</sup> and, together with Hsp90 (heat shock protein 90) and UFD-2 (ubiquitin fusion degradation 2), maintaining the functionality of myosin filaments during stress situations<sup>23,24</sup>. Mechanistic insight into the chaperone function of UNC-45 comes from structural studies revealing its 3-domain architecture<sup>19,25</sup>. UNC-45 is composed of an N-terminal TPR (tetratricopeptide repeat) domain mediating the interaction with Hsp70/Hsp90, an elongated UCS (UNC-45/Cro1/She4p) domain at the C-terminus providing a myosin-binding site<sup>14,19</sup>, and a central domain aligning the two functional TPR and UCS units to each other. Further analyses of UNC-45 from *C. elegans* revealed that the chaperone can form a linear protein chain, which constitutes a myosin assembly line licensing Hsp70 and Hsp90 to act in a defined periodicity on myosin heads protruding from the myofilaments<sup>19,26</sup>.

To address the myosin targeting mechanism of UNC-45, we reconstitute the chaperone-substrate interplay both *in vitro* and *in vivo*. Using insect cells as host system, we monitor the interaction between the *C. elegans* UNC-45 and MHC-B (myosin II heavy chain isoform B, also known as UNC-54) in a cellular context. Notably, co-expression of UNC-45 allowed production of fully functional MHC-B in large amounts, yielding about 15 mg muscle myosin per liter culture. The recombinant myosin was also key to address the basic mechanistic properties of the UNC-45 chaperone, revealing for example the molecular basis of *ts* motility defects of mutant worms harboring point-specific UNC-45 mutations. Our data show that these *ts* mutations affect the myosin-binding capability of UNC-45 rather than its protein stability.

## Results

**In vivo reconstitution of the UNC-45/myosin interplay.** An inherent problem in characterizing the substrate-targeting mechanism of the UNC-45 chaperone comprises the unavailability of the cognate substrate, muscle myosin II. We thus aimed

to establish an orthogonal *in vivo* assay to monitor the activity of myosin-specific chaperones. To this end, we used the motor domain of *C. elegans* body wall muscle myosin MHC-B as model system and co-expressed it with different *C. elegans* chaperones in insect cells (Fig. 1a). We first tested the production of an MHC-B muscle myosin variant comprising the motor domain (residues 1–790) in comparison to a non-muscle myosin motor (nematode NMY-2, residues 1–796). While the NMY-2 motor domain could be expressed in soluble form, even in the absence of any *C. elegans* helper chaperone (Fig. 1b), the expression of the MHC-B muscle myosin alone did not yield any soluble recombinant protein, a finding which is consistent with previous reports<sup>21,27</sup>. As it is known that the *C. elegans* chaperones UNC-45, HSP-1 (Hsp70) and DAF-21 (Hsp90) are critical for myosin folding and assembly<sup>14,19,28</sup>, we next tested whether co-expression of these chaperones improves the production of the MHC-B motor domain in its soluble form. The experiments revealed that the *C. elegans* Hsp70 and Hsp90 had only a moderate effect in yielding soluble muscle myosin in insect cells. However, co-expressing UNC-45 strongly increased the amount of the MHC-B motor domain in the soluble fraction of the cell lysate (Fig. 1c). These data imply that the nematode UNC-45 can team up with the insect cell chaperone machinery required for myosin folding, given that additional co-expression of the cognate partner chaperones Hsp70 and Hsp90 from *C. elegans* was not required to obtain soluble myosin (Fig. 1c). Indeed, we could pull-down endogenous Hsp70 and Hsp90 together with *C. elegans* UNC-45 from insect cell lysates (Fig. 1d). This interaction is abolished upon deletion of the UNC-45 TPR domain or mutating a key residue (K82E) in the Hsp70/90 binding groove, while deletion of the UCS domain does not impact the interaction with the partner chaperones (Fig. 1d). Finally, when purifying MHC-B and testing its actin-induced ATPase activity, we did not observe major differences in the amount and functionality of the myosin motor co-expressed with UNC-45 alone or together with *C. elegans* Hsp70 and Hsp90 (Fig. 1e and Supplementary Fig. 1). Taken together, our findings suggest that the *C. elegans* UNC-45 is the most critical chaperone for making MHC-B muscle myosin.

**Analyzing the UNC-45/myosin interplay in insect cells.** Since the recombinant production of functional MHC-B myosin fully depends on UNC-45, the insect cell co-expression system can be used as a cellular assay to determine the effect of site-specific UNC-45 mutations on its *de novo* myosin folding activity. To this end, we analyzed functional UNC-45 mutations that abrogated interactions with partner chaperones or substrate, prevented formation of multimeric UNC-45 chains or led to the well-known *ts* phenotype in nematodes (Fig. 2a). To assess the folding state of MHC-B co-expressed with different UNC-45 mutants, we monitored its solubility in insect cell lysates (Supplementary Fig. 2a) and, in parallel, analyzed the purified proteins *in vitro* by analytical SEC and ATPase assays. Fitting to our insect cell data (Fig. 2b), the strongest difference in SEC runs was observed for MHC-B expressed either alone or in the presence of the UNC-45 wild-type (wt) chaperone (Fig. 2c). In the absence of UNC-45, the produced MHC-B is mostly misfolded, eluting at the void volume of the SEC column (fractions 1–4, Fig. 2c, d). Contrary, in the presence of UNC-45, most of the MHC-B protein elutes in a pronounced peak that corresponds to the folded myosin motor (fractions 5–9, Fig. 2c, d). While the SEC runs allowed distinguishing between aggregated and folded protein, the ATPase assays confirmed that the isolated MHC-B motors, eluting in the folded peak, are enzymatically active, exhibiting comparable, actin-inducible ATPase activity (Supplementary Fig. 1). However, it should be noted that the SEC profiles strongly varied between

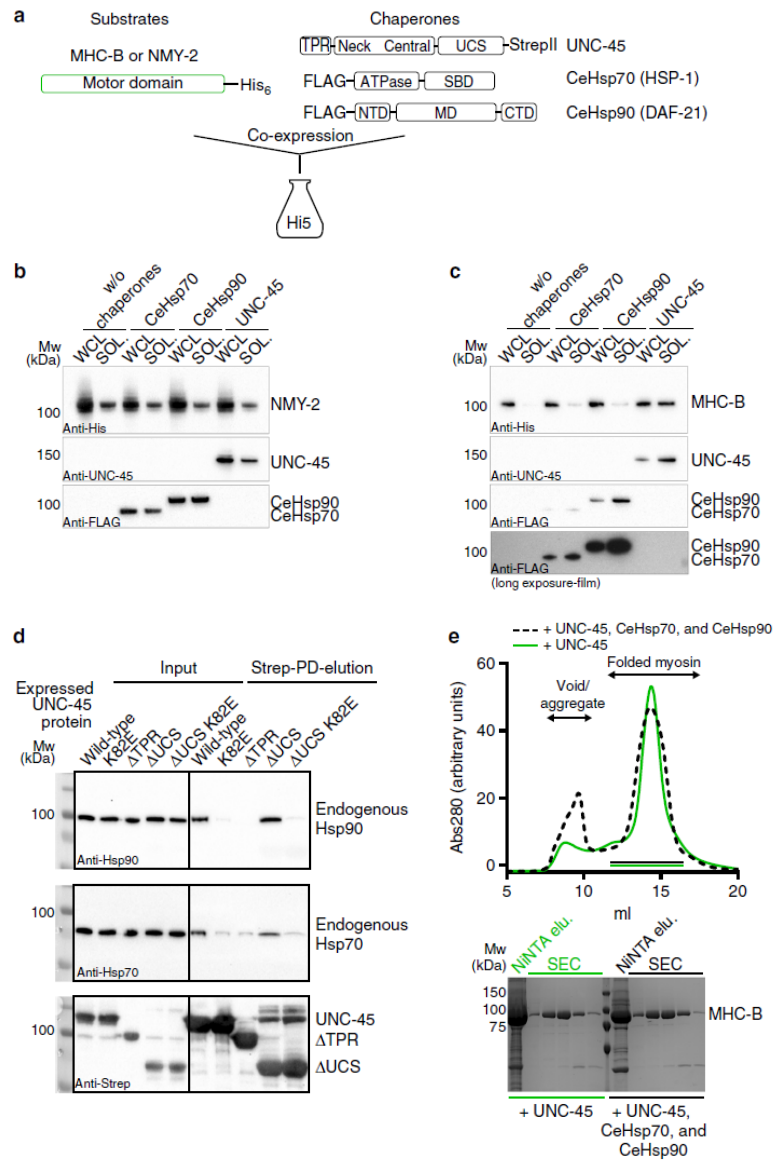


**Fig. 1** Producing functional myosin in insect cells. **a** Overview of constructs used for expression studies in insect cells. Western blot analysis of co-expression of NMY-2 (**b**) or MHC-B (**c**) with indicated chaperones in Hi5 insect cells. Whole cell lysates (WCL) and soluble fractions (SOL) are shown. 1/3rd of the WCL was applied with respect to the SOL fraction. (SBD-substrate binding domain, NBD-nucleotide binding domain, NTD-N-terminal domain, MD-middle domain, CTD-C-terminal domain). **d** Pull-down (PD) of Strep-tagged UNC-45 constructs from insect cells. Input samples and elutions were probed with Hsp70, Hsp90, and Strep-tag antibodies. **e** Upper panel: SEC traces of MHC-B purified from co-expression with the indicated *C. elegans* chaperones. Lower panel: SDS-PAGE gels showing the elution after NiNTA and indicated SEC fractions

different samples, depending on the co-expressed UNC-45 chaperone. We therefore used the SEC-purified amounts of monomeric, folded MHC-B (Fig. 2d) together with the data from our cellular assay (Fig. 2b and Supplementary Fig. 2a) as a readout to assess the chaperone activity of the different UNC-45 forms.

We first studied two mutants deficient in myosin binding, namely a deletion mutant lacking the UCS domain (residues 1–521, ΔUCS)<sup>14,24</sup> and a variant carrying a point mutation (N758Y) in the myosin-binding canyon<sup>19</sup>. Deletion of the UCS domain had a strong impact on UNC-45 chaperone function, as

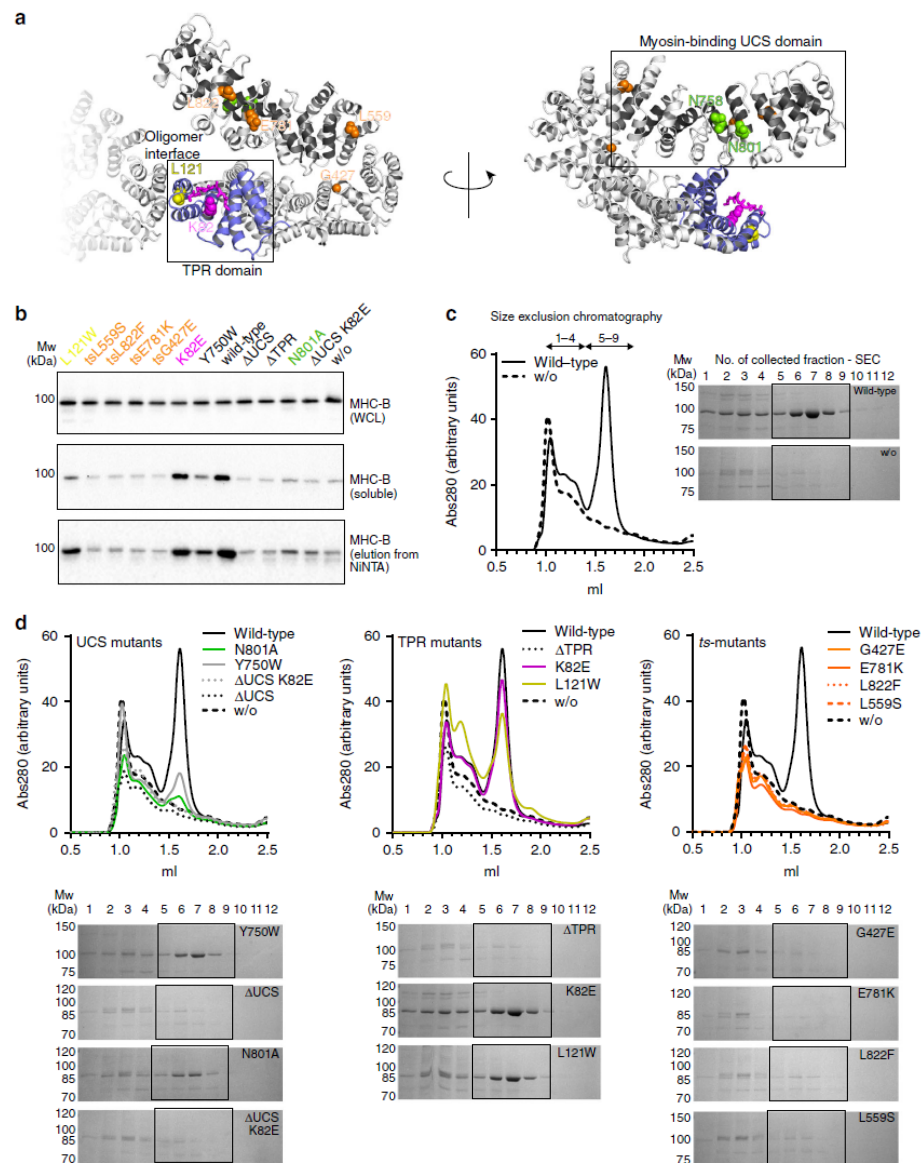


**Fig. 2** Effect of UNC-45 mutant proteins on myosin production in insect cells. **a** UNC-45 mutations that were analyzed in the chaperone assay are shown on the crystal structure of the wild-type protein (PDB code: 4i2z). **b** Western blot analysis of co-expression of MHC-B with indicated UNC-45 mutant proteins in insect cells. Whole cell lysates (WCL), soluble fractions and elutions after small-scale NiNTA purification are shown for MHC-B. **c** SEC traces and corresponding SDS-PAGE gels for MHC-B purified from insect cells with and without co-expression of UNC-45. Fractions 1–4 cover the void/aggregate peak, while fractions 5–9 correspond to the elution volume of monomeric functional myosin. **d** Same analysis as in **c** for MHC-B co-expressed with UNC-45 UCS domain mutants, TPR domain mutants and *ts*-mutants

seen by the reduced levels of soluble MHC-B in the insect cell co-expression system (Fig. 2b and Supplementary Fig. 2a). The site-specific N758Y mutant protein itself was not highly expressed in insect cells, likely because the mutation destabilizes the UCS

domain as observed for other point mutations bordering the myosin-binding groove<sup>24</sup>. We therefore excluded the N758Y mutant from our analysis. Instead, we used the cellular chaperone assay to look for a new site-specific UCS mutation having an

impaired myosin folding activity. A comparative analysis with beta-catenin, which is an armadillo (ARM) repeat protein structurally related to the UCS domain, suggested that Asn801 of UNC-45 may directly interact with myosin (Supplementary Fig. 3). The N801A variant is stable in insect cells, however compared to the wt protein, co-expression of the UCS mutant yielded only small amounts of soluble myosin (Fig. 2b and Supplementary Fig. 2a). Moreover, we observed only a minor peak of the folded MHC-B in the SEC analysis (Fig. 2d), indicating that the N801A mutation strongly impaired the myosin-folding function of UNC-45. Finally, we explored the effect of the UNC-45 mutation Y750W, which affects a residue located in the periphery of the myosin-binding canyon and did not show a clear phenotype when expressed in *C. elegans*<sup>19</sup>. While Y750W supported the production of soluble myosin in the cell (Supplementary Fig. 2a), the yield of functional MHC-B that could be purified is smaller than for wt UNC-45 (Fig. 2d). These data suggest that even subtle structural changes in proximity to the UCS myosin-binding site affect UNC-45 chaperone function.

The interaction of UNC-45 with its partner chaperones Hsp70/Hsp90 is mediated via its TPR domain<sup>14,19</sup>. When we assayed the activity of the K82E mutant, which is impaired in Hsp70/90 binding (Fig. 1d, and ref. <sup>19</sup>), we observed that it yielded similar levels of soluble myosin as the co-expressed wt UNC-45 (Fig. 2b). Notably, the SEC peaks of the folded MHC-B motor domain purified from the two samples almost completely overlap (Fig. 2d), implying that the K82E mutant exhibits full chaperone activity. These data suggest that a direct interaction between the Hsp70/Hsp90 chaperones and the UNC-45 TPR domain is not required to fold the motor domain of myosin. Surprisingly, however, deleting the entire TPR domain fully abolished the chaperone function of UNC-45 (Fig. 2b, d). Accordingly, the TPR domain does not only serve as Hsp70/Hsp90 docking site, but accomplishes further critical functions.

The linear UNC-45 chaperone chain has been shown to be essential for myofilament formation and sarcomere integrity in worms<sup>19</sup>. To test the importance of oligomer formation for myosin folding, we analyzed UNC-45 L121W, a single-site mutant known to disrupt the interface stabilizing UNC-45 chains. As seen in the insect cell chaperone assay, the L121W mutation led to a decrease in the amount of soluble MHC-B (Supplementary Fig. 2a). However, in our SEC analysis, a significant amount of the soluble MHC-B elutes as folded protein (Fig. 2d), suggesting that UNC-45 oligomerization is not required for the maturation of the myosin motor domain.

In *C. elegans*, four distinct UNC-45 point mutations (G427E, L559S, E781K, L822F) have been identified that underlie the so-called uncoordinated (*unc*) *ts*-phenotype<sup>10,11,13,29</sup>. *Ts*-worms grown at the permissive temperature of 15–18 °C during their larval development show no defects in myosin thick filament formation, while *ts*-worms grown at the restrictive temperature of 25 °C exhibit motility defects and a distorted sarcomere organization<sup>10,11</sup>. Though known for decades, the mechanistic details underlying the *ts*-phenotype of UNC-45 have remained elusive. Strikingly, in our cellular chaperone assay, all *ts*-mutations strongly reduced the production of soluble myosin (Fig. 2b). Moreover, applying the minimal amounts of soluble protein to a SEC column did not recover any folded protein (Fig. 2d). To test whether this defect in chaperone function relates to a reduced stability of the *ts*-proteins themselves, we repeated the cellular folding assays at a lower temperature (18 °C) that still supported survival of insect cells and corresponds to the permissive temperature in growing *ts*-worms. Also, at 18 °C we observed the same solubility defect for myosin co-expressed with the *ts*-mutants (Supplementary Fig. 2b). These results suggest that the UNC-45 *ts*-mutants, which were expressed at the same level

as the wt protein, affect the chaperone function of UNC-45 rather than its stability.

#### UNC-45 co-expression yields functional muscle myosin.

In addition to serving as a folding reporter in insect cells, we wanted to use the recombinant MHC-B motor domain as a substrate to characterize the UNC-45 chaperone in vitro. For this purpose, it was necessary to assess the structural and functional integrity of the produced muscle myosin in detail. We first tested the basal ATPase activity of purified, monomeric MHC-B in a stopped-flow setup by monitoring its tryptophan fluorescence (Fig. 3a). Upon ATP binding to the myosin motor domain Trp fluorescence is enhanced<sup>30,31</sup>, and by monitoring its decay over time we determined an MHC-B ATPase rate of 0.073 s<sup>-1</sup> showing that the recombinant protein is active. We then explored the interaction of recombinant MHC-B with rabbit skeletal muscle F-actin in a co-sedimentation assay (Fig. 3b). In the absence of nucleotide, MHC-B interacts strongly with F-actin, as demonstrated by the large amounts of MHC-B seen in the pelleted fraction. However, when adding ATP, myosin was released from F-actin and detected in the supernatant, reflecting the nucleotide-dependent interplay between the two proteins (Fig. 3b). Next, the activation of MHC-B ATPase activity by F-actin was quantified in an NADH-coupled assay (Fig. 3c). Upon elevating the actin concentration, we observed a 6-fold increase of its basal ATPase activity, which inclined from 0.043 ATP s<sup>-1</sup> in the absence of actin to a  $V_{max}$  of 0.257 ATP s<sup>-1</sup>. Finally, and most importantly, the large amount of recombinant MHC-B produced enabled us to perform a comprehensive analysis of the interaction with actin during the ATPase cross-bridge cycle. To compare the kinetic parameters of MHC-B and human cardiac myosin, which served as our reference, we performed stopped-flow measurements exploiting the strong quenching of pyrene-labelled actin by MHC-B. Rapid mixing of an excess of ATP with pyrene-actin: myosin results in dissociating of the complex and a return of the fluorescence to the starting value (inset Fig. 3d). Measuring the amplitude of the ATP induced transient gives an estimate of the amount of actin:myosin complex formed at each myosin concentration. The resulting fit of the binding isotherm reveals an affinity for actin of 10.3 nM, which is comparable with the affinity of the human cardiac muscle myosin isoform for the same actin (10 nM) (Fig. 3d, Supplementary Table 1, and ref. <sup>32</sup>). Using similar stopped-flow experiments, we carried out a broad kinetic characterization of the MHC-B myosin motor, determining the rate constants of ATP and ADP binding to myosin and the actin: myosin complex, respectively. In conclusion, the kinetic data demonstrate that the MHC-B variant produced in insect cells is a fully functional myosin motor, which exhibits similar kinetic properties to other muscle myosins (Supplementary Table 1, Supplementary Fig. 4).

Finally, we crystallized MHC-B and determined the structure of the ADP-bound state to a resolution of 1.9 Å (Supplementary Table 2). The motor domain adopts the canonical myosin ATPase fold being comprised of the N-terminal, the central (upper and lower 50 kDa region) and a C-terminal domain, with all residues (except loops 198–210 and 633–650) being well-defined by electron density. Notably, a DALI search<sup>33</sup> for related protein structures in the Protein Data Bank identified the human beta-cardiac muscle myosin (PDB 4db1) among the closest structural homologs of the determined MHC-B structure. The two motor domains are 59% identical and 72% similar (Supplementary Fig. 5), and could be superimposed with an RMSD of 2.1 Å for 696 Ca atoms (Fig. 3e). Indeed, the nucleotide binding site of MHC-B is virtually identical to that of the human beta cardiac myosin, with the sidechains that coordinate ADP present in



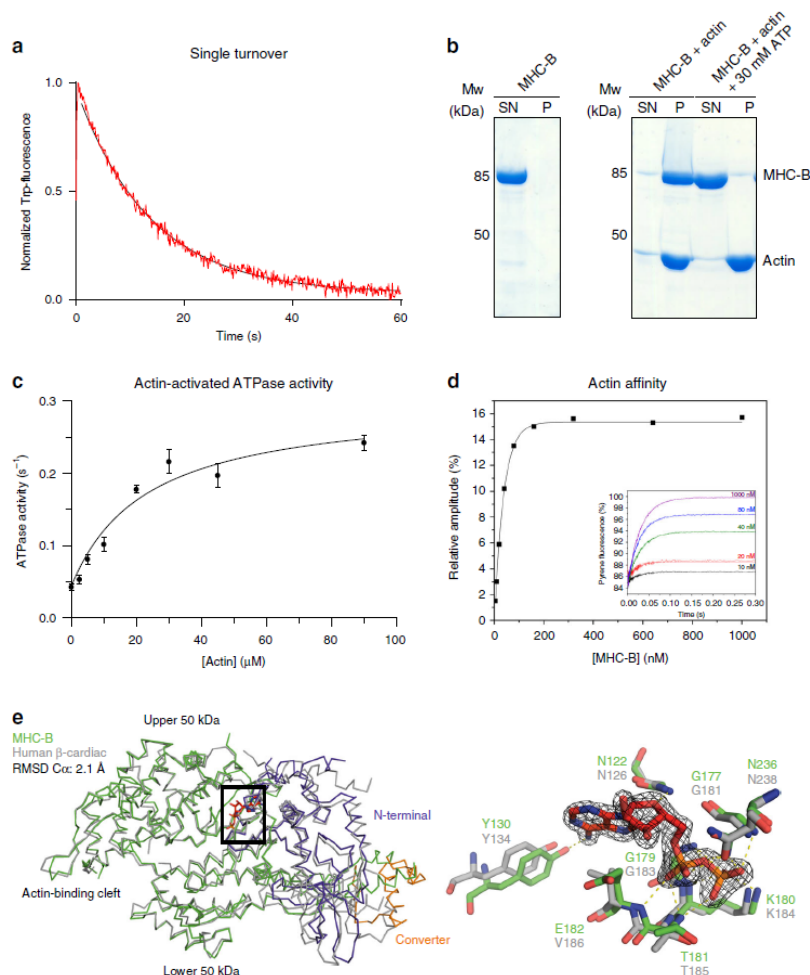


**Fig. 3** Characterization of functional MHC-B. **a** Single ATP turnover experiment monitoring Trp-fluorescence decay ( $K_{\text{obs}} = 0.073 \text{ s}^{-1}$ ). **b** F-actin co-sedimentation assay. In the presence of F-actin, MHC-B is detected in the pellet fraction (P) but is released upon addition of ATP and found in the supernatant (SN). **c** F-actin-stimulated ATPase activity of MHC-B, yielding  $V_{\text{max}} = 0.257 \text{ s}^{-1}$  and  $K_M = 23.1 \mu\text{M}$ . Error bars represent the s.e.m., of two biological replicates (MHC-B from different purifications), for which three technical replicates have been carried out each. **d** Stopped-flow analysis measuring dissociation of the actin:MHC-B complex. The inset illustrates example traces of the increase in pyrene fluorescence when  $20 \mu\text{M}$  ATP was mixed with  $50 \text{ nM}$  pyrene-labelled actin and varying concentrations of MHC-B (5–1000 nM). The increase in fluorescence can be described by an exponential function in which the rate constant is proportional to the ATP concentration and the amplitude of the fluorescence change is proportional to the fractional saturation of actin with MHC-B. The actin affinity derived by this experiment was  $10.3 \pm 3.7 \text{ nM}$  (average of three independent measurements). **e** Left panel: Structural alignment of ADP (red)-bound MHC-B (50 kDa domain in green, N-terminal domain in lilac, converter in orange) and human beta-cardiac myosin (PDB code: 4db1, gray). Right panel: Close-up view of the nucleotide-binding pocket of MHC-B in the ADP-bound state, overlaid with corresponding active site residues of the cardiac myosin. The ADP molecule (red) is shown together with the 2Fo-Fc omit electron density, contoured at  $1.5\sigma$ .

almost identical position (Fig. 3e). In contrast to the human protein, which has to be produced in a special mouse cell line requiring time- and resource-demanding procedures, the biochemical and structural analysis of MHC-B was performed with a recombinant protein that can be produced in large amounts in insect cells (15 mg myosin per liter cell culture) and is easily

accessible to genetic manipulations. Considering the high yields including the human beta-cardiac variant, the recombinant MHC-B should represent a valuable model system to address the assembly, function and regulation of muscle myosins in basic and in medical research.

**In vitro interaction of UNC-45 with damaged myosin.** To study how UNC-45 interacts with myosin molecules in vitro we used the recombinant MHC-B motor domain. Previous reports, in which non-cognate myosin variants and unrelated model substrates were used as chaperone substrates, implied that UNC-45 preferentially targets aberrant protein molecules<sup>34,35</sup>. However, the nature of the non-native myosin species targeted by UNC-45—either during de novo folding or when rescuing damaged myosin—is not known. Thus, the targeted state of myosin (e.g. partially unfolded, misfolded or aggregated protein) and the molecular details of forming cognate UNC-45/myosin complexes need to be resolved. Instead of applying the rather indirect aggregate prevention assay, we monitored formation of the UNC-45/myosin complex at two different temperatures, 4 and 27 °C, in a size-exclusion chromatography (SEC) based assay. The 4 °C condition served as control temperature, preserving the native state of the myosin substrate (Fig. 4a). The higher temperature, 27 °C, reflects a proteotoxic stress condition, as implied by the fact that *C. elegans* worms exhibit signs of heat-shock and sterility at this temperature<sup>36</sup>.

When evaluating the stability of the individual proteins at the elevated temperature (27 °C), we observed that myosin was destabilized and eluted in the void volume of the SEC column as expected for aberrant proteins. In contrast, all tested UNC-45 variants were stably folded, eluting at the same retention volume as the native chaperone at 4 °C (Fig. 4a, c). When myosin and UNC-45 were co-incubated at 27 °C, a prominent fraction of UNC-45 was present in complex with unfolded myosin eluting at higher molecular weight (HMW, Fig. 4a). Interestingly, when myosin and UNC-45 were separately incubated and mixed before loading, less UNC-45 was present in the corresponding HMW complex with myosin (Fig. 4a). This suggests that during myosin denaturation, a certain un-folding intermediate is formed that is preferentially targeted by UNC-45. To validate that the observed interaction is specific, we used bovine serum albumin (BSA) and the  $\Delta$ UCS mutant of UNC-45, deficient in myosin binding, as negative controls. When co-incubated at 27 °C, aberrant myosin did not influence the running behavior of BSA and  $\Delta$ UCS during SEC, as both control proteins eluted at the same retention volume as in the absence of myosin. In conclusion, the SEC experiments indicate that unfolded myosin binds to UNC-45 in a specific manner (Fig. 4b). We also analyzed the identified UNC-45 N801A mutant, deficient in myosin folding, in the in vitro assay (Supplementary Fig. 3b). Unexpectedly, the N801A mutant still interacts with damaged myosin under the applied conditions. These data suggest that the UNC-45 mutant protein, which has a partially obstructed myosin-binding site, can still bind to substrate, however, does not fully support the folding of myosin in the cell (Fig. 2b, d and Supplementary Fig. 2a).

The established in vitro interaction assay furthermore allowed us to address the molecular basis underlying the UNC-45 *ts*-mutations, which are among the most studied motility defects in *C. elegans*<sup>10,11,13</sup>. Of note, our cellular chaperone assay revealed that the UNC-45 *ts*-mutations have a negative effect on the myosin folding activity, however, did not resolve whether the *ts*-mutations directly impair the chaperone activity or exert rather indirect effects, destabilizing for example the UNC-45 protein. With regards to the latter point, we carried out circular dichroism (CD) measurements to determine the melting temperature ( $T_m$ ) and thus stability of the purified *ts*-proteins (Fig. 4c). The CD data demonstrate that all four UNC-45 *ts*-proteins exhibit the same or even slightly higher thermal stability than the wt chaperone. Moreover, the E781K mutant displayed a slightly different unfolding profile pointing to potential structural differences in the folded chaperone (Supplementary Fig. S6a). It should be also noted that it was even possible to crystallize

various *ts*-mutants at room temperature (19 °C) and determine their structure, as described later.

When addressing the interaction with myosin in the SEC-based assay, we observed that all UNC-45 *ts*-mutants showed a reduced ability to form a complex with the unfolded myosin, as judged by the smaller protein amounts co-eluting with the myosin substrate (Fig. 4c). To further confirm that the impaired chaperone activity of the *ts*-mutants is not due to an unstable UNC-45 protein, we repeated the in vitro chaperone assay, this time monitoring the interaction of *ts*-mutants with pre-misfolded myosin at low temperature. After pre-incubating myosin at 27 °C, the heat-damaged protein was mixed with different UNC-45 proteins at 4 °C and the samples were analyzed by SEC as described above. For the wt chaperone, we observed a shift of the UNC-45 fraction towards the HMW peak that should contain the chaperone-substrate complex (Supplementary Fig. S6b). In contrast, none of the *ts*-proteins shifted into the HMW fraction further confirming that the *ts*-mutants, present in a folded state, cannot interact with damaged myosin (Supplementary Fig. S6c). Together, the cellular folding assay, the CD data and the SEC-based reconstitution analysis demonstrate that the *ts*-mutations L559S, G427E, E781K and L822F have a direct effect on the myosin-binding function of UNC-45, abrogating the interaction with the heat-damaged myosin substrate. Thus, our data provide compelling evidence that the temperature-induced motility defect of *ts*-worms is caused by the impaired chaperone activity of UNC-45 rather than being the consequence of an unstable or misfolded *ts*-protein.

**Structural features of UNC-45 *ts*- and deletion mutants.** To address the structural basis of the impaired chaperone function of UNC-45 *ts*-mutants L822F and G427E, and UNC-45  $\Delta$ TPR, we analyzed the crystal structures of the three mutant proteins (Supplementary Table 2). The two UNC-45 *ts*-mutants L822F and G427E crystallized in the form of a linear filament, having the same periodicity (85 Å), hydrophobic interface and overall domain organization as the previously characterized wt oligomer. However, when we compared the UCS domains of wt and *ts* UNC-45, we noted two major differences. First, the *ts* UCS domains adopt different conformations, as most clearly seen for the C-terminal portion of the UCS domain that moves about 10–15 Å (Fig. 5a, b). Notably, a previous structural analysis revealed two different UCS domain conformations of the wt protein, in which the armadillo (ARM) repeats 14–17 compose either a curved (PDB code: 5mzu) or an extended (PDB code: 4i2z) UCS fold (Fig. 5a) and ARM repeat 13 serves as molecular hinge within the domain. Likewise, the relative orientation of the N- and C-terminal UCS subdomains varies markedly between G427E and wt UNC-45 (Fig. 5b). Importantly, this rearrangement remodels the myosin-binding canyon, thus providing different electrostatic and spatial constraints for recognizing and accommodating potential substrate proteins. Moreover, as revealed by the L822F structure, the entire UCS domain is able to move en bloc towards the TPR/central domain backbone of the UNC-45 molecule (Fig. 5c). Such gross domain rearrangement is expected to alter the geometry and thus the functionality of UNC-45 complexes with partner chaperones, in addition to modulating substrate binding and release via the UCS domain.

A second difference of wt UNC-45 and *ts* mutants comprises the dynamics of the UCS domain. For the wt protein, the two crystal forms capturing the alternate UCS conformations were grown from the same crystallization drops, suggesting that the observed states occur in equilibrium in solution<sup>19,24</sup>. In contrast, the two *ts* mutants crystallized exclusively in one state, even when testing a large number of crystals for an alternate crystal form. For G427E, the introduced mutation, which lies in the linker

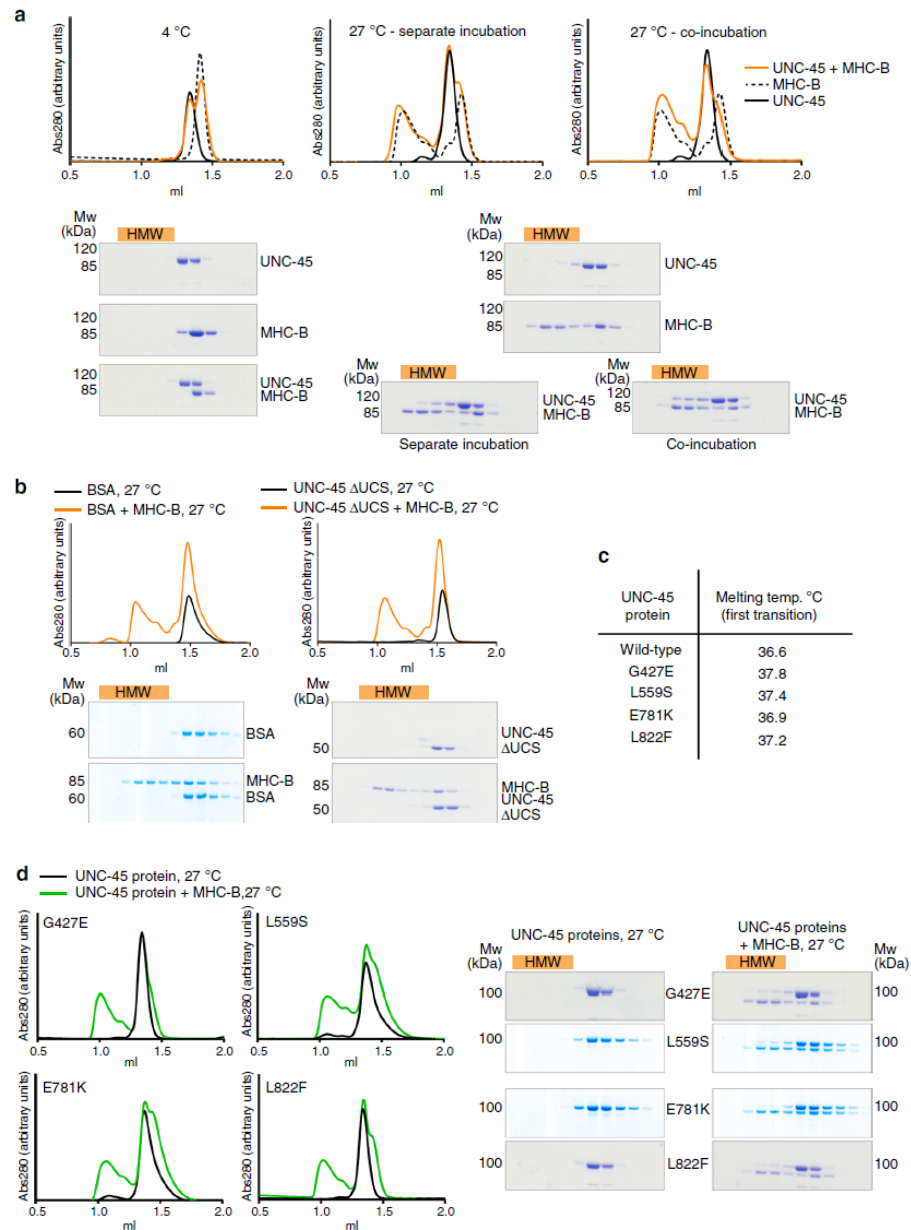


**Fig. 4** Interaction of UNC-45 proteins and myosin *in vitro*. **a** Analytical SEC and SDS-PAGE analysis of UNC-45 and myosin incubated together at 4 °C or at 27 °C and incubated separately at 27 °C and mixed before the SEC run. Misfolded myosin and bound UNC-45 proteins elute earlier from the SEC column, indicated as high molecular weight fractions (HMW, orange bar). **b** Controls for interaction studies shown in **a**. BSA or UNC-45  $\Delta$ UCS were incubated with myosin at 27 °C. **c** Melting temperature as determined by CD spectroscopy for the indicated UNC-45 proteins. **d** Same analysis as in **a** for the indicated UNC-45 ts-mutants and myosin, incubated together at 27 °C.

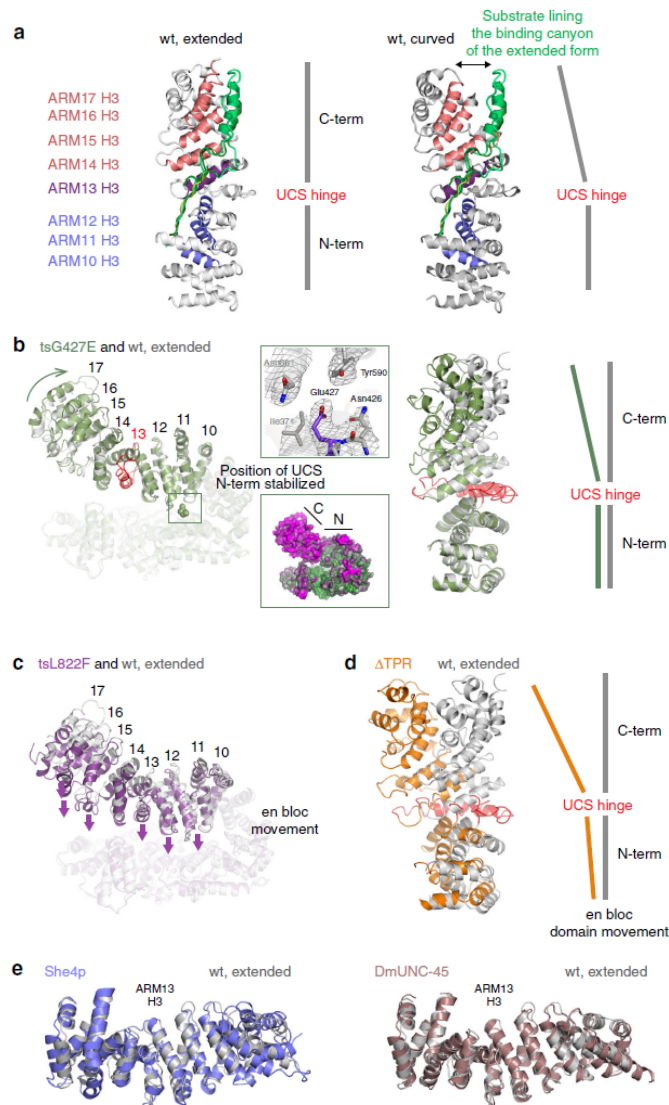


**Fig. 5** Structural analysis of UNC-45 mutant proteins. **a** Structural alignment of two different wild-type UNC-45 structures—PDB code: 4i2z, extended UCS domain conformation, PDB code 5mzu, curved UCS conformation. The three helices of each ARM repeat are organized such that helices H3 (colored) form the bottom of the myosin-binding canyon, whereas helices H1 and H2 compose the border of the molecular cleft. Substrates binding to the myosin binding-canyon are illustrated by overlay of ligands co-crystallized with the ARM domain of beta-catenin. **b** Structural alignment of wild-type UNC-45 (PDB code: 4i2z) and UNC-45 tsG427E—side view (left panel), top view (right panel). The top inset shows the E427 residue overlaid with 2fofc density contoured at 1 $\sigma$ . The bottom inset shows the thermal motion (**b**) factors displayed on the surface of the tsG427E mutant. N- and C-terminal subdomains of the UCS domain are indicated (green - rigid, magenta - flexible). **c** Structural alignment of wild-type UNC-45 (PDB code: 4i2z) and tsL822F. Arrows indicate the en bloc movement of the entire UCS domain towards the TPR/central domain. **d** Structural alignment of wild-type UNC-45 (PDB code: 4i2z) and UNC-45  $\Delta$ TPR molecule B. All structural alignments were performed with residues 1–523 as reference. **e** Structural alignment of wild-type UNC-45 (PDB code: 4i2z) and the UCS proteins She4p (PDB code: 3opb) and DmUNC-45 (PDB code: 3now). The center of the UCS myosin binding canyon (ARM 13 H3) is highlighted

region connecting the central and the UCS domain, induces small, local changes that propagate over the entire UCS domain (Fig. 5b). Movement of ARM repeats 11–15 toward the central domain results in the remodeling of the interface between UCS and central domain (Fig. 5b). This compaction of the UNC-45 molecule leads to additional van-der-Waals contacts between the domains, which in concert rigidify the UCS fold as suggested by its reduced dynamics (Fig. 5b). Likewise, the L822F *ts* mutation causes local changes inducing movement of the UCS domain towards the TPR/central backbone (Fig. 5c). As for the G427E mutant, the established inter-domain contacts reduce the conformational flexibility of the UCS domain, which seems to be a common property of the analyzed *ts* mutants.

Finally, we determined the crystal structure of the UNC-45  $\Delta$ TPR construct that represents a *C. elegans* UNC-45 variant in monomeric, non-filamentous form. The asymmetric unit of the  $\Delta$ TPR crystal form is built up by two molecules. In molecule A, the UCS domain adopts an extended conformation similar to wt UNC-45, whereas molecule B contains a UCS domain that is strongly bent, with the entire domain and even more strongly its C-terminal half (ARM repeats 14–17) extending away from the central domain (Fig. 5d). These data further highlight the pronounced structural flexibility of the myosin-binding UCS domain, which is held in place by non-covalent interactions with the adjacent central and TPR domains. Accordingly, deleting the TPR domain releases the flexible UCS domain to adopt various conformations, two of which were captured in the present crystal form.

To further characterize the identified UCS conformations, we performed a DALI search<sup>33</sup> and looked for related protein structures in the PDB database. This analysis revealed distinct sets of structural homologs (Supplementary Table 3). In notable contrast to UNC-45, the identified  $\beta$ -catenin, importin  $\alpha$ , and karyopherin  $\alpha$  seem to occur only in one major conformation. As the identified ARM proteins use distinct geometries to recognize and bind their cognate substrate proteins, the observed UCS shapes of UNC-45 could, in analogy, differ in their myosin-binding properties. To evaluate the possible predominance of one state, we compared the UCS domain of UNC-45 with that of the structurally and functionally related *Drosophila* Unc45 and yeast She4 proteins<sup>25,37</sup>. Remarkably, the UCS domains of DmUnc45 and She4p fit well to the extended fold of wt UNC-45,  $\Delta$ TPR molecule A, and L822F, as also reflected in the Z-scores of the DALI search (Fig. 5e and Supplementary Table 3). Since *C. elegans* UNC-45, DmUnc45 and She4p were crystallized in different crystal forms, the corresponding UCS conformation should not reflect a crystal packing artifact. We thus presume that the extended UCS conformation represents an important functional state of the myosin-binding site that is preferentially attained by the native chaperone. Taken together, our analysis demonstrates that the UCS domain can adopt distinct conformations leading to the rearrangement of its N- and C-terminal halves and thus of the engaged myosin-binding canyon. Moreover, we show that the myosin-binding deficient mutations, though being located at different portions of the UNC-45 molecule, influence the interaction of the UCS domain with the central and TPR domains, thereby modulating the overall conformation as well as flexibility of the myosin-binding module.

## Discussion

Although the role of UNC-45 in myosin assembly has been extensively studied, insights into the molecular mechanism of the chaperone is limited<sup>29</sup>. To better understand its myosin folding function, we established an orthogonal protein folding assay in insect cells, characterizing the interplay of the *C. elegans* muscle

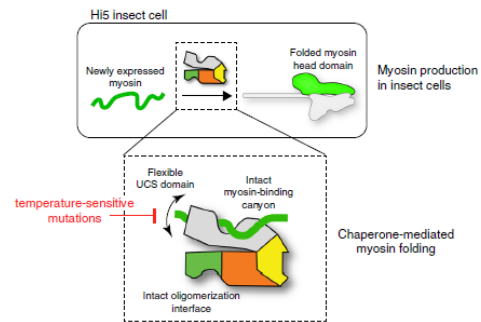


**Fig. 6** UNC-45 chaperone function in folding the myosin head domain. Fully functional myosin can be obtained by co-expression with its cognate chaperone UNC-45 in insect cells. UNC-45's ability to support myosin folding strongly depends on the flexibility of its UCS domain, the functionality of the myosin-binding canyon and its oligomerization properties. UNC-45 *ts*-mutations limit this conformational flexibility and therefore interfere with myosin binding and chaperone activity

myosin MHC-B with its cognate chaperone UNC-45 (Fig. 6). Moreover, the obtained muscle myosin II enabled us to directly monitor complex formation with UNC-45 in vitro using a SEC-based assay and to address the underlying effect of the long-studied UNC-45 *ts*-mutations, extensively characterized in vivo<sup>10</sup>. In fact, it is the limited ability of the *ts*-mutants to bind unfolded myosin (Fig. 4d) that should underlie their *unc* phenotype. Given the success in elucidating the long-sought molecular basis of the UNC-45 *ts*-mutations, we expect that the described in vitro and in vivo chaperone assays will be valuable tools for studying myosin folding in general. For example, the assays could be applied to characterize additional factors involved in myosin maturation, such as Smyd1b<sup>38–40</sup> or the Hsp70/Hsp90 cofactors<sup>14,19,28,41–44</sup>.

The present findings are also of interest for the recombinant production of muscle myosin. As the biochemical and structural characterization of myosin II is critical for understanding muscle function in health and disease, its recombinant production has been in the focus of research for decades. However, any attempts to express the motor domain of striated muscle myosin II in bacterial or insect cells failed<sup>27,45–47</sup>. So far, insect cell expression systems have been used to produce non-muscle myosin<sup>48</sup>, whereas co-expression of UNC-45 has further enabled production of an unconventional myosin<sup>49</sup>. Recombinant striated muscle myosin II could only be produced in C2C12 myoblasts<sup>21,50,51</sup> or specific *Drosophila* lines<sup>52</sup>; however, both systems are not suitable for large-scale protein expression and require specific expertise in working with the expression host. The UNC-45/myosin expression system presented here enables the production of large amounts of the motor domain of striated muscle myosin II, MHC-B, which may overcome this limitation. Importantly, protein expression and purification rely on simple standard procedures that can be carried out in short time and easily scaled up to obtain the required amounts of myosin II for detailed biochemical and structural studies, as exemplified by the presented crystal structure of MHC-B, which is one of the most highly resolved myosin structures in the Protein Data Bank. Given the similarity of human cardiac myosin II and MHC-B, our system offers an efficient way in producing myosin mutants that may reveal molecular details underlying human myopathies<sup>53–55</sup>.

Chaperones ensure the proper folding of newly synthesized proteins and prevent the formation of toxic protein aggregates

during stress situations. Here, we show that the myosin specific chaperone UNC-45 is essential for both processes. Structural data of various functional mutants clarify the role of the distinct UNC-45 domains in this process providing important mechanistic insight into its myosin folding activity.

The N-terminal TPR domain of UNC-45 is a well-characterized protein-protein interaction domain that serves as the major binding site for Hsp70 and Hsp90<sup>14,19,56</sup>. The developed cellular and in vitro chaperone assays revealed that the Hsp70/Hsp90 binding mutant UNC-45 K82E<sup>19</sup> did not have any negative effect on the yield of functional myosin suggesting that a direct interaction between the UNC-45 TPR domain and its partner chaperones is not required for the folding of the myosin II motor domain. Contrary, a UNC-45 mutant lacking the entire TPR domain did not support myosin folding in insect cells. These data indicate that the TPR domain of UNC-45 is not only critical to coordinate the interplay with partner chaperones, but has additional functions: (1) In the UNC-45 oligomer, the TPR domain is essential to connect neighboring molecules<sup>19</sup>. As shown in this study, the L121W mutation, which prevents oligomer formation, negatively affects the amount of produced myosin. (2) Our structural data suggest that the TPR domain obtains an additional intra-molecular scaffolding role. It undergoes van-der-Waals contacts with the UCS domain, thereby arranging the myosin binding site to accommodate substrate. Accordingly, formation of UNC-45 oligomers via the TPR domain may be critical to set up a functional UCS myosin-binding site, thus linking UNC-45 oligomerization to its myosin folding activity.

The most common characteristic for molecular chaperones is a structurally flexible binding site for client proteins<sup>57,58,59</sup>. The present data suggest this concept holds also true for the myosin-binding domain of UNC-45. The UCS domain adopts an extended ARM repeat scaffold that is penetrated by a long canyon serving as protein binding site. Our structural data reveal the capability of the UCS domain to adopt distinct defined conformations. Together, the wt, G427E, L822F, and ΔTPR crystal structures depict four different UCS conformations highlighting the pronounced dynamicity of the myosin-binding domain (Fig. 5). Even though the functionality of the characterized conformations remains to be elucidated, the switch between them should be carefully controlled as several states appear to be non-functional preventing the binding of the myosin substrate. In conclusion, the biochemical and structural data suggest that the conformational flexibility of the UCS domain is an important determinant of substrate selectivity. It appears that the plastic UCS domain offers a further layer of regulation. Induced-fit substrate binding, allosteric effects of the TPR domain, higher-order oligomer formation as well as post-translational modifications could thus have a strong impact on the function of the UNC-45 chaperone in bringing muscle proteins in shape.

## Methods

**Insect cell protein expression and purification.** MHC-B (1–796) and NMY-2 (1–796) were cloned from *C. elegans* cDNA into the pH promoter site of the pFastBac DUAL vector (Invitrogen) with a C-terminal His<sub>6</sub>-tag. FLAG-Hsp70 (*C. elegans* HSP-1), FLAG-Hsp90 (*C. elegans* DAF-21) or UNC-45-Strep were added into the p10 promoter site of the pFastBac DUAL vector. Previously described constructs served as DNA templates<sup>19</sup>. All primers used are listed in Supplementary Table 4. Baculovirus was produced by transfection of SF9 cells (Expression Systems) with PuGENE HD (Promega). For expression, High Five cells (Expression Systems) at a density of  $1 \times 10^6$  cells ml<sup>-1</sup> were infected with baculovirus (P1 amplification) and incubated for 72 h at 21 °C. The cells were collected by centrifugation, lysed by freeze-thaw, and resuspended in 50 mM Tris, pH 7.5, 300 mM NaCl (buffer A), containing 20 mM imidazole. The cleared cell lysate was loaded onto a NiNTA column (GE Healthcare) equilibrated with buffer A. After washing the column, myosin and associated UNC-45 were eluted with buffer A, containing 150 mM imidazole. The elution was applied to a Superdex 200 column equilibrated

with 20 mM Tris pH 8.0, 150 mM NaCl. For crystallization purposes, this buffer was optimized to 20 mM Tris pH 8.5, 20 mM NaCl.

For small scale myosin purifications (shown in Fig. 2), a pellet from 50 ml co-expression culture was lysed in 4 ml of 50 mM Tris pH 7.5, 150 mM NaCl, 20 mM imidazole containing benzonase. The cleared cell lysate was applied to 100 μl OPUS RoboColumns (Repligen) packed with Ni Sepharose 6 Fast Flow (GE Healthcare) using a Janus Liquid handling system (Perkin Elmer). The resin was washed with 2 ml of 50 mM Tris pH 7.5, 150 mM NaCl, 20 mM imidazole and 2 ml of 50 mM Tris pH 7.5, 150 mM NaCl, 40 mM imidazole and finally eluted in 400 μl of 50 mM Tris pH 7.5, 150 mM NaCl, 150 mM imidazole. Fifty microliter of the elution fraction was following loaded onto a Superdex 200 5/150 GL column pre-equilibrated with 50 mM Tris pH 7.5, 150 mM NaCl.

**Bacterial protein expression and purification.** UNC-45 point mutants (G427E, L559S, E781K, L822F, N801A) were generated by site-directed mutagenesis of the wild-type protein in pET21a. All primers used are listed in Supplementary Table 4. UNC-45 G427E SeMet protein was produced in B834-DE3 cells (Novagen) as previously described<sup>19</sup>. All native UNC-45 proteins were expressed and purified as previously described<sup>19,24</sup>. Briefly, expression was performed in BL21(RL) cells (Stratagene) induced with IPTG. The three-step purification procedure included NiNTA and anion exchange chromatography and a final SEC step in 20 mM Tris pH 8.0, 150 mM NaCl.

**Actin preparation.** Rabbit actin was purified by the method of Lehrer and Kewar<sup>60</sup> with minor modifications. Briefly, no ATP was added at the final step to polymerize actin and residual amounts of nucleotide were removed by sequential centrifugation of actin and dialysis steps. Actin was labeled with pyrene (pyr-actin) as previously described<sup>61</sup>.

**CD spectroscopy.** CD experiments were essentially performed as previously described<sup>24</sup>. Briefly, spectra (190–260 nm) of UNC-45 proteins at 0.7 mg ml<sup>-1</sup> were recorded on a Chirascan plus CD spectrometer (Applied Photophysics). Data were analyzed with the Global3 evaluation software.

**Western blot analysis of insect cell lysates.** For comparing the effect of different UNC-45 mutants on the solubility of MHC-B, UNC-45 proteins were cloned from previously described constructs<sup>19,24</sup> and bacterial expression constructs described above into a pIDC derivative encoding an N-terminal Twin-Strep-tag (former One-Strep-tag) followed by a 3C protease cleavage site. The MHC-B motor domain (1–790) was cloned into pACEBac1 with a C-terminal fusion to a His<sub>6</sub>-tag. FLAG-CeHsp90 and FLAG-CeHsp70 were cloned into pACEBac1 derivatives. All primers used are listed in Supplementary Table 4. The MultiBac was generated by Golden Gate assembly or Cre recombination (Geneva Biotech) and bacmid was generated by transposition of *E. coli* DH10EMBY (Geneva Biotech). Baculovirus production and protein expression was performed as described above. For expressions at 18 °C, cells were harvested after 96 h. High Five cells were harvested, lysed by freeze-thaw and resuspended in 50 mM sodium phosphate buffer pH 8, 300 mM NaCl. Whole cell lysates and cleared cell lysates (supernatant after centrifugation at 21130 g for 30 min at 4 °C) were analyzed by Western blot using anti-FLAG (Sigma F1804, used 1:1,000), anti-Penta-His (Qiagen, used 1:1,000) and anti-CeUNC-45 antibodies (used 1:10,000)<sup>24</sup>. For Supplementary Fig. 2a, samples were normalized to soluble UNC-45 levels.

**Pull-down of *C. elegans* UNC-45 from insect cells.** High Five cells (Expression Systems) at a density of  $1 \times 10^6$  cells ml<sup>-1</sup> were infected with baculovirus (P1 amplification) and incubated for 72 h at 21 °C. A pellet from 7.5 ml expression culture was lysed in 2 ml of 50 mM Tris pH 7.5, 20 mM NaCl containing benzonase. Cleared cell lysate was applied to 100 μl OPUS RoboColumns (Repligen) packed with Strep-Tactin Superflow (IBA Lifesciences) using a Janus Liquid handling system (Perkin Elmer). The resin was washed with 3 ml of 50 mM Tris pH 7.5, 20 mM NaCl and UNC-45 was eluted with 100 μl of 50 mM Tris pH 7.5, 20 mM NaCl, 5 mM d-Desthiobiotin. Elutions were analyzed by western blot using anti-Hsp70 (Santa Cruz Biotechnology, SC59572, used 1:1000), anti-Hsp90 (Abcam [EPR16621-67] (ab203126), used 1:250) and anti-Strep (Qiagen 34850, used 1:2500) antibodies.

**Analytical size exclusion.** UNC-45 proteins or BSA and myosin were incubated at a final concentration of 5 μM at 4 °C or 27 °C for 60 min. For the SEC analysis in Supplementary Fig. 6, myosin was incubated at 27 °C for 60 min followed by incubation with UNC-45 (wild-type or *ts*-mutant protein) on ice for 60 min. After incubation samples were applied to a S200 PC 3.2 column in 20 mM Tris pH 8.0, 150 mM NaCl. Indicated fractions were analyzed by SDS-PAGE.

**F-actin co-sedimentation assay.** F-actin was mixed with myosin (plus and minus 30 mM ATP) to a final concentration of 10 and 2.5 μM, respectively. The samples were centrifuged at 150,000 g, for 60 min at 4 °C. Supernatant and pellet fractions were analyzed by SDS-PAGE.

**Stopped-flow measurements.** Stopped-flow experiments to measure MHC-B single turnover were performed with a TgK stopped-flow apparatus (excitation wavelength 280 nm, emission filtered at 320 nm). The experimental data were fitted to a single exponential using Kinetic Studio, and the observed rate analyzed with Prism (GraphPad).

**Transient kinetics.** Fast kinetic data was performed as previously described<sup>62,63</sup>. All measurements were performed at 20 °C in 20 mM MOPS, 25 mM KCl, 5 mM MgCl<sub>2</sub>, 1 mM NaN<sub>3</sub> at pH 7.0, unless indicated otherwise. Rapid-mixing experiments were completed in triplicate using a High-Tec Scientific SF-61 DX2 stopped-flow system. Transient kinetic traces were initially fitted with Kinetic Studio (TgK Scientific) and subsequently plotted with Origin (OriginPro). For the single turnover experiment, 10 μM MHC-B and 5 μM ATP stock solutions (concentration before mixing) were prepared in 20 mM MOPS pH 7, 25 mM KCl, 5 mM MgCl<sub>2</sub>, 1 mM NaN<sub>3</sub>. For the actin affinity experiment, the amplitude dependence of the MHC-B concentration was fitted to the standard quadratic equation for a binding isotherm<sup>64</sup>.

$$\alpha = \frac{[M] + K_D + [A]_0 - \sqrt{([M] + K_D + [A]_0)^2 - 4[M][A]_0}}{2[A]_0} \quad (1)$$

Where  $\alpha$  = fraction of actin bound to MHC-B,  $[M]$  = concentration of MHC-B,  $K_D$  = the dissociation constant of MHC-B for actin and  $[A]_0$  = concentration of actin. For experiments probing the actin-myosin interaction with ATP and ADP the fluorescence signal for pyrene-labelled actin was recorded, which has an excitation wavelength at 365-nm and the emission was detected after passing through KV389-nm cut-off filter. In the absence of actin, intrinsic tryptophan fluorescence was monitored by excitation at 295-nm and emission detected with a WG-320 cut-off filter.

**ATPase assay and actin-stimulated ATPase activity.** ATPase activity was determined by a coupled enzymatic reaction<sup>65</sup>. In all, 2 μM MHC-B was incubated with 37.5 U ml<sup>-1</sup> pyruvate kinase, 42.9 U ml<sup>-1</sup> lactate dehydrogenase, 0.25 mM NADH, 15 mM phosphoenolpyruvate, and 2 mM ATP in a buffer containing 20 mM MOPS pH 7.0, 100 mM KCl, 5 mM MgCl<sub>2</sub>. The absorption at 340 nm was recorded for 30 min using a Pherastar FS plate reader. The experiment was performed in the presence of increasing concentrations of actin (ranging from 0 to 90 μM) and corrected by subtracting the ATPase activity of actin. The Michaelis-Menten equation was fit to the data to determine the maximal activity ( $V_{max}$ ) and the association constant of actin for myosin ( $K_m$ ) using Prism (GraphPad). For the activity measurement of MHC-B produced with different UNC-45 mutants, the experiment was performed with 90 μM actin concentration.

**Crystallization and data collection.** Crystals of MHC-B were grown in 96-well plates set up with a Mosquito robot (TTP Labtech) in 0.1 M MES/imidazole pH 6.5, 10% w/v PEG 4000, 20% v/v glycerol, 0.02 M Morphous alcohol mix (0.2 M 1,6-hexanediol, 0.2 M 1-butanol, 0.2 M (RS)-1,2-propanediol, 0.2 M 2-propanol, 0.2 M 1,4-butanediol, 0.2 M 1,3-propanediol). Crystals of the UNC-45 G427E mutant were obtained by manually mixing 2 μl protein (200 μM) with 0.3 μl additive (1.0 M (NH<sub>4</sub>)<sub>2</sub>SO<sub>4</sub>) and 1 μl reservoir solution (0.1 M HEPES pH 8.0, 5% Tacsimate, 15% PEG MME 5000). Crystals of UNC-45 L822F and UNC-45 ΔTPR were grown in 96-well plates set up with a Mosquito robot (TTP Labtech) in 0.1 M MES/NaOH pH 6.5, 0.2 M ammonium acetate, 30% glycerol ethoxylate and 0.1 M Tris pH 8.5, 32% glycerol ethoxylate, respectively. All crystals were grown by sitting drop vapor diffusion: MHC-B crystals at 4 °C, UNC-45 crystals at 19 °C. MHC-B, UNC-45 L822F and ΔTPR were directly frozen in liquid nitrogen, whereas UNC-45 G427E crystals were shortly incubated in reservoir solution containing 25% ethylene glycol, mounted into 90°-bent loops and frozen in liquid nitrogen as previously described<sup>19</sup>. Diffraction data were collected at the European Synchrotron Radiation Facility (ESRF) (wavelength: 0.979 Å): UNC-45 G427E anomalous diffraction dataset at beamline ID 29, UNC-45 L822F dataset at beamline ID 14-4; UNC-45 ΔTPR dataset at ID 23-1. Diffraction data for MHC-B were collected at Deutsches Elektronen-Synchrotron (DESY) (wavelength: 0.979 Å), beamline P13. Data were integrated with XDS and scaled with SCALA or XSCALE<sup>66,67</sup>.

**Structure solution and refinement.** The crystal structure of MHC-B was solved by molecular replacement with Phaser using chicken smooth muscle myosin motor domain as search model (PDB code: 5m05)<sup>68</sup>. The structure was built with Coot and O, and the final refinement performed using PHENIX<sup>69-71</sup>. The crystal structure of UNC-45 G427E was solved by using experimental SAD phases. Refinement proceeded smoothly in cycles of model rebuilding with O and crystallographic refinement with CNS<sup>71,72</sup>. The final model was refined with PHENIX<sup>69</sup>. The UNC-45 L822F and ΔTPR structures were solved by molecular replacement (MR) with PHASER<sup>68</sup>. The wild-type UNC-45 (PDB code: 4i2z) structure was split into three parts comprising residues 5–507, 525–760, and 761–930 to create an optimal search model for the MR of the UNC-45 L822F structure. For solution of the UNC-45 ΔTPR structure, the previous UNC-45 structure (PDB code: 4i2z) was divided into two fragments 135–507 and 525–930. Molecule A was clearly defined, while residues 719–828 and 829–930 had to be

placed as separate units into the density obtained for molecule B. Initial structural refinement of the UNC-45 L822F and ΔTPR structures was performed with CNS<sup>72</sup>. Following rebuilding of the structure using COOT and O, the final refinement was performed using PHENIX<sup>69-71</sup>. Structure figures were generated with PYMOL<sup>73</sup>. Data collection and refinement statistics are shown in Supplementary Table 2. Ramachandran statistics for the determined structures are as follows: UNC-45 L822F - favored 96.9%, allowed 3.1%, outliers 0.0%; UNC-45 G427E - favored 94.4%, allowed 5.3%, outliers 0.3%; UNC-45 ΔTPR - favored 97.3%, allowed 2.7%, outliers 0.0%; MHC-B - favored 97.7%, allowed 2.2%, outliers 0.1%.

**Reporting summary.** A reporting summary for this Article is available as a Supplementary Information file. Further information on research design is available in the Nature Research Reporting Summary linked to this article.

#### Data availability

Data supporting the findings of this paper manuscript are available from the corresponding authors upon reasonable request. The source data underlying Figs. 1b, c, e, 2b–d, 3a–d, and 4a, b, d and Supplementary Figs. 1–3 and 6b, c are provided as a Source Data file. Coordinates and structure factors were deposited in the Protein Data Bank under accession codes 6QDL (UNC-45 L822F), 6QDK (UNC-45 G427E), 6QDM (UNC-45 ΔTPR), and 6QDJ (MHC-B).

Received: 15 January 2019; Accepted: 21 September 2019;

Published online: 21 October 2019

#### References

- Krendel, M. & Mooseker, M. S. Myosins: tails (and heads) of functional diversity. *Physiol. (Bethesda)* **20**, 239–251 (2005).
- Odriontz, F. & Kollmar, M. Drawing the tree of eukaryotic life based on the analysis of 2,269 manually annotated myosins from 328 species. *Genome Biol.* **8**, R196 (2007).
- Meissner, B. et al. Determining the sub-cellular localization of proteins within *Caenorhabditis elegans* body wall muscle. *PLoS One* **6**, e19937 (2011).
- Meissner, B. et al. An integrated strategy to study muscle development and myofibrillar structure in *Caenorhabditis elegans*. *PLoS Genet* **5**, e1000537 (2009).
- Schnorner, F. et al. Systematic genetic analysis of muscle morphogenesis and function in *Drosophila*. *Nature* **464**, 287–291 (2010).
- Bai, J. et al. RNA interference screening in *Drosophila* primary cells for genes involved in muscle assembly and maintenance. *Development* **135**, 1439–1449 (2008).
- Frumkin, A. et al. Challenging muscle homeostasis uncovers novel chaperone interactions in *Caenorhabditis elegans*. *Front. Mol. Biosci.* **1**, 21 (2014).
- Smith, D. A., Carland, C. R., Guo, Y. & Bernstein, S. I. Getting folded: chaperone proteins in muscle development, maintenance and disease. *Anat. Rec.* **297**, 1637–1649 (2014).
- Goebel, H. H. & Laing, N. G. Actinopathies and myosinopathies. *Brain Pathol.* **19**, 516–522 (2009).
- Barral, J. M., Bauer, C. C., Ortiz, I. & Epstein, H. F. Unc-45 mutations in *Caenorhabditis elegans* implicate a CRO1/Shep-like domain in myosin assembly. *J. Cell Biol.* **143**, 1215–1225 (1998).
- Epstein, H. F. & Thomson, J. N. Temperature-sensitive mutation affecting myofibrillar assembly in *Caenorhabditis elegans*. *Nature* **250**, 579–580 (1974).
- Venolia, L., Ao, W., Kim, S., Kim, C. & Pilgrim, D. unc-45 gene of *Caenorhabditis elegans* encodes a muscle-specific tetratricopeptide repeat-containing protein. *Cell Motil. Cytoskeleton* **42**, 163–177 (1999).
- Venolia, L. & Waterston, R. H. The unc-45 gene of *Caenorhabditis elegans* is an essential muscle-affecting gene with maternal expression. *Genetics* **126**, 345–353 (1990).
- Barral, J. M., Hutagalung, A. H., Brinker, A., Hartl, F. U. & Epstein, H. F. Role of the myosin assembly protein UNC-45 as a molecular chaperone for myosin. *Science* **295**, 669–671 (2002).
- Geach, T. J. & Zimmerman, L. B. Paralysis and delayed Z-disc formation in the *Xenopus tropicalis* unc45b mutant dicky ticker. *BMC Dev. Biol.* **10**, 75 (2010).
- Wohlgemuth, S. L., Crawford, B. D. & Pilgrim, D. B. The myosin co-chaperone UNC-45 is required for skeletal and cardiac muscle function in zebrafish. *Dev. Biol.* **303**, 483–492 (2007).
- Lee, C. F. et al. *Drosophila* UNC-45 accumulates in embryonic blastoderm and in muscles, and is essential for muscle myosin stability. *J. Cell Sci.* **124**, 699–705 (2011).
- Melkani, G. C., Bodmer, R., Ocorr, K. & Bernstein, S. I. The UNC-45 chaperone is critical for establishing myosin-based myofibrillar organization

- and cardiac contractility in the *Drosophila* heart model. *PLoS One* **6**, e22579 (2011).
19. Gazda, L. et al. The myosin chaperone UNC-45 is organized in tandem modules to support myofibril formation in *C. elegans*. *Cell* **152**, 183–195 (2013).
  20. Price, M. G., Landsverk, M. L., Barral, J. M. & Epstein, H. F. Two mammalian UNC-45 isoforms are related to distinct cytoskeletal and muscle-specific functions. *J. Cell Sci.* **115**, 4013–4023 (2002).
  21. Chow, D., Srikakulam, R., Chen, Y. & Winkelmann, D. A. Folding of the striated muscle myosin motor domain. *J. Biol. Chem.* **277**, 36799–36807 (2002).
  22. Srikakulam, R. & Winkelmann, D. A. Chaperone-mediated folding and assembly of myosin in striated muscle. *J. Cell Sci.* **117**, 641–652 (2004).
  23. Etard, C., Roostalu, U. & Strahle, U. Shuttling of the chaperones Unc45b and Hsp90a between the A band and the Z line of the myofibril. *J. Cell Biol.* **180**, 1163–1175 (2008).
  24. Hellerschmied, D. et al. UFD-2 is an adaptor-assisted E3 ligase targeting unfolded proteins. *Nat. Commun.* **9**, 484 (2018).
  25. Lee, C. F. et al. X-ray crystal structure of the UCS domain-containing UNC-45 myosin chaperone from *Drosophila melanogaster*. *Structure* **19**, 397–408 (2011).
  26. Hellerschmied, D. & Clausen, T. Myosin chaperones. *Curr. Opin. Struct. Biol.* **25**, 9–15 (2014).
  27. Hutagalung, A. H., Landsverk, M. L., Price, M. G. & Epstein, H. F. The UCS family of myosin chaperones. *J. Cell Sci.* **115**, 3983–3990 (2002).
  28. Gaiser, A. M., Kaiser, C. J., Haslbeck, V. & Richter, K. Downregulation of the hsp90 system causes defects in muscle cells of *Caenorhabditis elegans*. *PLoS One* **6**, e25485 (2011).
  29. Lee, C. F., Melkani, G. C. & Bernstein, S. I. The UNC-45 myosin chaperone from worms to flies to vertebrates. *Int. Rev. Cell Mol. Biol.* **313**, 103–144 (2014).
  30. Malnasi-Csizmadia, A. et al. Kinetic resolution of a conformational transition and the ATP hydrolysis step using relaxation methods with a Dictyostelium myosin II mutant containing a single tryptophan residue. *Biochemistry* **40**, 12727–12737 (2001).
  31. Bagshaw, C. R. & Trentham, D. R. The reversibility of adenosine triphosphate cleavage by myosin. *Biochemical J.* **133**, 323–328 (1973).
  32. Nag, S. et al. Contractility parameters of human beta-cardiac myosin with the hypertrophic cardiomyopathy mutation R403Q show loss of motor function. *Sci. Adv.* **1**, e1500511 (2015).
  33. Holm, L. & Laakso, L. M. Dali server update. *Nucleic Acids Res* **44**, W351–W355 (2016).
  34. Melkani, G. C., Lee, C. F., Cammarato, A. & Bernstein, S. I. *Drosophila* UNC-45 prevents heat-induced aggregation of skeletal muscle myosin and facilitates refolding of citrate synthase. *Biochem Biophys. Res Commun.* **396**, 317–322 (2010).
  35. Kaiser, C. M. et al. Tracking UNC-45 chaperone-myosin interaction with a titin mechanical reporter. *Biophys. J.* **102**, 2212–2219 (2012).
  36. Begasse, M. L., Leaver, M., Vazquez, F., Grill, S. W. & Hymann, A. A. Temperature dependence of cell division timing accounts for a shift in the thermal limits of *C. elegans* and *C. briggsae*. *Cell Rep.* **10**, 647–653 (2015).
  37. Shi, H. & Blobel, G. UNC-45/CRO1/She4p (UCS) protein forms elongated dimer and joins two myosin heads near their actin binding region. *Proc. Natl Acad. Sci. USA* **107**, 21382–21387 (2010).
  38. Just, S. et al. The myosin-interacting protein SMYD1 is essential for sarcomere organization. *J. Cell Sci.* **124**, 3127–3136 (2011).
  39. Li, H. et al. SmYd1b is required for skeletal and cardiac muscle function in zebrafish. *Mol. Biol. Cell* **24**, 3511–3521 (2013).
  40. Tan, X., Rotllant, J., Li, H., De Deyne, P. & Du, S. J. SmYD1, a histone methyltransferase, is required for myofibril organization and muscle contraction in zebrafish embryos. *Proc. Natl Acad. Sci. USA* **103**, 2713–2718 (2006).
  41. Du, S. J., Li, H., Bian, Y. & Zhong, Y. Heat-shock protein 90alpha is required for organized myofibril assembly in skeletal muscles of zebrafish embryos. *Proc. Natl Acad. Sci. USA* **105**, 554–559 (2008).
  42. Liu, L., Srikakulam, R. & Winkelmann, D. A. Unc45 activates Hsp90-dependent folding of the myosin motor domain. *J. Biol. Chem.* **283**, 13185–13193 (2008).
  43. Srikakulam, R., Liu, L. & Winkelmann, D. A. Unc45b forms a cytosolic complex with Hsp90 and targets the unfolded myosin motor domain. *PLoS One* **3**, e2137 (2008).
  44. Srikakulam, R. & Winkelmann, D. A. Myosin II folding is mediated by a molecular chaperonin. *J. Biol. Chem.* **274**, 27265–27273 (1999).
  45. Mitchell, E. J., Jakes, R. & Kendrick-Jones, J. Localisation of light chain and actin binding sites on myosin. *Eur. J. Biochem.* **161**, 25–35 (1986).
  46. Mitchell, E. J. et al. Regulatory and essential light-chain-binding sites in myosin heavy chain subfragment-1 mapped by site-directed mutagenesis. *J. Mol. Biol.* **208**, 199–205 (1989).
  47. McNally, E. M., Goodwin, E. B., Spudich, J. A. & Leinwand, L. A. Coexpression and assembly of myosin heavy chain and myosin light chain in *Escherichia coli*. *Proc. Natl Acad. Sci. USA* **85**, 7270–7273 (1988).
  48. Billington, N., Wang, A., Mao, J., Adelstein, R. S. & Sellers, J. R. Characterization of three full-length human nonmuscle myosin II paralogs. *J. Biol. Chem.* **288**, 33398–33410 (2013).
  49. Bird, J. E. et al. Chaperone-enhanced purification of unconventional myosin 15, a molecular motor specialized for stereocilia protein trafficking. *Proc. Natl Acad. Sci. USA* **111**, 12390–12395 (2014).
  50. Wang, Q., Moncman, C. L. & Winkelmann, D. A. Mutations in the motor domain modulate myosin activity and myofibril organization. *J. Cell Sci.* **116**, 4227–4238 (2003).
  51. Resnicow, D. L., Deacon, J. C., Warrick, H. M., Spudich, J. A. & Leinwand, L. A. Functional diversity among a family of human skeletal muscle myosin motors. *Proc. Natl Acad. Sci. USA* **107**, 1053–1058 (2010).
  52. Caldwell, J. T., Melkani, G. C., Huxford, T. & Bernstein, S. I. Transgenic expression and purification of myosin isoforms using the *Drosophila* melanogaster indirect flight muscle system. *Methods* **56**, 25–32 (2012).
  53. Seidman, J. G. & Seidman, C. The genetic basis for cardiomyopathy: from mutation identification to mechanistic paradigms. *Cell* **104**, 557–567 (2001).
  54. Kurapati, R. et al. Myofibrillar myopathy caused by a mutation in the motor domain of mouse MyHC IIb. *Hum. Mol. Genet.* **21**, 1706–1724 (2012).
  55. Martinsson, T. et al. Autosomal dominant myopathy: missense mutation (Glu-706→Lys) in the myosin heavy chain IIa gene. *Proc. Natl Acad. Sci. USA* **97**, 14614–14619 (2000).
  56. Scheufler, C. et al. Structure of TPR domain-peptide complexes: critical elements in the assembly of the Hsp70-Hsp90 multichaperone machine. *Cell* **101**, 199–210 (2000).
  57. Hartl, F. U. & Hayer-Hartl, M. Converging concepts of protein folding in vitro and in vivo. *Nat. Struct. Mol. Biol.* **16**, 574–581 (2009).
  58. Kityk, R., Kopp, J., Sinning, I. & Mayer, M. P. Structure and dynamics of the ATP-bound open conformation of Hsp70 chaperones. *Mol. Cell* **48**, 863–874 (2012).
  59. Schlecht, R., Erbse, A. H., Bukau, B. & Mayer, M. P. Mechanics of Hsp70 chaperones enables differential interaction with client proteins. *Nat. Struct. Mol. Biol.* **18**, 345–351 (2011).
  60. Lehrer, S. S. & Kerwar, G. Intrinsic fluorescence of actin. *Biochemistry* **11**, 1211–1217 (1972).
  61. Criddle, A. H., Geeves, M. A. & Jeffries, T. The use of actin labelled with N-(1-pyrenyl)iodoacetamide to study the interaction of actin with myosin subfragments and troponin/tropomyosin. *Biochemical J.* **232**, 343–349 (1985).
  62. Deacon, J. C., Bloemink, M. J., Rezavandi, H., Geeves, M. A. & Leinwand, L. A. Erratum to: identification of functional differences between recombinant human alpha and beta cardiac myosin motors. *Cell Mol. Life Sci.* **69**, 4239–4255 (2012).
  63. Walklate, J., Vera, C., Bloemink, M. J., Geeves, M. A. & Leinwand, L. The most prevalent freeman-sheldon syndrome mutations in the embryonic myosin motor share functional defects. *J. Biol. Chem.* **291**, 10318–10331 (2016).
  64. Kurzawa, S. E. & Geeves, M. A. A novel stopped-flow method for measuring the affinity of actin for myosin head fragments using microgram quantities of protein. *J. Muscle Res Cell Motil.* **17**, 669–676 (1996).
  65. Norby, J. G. Coupled assay of Na<sup>+</sup>,K<sup>+</sup>-ATPase activity. *Methods Enzymol.* **156**, 116–119 (1988).
  66. Kabsch, W. Xds. *Acta Crystallogr D. Biol. Crystallogr* **66**, 125–132 (2010).
  67. Evans, P. Scaling and assessment of data quality. *Acta Crystallogr D. Biol. Crystallogr* **62**, 72–82 (2006).
  68. McCoy, A. J. et al. Phaser crystallographic software. *J. Appl. Crystallogr* **40**, 658–674 (2007).
  69. Adams, P. D. et al. PHENIX: building new software for automated crystallographic structure determination. *Acta Crystallogr D. Biol. Crystallogr* **58**, 1948–1954 (2002).
  70. Emsley, P. & Cowtan, K. Coot: model-building tools for molecular graphics. *Acta Crystallogr D. Biol. Crystallogr* **60**, 2126–2132 (2004).
  71. Jones, T. A., Zou, J. Y., Cowan, S. W. & Kjeldgaard, M. Improved methods for building protein models in electron density maps and the location of errors in these models. *Acta Crystallogr A* **47**(Pt 2), 110–119 (1991).
  72. Brunger, A. T. et al. Crystallography & NMR system: a new software suite for macromolecular structure determination. *Acta Crystallogr D. Biol. Crystallogr* **54**, 905–921 (1998).
  73. DeLano, W. L. *The PyMol molecular graphics system*. (DeLano Scientific, San Carlos, 2002).

#### Acknowledgements

We thank the VBCF Protech Facility for the support with biophysical measurements. R.A. was supported by the Austrian Science Fund (FWF) DK W1258-B22. C.J. and M.A.G. were supported by NIH grant GM029090. The IMP is funded by Boehringer Ingelheim.



**Author contributions**

D.H., A.L. and N.F. performed the UNC-45 biochemistry. A.L, N.F. and R.K. performed the insect cell studies. N.F., R.A., C.J. and M.A.G. performed the myosin biochemistry and kinetic analysis. D.H., R.A., A.M., L.D., L.G. and T.C. performed the structural analysis. D.H. and T.C. outlined the study and prepared the paper with input from all authors.

**Competing interests**

The authors declare no competing interests.

**Additional information**

**Supplementary Information** accompanies this paper at <https://doi.org/10.1038/s41467-019-12667-8>.

**Correspondence** and requests for materials should be addressed to D.H. or T.C.

**Peer review information** *Nature Communications* thanks Donald Winkelmann and the other, anonymous, reviewer(s) for their contribution to the peer review of this work. Peer reviewer reports are available.

**Reprints and permission information** is available at <http://www.nature.com/reprints>

**Publisher's note** Springer Nature remains neutral with regard to jurisdictional claims in published maps and institutional affiliations.



**Open Access** This article is licensed under a Creative Commons Attribution 4.0 International License, which permits use, sharing, adaptation, distribution and reproduction in any medium or format, as long as you give appropriate credit to the original author(s) and the source, provide a link to the Creative Commons license, and indicate if changes were made. The images or other third party material in this article are included in the article's Creative Commons license, unless indicated otherwise in a credit line to the material. If material is not included in the article's Creative Commons license and your intended use is not permitted by statutory regulation or exceeds the permitted use, you will need to obtain permission directly from the copyright holder. To view a copy of this license, visit <http://creativecommons.org/licenses/by/4.0/>.

© The Author(s) 2019

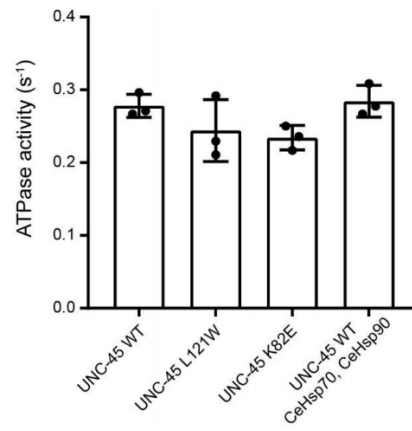
*Hellerschmied (2019) Recapitulating the myosin/UNC-45 interplay*

**Supplementary Information**

**Molecular features of the UNC-45 chaperone critical for  
binding and folding muscle myosin**

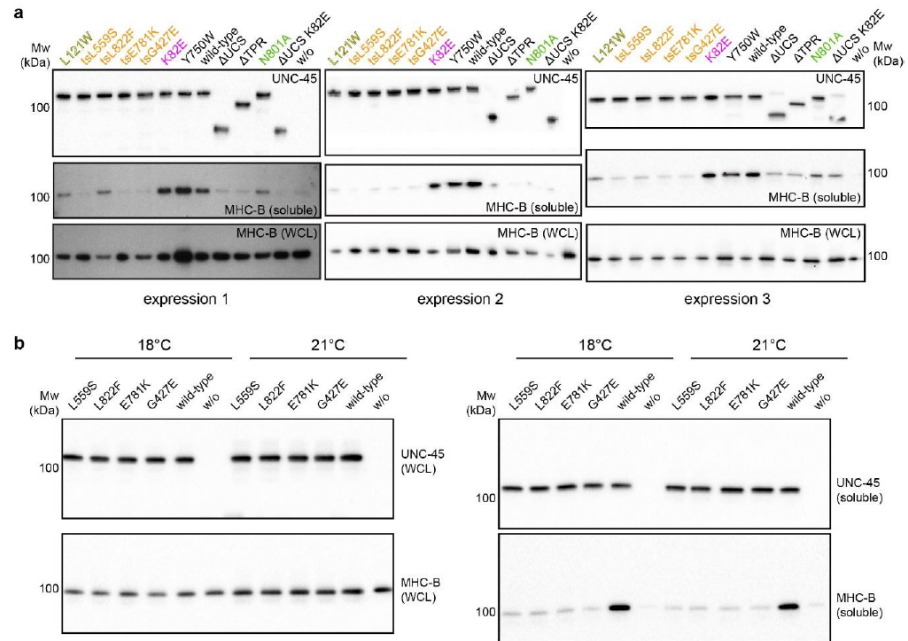
**CONTENT**

Supplementary Figures 1-6, Supplementary Tables 1-4

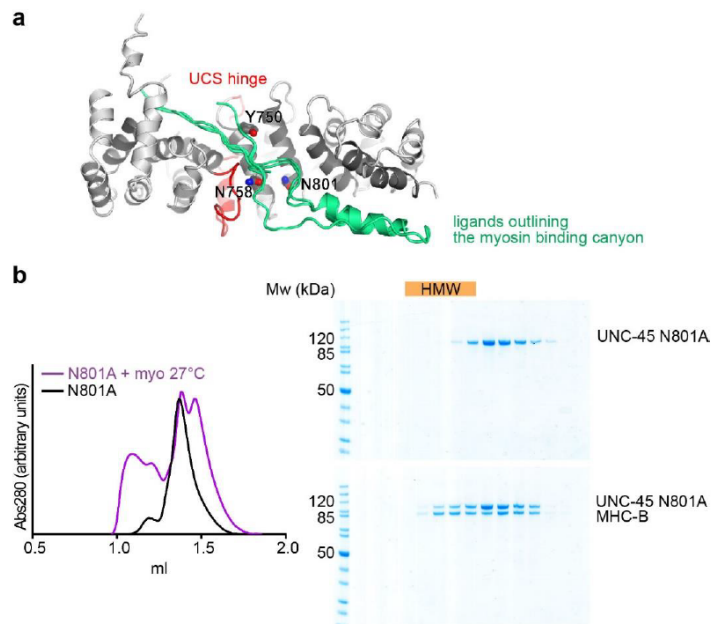


**Supplementary Figure 1. Actin-activated ATPase activity determined for the monomeric MHC-B peak after SEC from the indicated co-expression studies (n = 3, data represent mean  $\pm$  s.d.)**

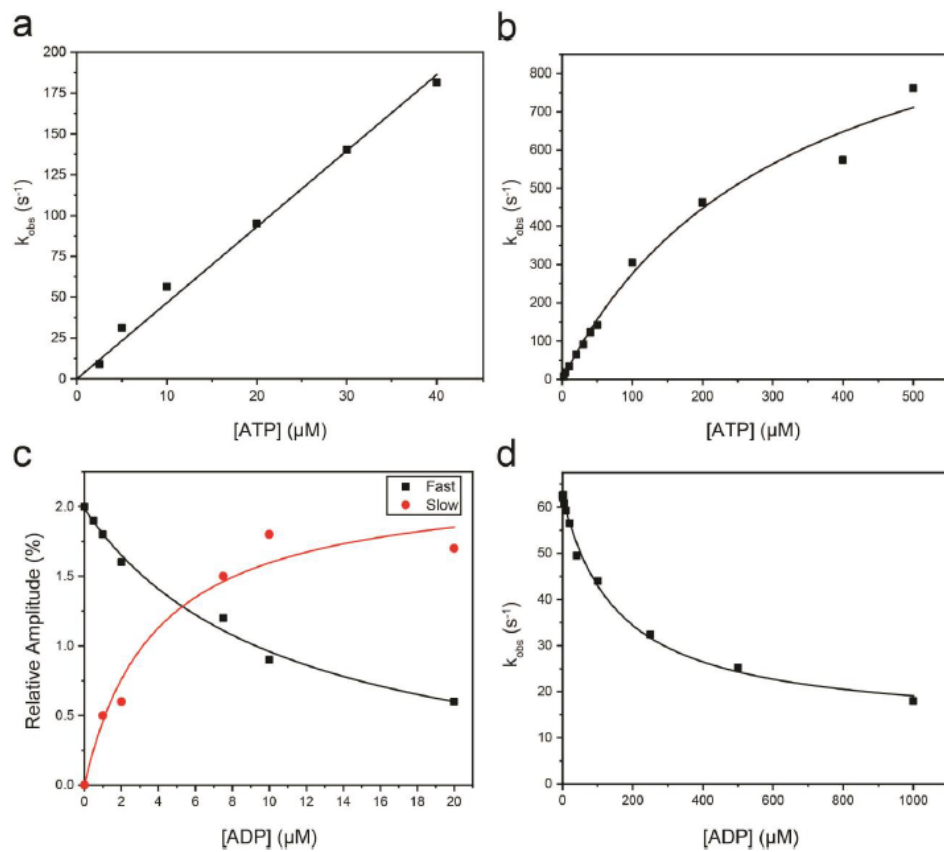
Hellerschmied (2019) Recapitulating the myosin/UNC-45 interplay



**Supplementary Figure 2. Co-expression of MHC-B with UNC-45 mutant proteins.** (a) Western blot analysis of co-expression of MHC-B with indicated UNC-45 mutant proteins in insect cells. Whole cell lysates (WCL) and soluble fractions are shown for MHC-B. Input was normalized to soluble UNC-45 levels (top panels). (b) Comparison of co-expression of MHC-B with UNC-45 *ts*-mutants at 18°C (permissive temperature for *ts*-worm development) and 21°C (standard temperature for insect cell expression in this study). Western blots show whole cell lysates (WCL) and soluble fractions for the UNC-45 proteins and MHC-B.



**Supplementary Figure 3. Analysis of UCS domain to identify myosin folding mutants.** (a) Ligands co-crystallized with the ARM repeat domain of  $\beta$ -catenin (green) mapped onto the UCS domain of wild-type UNC-45 (grey, PDB code: 4i2z). Residues at the center of the outlined myosin binding canyon (N758 and N801) or bordering the canyon (Y750) are highlighted. (b) Analytical SEC and SDS-PAGE analysis of UNC-45 N801A incubated with and without myosin at 27°C. High molecular weight fractions (HMW) are indicated.



**Supplementary Figure 4. Biochemical characterization of MHC-B by stopped-flow analysis.**

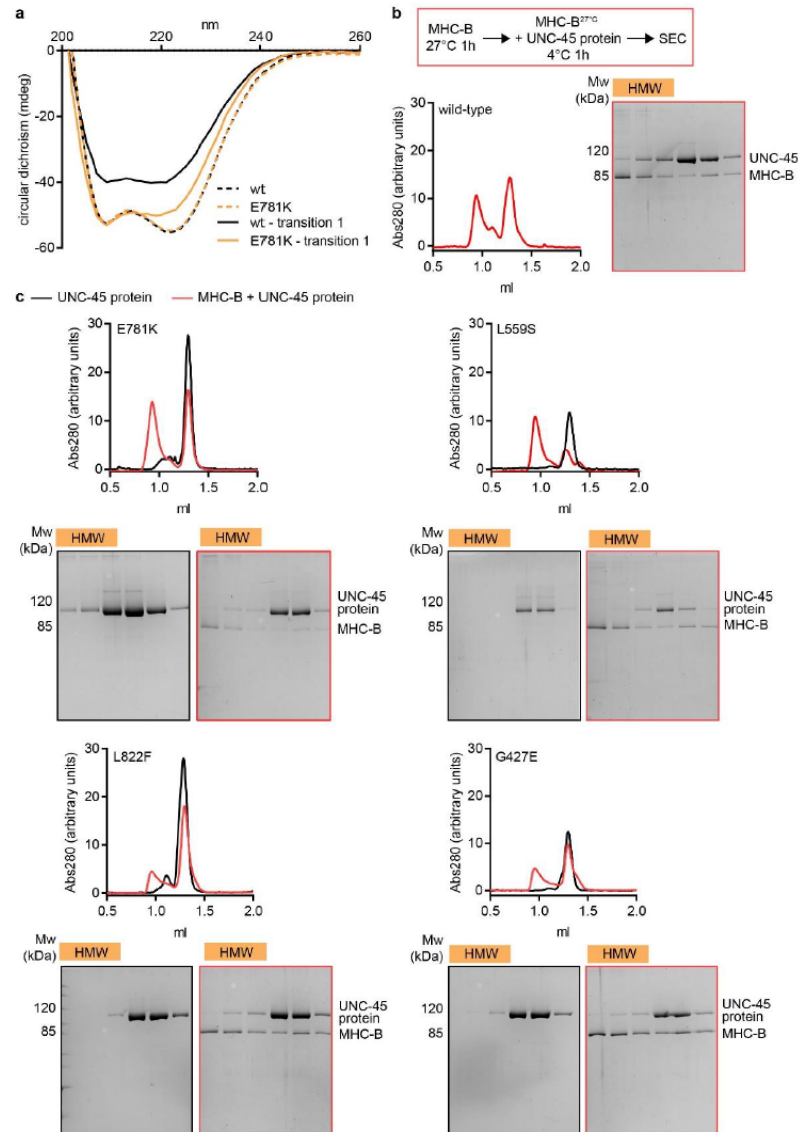
The average of two independent measurements are given in Supplementary Table 1. **(a)** ATP binding to MHC-B. The effect of ATP concentration on  $k_{obs}$  for ATP-induced dissociation of pyrene-actin:MHC-B. The gradient generates second order rate constant of ATP binding ( $K_1k_{+2}$ ) value of  $6.1 \mu\text{M}^{-1}\text{s}^{-1}$ . **(b)** The effect of ATP concentration on  $k_{obs}$  for ATP-induced dissociation of pyrene-actin:MHC-B. The gradient generates a second order rate constant of ATP binding,  $K_1k'_{+2}$ , value of  $3.6 \mu\text{M}^{-1}\text{s}^{-1}$ . The affinity of MHC-B for ATP,  $1/K'_1$ , is  $340 \mu\text{M}$  and the maximum rate of ATP-induced dissociation,  $k'_{+2}$ , is  $1198 \text{ s}^{-1}$ . **(c)** Affinity of MHC-B for ADP. The relative amplitudes of the fast and slow phases plotted against ADP concentration, which has a hyperbolic dependence and generates an ADP affinity of  $7.7 \mu\text{M}$ . **(d)** ADP affinity for actin:MHC-B.  $k_{obs}$  plotted as a function of ADP concentration fitted with a hyperbolic equation resulting in an ADP affinity ( $K'_6K'_7$ ) value of  $143 \mu\text{M}$ .

Hellerschmied (2019) Recapitulating the myosin/UNC-45 interplay

|          |     |   |  |
|----------|-----|---|--|
| Ce_MHC-B | 1   | MEHEKD----FGWQYLRRTREQVLEDDOSRPFYDSKKNVWIPDPEEGYLAGEITATKGDQCVT |  |
| Hs_Bcard | 1   | MGDSEMAVFGAAAFYLRKSEKERLEAQTFRPFDLKKDVFVDDKQEFVVKAKIVSREGKGVIT  |  |
| Ce_MHC-B | 57  | IVTARGNEVTLKKELVQEMNPPKFEKTEDMSNLSFLINDASVHLNLSRYAAMLIYTYSGL    |  |
| Hs_Bcard | 61  | AETFEYCKTIVTKKELVQEMNPPKFEKTEDMAMLIFFLHSPAVLYNLRDREYSWMTIYTYSGL |  |
| Ce_MHC-B | 117 | FCVVTNPKYKRFETYTDSCARMTMGKRKTEMPPHIFAVSDBAYRNMLQDHENQSMILITGES  |  |
| Hs_Bcard | 121 | FCVVTNPKYKRFVYTPVVAAVRGKRKSEAPPHTFSLSDNAYQYMLTDRENQSMILITGES    |  |
| Ce_MHC-B | 177 | GAGKTENTKRVICYFAAVGASQEGGAIVDINPKKRVLTLEDQIVQINPVLFAFGNAKTVRN   |  |
| Hs_Bcard | 181 | GAGKTVNTRVVIQYPAVIAAIGDRSKKIOSP--GKGTLEDQIQANPALEAFGNAKTVRN     |  |
| Ce_MHC-B | 237 | NSSRFGKFIRIHFNKHGRLASCDIEHYLLEKSRVIRQAPGERCYHIFYQLYSDFRPELK     |  |
| Hs_Bcard | 239 | DSSRFGKFIRIHFGATGKLASADIETYLLEKSRVIRQLKAEEDYHIFYQLYSNKKPELL     |  |
| Ce_MHC-B | 297 | KELLIDLPIKDYMEWAQELIDGIDDVVEEFQLTDEAFDILNFAVEKQDCYRLMSAHMH      |  |
| Hs_Bcard | 299 | DMLLTNNPYDYAFISQGETTVASTDDAEELMADNADFVLAGFISEKKNMSYKLTGARMH     |  |
| Ce_MHC-B | 357 | MGNMKFKQRPREEQAEPDGTDEAFKASNMYCIGCEHFLKALTKPRVKVGTETVSKGQNCCE   |  |
| Hs_Bcard | 359 | FGNMKFKLQREEQAEPDGTDEADKSAYLMGLNSADLLKGLCHPRVKVGNEMVITKGQNVQ    |  |
| Ce_MHC-B | 417 | QVNVAVGAMAKGLYSRVFNWLVKRCNLTLDQKIDRDYFIGVLDIAGFEIFDFNSFEQLW     |  |
| Hs_Bcard | 419 | QVIVATGALAKAVYERMFNWMVTRINATLETKQ-PRQYFIGVLDIAGFEIFDFNSFEQLC    |  |
| Ce_MHC-B | 477 | INFTNEKLQQFFNHHMFVLEQEEYAREGIIQWVDFGLDLQACIEILIEKPLGIIISMLDEE   |  |
| Hs_Bcard | 478 | INFTNEKLQQFFNHHMFVLEQEEYKKEGIEHTFIDFGMDLQACIEILIEKPMGIIISMLDEE  |  |
| Ce_MHC-B | 537 | CTVPKATDITLASKLIVDCHLGKHPNFKPKPPKCKQGEAHFAMRHYACTVRYNCHNWLEK    |  |
| Hs_Bcard | 538 | CTVPKATDITFKAKLFDNHLGKSNFQKPRNICKKP-BAHESLIHYACTVDYNIICWLEK     |  |
| Ce_MHC-B | 657 | LYRESLNNLMTMLNKTTHPHFVRCIIPNEKKSQGMIDAAFLVNLTCNGVLEGIRICRKGK    |  |
| Hs_Bcard | 650 | LYRENLNKLMTNLRSHTPHFVRCIIPNEKKSFGVMDNPLVNHQLRCNGVLEGIRICRKGK    |  |
| Ce_MHC-B | 717 | PNRITLHPDFVQRYAALLAA--KEAKSDDDKKKCAEALMSKLVNDGSLSEEMFRICHTKVVFF |  |
| Hs_Bcard | 710 | PNRILYGDPRQRYRIINPAAIPEGQFIDSRKGAERLLSSLD----IDHNQYKFGHTKVVFF   |  |
| Ce_MHC-B | 775 | KAGVLAHLEDIRDEKL  | • mutations connected to hypertrophic cardiomyopathy |
| Hs_Bcard | 766 | KAGLGLLEEMRDERL   |  |

**Supplementary Figure 5. Sequence alignment of MHC-B and human  $\beta$ -cardiac myosin motor domains.** Identical residues are highlighted in black, similar residues in grey. Mutations connected with hypertrophic cardiomyopathy are indicated by a red dot.

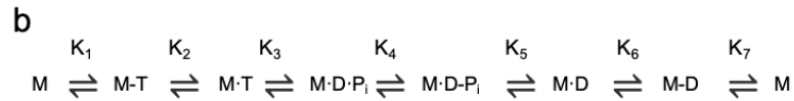
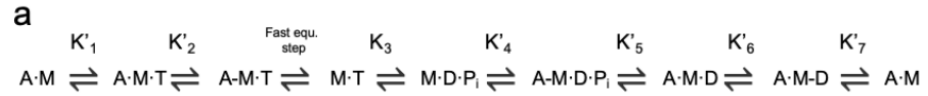
Hellerschmied (2019) Recapitulating the myosin/UNC-45 interplay



**Supplementary Figure 6. Analysis of UNC-45 *ts*-mutants in *in vitro* assays.** (a) CD spectra for wild-type UNC-45 and E781K. (b) Experimental outline illustrating the sequence of events: MHC-B was first incubated at 27°C for 60 min to induce protein unfolding. Following this step UNC-45 and MHC-B were incubated together at 4°C for 60 min and analyzed by SEC. UNC-45 which interacts with unfolded MHC-B is present in the high molecular weight (HMW) fractions. (c) Same analysis as in (b) for the indicated UNC-45 *ts*-mutants.



**Supplementary Table 1: Kinetic properties of MHC-B compared to human  $\beta$ -cardiac S1.** Data represent mean  $\pm$  s.e.m. Raw data and calculations are shown in Supplementary Figure 4. Data are shown for the constants depicted for the actin-myosin (a) and myosin (b) ATPase cycle. M = myosin; A = actin; T = ATP; D = ADP; P = P<sub>i</sub>. Dashed (-) interactions represent a weakly bound complex, and dotted (·) interactions represent a strongly bound state. An equilibrium constant, K<sub>i</sub> can be defined as k<sub>+/k<sub>i</sub></sub>.



|  | <i>C. elegans</i> MHC-B | human $\beta$ -cardiac S1 |
|--|-------------------------|---------------------------|
| <b>ATP binding to myosin</b>   |                         |                           |
| K <sub>1</sub> k <sub>+2</sub> ( $\mu\text{M}^{-1}\text{s}^{-1}$ )           | 6.8 $\pm$ 1.2           | 5.8 $\pm$ 0.2             |
| <b>ADP binding to myosin</b>   |                         |                           |
| K <sub>6</sub> K <sub>7</sub> ( $\mu\text{M}$ )                              | 7.55 $\pm$ 0.5          | 0.53 $\pm$ 0.06           |
| k <sub>+6</sub> ( $\text{s}^{-1}$ )  | 12.7 $\pm$ 0.7          | 0.63 $\pm$ 0.03           |
| <b>ATP binding to actomyosin</b>   |                         |                           |
| K' <sub>1</sub> k' <sub>+2</sub> ( $\mu\text{M}^{-1}\text{s}^{-1}$ ) at 20°C | 3.6 $\pm$ 0.4           | 4.4 $\pm$ 0.3             |
| 1/K' <sub>1</sub> ( $\mu\text{M}$ )  | 324.2 $\pm$ 67.9        | 327.9 $\pm$ 53.3          |
| k' <sub>+2</sub> ( $\text{s}^{-1}$ )   | 1172.8 $\pm$ 125.6      | 1543 $\pm$ 100            |
| <b>ADP affinity for actomyosin</b>   |                         |                           |
| K' <sub>6</sub> K' <sub>7</sub> ( $\mu\text{M}$ )                            | 131.5 $\pm$ 19.3        | 6.1 $\pm$ 0.7             |
| k' <sub>+6</sub> ( $\text{s}^{-1}$ )   | 189 $\pm$ 42.5          | 58.7 $\pm$ 3.3            |
| <b>S1 affinity for actin</b>   |                         |                           |
| K <sub>A</sub> (nM)  | 10.3 $\pm$ 3.7          | 10 $\pm$ 1.8              |

**Supplementary Table 2: Data collection and refinement statistics.**

|   | MHC-B                   | Unc-45 G427E               | Unc-45 L822F            | Unc-45 ΔTPR           |
|---|-------------------------|----------------------------|-------------------------|-----------------------|
| PDB code  | 6QDJ                    | 6QDK                       | 6QDL                    | 6QDM                  |
| <b>Data collection</b>                              |                         |                            |                         |                       |
| Space group   | <i>P</i> 2 <sub>1</sub> | <i>P</i> 6 <sub>1</sub> 22 | <i>P</i> 2 <sub>1</sub> | <i>C</i> 2            |
| Cell dimensions                                     |                         |                            |                         |                       |
| <i>a</i> , <i>b</i> , <i>c</i> (Å)                  | 54.11, 111.96, 84.74    | 86.91, 86.91, 718.54       | 54.12, 114.32, 85.01    | 157.39, 97.61, 148.88 |
| α, β, γ (°)   | 90, 97.44, 90           | 90, 90, 120                | 90, 107.99, 90          | 90, 93.41, 90         |
| Resolution (Å)                                      | 85-1.9 (2.05-1.90) *    | 30-3.4 (3.49-3.4)          | 47-2.9 (3.09-2.9)       | 49-3.8 (4.01-3.80)    |
| <i>R</i> <sub>meas</sub> (%)                        | 4.5(45.4)               | 12.0 (84.8)                | 11.9 (67.5)             | 6.2 (127.5)           |
| <i>I</i> / σ <i>I</i>                               | 19.6(3.1)               | 12.0 (1.9)                 | 8.5 (1.4)               | 9.1 (1.1)             |
| Completeness (%)                                    | 93.8(78.0)              | 99.6 (96.2)                | 97.0 (82.3)             | 98.9 (96.2)           |
| Redundancy  | 3.3(2.9)                | 18.2 (8.8)                 | 3.1 (2.7)               | 3.3 (3.1)             |
| <b>Refinement</b>                                   |                         |                            |                         |                       |
| Resolution (Å)                                      | 85-1.9                  | 30-3.4                     | 47-2.9                  | 49-3.8                |
| No. reflections                                     | 76,202                  | 23,652                     | 20,543                  | 22,138                |
| <i>R</i> <sub>work</sub> / <i>R</i> <sub>free</sub> | 18.5/21.3               | 28.7/32.0                  | 22.1/26.8               | 28.0/31.0             |
| No. atoms   |                         |                            |                         |                       |
| Protein   | 6,130                   | 6,851                      | 6,931                   | 11,815                |
| Ligand/ion  | 131                     | -                          | -                       | -                     |
| Water   | 237                     | -                          | -                       | -                     |
| <i>B</i> -factors                                   |                         |                            |                         |                       |
| Protein   | 38.6                    | 96.5                       | 63.5                    | 200                   |
| Ligand/ion  | 45.5                    | -                          | -                       | -                     |
| Water   | 40.6                    | -                          | -                       | -                     |
| R.m.s. deviations                                   |                         |                            |                         |                       |
| Bond lengths (Å)                                    | 0.012                   | 0.008                      | 0.007                   | 0.013                 |
| Bond angles (°)                                     | 1.32                    | 1.07                       | 0.99                    | 1.48                  |

\*Number of xtals: 1. \*Values in parentheses are for highest-resolution shell.

Supplementary Table 3: Structural homologs of indicated UCS domains identified by a DALI search.

| rank                    | wt, extended (4i2z)                   |         | wt, curved (5mzu)                         |         | $\Delta$ TPR, molecule B |         | tsL822F                            |         | tsG427E                         |         |
|-------------------------|---------------------------------------|---------|---|---------|--------------------------|---------|------------------------------------|---------|---------------------------------|---------|
|                         | structural homolog                    | Z-score | structural homolog                        | Z-score | structural homolog       | Z-score | structural homolog                 | Z-score | structural homolog              | Z-score |
| <b>UCS proteins</b>     |                                       |         |   |         |                          |         |                                    |         |                                 |         |
|                         | DmUNC-45                              | 35.3    | DmUNC-45                                  | 26.5    | DmUNC-45                 | 31.6    | DmUNC-45                           | 36.9    | DmUNC-45                        | 29.6    |
|                         | She4p                                 | 28.1    | CeUNC-45, extended                        | 23.1    | She4p                    | 25.4    | CeUNC-45, extended                 | 31.3    | She4p                           | 24.0    |
|                         | CeUNC-45, curved                      | 17.0    | She4p                                     | 22.2    | CeUNC-45, extended       | 24.8    | She4p                              | 28.8    | CeUNC-45, extended              | 23.8    |
|                         |                                       |         |   |         | CeUNC-45, curved         | 19.4    | CeUNC-45, curved                   | 16.0    | CeUNC-45, curved                | 16.4    |
| <b>Non UCS proteins</b> |                                       |         |   |         |                          |         |                                    |         |                                 |         |
| 1                       | $\beta$ -catenin                      | 24.2    | catenin delta-1                           | 19.3    | $\beta$ -catenin         | 20.9    | importin $\alpha$                  | 24.9    | vacuolar protein 8              | 20.4    |
| 2                       | engineered protein OR497              | 24.0    | $\beta$ -catenin                          | 18.9    | importin $\alpha$        | 20.5    | engineered protein or497           | 24.7    | importin $\alpha$               | 20.1    |
| 3                       | importin $\alpha$                     | 23.9    | importin $\alpha$                         | 18.6    | vacuolar protein 8       | 19.9    | xpg2 peptide                       | 24.7    | GTP-binding nuclear protein ran | 19.8    |
| 4                       | vacuolar protein 8                    | 23.8    | GEF srm1                                  | 17.8    | GEF srm1                 | 19.8    | karyopherin $\alpha$               | 24.4    | GEF srm1                        | 19.8    |
| 5                       | GEF srm1                              | 23.8    | engineered protein OR497                  | 17.1    | karyopherin $\alpha$     | 19.5    | GEF srm1                           | 24.3    | $\beta$ -catenin                | 19.6    |
| 6                       | karyopherin $\alpha$                  | 23.4    | plakoglobin                               | 17.1    | protein humpback-2       | 19.0    | $\beta$ -catenin                   | 24.2    | karyopherin $\alpha$            | 19.6    |
| 7                       | GTP-binding nuclear protein ran       | 22.8    | RAP1 GTPase-GDP dissociation stimulator 1 | 16.4    | plakoglobin              | 18.0    | vacuolar protein 8                 | 23.9    | protein humpback-2              | 19.1    |
| 8                       | nuclear cap-binding protein subunit 1 | 22.7    | adenomatous polyposis coli protein        | 16.3    | APC variant protein      | 17.8    | flap endonuclease 1 (fen1) peptide | 23.8    | plakoglobin                     | 18.1    |

**Supplementary Table 4: Primers used in this study.**

| Primers used for site-directed mutagenesis of UNC-45 constructs in pET21a |  |  |
|---|--|--|
| tsUNC-45 G427E  | ATTACAATGCTTCAAGAACCAGTTGATATTGGA  |  |
| tsUNC-45 L559S  | CTCTCCTATTTGTCTTCGGATGCTGATGTTAAG  |  |
| tsUNC-45 E781K  | ATTCCAAGATTGAGAAATTCGGTTTATGACG  |  |
| tsUNC-45L822F   | ACCGATCGTCTGAAATTCGGGTTCTCTACTCG   |  |
| UNC-45 N801A  | Forward:<br>CGCTGAGCTTCTTCTCGCGTTGCTCTTTTTTCGAGA<br>Reverse:<br>TCTCGAAAAGAGCAACGCGAGAAGAAGCTCAGCG |  |
| Primers used for generating expression constructs for insect cells        |  |  |
|   | Forward  | Reverse  |
| MHC-B in pFastBacDual   | GATCGAATTCATGGAGCACGAGAAGGAC   | CATGCTAGACTAGTGATGGTGGTGATGGTG<br>GAGCTTCTCGTCACGGAT                               |
| NMY-2 in pFastBacDual   | GATCGCGCGCATGACATCATCTCGACAA   | CATGCTAGACTAGTGATGGTGGTGATGGTG<br>AAGCTTCTGATCAGCCAT                               |
| UNC-45 in pFastBacDual  | GATGCCCGGGATGGTTGCTCGAGTACAG   | together with MHC-B:<br>GATGGCATGCTTATTTTTCGAACTGCGGGTG<br>GCTCCATTCTGAATGGTGCTCAT |
|   |  | together with NMY-2:<br>GATGCCATGGTTATTTTTCGAACTGCGGGTG<br>GCTCCATTCTGAATGGTGCTCAT |
| Hsp70 in pFastBacDual   | GATGCCCGGGATGGACTACAAAGACGAT<br>GACGACAAGAGTAAGCATAACGCTGTT  | GATCGCTAGCTTAGTCGACCTCCTCGAT   |
| Hsp90 in pFastBacDual   | GATGCCCGGGATGGACTACAAAGACGAT<br>GACGACAAGTCCGAGAACGCGAAACC   | GATCGCTAGCTTAGTCGACCTCCTCCAT   |
| MHC-B in pACEBac1   | CGGATCCCGGTCCGAAACCATGGAGCAC<br>GAGAAGGACCCAG  | CCCCAGAACATCAGGTTAATGGCGCTAATGA<br>TGGTGGTGATGGTGGAGC                              |
| UNC-45 full-length proteins in pIDC derivative                            | CTGGAAGTTCTGTTCCAGGGGCCCATGG<br>TTGCTCGAGTACAGACTGC  | CCCCAGAACATCAGGTTAATGGCGTTATTCC<br>TGAATGGTGCTCATTGATTTTCG                         |
| UNC-45 ΔUCS in pIDC derivative  | CTGGAAGTTCTGTTCCAGGGGCCCATGG<br>TTGCTCGAGTACAGACTGC  | CCCCAGAACATCAGGTTAATGGCGTTATTTC<br>ATCGTTGCTTTTCGAAATGTCGTC                        |
| UNC-45 ΔTPR in pIDC derivative  | CTGGAAGTTCTGTTCCAGGGGCCCATGG<br>TTGCTCGAGTACAGACTGC  | CCCCAGAACATCAGGTTAATGGCGTTATTTC<br>ATCGTTGCTTTTCGAAATGTCGTC                        |
| UNC-45 ΔTPR in pIDC derivative  | CTGGAAGTTCTGTTCCAGGGGCCCACCA<br>CTTCACTGGCTAATAAGGTAAGTGC  | CCCCAGAACATCAGGTTAATGGCGTTATTTC<br>TGAATGGTGCTCATTGATTTTCG                         |
| Hsp90 in pACEBac1 derivative  | CGGATCCCGGTCCGAAACCATGGACTAC<br>AAAGACGATGACGACAAG   | CCCCAGAACATCAGGTTAATGGCGTTAGTCG<br>ACCTCCTCCATGCG                                  |
| Hsp70 in pACEBac1 derivative  | CCCATACGATGTTCCAGATTACGCTAGT<br>AAGCATAACGCTGTTGGAATCG   | CCCCAGAACATCAGGTTAATGGCGTTAGTCG<br>ACCTCCTCGATCGTTG                                |
| MHC-B in pACEBac1 derivative  | GATCCCGGTCCGAAACCATGGAGCACGA<br>GAAGGACCCAG  | CCCCAGAACATCAGGTTAATGGCGCTAATGA<br>TGGTGGTGATGGTGGAGC                              |

## **7. Discussion**

As described in Chapter 1.7, the aims of this thesis were part of an effort to understand the mechanism by which the properties of myosin can be modulated to achieve a multitude of functions. With a focus on class II myosins, this was achieved by looking at different contraction characteristics between class II isoforms, the way in which MyHC- $\beta$  myosin can modulate ADP release and velocity, and how single point mutations can disrupt myosin function. To improve the current methodology to produce recombinant myosin that allow us to answer such questions, we also attempted to address if the myosin chaperone UNC-45 could be utilised to increase protein yields, and characterised the MHC-B myosin from the body wall of *C. elegans*. The extent to which this work has successfully addressed these problems will be discussed below, chapter by chapter.

### ***7.1 The ATPase cycle of Human Muscle Myosin II isoforms: Adaptation of a single mechanochemical cycle for different physiological roles***

The first aim of this thesis was to predict how human sarcomeric myosins may adapt their mechanochemical ATP-driven cross-bridge cycle to perform different functions within different muscle types. The physiology of a muscle is determined by the muscle fibres present, which typically express a single myosin isoform. Chapter 3 demonstrated that all isoforms studied have unique fractional occupancies of the states in the ATPase cycle, and the balance between the different molecular events in the cycle can be altered to produce a range of mechanical activities.

The work presented in Chapter 3 is the first of its kind, combining data from multiple groups and applying a novel modelling approach to predict how parameters of the cross-bridge cycle govern the major physiological characteristics of a muscle fibre. Some key conclusions from this work include the finding that each isoform has a unique relationship between the ATPase cycling rate and the three significant events in the cycle (phosphate release, ATP hydrolysis and ADP release). Interestingly, whilst being a developmental myosin, the MyHC-peri isoform shared similar characteristics with the fast skeletal isoforms rather than the MyHC-emb isoform. Our results additionally demonstrated that the slow isoforms are more economical at holding loads. This allows the slow isoforms to sustain force and velocity when contracting for longer periods compared to the fast isoforms. Taken

together, these findings reveal distinct characteristics between different sarcomeric myosin isoforms.

One of the parameters that is predicted from the modelling approach is the rate constant of ATP hydrolysis. The rate and equilibrium constants that control this step precedes the entry into the M.D.Pi state (see Figure 1.28). The rate of ATP hydrolysis, along with phosphate release, is thought to control the rate of force development (Sleep, Irving, and Burton 2005). To determine the rate and equilibrium constant of ATP hydrolysis, previous assays in our laboratory use a combination of quenched-flow spectroscopy and High Performance Liquid Chromatography (HPLC) (Bloemink et al. 2007). This assay measures the time dependence of phosphate production using a quench-flow apparatus; myosin is mixed with ATP, aged for a specified time, and then quenched with acid, which denatures the myosin and stops the ATPase reaction. Phosphate that was sequestered in the active site in the M.ADP.Pi state is also measured. Phosphate, along with ADP and ATP nucleotides can be then be quantified using HPLC. The limitation of using this assay with the human proteins generated from C2C12 expression and purification is the large quantity of protein required. The assay generally uses 2 mg for one experiment, which is double the 1 mg of protein generated from one batch of culture of C212 cells. However, the parameter has been measured in other species for the MyHC- $\beta$  and MyHC-IIa isoforms. MyHC- $\beta$  from bovine masseter muscle has a rate constant of  $18 \text{ s}^{-1}$  (Bloemink et al. 2007), from rabbit  $21.6 \text{ s}^{-1}$  (Iorga, Adamek, and Geeves 2007), and from porcine  $24.5 \text{ s}^{-1}$  (Stein, White, and Annis 1989). This agrees well with the modelled human value of  $12.5 \text{ s}^{-1}$ . MyHC-IIa from rabbit had a rate constant for ATP hydrolysis of  $131 \text{ s}^{-1}$  (Ritchie et al. 1993); our model predicts the human fast skeletal isoforms to have values  $92.8\text{-}125.2 \text{ s}^{-1}$ . This demonstrates the accuracy of the model to predict unknown parameters, therefore we applied the model to other isoforms (such as the perinatal and extraocular isoforms) for which this parameter has not been reported.

Another parameter predicted from the modelling is the rate constant of phosphate release. This is a significant part of the cycle, as it precedes the force-holding, strongly attached AMD state. The work of White et al and Heeley et al estimated Pi release to be  $75\text{--}77 \text{ s}^{-1}$  for rabbit skeletal S1 (White, Belknap, and Webb 1997; Heeley, Belknap, and White 2002). The modelled human IIa isoform was predicted to be  $44.5 \text{ s}^{-1}$ . Whilst the measured value is almost double our predicted value, it should be noted that it was obtained at different ionic strength to our solution data. The salt dependence of this parameter is not known. However, measurements performed at identical salt conditions to our experiments on porcine MyHC- $\beta$  S1, which has a sequence identity to human MyHC- $\beta$  of 95%, estimates

phosphate release to be  $17 \text{ s}^{-1}$ . This compares well with our estimate of  $15.95 \text{ s}^{-1}$  (Liu et al. 2015), further highlighting the precision of the model.

To constrain our model further, we could measure the rate constant or equilibrium constant of ATP hydrolysis. Classically the method to measure this constant used radioactively-labelled nucleotides. Other methods that have the sensitivity to measure nucleotides at low concentrations could be explored. In 2017, Olafsson et al described the combination of HPLC with mass spectrometry to measure deoxyribonucleoside triphosphate concentrations in tissues and isolated cells (Olafsson et al. 2017). The assay successfully separated and quantified down to the femtomole level dCTP, dTTP, dATP, and dGTP nucleotides. If this resolution could be applied to ATP and ADP nucleotides, it may present an attractive method to measure the rate constant of ATP hydrolysis. My initial studies (not presented in this thesis) have investigated the use of NMR spectrometry. Guo et al reported the use of one-dimensional proton NMR spectroscopy to measure the ratios of different nucleotides, which can then be used to infer information about ATPase and kinase activities (Guo et al. 2014). The authors also claim that the technique can directly monitor ATP turnover. I performed initial experiments testing this method and proof-of-concept measurements were successful. Optimising this method is an area that could enhance the current scope of our modelling approach, and may also have implications for the work described in Chapter 5, as will be discussed in section 7.3.

The modelling conducted with MUSICO in this thesis is not reflective of the sarcomere environment in which actin and myosin are found. The larger aim of MUSICO is the development of an accurate multiscale model of a contracting sarcomere (Mijailovich et al. 2016). Such complex modelling would require the combination of single molecule force measurements, muscle fibre data, motility assays and transient ATPase kinetics. The modelling performed in Chapter 3 does not take into account regulatory proteins such as tropomyosin and troponin, thin filament regulation,  $\text{Ca}^{2+}$  sensitivity or thick filament regulation (such as myosin binding to MyBP-C and titin, phosphorylation of RLC). However, whilst the modelling approach used here is simple, and does not fully exploit the capabilities of the MUSICO programme, the basics of the ATPase cycle have to be understood before progressing to more complex models. To obtain a highly constrained model, the ATPase cycle should be well-defined, which the data in Chapter 3 achieves.

To fully understand the mechanical behaviour of a muscle fibre, the force-velocity relationship needs to be defined. When studying the *in vivo* mechanics of a muscle, maximum shortening velocity is not the most relevant parameter. Muscles contracting *in*

*vivo* do not shorten at their maximum shortening velocity, but rather at the velocity at which power output is maximal (i.e. the optimum performing conditions for a muscle) (Bottinelli et al. 1996). The force generated by a muscle is a function of its velocity; power = force x velocity. The force of a muscle defines the velocity at which power output is maximal. Currently, our data is on single protein, and extrapolating solution biochemistry to muscle fibre data is beyond the scope of the model. However, of note is the work of Fenwick et al, who used a modelling approach to show how myosin force production is co-ordinated with energy utilisation during lengthening and shortening (Fenwick, Wood, and Tanner 2017). They report that the fraction of bound cross-bridges increased during slow-velocity concentric and eccentric contractions, but that ATP utilization increased during shortening transients due to faster cross-bridge cycling. This work demonstrates how contractile efficiency and power output are modulated throughout dynamic contractions, which may be another way in which myosin can fine-tune its properties.

As with any modelling approach, there are a number of assumptions that are made to allow a detailed description of the system to be achieved. For the class II myosins, load dependence has only been measured for the human MyHC- $\beta$ . We applied this load dependence to all isoforms studied in our analysis; this is unlikely to be the same between the isoforms. This parameter needs to be determined for more isoforms. The recent developments in force measurements using single molecule assays will enable this (Greenberg, Shuman, and Ostap 2014; Sung et al. 2015). Another assumption in our modelling was the effect of temperature on myosin ATPase. The experimental ATPase data for the perinatal, extraocular and fast skeletal isoforms were conducted at 37 °C; a  $Q_{10}$  value of 1.5 has been reported for the ATPase of MyHC- $\beta$  (Siemankowski, Wiseman, and White 1985), and so this value was used to correct value to a temperature of 20 °C. However, it is possible that this temperature-dependence is different between isoforms, thus this remains a limitation of the data.

One of the limitations of using such an approach as kinetic modelling is the varying experimental conditions between different labs if parameters are not all collected within the same group. All the assays included in the model in Chapter 5 were completed under the same experimental conditions (i.e., ionic strength, temperature). Where possible this was also true for the data in Chapter 3, with a few exceptions. Kinetic data for the fast skeletal and extraocular isoforms were completed at 100 mM KCl (Deacon et al. 2012), but all other data was collected at 25 mM KCl (Nag et al. 2015; Walklate et al. 2016). However, salt dependence has been reported for rabbit MyHC-IIa and human MyHC- $\beta$  kinetics (Mijailovich et al. 2017), so we corrected for this difference. Perhaps one limitation is the different tags



that have been added to the recombinant myosins as the production process has been refined over the last decade. The fast skeletal and extraocular isoforms were purified with a GFP-tagged moiety, which was absent in all other isoforms. Bloemink et al demonstrated that there were few differences in measured parameters of MyHC- $\beta$  with and without a GFP-tag (Bloemink et al. 2013), but the effect of the presence of the GFP-tag on the steady-state ATPase rates has not been measured.

All kinetic parameters in the model were collected in solutions containing 25 mM salt, and simulations were run assuming this ionic strength. Simulations were performed at this ionic strength to allow comparison between stopped-flow and ATPase data, the latter of which requires low salt to achieve saturation of the actin-activated ATPase. This is not reflective of physiologically relevant salt conditions, but as the modelling is dependent on steady-state ATPase parameters, this must be a well-defined parameter. Whilst this may not be physiologically relevant, as all isoforms were under the same conditions, a direct comparison between them can be made.

As the fundamental ATPase cycle, which the model is based on (Figure 1.28) is conserved between myosins, this analysis can be performed for myosins from different classes. The work presented in Chapter 3 was focussed on human sarcomeric myosins, which contain a wide repertoire of properties alone. Whether the difference in structural domains are coupled with changes in mechanochemical cross-bridge cycle properties to give rise to different functions between different myosin classes could be explored. A further application of the model could be in the use for predicting potential therapeutic agents for disease from small molecule screens. If kinetic parameters of disease-causing mutations were known, the model could be used to assess if the parameters are restored to WT values when in the presence of a potential therapeutic agent.

## ***7.2 Cardiac contraction velocity has evolved to match heart rate with body size through variation in $\beta$ -cardiac myosin sequence***

The work from Chapter 3 demonstrated some of the different contractile properties of different myosin class II isoforms, but the question still remains as to how these differences arise from the sequences of myosin. Chapter 4 aimed to address this question by focusing on MyHC- $\beta$  and its adaptation of the rate of ADP-release to control velocity as body mass increases through evolution.

The instructions for life are encoded within the DNA sequence of proteins, so we analysed the sequences of class II myosins. As described in section 1.3.2, the work of McGreig et al demonstrated a correlation in sequence identity with body mass for MyHC- $\beta$ , MyHC-IIa and MyHC-IIb isoforms (McGreig et al. 2019). In this study we focussed on the MyHC- $\beta$  isoform. Velocity data of the MyHC-IIa and MyHC-IIb isoforms are only available for a few species, whereas heart rates have been recorded for a large cohort of mammals. To be clear, heart rate is not solely a function of myosin composition within the heart; it is a function of very many inter-species variables. These variables exist at the protein, anatomical and physiological levels. However, the maximum shortening velocity, which is one of the parameters that defines the force-velocity relationship of a muscle, is a property of the myosin isoform expressed. We therefore propose MyHC- $\beta$  can be used to probe adaptation of contraction velocity with increasing body mass.

MyHC- $\beta$  is expressed both within slow skeletal muscle and the ventricles of large mammals, including humans. The endogenous rat protein which was used as a control in Chapter 4 was obtained from the soleus muscle, not cardiac tissue. Cardiac muscle contains an abundance of fibroblasts and other cell types, which makes purifying cardiac MyHC- $\beta$  less efficient. One consideration is that different post-translational modifications (PTMs) may occur in cardiac and skeletal muscle. To understand the effects of PTMS such as phosphorylation, serine to aspartate mutations can be introduced into a protein to mimic the phosphorylated states. Kampourakis and colleagues recently reported the limitations of generating and studying such mutations (Kampourakis et al. 2018). They found three Ser-Asp mutations in cardiac MyBP-C did not reproduce the same effects as tri-phosphorylation of these sites Protein Kinase A. This is likely due to the additional negative charges introduced with phospho-mimetic mutations. It can therefore be misleading to interpret the effects of phosphorylation sites in a protein using such an approach. Whilst the full extent of the effect of PTMs on MyHC- $\beta$  is currently unknown, it is unlikely that such modifications generate significant alterations to the rate of ADP-release or maximum

shortening velocity. Bloemink et al demonstrated that the ADP release rate was not significantly different between MyHC- $\beta$  from bovine masseter and cardiac muscles. Therefore, rat MyHC- $\beta$  purified from soleus muscle is expected to have the same kinetic properties as that of cardiac MyHC- $\beta$ .

The sequence changes introduced into the MyHC- $\beta$  were found in three distinct clusters of the motor domain. Whether all three of these regions contribute equally to the changes in ADP release, and hence velocity, or if they all work in unison is not yet defined. As shown by the table in Figure 6 in Chapter 4, the rate of ADP release is modified step-wise. It is therefore unlikely that a single one of these residues is the sole determinant of the change in the rate of ADP release and velocity between the rat and human MyHC- $\beta$ . Instead, we predict that each of the nine residues will contribute a fraction of the difference in the measured parameters. What would be interesting is whether 3 locations in the motor domain are also responsible for the adaptation to body mass in the MyHC-IIa and MyHC-IIb isoforms, or if these isoforms vary alternate regions of the motor domain to suit their physiological requirement. It should be noted that any changes made to the sequence of the motor domain are likely to be subtle; to alter the function of the protein in a positive manner without exerting any negative consequences requires a careful balance of tuning the ADP-release rate whilst maintaining motor function.

Whilst the work in Chapters 3 and 5 were completed with sS1, the WT human MyHC- $\beta$  and chimera proteins in Chapter 4 were extended S1 molecules. These S1 constructs contained 2 IQ domains, and so were purified with the endogenous mouse essential and regulatory light chains. Deacon et al demonstrated no significant difference in kinetic parameters between sS1 and S1 (Deacon et al. 2012).

The velocity value for human MyHC- $\beta$  obtained in Chapter 4 was  $0.49 \pm 0.129 \mu\text{m}\cdot\text{s}^{-1}$ . A similar experiment in Ujfalusi et al reported a motility of  $0.612 \pm 0.21 \mu\text{m}\cdot\text{s}^{-1}$  (Ujfalusi et al. 2018), although this value was obtained at 23 °C (compared with our experimental condition of 20 °C). It has been reported previously that the effects of salt, pH and temperature can alter velocity values (Homsher, Wang et al. 1992). Higher temperatures can increase motility by a factor of 4 over 10 °C, as shown by Sheetz et al (Sheetz, Chasan, and Spudich 1984). Moreover, the construct used in Ujfalusi et al was sS1 with only single light chain, compared to the S1 construct with two light chains used in this study. Lowey et al showed that light chain content can affect velocity (Lowey, Waller, and Trybus 1993a). Indeed, in skeletal muscle removal of both light chains slowed velocity by a factor of 10, but reconstitution of a single light chain restored velocity only to an intermediate level (Lowey, Waller, and Trybus

1993b). Other studies have also shown the importance of light chain content on velocity (Fewell et al. 1998; Matthew et al. 1998; Toepfer et al. 2013; Kim et al. 2019). Thus, the differences in temperature and light chain content may account for the differing velocity values.

Velocity values for human MyHC- $\beta$  are also reported in Chapter 5, which were collected by the Spudich group. They report a range of velocity values; data in Table S8 show that values range from 0.579 to 0.858  $\mu\text{m}\cdot\text{s}^{-1}$  between different protein preparations. This suggests there is variability between protein preparations. In this study, all measurements were completed from 3 independent protein preparations from different cell pellets. Despite this, all cell pellets were transfected with the same adenovirus stock, and were grown simultaneously in the same incubator, resulting in growth under identical conditions. This reduced the variability we observed in our measurements. To note, the errors are larger in our velocity values as the errors from the Spudich laboratory represent Standard Error of the Mean (SEM), whereas we report Half Width at Half Maximum (HWHM). This is to account for the distribution of the velocity values around the mean.

The site of cleavage by chymotrypsin is found after the first IQ domain; therefore, the chymotryptic-digested rat soleus myosin contained 1 IQ domain and hence 1 light chain. As the light chain content differs from the recombinant human MyHC- $\beta$  and chimera proteins, and because light chain content affects motility as outlined above, a direct comparison of motility cannot be made between the recombinant proteins and the native rat soleus S1. Whilst a motility assay was not performed for the native rat protein, studies in the literature indicate that rat myosin moves 3-5 times faster than the human myosin (the absolute value varies depending on conditions of the experiment) (Pellegrino et al. 2003). Velocity data has been reported for rat and human fibres. However, comparison of velocity data from muscle fibres does not directly correspond to values obtained with single protein. It is thought that the orientation of the myosin on the surface will contribute to this (Homsher, Wang et al. 1992). Indeed, the presence of the C-terminal extension on the MyHC- $\beta$  and chimeric proteins tether the myosin to the surface resulting in a uniform attachment of proteins to the coverslip and stable geometry, which is not the case for fibre data. Whilst the absolute values cannot be directly compared, the ratio of rat-human motility is comparable to our chimera-human ratio.

The motility assay was performed under unloaded conditions. It would be interesting to measure the load-dependence of the chimera protein with harmonic force microscopy (Sung et al. 2015). Both load-dependence and the step-size of human MyHC- $\beta$  have been

measured, although we would not expect to see a difference in these parameters in the chimera protein. The force-velocity relationship defines the mechanical performance under various loads as a function of maximum force and maximum velocity. For individual muscle myosins the maximum force is a property of a myosin isoform but is largely invariant amongst different orthologues. Maximum shortening velocity of a single myosin type, however, does vary among orthologues. This would suggest that the load-dependence of the chimera protein would be equivalent to the human MyHC- $\beta$ , although this remains a prediction and has not been experimentally determined.

Figure 5 in Chapter 4 shows the location of the residues changed in the chimera protein. Interestingly, none of the changes were found in the converter domain, which, as described previously, is a hot-spot for cardiomyopathy-causing mutations. This suggests that mutations introduced into this domain are not well-tolerated. Whilst none of the residues have been reported in ClinVar (a database that reports human variations and phenotypes, with supporting evidence), a study from Robert-Paganin et al reported two of the residues as sites with reported disease-causing mutations (Robert-Paganin, Auguin, and Houdusse 2018). This study was a comprehensive analysis of 178 reported HCM-causing mutations which aimed to categorise the mutations based on the effects on the motor. At residue 349, a methionine to threonine substitution has been reported in a single adolescent by Jeschke et al (Jeschke et al. 1998). The authors predict that this mutation leads to altered motor function. Similarly at residue 434, an arginine to threonine substitution is predicted to likely effect both motor function and stability. However, like the 349 residue, this mutation has only been seen in one patient (Wang et al. 2014). It is therefore hard to predict whether the mutations are clearly causative of HCM; the two mutations could be normal variants in the population.

This study may have wider implications on the field of evolutionary biology. One of the fundamental challenges in current molecular and structural biology is to understand how a protein can adapt, over evolutionary time frames, to different physiological requirements. To begin to understand this, we must grasp how DNA sequence variation alters protein function. This is pivotal to our understanding of evolution and the role of genetic variation. Now with the availability of the genomes of different species and many individual human genomes, it would be possible to use this approach for any measurable phenotype.

As shown in Figure 1.16, point mutations can have long-reaching effects on protein function, both locally and globally. Of the ~800 amino acid motor domain, 9 amino acid substitutions were sufficient to alter properties of the motor such that the behaviour of the

protein was altered to match that of a different species. Physiologically, multiple mutations are not well tolerated within the myosin protein. Table 1.5 demonstrates the sheer number of mutations identified in MyHC- $\beta$ . Just single amino acid substitutions are sufficient to cause HCM. The molecular mechanisms underpinning the cause and progression of this disease are incompletely understood. Chapter 5 aimed to address this and is discussed in more detail below.

### ***7.3 Myosin motor domains carrying mutations implicated in early or late onset hypertrophic cardiomyopathy have similar properties***

Chapter 5 described a large-scale study on seven well-known heart HCM-causing mutations to identify the molecular changes in the MyHC- $\beta$  motor that give rise to either early or late onset disease. This work is the key for understanding disease progression and identifying potential therapeutic targets for HCM. We initially hypothesised that early onset mutations would be more severe in their properties compared to late onset. Interestingly, we disproved our original hypothesis.

Whilst no clear distinction was observed between early and late mutations, a pattern of behaviour was observed based on the location of the mutation within the motor domain. As discussed previously, the converter domain is a hotspot for HCM mutations, and is critical for the swing of the myosin lever arm during force production. All three late onset and two of the four early onset mutations studied in Chapter 5 are located in the converter domain. These five mutations showed some distinct characteristics which were not observed in the two non-converter domain mutations. For example, all converter domain mutations had a lower actin-activated ATPase rate, a lower duty ratio, and a lower AMD state. As stated in Chapters 3 and 5, the AMD state represents the ADP-bound myosin head in a force-producing state bound to actin. A decrease in the AMD population will result in a decrease in the population of myosin heads strongly bound to actin in a force-producing state, suggesting a decrease in the ensemble force. Recent data shows that the myosin intrinsic force is little affected by adult-onset HCM converter mutations (Kawana et al. 2017). Taking together, these results suggest there exists a more complex mechanism by which mutations alter myosin activity or its regulation, leading to HCM pathology.

Recently, a hypothesis has been proposed that suggests the number of myosin heads in a sequestered state in cardiac filaments is altered during disease. Myosin can form an auto-inhibited state, termed the interacting-heads motif (IHM). It has been reported that when myosin filaments disassemble, the tail folds into three segments and the heads bend back and interact both with each other and with the folded tail (Lee et al. 2018). The activity of the two heads are highly inhibited; the so-called blocked head is prevented from binding to actin through its interaction with the other free head. The free head, in turn, has its ATPase activity inhibited by binding to the blocked head. It has been suggested that these head-head and head-tail interactions may be the basis of the super-relaxed (SRX) state of myosin (Stewart et al. 2010).

The work of Cooke and colleagues first hypothesised that myosin exists in three states with different nucleotide turnover lifetimes; active ( $1 \text{ s}^{-1}$ ), disordered relaxed ( $\sim 30 \text{ s}^{-1}$ ) and super relaxed ( $150 \text{ s}^{-1}$  in cardiac muscle fibres,  $\sim 300 \text{ s}^{-1}$  in skeletal muscle fibres). The super relaxed state (SRX) of myosin was first identified in single nucleotide turnover experiments on permeabilized, relaxed skeletal muscle fibres, which showed a biphasic decay in fluorescence intensity. The authors postulated that there exist two subpopulations of relaxed cross-bridges (disordered relaxed and super-relaxed) with ATP-turnover rates that differ by approximately a factor of 10. The two subpopulations were also observed in experiments performed on rabbit ventricular muscle fibres (Hooijman, Stewart, and Cooke 2011). Intriguingly, the proportion of SRX can be fully abolished in skeletal fibres upon activation of myosin heads, although this is not observed in cardiac muscle fibres (Hooijman, Stewart, and Cooke 2011). This suggests a subset of myosin molecules remain in the SRX even during activation of the muscle and thus may slightly reduce the total metabolic rate of working cardiac muscle. It should be noted that the definition of the SRX is the state of myosin with an extremely slow ATPase turnover rate; it is not defined as a folded-back state of myosin.

Both SRX and IHM are becoming increasingly discussed in the field. It has been suggested that hypercontractility may arise from an increase in the number of functionally accessible heads in the sarcomere for interaction with actin (Trivedi et al. 2018; Spudich 2019). It has been observed that a number of HCM-causing mutations are located close to the junction of the myosin S2 tail and the IHM. One of these mutations occur in an area of the “free” myosin head termed the cardiomyopathy loop, while others occur in the region of the S2 rod with which this loop interacts (Alamo et al. 2008). Mutations near this interface may destabilise the ordered structure of the thick filaments thereby reducing the proportion of SRX. Spudich and colleagues have also hypothesised how the number of available myosin heads available to interact with actin may lead to hypercontractility (Nag et al. 2017). They reported that myosin contains a relatively flat surface on the S1 domain which is a hot-spot for HCM mutations (Spudich 2015; Homburger et al. 2016). This surface has a positively charged cluster of arginine residues, all of which when mutated are causative of HCM (Homburger et al. 2016). This cluster was suggested to act as a binding interface for MyBP-C and the proximal S2 region of myosin (Spudich 2015; Spudich et al. 2016). The authors suggested that such binding interactions could sequester myosin heads in an ‘off-state,’ thereby regulating the number of myosin heads functionally accessible for interaction with actin. A primary effect of HCM mutations could be to weaken such associations, causing an increase in the number of heads available to bind to actin, thereby explaining the hypercontractility observed in HCM patients.



It is currently beyond the scope of our kinetic measurements to predict the number of myosin heads that may exist in the SRX. Similarly, the MUSICO programme does not take into account the proportion of myosin in a sequestered state. However, as discussed in 7.1, the ability to measure the  $K_3$  parameter would be crucial for elucidating the equilibrium between myosin heads in active and relaxed states. The myosin heads in the SRX would exist in the pre-stroke state, with ADP and Pi in the nucleotide pocket, before interaction with actin accelerates the ATPase activity releasing the heads out of the SRX. A shift in either the rate or equilibrium constant of this state could alter the amount of myosin that is able to form the SRX. Studies mentioned above indicate that HCM mutations may weaken the IHM, which would result in an increased number of active myosin heads. Measuring the  $K_3$  parameter would test this hypothesis.

The stopped-flow experiments described were performed with sS1 protein (the myosin motor domain with a single IQ domain and myosin ELC). This means that head-head and head-tail interactions of the IHM cannot occur, and their effects not observed. To address this, work should now focus on performing experiments with HMM. The presence of the S2 region would provide the myosin head with a platform to fold onto, and the dimeric structure would bring the two S1 heads into close proximity to interact. Adhikari et al have recently performed ATPase and *in vitro* motility experiments for 5 HCM mutations with HMM-like two-headed molecules (Adhikari et al. 2019). This is the first study to describe functional parameters of HCM mutations using HMM-like constructs. The H251N, D382Y and R719W mutations studied in Chapter 5 were included in the Adhikari study. They found that the mutations do indeed decrease the level of SRX and make more heads available for interaction with actin.

The stopped-flow experiments were performed with homogenous solutions of protein. Whilst this is not representative of the mixture of protein found in patient muscle fibres, this is required to understand the fundamental parameters of mutated protein. None of the mutations studied in Chapter 5 have been reported in homozygous patients, suggesting that homozygous mutations are incompatible with life. Patients will contain a mixture of both WT and mutated protein in their cardiomyocytes. As both genes are co-dominantly expressed, an equimolar ratio of WT and mutated protein would be expected. However, a study by Tripathi et al found that the ratios of five different HCM-causing MyHC- $\beta$  mutations showed an allelic imbalance at both the mRNA and protein level (Tripathi et al. 2011). Two of the mutations included in the study included R719W and R723G, which were analysed in Chapter 5. Both of these mutations accounted for 2/3 of total *MYH7* mRNA transcripts. It has been suggested that this is due to increase splicing efficacy, as the

mutations are located at hairpin structures at intron-exon boundaries (Tripathi et al. 2011). The kinetic properties of a myosin solution containing a combination of WT and mutated protein is yet to be elucidated.

As mutations are found in many regions within the motor domain, it is unlikely there is one single mechanism by which mutations cause disease. The question as to how the large number of reported mutations lead to the same phenotype remains a valid question. Robert-Paganin et al recently classified HCM and DCM mutations in *MYH7*, based on the resulting effects on the motor (Robert-Paganin, Auguin, and Houdusse 2018). The classification of the seven mutations studied in this thesis are summarised in Table 7.1. All 3 late onset mutations were described as destabilising the sequestered state destabilized due to effect on IHM contacts. All seven mutations had different resulting impairments on the protein. This again highlights that it is unlikely there exists a common mechanism for disease progression that arises from the presence of these mutations alone. The prediction of the H251N and the three late onset mutations affecting motor function is consistent with our observations. Whilst the Robert-Paganin study was comprehensive, many of the mutations included in the analysis are reported as VUS. This is true for the H251N, P710R and V763M early onset mutations that we characterised. Thus, caution must be taken to describe these mutations as causative of disease.

The study of MyHC- $\beta$  and its role in HCM has changed the field of myosin research from one of basic science to a relevant subject for clinical study. However, the field remains limited by the lack of protein in order to conduct large-scale studies on the molecular basis of disease and therapeutic target design. We attempted to address this issue in Chapter 6, as will be discussed below.

| <b>Mutation</b> | <b>Early or late onset?</b> | <b>Predicted effect of mutation</b>   | <b>Resulting impairment</b>  |
|-----------------|-----------------------------|---|--|
| H251N           | Early                       | Sequestered state destabilized due to effect on IHM contacts. Motor function altered  | Interaction with U50 linker within the transducer. May affect the motor transitions and the stability of the PPS state<br>Involved in stabilisation of the IHM motif |
| D382Y           | Early                       | Sequestered state destabilized by direct effect on IHM without impairment in motor activity                                 | Surface – no effect on motor function<br>(unless the tyrosine side chain gets buried and allosterically changes this actin-binding interface)                        |
| P710R           | Early                       | Sequestered state destabilized due to effect on PPS stability or off state formation. Motor function altered                | Alters the transitions of the SH1 helix and the stability of the primed lever arm –likely alters motor function<br>PPS stability affected                            |
| V763M           | Early                       | Protein stability likely altered as well as motor function possible effect on the off state if the PPS stability is altered | Destabilisation of the converter fold<br>Would affect function and the stability of the sequestered state  |
| R719W           | Late                        | Sequestered state destabilized due to effect on IHM contacts. Motor function altered  | Modifies the top-loop conformation<br>Small effect on compliance   |
| R723G           | Late                        | Sequestered state destabilized due to effect on IHM contacts. Motor function altered  | Change in top-loop conformation<br>Change in lever arm compliance  |
| G741R           | Late                        | Sequestered state destabilized due to effect on IHM contacts. Motor function altered  | No major effect on the compliance of the lever arm<br>Destabilised the converter at the top loop   |

**Table 7.1 Classification of the seven mutations studied in Chapter 6. PPS – pre-powerstroke. Data from (Robert-Paganin, Auguin, and Houdusse 2018).**

#### **7.4 Molecular features of the UNC-45 chaperone critical for binding and folding muscle myosin**

The fourth aim of this thesis was to improve the current recombinant myosin expression and production system. The importance of UNC-45 in myosin folding has been utilised to produce recombinant myosin over the past two decades. Winkelmann and colleagues demonstrated that muscle myosin requires a muscle environment to fold into a functional molecule (Srikakulam and Winkelmann 1999; Chow et al. 2002; Srikakulam and Winkelmann 2004). As shown by Price et al, skeletal muscle UNC-45 is expressed specifically in cardiac and skeletal muscle (Price et al. 2002). The current system to produce recombinant myosin uses an immortalised mouse myoblast cell line, called C2C12 (Resnicow et al. 2010). The C2C12 cell line differentiates rapidly upon hormonal treatment, forming contractile myotubes and produces characteristic muscle proteins. As the protein is being produced in a muscle environment, all necessary chaperones and folding factors are present to enable fully folded motor domain to be extracted.

The work of the Winkelmann and Leinwand labs revolutionised the field, as it became possible to study single myosin class II isoforms for the first time. Whilst Reggiani showed that a single muscle fibre typically expresses one myosin isoform, a muscle may consist of multiple fibre types (Bottinelli and Reggiani 2000), making the isolation of a single isoform difficult. The C2C12 cell methodology enabled the characterisation of seven of the class II isoforms (Deacon et al. 2012; Bloemink et al. 2013; Walklate et al. 2016). In Chapter 3, we characterised another developmental class II isoform; MyHC-Peri. Despite the achievements of this production system, there are limitations. Firstly, the process is time consuming. The time from viral expression to protein purification is typically three months. Secondly, the protocol requires specialist equipment and expertise; a methodology that uses standard lab chemicals would be advantageous. Furthermore, little protein is generated; typically, 1 mg from a 1 litre culture. To address these issues, and utilise the information we have about the role of UNC-45 in myosin folding, colleagues in the Clausen lab in Vienna attempted to produce sarcomeric myosin using a standard baculoviral expression system in a non-muscle environment.

Using the High Five insect cell line and baculovirus expression system, the motor domain of a sarcomeric *C. elegans* myosin was successfully produced. Baculovirus has been used previously to produce smooth non-muscle myosins, but this is the first time it has been used to produce a sarcomeric myosin. The gene for the body wall myosin, MHC-B,

was co-expressed with the gene for UNC-45. The expression and purification system were able to generate 15 mg protein per litre of insect cell culture. This is almost 15x the yield of that obtained from the C2C12 system. Not only was the protein produced folded and soluble, it was also fully active. We confirmed this by stopped-flow spectroscopy to characterise the activity of the protein. This characterisation is novel, as no kinetic measurements have been performed on a *C. elegans* myosin previously. The data in Supplementary Table 1 of Chapter 6 demonstrates that the *C. elegans* MHC-B has similar properties to the slow-type MyHC- $\beta$ . The two proteins had a similar affinity for actin ( $K_A$ ), second order rate constant of ATP binding to S1 ( $K_1k_{+2}$ ) and actin.S1 ( $K'_1k'_{+2}$ ), and ATP affinity for acto.S1 ( $1/K'_1$ ). The major differences were the ADP affinity for S1 ( $K_6K_7$ ) value - which was 14-fold weaker - and the ADP affinity for actin.S1 ( $K'_6K'_7$ ) value, which was 2-fold weaker. The ADP release rate from acto.S1 ( $k'_{+6}$ ) was over three times faster, with a value of  $189\text{ s}^{-1}$ , compared to  $59\text{ s}^{-1}$  for the MyHC- $\beta$  (Deacon et al. 2012; Bloemink et al. 2013). This is rather surprising, due to the very similar nucleotide binding sites between the two proteins. To validate the results of the recombinant MHC-B, a characterisation of endogenous MHC-B purified from *C. elegans* would be required.

It is worth noting that the MHC-B construct was expressed in the absence of any IQ domains, and hence light chains, whereas the MyHC- $\beta$  was co-expressed with the human essential light chain, MYL3. However, this is unlikely to cause the differences in ADP affinity or ADP off-rate reported. Deacon et al compared MyHC- $\beta$  with 1 and 2 light chains (Deacon et al. 2012), and saw no significant differences in these parameters. Similarly, Woodward et al demonstrated that removal of the light chain in *Dictyostelium discoideum* myosin did not alter enzymatic properties of the motor domain (Woodward, Geeves, and Manstein 1995). As mentioned above, Lowey et al showed with rabbit skeletal S1 that the absence of light chains altered velocity but not ATPase activity (Lowey, Waller, and Trybus 1993b). Therefore, it is unlikely that the lack of IQ domains and light chains altered the kinetic properties of the purified MHC-B.

The limitation of the production system is the so-far inability to produce mammalian myosin. Attempts to produce the motor domain of human MyHC- $\beta$  resulted in successful expression of the gene, but when purified the protein aggregated and no-soluble myosin was present. To address this, a chaperone screen using a proteomics approach could be employed to identify chaperones that are required for mammalian myosin folding that are not present in simpler model systems, such as *C. elegans*. It could also be that the recombinant protein is lacking in PTMs that would exist if the myosin was produced in a muscle environment – this could be critical for correct myosin folding, and has yet to be

explored. Another potential use of the insect cell system would be the ability to produce HMM, rather than S1. As discussed above, the HCM mutations studied to date are often conducted on S1, which is not representative of the double headed conformation that exists within a sarcomere. Work to produce HMM using the insect cell system is not presented here, but is on-going in the Clausen laboratory.

An inherent limitation in characterising the substrate-targeting mechanism of UNC-45 thus far has been the lack of sufficient quantities of its substrate (due to reasons outlined above). The higher protein yields from the insect cell system therefore enabled the importance of various folding factors in myosin folding to be explored. Soluble myosin was only obtained during co-expression with UNC-45, not with Hsp70 or Hsp90, highlighting the essential requirement of UNC-45 even in the absence of its co-chaperones. Because of the high protein yield we propose that it would also be easier to obtain high resolution crystal structures of human cardiac myosins in multiple states, attempts of which have yet to produce such structures. This is also important for the elucidation of the previously mentioned SRX state of myosin, which has yet to be crystallised. Obtaining a crystal structure of the SRX state is challenging due to the requirement of the sample containing intact filament. A technique such as cryo-electron microscopy is more likely to reveal the 3D-structure of such a complex. This technique would still require HMM constructs, so that the sequestered heads folded back onto the myosin tail can be resolved.

Whilst no mammalian myosin has been expressed, as noted above, the work on HCM could benefit from a model organism. A DALI search (a database for comparing 3D structures of proteins) found that of 36 related protein structures in the Protein Data Bank, the human MyHC- $\beta$  myosin was the closest structural homolog of the MHC-B structure. The two motor domains are 59% identical and 72% similar. The work of Bernstein and colleagues use *Drosophila melanogaster* as a model for cardiomyopathy, which they have successfully used to characterise the K146N and R2249Q HCM mutations (Kronert et al. 2018; Bell et al. 2019). Since *D. melanogaster* is 58% identical to human MyHC- $\beta$ , which is comparable to the *C. elegans* MHC-B, and because *C. elegans* is a widely used genetic model for muscle biology, we propose that *C. elegans* could be used as a model organism for both myosin folding and disease. To test the suitability of *C. elegans* as a model organism, a well-studied HCM-causing mutation, such as R403Q or R453C, could be inserted into the MHC-B, and observe if the same kinetic parameters are changed compared to WT. Further, the role of UNC-45 in cardiomyopathies could be explored using this system. Melkani et al showed the importance of UNC-45 in maintaining cardiac contractility during remodelling of the myocardium in fly heart muscle (Melkani et al. 2011).

The study showed that UNC-45 knockdown in *Drosophila* heart leads to conditions similar to cardiomyopathies. The precise mechanism that generates this phenotype is not yet fully understood.

An interesting question that still remains is how the UNC-45b isoform is specific for myosin, compared to the more generic UNC-45a. The two isoforms have a 57% sequence homology. Studying the isoform-specific activities of UNC-45 and their regulation will be critical to enhance our understanding of myosin chaperone function in health and disease. It is also currently unknown if they are differentially regulated. Another interesting question is whether or not the assembly of UNC-45 oligomers regulates chaperone activity. The equilibrium between monomeric and oligomeric UNC-45 has yet to be defined, and transition between the two states may direct different chaperone activities. Whether this equilibrium is altered when a muscle undergoes stress may further yield insights into the protective role of UNC-45 in stress response.

## **7.5 Concluding remarks and future perspectives**

The work of this thesis has elucidated how sarcomeric myosins have fine-tuned their properties to give rise to different physiological functions. Disruption of these processes in diseased-states is crucial for understanding the mechanism of disease onset and progression. There are still a number of interesting questions that remain within the fields of muscle physiology and myosin biochemistry. I have outlined below a few areas I think will shape these fields in the coming years.

Fundamental to myosin biochemistry is the mechanochemical cycle, which is conserved across myosin classes. As discussed in 1.6.2, force generation during the working stroke of the cross-bridge cycle includes phosphate release and movement of the lever arm, although the precise order of these two events remains under debate. It is also unknown whether this order varies between different classes of myosin. Elucidating the precise process of force generation remains a challenge in the field.

The design and testing of small molecules or MyHC- $\beta$  inhibitors to treat HCM is required to advance the current therapeutic options available to patients. It is unlikely there is one single modulator of MyHC- $\beta$  that could successfully treat all cases of HCM, due to the array of different impairments reported in the protein (see Table 7.1). The phenomenon of myosin in a SRX may pose a potential mechanism to target for both prevention of disease progression and treatment of existing cardiac conditions. The structural state of the SRX is yet to be elucidated. Whilst not only advancing our potential understanding of cardiac disease pathology, it will yield insights into fundamental thick filament behaviour and regulation.

The IHM and SRX state of myosin heads which are unable to bind to actin and hydrolyse ATP raises the question of how the motors can sense the state of the thin filament during activation. A thick-filament mechanosensing mechanism in skeletal muscle has been proposed (Linari et al. 2015), whereby a small fraction of constitutively active motors allows the muscle to respond immediately to calcium activation and initiates a positive feedback loop. Such a mechanism in cardiac muscle may represent a potential target for therapeutic intervention in disease.



## **8. Non-publication References**

- Ackermann, M.A. and Kontrogianni-Konstantopoulos, A., 2011. "Myosin Binding Protein-C: A Regulator of Actomyosin Interaction in Striated Muscle." *Journal of Biomedicine and Biotechnology* 2011: 1–9.
- Adamek, N., Coluccio, L.M. and Geeves, M.A., 2008. "Calcium Sensitivity of the Cross-Bridge Cycle of Myo1c, the Adaptation Motor in the Inner Ear." *Proceedings of the National Academy of Sciences* 105 (15): 5710–15.
- Adhikari, A.S., Kooiker, K.B., Sarkar, S.S., Liu, C., Bernstein, D., Spudich, J.A. and Ruppel, K.M., 2016. "Early-Onset Hypertrophic Cardiomyopathy Mutations Significantly Increase the Velocity, Force, and Actin-Activated ATPase Activity of Human  $\beta$ -Cardiac Myosin." *Cell Reports* 17 (11): 2857–64.
- Adhikari, A.S., Trivedi, D.V., Sarkar, S.S., Song, D., Kooiker, K.B., Bernstein, D., Spudich, J.A. and Ruppel, K.M., 2019. " $\beta$ -Cardiac Myosin Hypertrophic Cardiomyopathy Mutations Release Sequestered Heads and Increase Enzymatic Activity." *Nature Communications* 10 (1): 2685.
- Agarkova, I. and Perriard, J.C., 2005. "The M-Band: An Elastic Web That Crosslinks Thick Filaments in the Center of the Sarcomere." *Trends in Cell Biology* 15 (9): 477–85.
- Agbulut, O., Noirez, P., Beaumont, F. and Butler-Browne, C., 2003. "Myosin Heavy Chain Isoforms in Postnatal Muscle Development of Mice." *Biology of the Cell* 95: 399–406.
- Aksel, T., ChoeYu, E., Sutton, S., Ruppel, K.M., and Spudich, J.A., 2015. "Ensemble Force Changes That Result from Human Cardiac Myosin Mutations and a Small-Molecule Effector." *Cell Reports* 11 (6): 910–20.
- AL-Khayat, H. A., Kensler, R.W., Squire, J.M., Marston, S.B and Morris, E.P., 2013. "Atomic Model of the Human Cardiac Muscle Myosin Filament." *Proceedings of the National Academy of Sciences* 110 (1): 318–23.
- Anan, R, Greve, G., Thierfelder, L., Watkins, H., McKenna, W.J., Solomon, S., Vecchio, C., Shono, H., Nakao, S. and Tanaka, H., 1994. "Prognostic Implications of Novel Beta Cardiac Myosin Heavy Chain Gene Mutations That Cause Familial Hypertrophic Cardiomyopathy." *Journal of Clinical Investigation* 93 (1): 280–85.
- Ao., Wanyuan. and Pilgrim., 2000. "Caenorhabditis Elegans Unc-45 Is a Component of Muscle Thick Filaments and Colocalizes with Myosin Heavy Chain B, but Not Myosin Heavy Chain A." *The Journal of Cell Biology* 148 (2): 375–84.
- Attanapola., Sheran, L, Alexander, C.J. and Mulvihill, D.P., 2009. "Ste20-Kinase-Dependent TEDS-Site Phosphorylation Modulates the Dynamic Localisation and Endocytic Function of the Fission Yeast Class I Myosin, Myo1." *Journal of Cell Science* 122 (Pt 21): 3856–61.
- Bagshaw, C.R., 2013a. "Stopped-Flow Techniques." In *Encyclopedia of Biophysics*, 2460–66. Berlin, Heidelberg: Springer Berlin Heidelberg.
- Bagshaw, C.R., 2013b. "Transient-State Kinetic Methods." In *Encyclopedia of Biophysics*, 2638–44. Berlin, Heidelberg: Springer Berlin Heidelberg.
- Bähler, M. and Rhoads, A., 2002. "Calmodulin Signaling via the IQ Motif." *FEBS Letters* 513 (1): 107–13.

- Barbet, J.P., Thornell, L.E. and Butler-Browne, G.S., 1991. "Immunocytochemical Characterisation of Two Generations of Fibers during the Development of the Human Quadriceps Muscle." *Mechanisms of Development* 35: 3–11.
- Barral, J.M., Hutagalung, A.H., Brinker, A., Hartl, F.U. and Epstein, H.F., 2002. "Role of the Myosin Assembly Protein UNC-45 as a Molecular Chaperone for Myosin." *Science* 295 (5555): 669–71.
- Barral, J.M., Bauer, C.C., Ortiz, I. and Epstein, H.F., 1998. "Unc-45 Mutations in *Caenorhabditis Elegans* Implicate a CRO1/She4p-like Domain in Myosin Assembly." *The Journal of Cell Biology* 143 (5): 1215–25.
- Batters, C., Arthur, C.P., Lin, A., Porter, J., Geeves, M.A., Milligan, R.A., Molloy, J.E. and Coluccio, L., 2004. "Myo1c Is Designed for the Adaptation Response in the Inner Ear." *The EMBO Journal* 23 (7): 1433–40.
- Bazzaro, M., Santillan, A., Lin, Z., Tang, T., Lee, M.K., Bristow, R.E., Shih, L.M. and Roden, R.B.S., 2007. "Myosin II Co-Chaperone General Cell UNC-45 Overexpression Is Associated with Ovarian Cancer, Rapid Proliferation, and Motility." *The American Journal of Pathology* 171 (5): 1640–49.
- Bell, K.M., Kronert, W.A., Huang, A., Bernstein, S.I. and Swank, D.M., 2019. "The R249Q Hypertrophic Cardiomyopathy Myosin Mutation Decreases Contractility in *Drosophila* by Impeding Force Production." *The Journal of Physiology* 597 (9): 2403–20.
- Bell, M.L., Buvoli, M. and Leinwand, L.A., 2010. "Uncoupling of Expression of an Intronic MicroRNA and Its Myosin Host Gene by Exon Skipping." *Molecular and Cellular Biology* 30 (8): 1937–45.
- Bennett, P., Craig, R., Starr, R. and Offer, G., 1986. "The Ultrastructural Location of C-Protein, X-Protein and H-Protein in Rabbit Muscle." *Journal of Muscle Research and Cell Motility* 7 (6): 550–67.
- Bloemink, M.J., Deacon, J., Resnicow, D., Leinwand, L.A., and Geeves, M.A., 2013. "The Superfast Human Extraocular Myosin Is Kinetically Distinct from the Fast Skeletal IIa, IIb, and IIc Isoforms." *The Journal of Biological Chemistry* 288 (38): 27469–79.
- Bloemink, M.J., Adamek, N., Reggiani, C. and Geeves, M.A., 2007. "Kinetic Analysis of the Slow Skeletal Myosin MHC-1 Isoform from Bovine Masseter Muscle." *Journal of Molecular Biology* 373 (5): 1184–97.
- Bloemink, M.J. and Geeves, M.A., 2011. "Shaking the Myosin Family Tree: Biochemical Kinetics Defines Four Types of Myosin Motor." *Seminars in Cell and Developmental Biology* 22 (9): 961–7.
- Bloemink, M.J., Deacon, J.C., Langer, S., Vera, C., Combs, A., Leinwand, L.A. and Geeves, M.A., 2014. "The Hypertrophic Cardiomyopathy Myosin Mutation R453C Alters ATP Binding and Hydrolysis of Human Cardiac  $\beta$ -Myosin." *Journal of Biological Chemistry* 289 (8): 5158–67.
- Bottinelli, R., Canepari, M., Pellegrino, M.A. and Reggiani, C., 1996. "Force-Velocity Properties of Human Skeletal Muscle Fibres: Myosin Heavy Chain Isoform and Temperature Dependence." *The Journal of Physiology* 495 (Pt 2): 573.
- Bottinelli, R. and Reggiani, C., 2000. "Human Skeletal Muscle Fibres: Molecular and Functional Diversity." *Progress in Biophysics and Molecular Biology* 73 (2–4): 195–262.
- Briggs, M.M. and Schachat, F., 2000. "Early Specialization of the Superfast Myosin in Extraocular and Laryngeal Muscles." *Journal of Experimental Biology* 203: 2485–94.

- Burkholder, T. J and Lieber. R. L., 2001. "Sarcomere Length Operating Range of Vertebrate Muscles during Movement." *Journal of Experimental Biology* 204 (9): 1529–36.
- Buvoli, M., Hamady, M., Leinwand, L.A. and Knight, R., 2008. "Bioinformatics Assessment of  $\beta$ -Myosin Mutations Reveals Myosin's High Sensitivity to Mutations." *Trends in Cardiovascular Medicine* 18 (4): 141–49.
- Cahill, T.J., Ashrafian, H. and Watkins, H., 2013. "Genetic Cardiomyopathies Causing Heart Failure." *Circulation Research* 113 (6): 660–75.
- Cavalier-Smith, T., 2002. "The Phagotrophic Origin of Eukaryotes and Phylogenetic Classification of Protozoa." *International Journal of Systematic and Evolutionary Microbiology* 52 (2): 297–354.
- Chadli, A., Graham, J.D., Abel, M.G., Jackson, T.A., Gordon, D.F., Wood, W.M., Felts, S.J., Horwitz, K.B. and Toft, D., 2006. "GCUNC-45 Is a Novel Regulator for the Progesterone Receptor/Hsp90 Chaperoning Pathway." *Molecular and Cellular Biology* 26 (5): 1722–30.
- Chadli, A., Bruinsma, E.S., Stensgard, B. and Toft, D., 2008. "Analysis of Hsp90 Cochaperone Interactions Reveals a Novel Mechanism for TPR Protein Recognition †." *Biochemistry* 47 (9): 2850–57.
- Chadli, A., Felts, S.J. and Toft, D.O., 2008. "GCUNC45 Is the First Hsp90 Co-Chaperone to Show  $\alpha/\beta$  Isoform Specificity." *Journal of Biological Chemistry* 283 (15): 9509–12.
- Cho, M., Webster, S.G. and Blau, H.M., 1993. "Evidence for Myoblast-Extrinsic Regulation of Slow Myosin Heavy Chain Expression during Muscle Fiber Formation in Embryonic Development." *Journal of Cell Biology* 121: 795–810.
- Chung, C.S., Bogomolovas, J., Gasch, A., Hidalgo, C.G., Labeit, S. and Granzier, H.L., 2011. "Titin-Actin Interaction: PEVK-Actin-Based Viscosity in a Large Animal." *Journal of Biomedicine & Biotechnology* 2011: 310791.
- Close, R.I. and Luff, A.R., 1974. "Dynamic Properties of Inferior Rectus Muscle of the Rat." *The Journal of Physiology* 236 (2): 259–70.
- Colan, S.D., Lipshultz, S.E., Lowe, A.M., Sleeper, L.A., Messere, J., Cox, G.F., Lurie, P.R., Orav, E.J. and Towbin, J.A., 2007. "Epidemiology and Cause-Specific Outcome of Hypertrophic Cardiomyopathy in Children: Findings from the Pediatric Cardiomyopathy Registry." *Circulation* 115 (6): 773–81.
- Colegrave, M., and Peckham, M., 2014. "Structural Implications of  $\beta$ -Cardiac Myosin Heavy Chain Mutations in Human Disease." *The Anatomical Record* 297 (9): 1670–80.
- Condon, K., Silberstein, L., Blau, H.M. and Thompson, W.J., 1990. "Development of Muscle Fiber Types in the Prenatal Rat Hindlimb." *Developmental Biology* 138 (2): 256–74.
- Craig, R. and G. Offer. 1976. "The Location of C Protein in Rabbit Skeletal Muscle." *Proceedings of the Royal Society of London - Biological Sciences* 192 (1109): 451–61.
- Cremonesi, C.R. and Geeves, M.A., 1998. "Interaction of Actin and ADP with the Head Domain of Smooth Muscle Myosin: Implications for Strain-Dependent ADP Release in Smooth Muscle." *Biochemistry* 37 (7): 1969–78.
- Criddle, A.H., Geeves, M.A. and Jeffries, T., 1985. "The Use of Actin Labelled with N-(1-Pyrenyl)Iodoacetamide to Study the Interaction of Actin with Myosin Subfragments and Troponin/Tropomyosin." *The Biochemical Journal* 232 (2): 343–49.

- Das, A.K., Cohen, P.W. and Barford, D., 1998. "The Structure of the Tetratricopeptide Repeats of Protein Phosphatase 5: Implications for TPR-Mediated Protein-Protein Interactions." *The EMBO Journal* 17 (5): 1192–99.
- Deacon, J.C., Bloemink, M.J., Rezavandi, H., Geeves, M.A., and Leinwand, L.A., 2012. "Erratum to: Identification of Functional Differences between Recombinant Human  $\alpha$  and  $\beta$  Cardiac Myosin Motors." *Cellular and Molecular Life Sciences* : CMLS 69 (24): 4239–55.
- De La Cruz, E.M., Wells, A.L., Rosenfeld, S.S., Ostap, E.M. and Sweeney, H.L., 1999. "The Kinetic Mechanism of Myosin V." *Proceedings of the National Academy of Sciences of the United States of America* 96 (24): 13726–31.
- De La Cruz, E.M., and Ostap, E.M., 2009. "Kinetic and Equilibrium Analysis of the Myosin ATPase." In *Methods in Enzymology; Biothermodynamics*, 455:157–92.
- De La Cruz, E.M., Ostap, E.M. and Sweeney, H.L., 2001. "Kinetic Mechanism and Regulation of Myosin VI." *Journal of Biological Chemistry* 276 (34): 32373–81.
- De La Cruz, E.M. and Ostap, E.M., 2004. "Relating Biochemistry and Function in the Myosin Superfamily." *Current Opinion in Cell Biology* 16 (1): 61–67.
- DeNardi, C., Ausoni, S., Moretti, P., Gorza, L., Velleca, M., Buckingham, M. and Schiaffino, S., 1993. "Type 2X-Myosin Heavy Chain Is Coded by a Muscle Fiber Type-Specific and Developmentally Regulated Gene." *Journal of Biological Chemistry* 268 (4): 823–35.
- Dominguez, R., Freyzon, Y., Trybus, K.M. and Cohen., 1998. "Crystal Structure of a Vertebrate Smooth Muscle Myosin Motor Domain and Its Complex with the Essential Light Chain: Visualization of the Pre-Power Stroke State." *Cell* 94 (5): 559–71.
- Draeger, A., Weeds, A.G. and Fitzsimons, R.B., 1987. "Primary, Secondary and Tertiary Myotubes in Developing Skeletal Muscle: A New Approach to the Analysis of Human Myogenesis." *Journal of the Neurological Sciences* 81: 19–43.
- Du, S.J., Li, H., Bian, Y. and Zhong, Y., 2008. "Heat-Shock Protein 90 1 Is Required for Organized Myofibril Assembly in Skeletal Muscles of Zebrafish Embryos." *Proceedings of the National Academy of Sciences* 105 (2): 554–59.
- Dugina, V.B., Shagieva, G.S. and Kopnin, P.B., 2019. "Biological Role of Actin Isoforms in Mammalian Cells." *Biochemistry (Moscow)* 84 (6): 583–92.
- Durrwang, U., Fujita-Becker, S., Erent, M., Kull, F.J., Tsiavaliaris, G., Geeves, M.A. and Manstein, D.J., 2006. "Dictyostelium Myosin-IE Is a Fast Molecular Motor Involved in Phagocytosis." *Journal of Cell Science* 119 (3): 550–58.
- Ecob-Prince, M., Hill, M. and Brown, W., 1989. "Immunocytochemical Demonstration of Myosin Heavy Chain Expression in Human Muscle." *Journal of the Neurological Sciences* 91: 71–78.
- Enjuto, M., Francino, A., Navarro-López, F., Viles, D., Paré, J.C. and Ballesta, A.M., 2000. "Malignant Hypertrophic Cardiomyopathy Caused by the Arg723Gly Mutation in  $\beta$ -Myosin Heavy Chain Gene." *Journal of Molecular and Cellular Cardiology* 32 (12): 2307–13.
- Ennion, S., Pereira, J.S., Sargeant, A.J., Young, A. and Goldspink, G., 1995. "Characterization of Human Skeletal Muscle Fibres According to the Myosin Heavy Chains They Express." *Journal of Muscle Research and Cell Motility* 16 (1): 35–43.

- van den Ent, F., Amos, L.A. and Löwe, J., 2001. "Prokaryotic Origin of the Actin Cytoskeleton." *Nature* 413 (6851): 39–44.
- Epstein, H.F. and Thomson, J.N., 1974. "Temperature-Sensitive Mutation Affecting Myofilament Assembly in *Caenorhabditis Elegans*." *Nature* 250 (5467): 579–80.
- Etard, C., Behra, M., Fischer, N., Hutcheson, D., Geisler, R. and Strähle, U., 2007. "The UCS Factor Steif/Unc-45b Interacts with the Heat Shock Protein Hsp90a during Myofibrillogenesis." *Developmental Biology* 308 (1): 133–43.
- Etard, C., Roostalu, U. and Strähle, U., 2008. "Shuttling of the Chaperones Unc45b and Hsp90a between the A Band and the Z Line of the Myofibril." *The Journal of Cell Biology* 180 (6): 1163–75.
- Etheridge, L., Diorio, P. and Sagerström, C.G., 2002. "A Zebrafish Unc-45 -Related Gene Expressed during Muscle Development." *Developmental Dynamics* 224 (4): 457–60.
- Fananapazir, L., Dalakas, M.C., Cyran, F., Cohn, G. and Epstein, N.D., 1993. "Missense Mutations in the Beta-Myosin Heavy-Chain Gene Cause Central Core Disease in Hypertrophic Cardiomyopathy." *Proceedings of the National Academy of Sciences* 90 (9): 3993–97.
- Fatkin, D. and Graham, R.M., 2002. "Molecular Mechanisms of Inherited Cardiomyopathies." *Physiological Reviews* 82 (4): 945–80.
- Fenwick, A.J., Wood, A.M. and Tanner, B.C.W., 2017. "Effects of Cross-Bridge Compliance on the Force-Velocity Relationship and Muscle Power Output." Edited by Daniel A Beard. *PloS One* 12 (12): e0190335.
- Fewell, J.G., Hewett, T.E., Sanbe, A., Klevitsky, R., Hayes, E., Warshaw, D., Maughan, D. and Robbins, J., 1998. "Functional Significance of Cardiac Myosin Essential Light Chain Isoform Switching in Transgenic Mice." *The Journal of Clinical Investigation* 101 (12): 2630–39.
- Flashman, E., Redwood, C., Moolman-Smook, J. and Watkins, H., 2004. "Cardiac Myosin Binding Protein C: Its Role in Physiology and Disease." *Circulation Research*.
- Franklin, A.J., Baxley, T., Kobayashi, T. and Chalovich, J.M., 2012. "The C-Terminus of Troponin T Is Essential for Maintaining the Inactive State of Regulated Actin." *Biophysical Journal* 102 (11): 2536–44.
- Fratev, F., Sónsdóttir, S.O. and Pajeva, I., 2013. "Structural Insight into the UNC-45-Myosin Complex." *Proteins: Structure, Function, and Bioinformatics* 81 (7): 1212–21.
- Freiburg, A. and Gautel, M., 1996. "A Molecular Map of the Interactions between Titin and Myosin-Binding Protein C. Implications for Sarcomeric Assembly in Familial Hypertrophic Cardiomyopathy." *European Journal of Biochemistry* 235: 317–23.
- Fujita-Becker, S., Dürrwang, U., Erent, M., Clark, R.J., Geeves, M.A. and Manstein, D.J., 2005. "Changes in M<sup>2+</sup> Ion Concentration and Heavy Chain Phosphorylation Regulate the Motor Activity of a Class I Myosin." *Journal of Biological Chemistry* 280 (7): 6064–71.
- Gaiser, A.M., Kaiser, C.J.O., Haslbeck, V. and Richter, K., 2011. "Downregulation of the Hsp90 System Causes Defects in Muscle Cells of *Caenorhabditis Elegans*." Edited by Ellen A. A. Nollen. *PLoS ONE* 6 (9): e25485.
- Garrels, J.I. and Gibson, W., 1976. "Identification and Characterization of Multiple Forms of Actin." *Cell* 9 (4 PT 2): 793–805.

Gazda, L., Pokrzywa, W., Hellerschmied, D., Löwe, T., Forné, I., Mueller-Planitz, F., Hoppe, T. and Clausen, T., 2013. "The Myosin Chaperone UNC-45 Is Organized in Tandem Modules to Support Myofilament Formation in *C. Elegans*." *Cell* 152 (1–2): 183–95.

Geach, T.J. and Zimmerman, L.B., 2010. "Paralysis and Delayed Z-Disc Formation in the *Xenopus Tropicalis* Unc45b Mutant Dicky Ticker." *BMC Developmental Biology* 10 (1): 75.

Geeves, M.A., edorov, R. and Manstein, D.J., 2005. "Molecular Mechanism of Actomyosin-Based Motility." *Cellular and Molecular Life Sciences* 62: 1462–77.

Geeves, M.A. and Holmes, K.C., 2005. "The Molecular Mechanism of Muscle Contraction." In *Advances in Protein Chemistry*, 71:161–93.

Geisterfer-Lowrance, A.A.T., Kass, S., Tanigawa, G., Vosberg, H.P., McKenna, W., Seidman, C.E. and Seidman, J.G., 1990. "A Molecular Basis for Familial Hypertrophic Cardiomyopathy: A  $\beta$  Cardiac Myosin Heavy Chain Gene Missense Mutation." *Cell* 62 (5): 999–1006.

Gergely, J., Gouvea, M.A. and Karibian, D., 1955. "Fragmentation of Myosin by Chymotrypsin." *The Journal of Biological Chemistry* 212 (1): 165–77.

Gilbert, R., Cohen, J.A., Pardo, S., Basu, A. and Fischman D.A., 1999. "Identification of the A-Band Localization Domain of Myosin Binding Proteins C and H (MyBP-C, MyBP-H) in Skeletal Muscle." *Journal of Cell Science* 112 ( Pt 1) (January): 69–79.

Goodson, H.V. and Spudich, J.A., 2006. "Molecular Evolution of the Myosin Family: Relationships Derived from Comparisons of Amino Acid Sequences." *Proceedings of the National Academy of Sciences* 90 (2): 659–63.

Gordon, A.M., Homsher, E. and Regnier, M., 2000. "Regulation of Contraction in Striated Muscle." *Physiological Reviews* 80 (2): 853–924.

Graceffa, P. and Dominguez, R., 2003. "Crystal Structure of Monomeric Actin in the ATP State." *Journal of Biological Chemistry* 278 (36): 34172–80.

Greaser, M.L. and Gergely, J., 1973. "Purification and Properties of the Components from Troponin." *The Journal of Biological Chemistry* 248 (6): 2125–33.

Greber-Platzer, S., Marx, M., Fleischmann, C., Suppan, C., Dobner, M. and Wimmer M., 2001. "Beta-Myosin Heavy Chain Gene Mutations and Hypertrophic Cardiomyopathy in Austrian Children." *Journal of Molecular and Cellular Cardiology* 33 (1): 141–48.

Greenberg, M.J., Shuman, H. and Ostap, E.M., 2014. "Inherent Force-Dependent Properties of  $\beta$  - Cardiac Myosin Contribute to the Force-Velocity Relationship of Cardiac Muscle." *Biophysical Journal* 107 (12): L41–44.

Gruen, M. and Gautel, M., 1999. "Mutations in Beta-Myosin S2 That Cause Familial Hypertrophic Cardiomyopathy (FHC) Abolish the Interaction with the Regulatory Domain of Myosin-Binding Protein-C." *Journal of Molecular Biology* 286 (3): 933–49.

Guo, B., Gurel, P.S., Shu, R., Higgs, H.N., Pellegrini, M. and Mierke, D.F., 2014. "Monitoring ATP Hydrolysis and ATPase Inhibitor Screening Using 1H NMR." *Chemical Communications* 50 (81): 12037–39.

Harridge, S.D., Bottinelli, R., Canepari, M., Pellegrino, M.A., Reggiani, C., Esbjörnsson, M. and Saltin, B., 1996. "Whole-Muscle and Single-Fibre Contractile Properties and Myosin Heavy Chain Isoforms in Humans." *Pflugers Archiv : European Journal of Physiology* 432 (5): 913–20.

- Hartzell, H.C., 1985. "Effects of Phosphorylated and Unphosphorylated C-Protein on Cardiac Actomyosin ATPase." *Journal of Molecular Biology* 186 (1): 185–95.
- Harvey, PA. and Leinwand, L.A., 2011. "Cellular Mechanisms of Cardiomyopathy." *Journal of Cell Biology* 194 (3): 355–65.
- Hawkins, T.A., Haramis, A.P., Etard, C., Prodromou, C., Vaughan, C.K., Ashworth, R., Ray, S., et al. 2008. "The ATPase-Dependent Chaperoning Activity of Hsp90a Regulates Thick Filament Formation and Integration during Skeletal Muscle Myofibrillogenesis." *Development* 135 (6): 1147–56.
- Heeley, D.H., Belknap, B. and White, H.D., 2002. "Mechanism of Regulation of Phosphate Dissociation from Actomyosin-ADP-Pi by Thin Filament Proteins." *Proceedings of the National Academy of Sciences* 99 (26): 16731–36.
- Heissler, S.M. and Sellers J.R., 2016. "Kinetic Adaptations of Myosins for Their Diverse Cellular Functions." *Traffic (Copenhagen, Denmark)* 17 (8): 839–59.
- Hellerschmied, D. and Clausen, T., 2014. "Myosin Chaperones." *Current Opinion in Structural Biology* 25 (100): 9–15.
- Henderson, C.A. and Gregorio, C., 2015. "Dynamics of Actin in the Heart: Defining Thin Filament Length." In *Cardiac Cytoarchitecture: How to Maintain a Working Heart*, 71–88.
- Herron, T.J. and McDonald, K.S., 2002. "Small Amounts of Alpha-Myosin Heavy Chain Isoform Expression Significantly Increase Power Output of Rat Cardiac Myocyte Fragments." *Circulation Research* 90 (11): 1150–52.
- Ho, C.Y., López, B., Coelho-Filho, O.R., Lakdawala, N.K., Cirino, A.L., Jarolim, P., Kwong, R., et al. 2010. "Myocardial Fibrosis as an Early Manifestation of Hypertrophic Cardiomyopathy." *New England Journal of Medicine* 363 (6): 552–63.
- Ho, C.Y., Sweitzer, N.K., McDonough, B., Maron, B.J., Casey, S.A., Seidman, J.G., Seidman, C.E. and Solomon, S.D., 2002. "Assessment of Diastolic Function With Doppler Tissue Imaging to Predict Genotype in Preclinical Hypertrophic Cardiomyopathy." *Circulation* 105 (25): 2992–97.
- Hodge, T. and Cope, M.J., 2000. "A Myosin Family Tree." *Journal of Cell Science* 113 Pt 19 (October): 3353–54.
- Homburger, J.R., Green, E.M., Caleshu, C., Munitha, S., Taylor, R.E., Ruppel, K.M., Metpally, R.P.R., et al. 2016. "Multidimensional Structure-Function Relationships in Human  $\beta$ -Cardiac Myosin from Population-Scale Genetic Variation." *Proceedings of the National Academy of Sciences* 113 (24): 6701–6.
- Homsher, E., Wang, F. and Sellers, J.R., 1992. "Factors Affecting Movement of F-Actin Filaments Propelled by Skeletal Muscle Heavy Meromyosin." *American Journal of Physiology* 263 (3 Pt 1): 741–23. <https://doi.org/10.1152/ajpcell.1992.262.3.C714>.
- Hooijman, P., Stewart, M.A. and Cooke, R., 2011. "A New State of Cardiac Myosin with Very Slow ATP Turnover: A Potential Cardioprotective Mechanism in the Heart." *Biophysical Journal* 100 (8): 1969–76.
- Hooper, S.L and Thuma, J.B., 2005. "Invertebrate Muscles: Muscle Specific Genes and Proteins." *Physiological Reviews* 85 (3): 1001–60.

- Hoppe, T., Cassata, G., Barral, J.M., Springer, W., Hutagalung, A.H., Epstein, H.F. and Baumeister, R., 2004. "Regulation of the Myosin-Directed Chaperone UNC-45 by a Novel E3/E4-Multiubiquitylation Complex in *C. Elegans*." *Cell* 118 (3): 337–49.
- Horton, M.J, Brandon, C.A., Morris, T.J., Braun, T.W., Yaw, K.M. and Sciote, J.J., 2001. "Abundant Expression of Myosin Heavy-Chain IIB RNA in a Subset of Human Masseter Muscle Fibres." *Archives of Oral Biology* 46 (11): 1039–50.
- Horton, M.J., Rosen, C., Close, J.M. and Sciote, J.J., 2008. "Quantification of Myosin Heavy Chain RNA in Human Laryngeal Muscles: Differential Expression in the Vertical and Horizontal Posterior Cricoarytenoid and Thyroarytenoid." *The Laryngoscope* 118 (3): 472–77.
- Houdusse, A. and Sweeney, H.L., 2016. "How Myosin Generates Force on Actin Filaments." *Trends in Biochemical Sciences* 41 (12): 989.
- Houmeida, A., Holt, J., Tskhovrebova, L. and Trinick J., 1995. "Studies of the Interaction between Titin and Myosin." *Journal of Cell Biology* 131: 1471–81.
- Hutagalung, A.H., Landsverk, M.L., Price, M.G. and Epstein, H.F., 2002. "The UCS Family of Myosin Chaperones." *Journal of Cell Science* 115 (21): 3983–90.
- Huxley, A.F. and Niedergerke, R., 1953. "Structural Changes in Muscle during Contraction: Interference Microscopy of Living Muscle Fibres." *Nature* 173: 971–73.
- Huxley, H.E. and Hanson, E.J., 1953. "Structural Basis of the Cross-Striations in Muscle." *Nature* 172: 530–32.
- Ingles, J., Burns, C., Bagnall, R.D., Lam, L., Yeates, L., Sarina, T., Puranik, R., et al. 2017. "Nonfamilial Hypertrophic Cardiomyopathy - Prevalence, Natural History, and Clinical Implications." *Circulation: Cardiovascular Genetics* 10 (2).
- Iorga, B., Adamek, N. and Geeves, M.A., 2007. "The Slow Skeletal Muscle Isoform of Myosin Shows Kinetic Features Common to Smooth and Non-Muscle Myosins." *Journal of Biological Chemistry* 282 (6): 3559–70.
- Jacoby, J., Ko, K., Weiss, C. and Rushbrook, J.I., 1990. "Systematic Variation in Myosin Expression along Extraocular Muscle Fibres of the Adult Rat." *Cell Motility* 11: 24–40.
- Janco, M., Suphamungmee, W., Li, X., Lehman, W., Lehrer, S.S. and Geeves, M.A., 2013. "Polymorphism in Tropomyosin Structure and Function." *Journal of Muscle Research and Cell Motility* 34 (3–4): 177–87.
- Janiesch, P.C., Kim, J., Mouysset, J., Barikbin, R., Lochmüller, H., Cassata, G., Krause, S. and Hoppe, T., 2007. "The Ubiquitin-Selective Chaperone CDC-48/P97 Links Myosin Assembly to Human Myopathy." *Nature Cell Biology* 9 (4): 379–90.
- Jeschke, B., Uhl, K., Weist, B., Schröder, D., Meitinger, T., Döhlemann, C. and Vosberg, H.P., 1998. "A High Risk Phenotype of Hypertrophic Cardiomyopathy Associated with a Compound Genotype of Two Mutated Beta-Myosin Heavy Chain Genes." *Human Genetics* 102 (3): 299–304.
- Johnson, M., East, D.A. and Mulvihill, D.P., 2014. "Formins Determine the Functional Properties of Actin Filaments in Yeast." *Current Biology* 24 (13): 1525–30.
- Jones, L.J., Carballido-López, R. and Errington, J., 2001. "Control of Cell Shape in Bacteria: Helical, Actin-like Filaments in *Bacillus Subtilis*." *Cell* 104 (6): 913–22.



Kabsch, W., Mannherz, H.G., Suck, D., Pai, E.F. and Holmes, K.C., 1990. "Atomic Structure of the Actin: DNase I Complex." *Nature* 347 (6288): 37–44.

Kachur, T. and Pilgrim, D., 2008. "Myosin Assembly, Maintenance and Degradation in Muscle: Role of the Chaperone UNC-45 in Myosin Thick Filament Dynamics." *International Journal of Molecular Sciences* 9 (9): 1863–75.

Kampourakis, T., Ponnampalasa, S., Sun, Y.B., Sevriva, I and Irving. M., 2018. "Structural and Functional Effects of Myosin-Binding Protein-C Phosphorylation in Heart Muscle Are Not Mimicked by Serine-to-Aspartate Substitutions." *Journal of Biological Chemistry* 293 (37): 14270–75.

Kampourakis, T., Yan, Z., Gautel, M., Sun, Y.B. and Irving, M., 2014. "Myosin Binding Protein-C Activates Thin Filaments and Inhibits Thick Filaments in Heart Muscle Cells." *Proceedings of the National Academy of Sciences of the United States of America* 111 (52): 18763–68.

Karatzafieri, C., Adamek, N., and Geeves, M.A., 2017. "Modulators of Actin-Myosin Dissociation: Basis for Muscle Type Functional Differences during Fatigue." *American Journal of Physiology-Cell Physiology* 313 (6): C644–C654.

Kaski, J.P., Syrris, P., Teresa M., Esteban, T., Jenkins, S., Pantazis, A., Deanfield, J.E., McKenna, W.J. and Elliott, P.M., 2009. "Prevalence of Sarcomere Protein Gene Mutations in Preadolescent Children With Hypertrophic Cardiomyopathy." *Circulation: Cardiovascular Genetics* 2 (5): 436–41.

Kawana, M., Sarkar, S.S., Sutton, S., Ruppel, K.M. and Spudich, J.A., 2017. "Biophysical Properties of Human  $\beta$ -Cardiac Myosin with Converter Mutations That Cause Hypertrophic Cardiomyopathy." *Science Advances* 3 (2): e1601959.

Kim, J.H., Graber, T.G., Liu, H., Asakura, A. and Thompson, L.D.V., 2019. "Increasing Myosin Light Chain 3f (MLC3f) Protects against a Decline in Contractile Velocity." Edited by Ashok Kumar. *PLoS One* 14 (4): e0214982.

Kobayashi, T., Jin, L. and de Tombe, P.P., 2008. "Cardiac Thin Filament Regulation." *Pflügers Archiv : European Journal of Physiology* 457 (1): 37–46.

Kominz, D.R., Mitchell, E.R., Nihei, T. and Kay, C.M., 1965. "The Papain Digestion of Skeletal Myosin A." *Biochemistry* 4 (11): 2373–82.

Koppole, S, Smith, J.C. and Fischer, S., 2006. "Simulations of the Myosin II Motor Reveal a Nucleotide-State Sensing Element That Controls the Recovery Stroke." *Journal of Molecular Biology* 361 (3): 604–16.

Korn, E.D., 2000. "Coevolution of Head, Neck, and Tail Domains of Myosin Heavy Chains." *Proceedings of the National Academy of Sciences* 97 (23): 12559–64.

Kronert, W.A., Bell, K.M., Viswanathan, M.C., Melkani, G.C., Trujillo, A.S., Huang, A., Melkani, A., Cammarato, A., Swank, D.M. and Bernstein, S.I., 2018. "Prolonged Cross-Bridge Binding Triggers Muscle Dysfunction in a Drosophila Model of Myosin-Based Hypertrophic Cardiomyopathy." *ELife* 7: e38064

Kurzawa, S.E., and Geeves, M.A., 1996. "A Novel Stopped-Flow Method for Measuring the Affinity of Actin for Myosin Head Fragments Using Microgram Quantities of Protein." *Journal of Muscle Research and Cell Motility* 17 (6): 669–76.

Labeit, S., Gautel, M., Lakey, A. and Trinick, J., 1992. "Towards a Molecular Understanding of Titin." *The EMBO Journal* 11 (5): 1711–16.

- Labeit, S. and Kolmerer, B., 1995. "Titins: Giant Proteins in Charge of Muscle Ultrastructure and Elasticity." *Science* 270: 293–96.
- Leavis, P.C. and Gergely, J., 1984. "Thin Filament Proteins and Thin Filament-Linked Regulation of Vertebrate Muscle Contraction." *CRC Critical Reviews in Biochemistry* 16 (3): 235–305.
- Lee, C.F., Melkani, G.C., Yu, Q., Suggs, J.A., Kronert, W.A., Suzuki, Y., Hipolito, L., Price, M.G., Epstein, H.F. and Bernstein, S.I., 2011. "Drosophila UNC-45 Accumulates in Embryonic Blastoderm and in Muscles, and Is Essential for Muscle Myosin Stability." *Journal of Cell Science* 124 (5): 699–705.
- Lee, C.F., Hauenstein, A.V., Fleming, J.K., Gasper, W.C., Engelke, V., Sankaran, B., Bernstein, S.I. and Huxford, T., 2011. "X-Ray Crystal Structure of the UCS Domain-Containing UNC-45 Myosin Chaperone from *Drosophila Melanogaster*." *Structure (London, England : 1993)* 19 (3): 397–408.
- Lee, C.F., Melkani, G.C. and Bernstein, S.I., 2014. "The UNC-45 Myosin Chaperone: From Worms to Flies to Vertebrates." *International Review of Cell and Molecular Biology* 313: 103–44.
- Lee, K.H., Sulbarán, G., Yang, S., Young Mun, J., Alamo, L., Pinto, A., Sato, O., et al. 2018. "Interacting-Heads Motif Has Been Conserved as a Mechanism of Myosin II Inhibition since before the Origin of Animals." *Proceedings of the National Academy of Sciences of the United States of America* 115 (9): E1991–2000.
- Lee, L.A., Karabina, A., Broadwell, L.J. and Leinwand, L.A., 2019. "The Ancient Sarcomeric Myosins Found in Specialized Muscles." *Skeletal Muscle* 9 (1): 1–15.
- Lefaucheur, L., Hoffman, R.K., Gerrard, D.E., Okamura, C.S., Rubinstein, N. and Kelly, A., 1998. "Evidence for Three Adult Fast Myosin Heavy Chain Isoforms in Type II Skeletal Muscle Fibers in Pigs." *Journal of Animal Science* 76 (6): 1584–93.
- Lehman, W., Rosol, M., Tobacman, L.S. and Craig, R., 2001. "Troponin Organization on Relaxed and Activated Thin Filaments Revealed by Electron Microscopy and Three-Dimensional Reconstruction." *Journal of Molecular Biology* 307 (3): 739–44.
- Lehrer, S.S., and Kerwar, G., 1972. "Intrinsic Fluorescence of Actin." *Biochemistry* 11 (7): 1211–17.
- Linari, M., Brunello, E., Reconditi, M., Fusi, L., Caremani, M., Narayanan, T., Piazzesi, G., Lombardi, V. and Irving, M., 2015. "Force Generation by Skeletal Muscle Is Controlled by Mechanosensing in Myosin Filaments." *Nature* 528 (7581): 276–79.
- Liu, X., Shu, S., Kovács, M. and Korn, E.D., 2005. "Biological, Biochemical, and Kinetic Effects of Mutations of the Cardiomyopathy Loop of Dictyostelium Myosin II: Importance of ALA400." *The Journal of Biological Chemistry* 280 (29): 26974–83.
- Liu, Y., White, H.D., Belknap, B., Winkelmann, D.A. and Forgacs, E., 2015. "Omecamtiv Mecarbil Modulates the Kinetic and Motile Properties of Porcine  $\beta$ -Cardiac Myosin." *Biochemistry* 54 (10): 1963–75.
- Llinas, P., Isabet, T., Song, L., Ropars, V., Zong, B., Benisty, H., Sirigu, S., et al. 2015. "How Actin Initiates the Motor Activity of Myosin." *Developmental Cell* 33 (4): 401–12.
- Lompré, A.M., Nadal-Ginard, B. and Mahdavi, V., 1984. "Expression of the Cardiac Ventricular Alpha- and Beta-Myosin Heavy Chain Genes Is Developmentally and Hormonally Regulated." *The Journal of Biological Chemistry* 259 (10): 6437–46.

- Lord, M. and Pollard, T.D., 2004. "UCS Protein Rng3p Activates Actin Filament Gliding by Fission Yeast Myosin-II." *The Journal of Cell Biology* 167 (2): 315–25.
- Loughna, P.T., Izumo, S., Goldspink, G. and Nadal-Ginard, B., 1990. "Disuse and Passive Stretch Cause Rapid Alterations in Expression of Developmental and Adult Contractile Protein Genes in Skeletal Muscle." *Development (Cambridge, England)* 109 (1): 217–23.
- Lowey, S., Waller, G.S. and Trybus, K.M., 1993a. "Function of Skeletal Muscle Myosin Heavy and Light Chain Isoforms by an in Vitro Motility Assay." *The Journal of Biological Chemistry* 268 (27): 20414–18.
- Lowey, S., Waller, G.S. and Trybus, K.M., 1993b. "Skeletal Muscle Myosin Light Chains Are Essential for Physiological Speeds of Shortening." *Nature* 365 (6445): 454–56.
- Lu, B.D., D L Allen, L A Leinwand, and G E Lyons. 1999. "Spatial and Temporal Changes in Myosin Heavy Chain Gene Expression in Skeletal Muscle Development." *Developmental Biology* 216 (1): 312–26.
- Lucas, C.A., Rughani, A. and Hoh. J.F., 1995. "Expression of Extraocular Myosin Heavy Chain in Rabbit Laryngeal Muscle." *Journal of Muscle Research and Cell Motility* 16 (4): 368–78.
- Lymm, R.W., and E.W Taylor. 1971. "Mechanism of Adenosine Triphosphate Hydrolysis by Actomyosin." *Biochemistry* 10 (25): 4617–24.
- Lynch, G.S., Frueh, B.R. and Williams, D.A., 1994. "Contractile Properties of Single Skinned Fibres from the Extraocular Muscles, the Levator and Superior Rectus, of the Rabbit." *The Journal of Physiology* 475 (2): 337–46.
- Lyons, G.E., Ontell, M., Cox, R., Sassoon, D. and Buckingham, M., 1990. "The Expression of Myosin Genes in Developing Skeletal Muscle in the Mouse Embryo." *The Journal of Cell Biology* 111: 1465–76.
- Mansson, A., Rassier, D. and Tsiavaliaris, G., 2015. "Poorly Understood Aspects of Striated Muscle Contraction." *Biomed Research International*, Epub 2015 Apr 16.
- Margossian, S.S. and Lowey, S., 1982. "Preparation of Myosin and Its Subfragments from Rabbit Skeletal Muscle." *Methods in Enzymology* 85: 55–71.
- Maron, B.J., 2004. "Hypertrophic Cardiomyopathy in Childhood." *Pediatric Clinics of North America* 51 (5): 1305–46.
- Maron, B.J., Gardin, J.M., Flack, J.M., Gidding, S.S., Kurosaki, T.T. and Bild, D.E., 1995. "Prevalence of Hypertrophic Cardiomyopathy in a General Population of Young Adults." *Circulation* 92 (4): 785–89.
- Maron, B.J. and Maron, M.S., 2013. "Hypertrophic Cardiomyopathy." *The Lancet* 381 (9862): 242–55.
- Maron, B.J., McKenna, W.J., Danielson, G.K., Kappenberger, L.J., Kuhn, H.J., Seidman, C.E., Shah, P.M., et al. 2003. "American College of Cardiology/European Society of Cardiology Clinical Expert Consensus Document on Hypertrophic Cardiomyopathy. A Report of the American College of Cardiology Foundation Task Force on Clinical Expert Consensus Documents and the European Society of Cardiology Committee for Practice Guidelines." *Journal of the American College of Cardiology* 42 (9): 1687–1713.

- Marston, S., 2018. "The Molecular Mechanisms of Mutations in Actin and Myosin That Cause Inherited Myopathy." *International Journal of Molecular Sciences* 19 (7).
- Maruyama, K. and Ebashi, S., 1965. " $\alpha$ -Actinin, a New Structural Protein from Striated Muscle. II. Action on Actin." *Journal of Biochemistry* 58: 13–19.
- Masters, T.A., Kendrick-Jones, J. and Buss, F., 2016. "Myosins: Domain Organisation, Motor Properties, Physiological Roles and Cellular Functions." In *Handbook of Experimental Pharmacology*, 235:77–122.
- Matthew, J.D., Khromov, A.S., Trybus, K.M., Somlyo, A.P. and Somlyo, A.V., 1998. "Myosin Essential Light Chain Isoforms Modulate the Velocity of Shortening Propelled by Nonphosphorylated Cross-Bridges." *The Journal of Biological Chemistry* 273 (47): 31289–96.
- McElhinny, A.S., Kolmerer, B., Fowler, V.M., Labeit, S. and Gregorio, C.C., 2001. "The N-Terminal End of Nebulin Interacts with Tropomodulin at the Pointed Ends of the Thin Filaments." *Journal of Biological Chemistry*, no. 276: 583–92.
- McGreig, J.E., Jeanfavre, S.T., Henson, C., Coghlan, M.P., Walklate, J., Ridout, M, Baines, A.J., Geeves, M.A. and Wass, M.N., 2019. "Adaptation of Mammalian Myosin II Sequences to Body Mass," 1–25. *bioRxiv* 680413; doi: <https://doi.org/10.1101/680413>
- McKay, R.T., Tripet, B.P., Hodges, R.S. and Sykes, B.D., 1997. "Interaction of the Second Binding Region of Troponin I with the Regulatory Domain of Skeletal Muscle Troponin C as Determined by NMR Spectroscopy." *The Journal of Biological Chemistry* 272 (45): 28494–500.
- Melkani, G.C., Bodmer, R., Ocorr, K. and Bernstein, S.I., 2011. "The UNC-45 Chaperone Is Critical for Establishing Myosin-Based Myofibrillar Organization and Cardiac Contractility in the *Drosophila* Heart Model." Edited by Edathara Abraham. *PLoS ONE* 6 (7): e22579.
- Melkani, G.C., Lee, C.F., Cammarato, A. and Bernstein, S.I., 2010. "Drosophila UNC-45 Prevents Heat-Induced Aggregation of Skeletal Muscle Myosin and Facilitates Refolding of Citrate Synthase." *Biochemical and Biophysical Research Communications* 396 (2): 317–22.
- Mihalyi, E. and Harrington, W.F., 1959. "Studies on the Tryptic Digestion of Myosin." *Biochimica et Biophysica Acta* 36 (2): 447–66.
- Mijailovich, S.M., Nedic, D., Svcevic, M., Stojanovic, B., Walklate, J., Ujfalusi, Z. and Geeves, M.A., 2017. "Modeling the Actin-Myosin ATPase Cross-Bridge Cycle for Skeletal and Cardiac Muscle Myosin Isoforms." *Biophysical Journal* 112 (5).
- Mijailovich, S.M., Li, X., del Álamo, J.C., Griffiths, R.H., Kecman, V. and Geeves, M.A., 2010. "Resolution and Uniqueness of Estimated Parameters of a Model of Thin Filament Regulation in Solution." *Computational Biology and Chemistry* 34 (1): 19–33.
- Mijailovich, S.M., Kayser-Herold, O., Stojanovic, B., Nedic, D., Irving, T.C. and Geeves, M.A., 2016. "Three-Dimensional Stochastic Model of Actin-Myosin Binding in the Sarcomere Lattice." *The Journal of General Physiology* 148 (6): 459–88.
- Miyata, S., Minobe, W., Bristow, M.R. and Leinwand, L.A., 2000. "Myosin Heavy Chain Isoform Expression in the Failing and Nonfailing Human Heart." *Circulation Research* 86 (4): 386–90.
- Moos, C., Offer, G., Starr, R. and Bennett, P., 1975. "Interaction of C-Protein with Myosin, Myosin Rod and Light Meromyosin." *Journal of Molecular Biology* 97 (1): 1–9.

- Morita, H., Rehm, H.L., Menesses, A., McDonough, B., Roberts, A.E., Kucherlapati, R., Towbin, J.A., Seidman, J.G. and Seidman, C.E., 2008. "Shared Genetic Causes of Cardiac Hypertrophy in Children and Adults." *The New England Journal of Medicine* 358 (18): 1899–1908.
- Mornet, D., Pantel, P., Audemard, E. and Kassab, R., 1979. "The Limited Tryptic Cleavage of Chymotryptic S-1: An Approach to the Characterization of the Actin Site in Myosin Heads." *Biochemical and Biophysical Research Communications* 89 (3): 925–32.
- Mouton, J., Loos, B., Moolman-Smook, J.C. and Kinnear, C.J., 2015. "Ascribing Novel Functions to the Sarcomeric Protein, Myosin Binding Protein H (MyBPH) in Cardiac Sarcomere Contraction." *Experimental Cell Research* 331 (2): 338–51.
- Muretta, J.M., Rohde, J.A., Johnsrud, D.O., Cornea, S. and Thomas, D.D., 2015. "Direct Real-Time Detection of the Structural and Biochemical Events in the Myosin Power Stroke." *Proceedings of the National Academy of Sciences* 112 (46): 14272–77.
- Nag, S., Sommese, R.F., Ujfalusi, Z., Combs, A., Langer, S., Sutton, S., Leinwand, L.A., Geeves, M.A., Ruppel, K.M. and Spudich, J.A., 2015. "Contractility Parameters of Human  $\beta$ -Cardiac Myosin with the Hypertrophic Cardiomyopathy Mutation R403Q Show Loss of Motor Function." *Science Advances* 1 (9): e1500511.
- Nag, S., Trivedi, D.V., Sarkar, S.S., Adhikari, A.S., Sunitha, M.S., Sutton, S., Ruppel, K.M. and Spudich, J.A., 2017. "The Myosin Mesa and the Basis of Hypercontractility Caused by Hypertrophic Cardiomyopathy Mutations." *Nature Structural & Molecular Biology* 24 (6): 525–33.
- Nagase, T., Ishikawa, K., Miyajima, N., Tanaka, A., Kotani, H., Nomura, N. and Ohara, O., 1998. "Prediction of the Coding Sequences of Unidentified Human Genes. IX. The Complete Sequences of 100 New CDNA Clones from Brain Which Can Code for Large Proteins in Vitro." *DNA Research: An International Journal for Rapid Publication of Reports on Genes and Genomes* 5 (1): 31–39.
- Nakao, K., Minobe, W., Roden, R., Bristow, M.R. and Leinwand, L.A., 1997. "Myosin Heavy Chain Gene Expression in Human Heart Failure." *Journal of Clinical Investigation* 100 (9): 2362–70.
- Narusawa, M., Fitzsimons, R.B., Izumo, S., Nadal-Ginard, B., Rubinstein, N.A. and Kelly, A.M., 1987. "Slow Myosin in Developing Rat Skeletal Muscle." *Journal of Biological Chemistry* 104 (3): 447–50.
- Nishikawa, K., Dutta, S., DuVall, M., Nelson, B., Gage, M.J. and Monroy, J.A., 2019. "Calcium-Dependent Titin–Thin Filament Interactions in Muscle: Observations and Theory." *Journal of Muscle Research and Cell Motility*, July.
- Novak, K.D. and Titus, M.A., 1998. "The Myosin I SH3 Domain and TEDS Rule Phosphorylation Site Are Required for in Vivo Function." *Molecular Biology of the Cell* 9 (1): 75–88.
- Nyitrai, M. and Geeves, M.A., 2004. "Adenosine Diphosphate and Strain Sensitivity in Myosin Motors." *Philosophical Transactions of the Royal Society B: Biological Sciences* 359 (1452): 1867–77.
- Nyitrai, M., Rossi, R., Adamek, N., Pellegrino, M., Bottinelli, R., and Geeves, M.A., 2006. "What Limits the Velocity of Fast-Skeletal Muscle Contraction in Mammals?" *Journal of Molecular Biology* 355 (3): 432–42.
- O'Connell, C.B., Tyska, M.J. and Mooseker, M.S., 2007. "Myosin at Work: Motor Adaptations for a Variety of Cellular Functions." *Biochimica et Biophysica Acta* 1773 (5c): 615–30.
- Odrionitz, F. and Kollmar, M., 2007. "Drawing the Tree of Eukaryotic Life Based on the Analysis of 2,269 Manually Annotated Myosins from 328 Species." *Genome Biology* 8 (9): 196.

- Olafsson, S., Whittington, D., Murray, J., Regnier, M. and Moussavi-Harami, F., 2017. "Fast and Sensitive HPLC–MS/MS Method for Direct Quantification of Intracellular Deoxyribonucleoside Triphosphates from Tissue and Cells." *Journal of Chromatography B: Analytical Technologies in the Biomedical and Life Sciences* 1068–1069 (June): 90–97.
- Olivotto, I, Cecchi, F., Poggesi, C. and Yacoub, M.H., 2012. "Patterns of Disease Progression in Hypertrophic Cardiomyopathy: An Individualized Approach to Clinical Staging." *Circulation. Heart Failure* 5 (4): 535–46.
- OOta, S. and Saitou, N., 1999. "Phylogenetic Relationship of Muscle Tissues Deduced from Superimposition of Gene Trees." *Molecular Biology and Evolution* 16 (6): 856–67.
- Ostap, E.M., Lin, T., Rosenfeld, S.S. and Tang, N., 2002. "Mechanism of Regulation of Acanthamoeba Myosin-1C by Heavy-Chain Phosphorylation." *Biochemistry* 41 (41): 12450–56.
- Otterbein, L.R., Graceffa, P. and Dominguez, R., 2001. "The Crystal Structure of Uncomplexed Actin in the ADP State." *Science* 293: 708–11.
- Park, H., Li, A., Chen, L.Q., Houdusse, A., Selvin, P.R. and Sweeney, H.L., 2007. "The Unique Insert at the End of the Myosin VI Motor Is the Sole Determinant of Directionality." *Proceedings of the National Academy of Sciences of the United States of America* 104 (3): 778–83.
- Park, K., Lim, J., Sohn, S. and Yeul, S., 2012. "Myosin Heavy Chain Isoform Expression in Human Extraocular Muscles: Longitudinal Variation and Patterns of Expression in Global and Orbital Layers." *Muscle & Nerve* 45: 713–20.
- Pellegrino, M.A., Canepari, M., Rossi, R., D'Antona, G., Reggiani, C. and Bottinelli, R., 2003. "Orthologous Myosin Isoforms and Scaling of Shortening Velocity with Body Size in Mouse, Rat, Rabbit and Human Muscles." *The Journal of Physiology* 546 (Pt 3): 677–89.
- Pette, D. and Vrbová, G., 1985. "Neural Control of Phenotypic Expression in Mammalian Muscle Fibers." *Muscle & Nerve* 8 (8): 676–89.
- Piroddi, N., Belus, A., Scellini, B., Tesi, C., Giunti, G., Cerbai, E., Mugelli, A. and Poggesi, C., 2007. "Tension Generation and Relaxation in Single Myofibrils from Human Atrial and Ventricular Myocardium." *Pflügers Archiv - European Journal of Physiology* 454 (1): 63–73.
- Pokrzywa, W. and Hoppe, T., 2013. "Chaperoning Myosin Assembly in Muscle Formation and Aging." *Worm* 2 (3): e25644.
- Porter, J.D. and Baker, R.S., 1996. "Muscles of a Different 'Color': The Unusual Properties of the Extraocular Muscles May Predispose or Protect Them in Neurogenic and Myogenic Disease." *Neurology* 46 (1): 30–37.
- Potter, J.D., Sheng, Z., Pan, B.S. and Zhao, J., 1995. "A Direct Regulatory Role for Troponin T and a Dual Role for Troponin C in the Ca<sup>2+</sup> Regulation of Muscle Contraction." *The Journal of Biological Chemistry* 270 (6): 2557–62.
- Poutanen, T., Tikanoja, T., Jääskeläinen, P., Jokinen, E., Silvast, A., Laakso, M. and Kuusisto, J., 2006. "Diastolic Dysfunction without Left Ventricular Hypertrophy Is an Early Finding in Children with Hypertrophic Cardiomyopathy-Causing Mutations in the Beta-Myosin Heavy Chain, Alpha-Tropomyosin, and Myosin-Binding Protein C Genes." *American Heart Journal* 151 (3): 725.e1-725.e9.
- Price, M.G., Landsverk, M.L., Barral, J.M. and Epstein, H.F., 2002. "Two Mammalian UNC-45 Isoforms Are Related to Distinct Cytoskeletal and Muscle-Specific Functions." *Journal of Cell Science* 115 (21): 4013–23.

- Racca, A.W., Beck, A.E., Rao, V.S., Flint, G.V., Lundy, S.D., Born, D.E., Bamshad, M.J. and Regnier, M., 2013. "Contractility and Kinetics of Human Fetal and Human Adult Skeletal Muscle." *Journal of Physiology* 591: 3049–61.
- Rajani S. and Winkelmann, D.A., 2004. "Chaperone-Mediated Folding and Assembly of Myosin in Striated Muscle." *Journal of Cell Science* 117 (4): 641–52.
- Rayment, I., Rypniewski, W.R., Schmidt-bäse, K., Smith, R., Tomchick, R., Benning, M.M., Winkelmann, D.A., Wesenberg, G., Holden, H.M. and Tomchick, D.R., 1993. "Structure of Three-Dimensional A Molecular Motor." *Science* 261 (5117): 50–58.
- Resnicow, D.I., Deacon, J.C., Warrick, H.M., Spudich, J.A. and Leinwand, L.A., 2010. "Functional Diversity among a Family of Human Skeletal Muscle Myosin Motors." *Proceedings of the National Academy of Sciences of the United States of America* 107 (3): 1053–58.
- Richards, C.S., Bale, S., Bellissimo, D.B., Das, S., Grody, W.W., Hegde, M.R., Lyon, E., Ward, B.E. and Molecular Subcommittee of the ACMG Laboratory Quality Assurance Committee., 2008. "ACMG Recommendations for Standards for Interpretation and Reporting of Sequence Variations: Revisions 2007." *Genetics in Medicine : Official Journal of the American College of Medical Genetics* 10 (4): 294–300.
- Richards, T.A. and Cavalier-Smith, T., 2005. "Myosin Domain Evolution and the Primary Divergence of Eukaryotes." *Nature* 436 (7054): 1113–18.
- Ritchie, M.D., Geeves, M.A., Woodward, S.K. and Manstein, D.J., 1993. "Kinetic Characterization of a Cytoplasmic Myosin Motor Domain Expressed in Dictyostelium Discoideum." *Proceedings of the National Academy of Sciences* 90 (18): 8619–23.
- Robert-Paganin, J., Auguin, D. and Houdusse, A., 2018. "Hypertrophic Cardiomyopathy Disease Results from Disparate Impairments of Cardiac Myosin Function and Auto-Inhibition." *Nature Communications* 9 (1): 4019.
- Rooij, E.V., Liu, N. and Olson, E.N., 2008. "MicroRNAs Flex Their Muscles." *Trends in Genetics : TIG* 24 (4): 159–66.
- Rooij, E.V., Quiat, D., Johnson, B.A., Sutherland, L.B., Qi, X., Richardson, J.A., Kelm, R.J. and Olson, E.N., 2009. "A Family of MicroRNAs Encoded by Myosin Genes Governs Myosin Expression and Muscle Performance." *Developmental Cell* 17 (5): 662–73.
- Rubinstein, N.A. and Kelly, A.M., 1981. "Development of Muscle Fibre Specialization in the Rat Hindlimb." *Journal of Biological Chemistry* 90 (1): 128–44.
- Rubinstein, N.A., Porter, J.D. and Hoh, J.F.Y., 2004. "The Development of Longitudinal Variation of Myosin Isoforms in the Orbital Fibers of Extraocular Muscles of Rats." *Investigative Ophthalmology & Visual Science* 45: 3067–72.
- Sanger, J.W., Kang, S., Siebrands, C.C., Freeman, N., Du, A., Wang, J., Stout, A.L. and Sanger, J.M., 2006. "How to Build a Myofibril." *Journal of Muscle Research and Cell Motility* 26 (6–8): 343–54.
- Sartore, S., Gorza, L. and Schiaffino, S., 1982. "Fetal Myosin Heavy Chains in Regenerating Muscle." *Nature* 298 (5871): 294–96.
- Sartore, S., Mascarello, F., Rowlerson, A., Gorza, L., Ausoni, S., Vianello, M. and Schiaffino, S., 1987. "Fibre Types in Extraocular Muscles: A New Myosin Isoform in the Fast Fibres." *Journal of Muscle Research and Cell Motility* 8 (2): 161–72.

- Sasaki, N., Ohkura, R. and Sutoh, K., 2000. "Insertion or Deletion of a Single Residue in the Strut Sequence of Dictyostelium Myosin II Abolishes Strong Binding to Actin." *Journal of Biological Chemistry* 275 (49): 38705–9.
- Savage, V.M., Allen, A.P., Brown, J.H., Gillooly, J.F., Herman, A.B., Woodruff, W.H. and West, G.B., 2007. "Scaling of Number, Size, and Metabolic Rate of Cells with Body Size in Mammals." *Proceedings of the National Academy of Sciences* 104 (11): 4718–23.
- Schachat, F. and Briggs, M.M., 2002. "Phylogenetic Implications of the Superfast Myosin in Extraocular Muscles." *Journal of Experimental Biology* 205: 2189–2201.
- Scheufler, C., Brinker, A., Bourenkov, G., Pegoraro, S., Moroder, L., Bartunik, H., Hartl, F.U. and Moarefi, I., 2000. "Structure of TPR Domain–Peptide Complexes." *Cell* 101 (2): 199–210.
- Schiaffino, S. and Reggiani, C., 2011. "Fiber Types in Mammalian Skeletal Muscles." *Physiological Reviews* 91 (4): 1447–1531.
- Schiaffino, S., Rossi, A.C., Smerdu, V., Leinwand, L.A. and Reggiani, C., 2015. "Developmental Myosins: Expression Patterns and Functional Significance." *Skeletal Muscle* 5 (1): 1–14.
- Sebé-Pedrós, A., Grau-Bové, X., Richards, T.A. and Ruiz-Trillo, I., 2014. "Evolution and Classification of Myosins, a Eukaryotic Whole-Genome Approach." *Genome Biology and Evolution* 6 (2): 290–305.
- Sellers, J.R., 2000. "Myosins: A Diverse Superfamily." *Biochimica et Biophysica Acta* 1496 (1): 3–22.
- Semsarian, C., Ingles, J., Maron, M.S. and Maron, B.J., 2015. "New Perspectives on the Prevalence of Hypertrophic Cardiomyopathy." *Journal of the American College of Cardiology* 65 (12): 1249–54. <https://doi.org/10.1016/j.jacc.2015.01.019>.
- Sheetz, M.P., Chasan, R. and Spudich, J.A., 1984. "ATP-Dependent Movement of Myosin in Vitro: Characterization of a Quantitative Assay." *Journal of Cell Biology* 99 (5): 1867–71.
- Shi, H. and Blobel, G., 2010. "UNC-45/CRO1/She4p (UCS) Protein Forms Elongated Dimer and Joins Two Myosin Heads near Their Actin Binding Region." *Proceedings of the National Academy of Sciences* 107 (50): 21382–87.
- Siegfried, L., Ottenheijm, C.A.C. and Granzier, H., 2011. "Nebulin, a Major Player in Muscle Health and Disease." *FASEB Journal* 25 (3): 822–29.
- Siemankowski, R.F. and White, H.D., 1984. "Kinetics of the Interaction between Actin, ADP, and Cardiac Myosin-S1." *The Journal of Biological Chemistry* 259 (8): 5045–53.
- Siemankowski, R.F., Wiseman, M.O. and White, H., 1985. "ADP Dissociation from Actomyosin Subfragment 1 Is Sufficiently Slow to Limit the Unloaded Shortening Velocity in Vertebrate Muscle." *Proceedings of the National Academy of Science of the United States of America* 82 (February): 658–62.
- Sleep, J., Irving, M. and Burton, K., 2005. "The ATP Hydrolysis and Phosphate Release Steps Control the Time Course of Force Development in Rabbit Skeletal Muscle." *The Journal of Physiology* 563 (3): 671–87.
- Smerdu, V., Karsch-Mizrachi, I., Campione, M., Leinwand, L. and Schiaffino, S., 1994. "Type IIx Myosin Heavy Chain Transcripts Are Expressed in Type IIb Fibers of Human Skeletal Muscle." *American Journal of Physiology-Cell Physiology* 267 (6): C1723–28.



- Smith, D.A., and Geeves, M.A., 1995. "Strain-Dependent Cross-Bridge Cycle for Muscle. II. Steady-State Behavior." *Biophysical Journal* 69 (2): 538–52.
- Soler, R., Méndez, C., Rodríguez, E., Barriales, R., Ochoa, J.P. and Monserrat, L., 2018. "Phenotypes of Hypertrophic Cardiomyopathy. An Illustrative Review of MRI Findings." *Insights into Imaging* 9 (6): 1007–20.
- Soteriou, A., Gamage, M. and Trinick, J., 1993. "A Survey of Interactions Made by the Giant Protein Titin." *Journal of Cell Science*, no. 104: 119–23.
- Spudich, J.A., 2015. "The Myosin Mesa and a Possible Unifying Hypothesis for the Molecular Basis of Human Hypertrophic Cardiomyopathy." *Biochemical Society Transactions* 43 (1): 64–72.
- Spudich, J.A., 2019. "Three Perspectives on the Molecular Basis of Hypercontractility Caused by Hypertrophic Cardiomyopathy Mutations." *Pflugers Archiv : European Journal of Physiology* 471 (5): 701–17.
- Squire, J.M., Luther, P.K. and Knupp, C., 2003. "Structural Evidence for the Interaction of C-Protein (MyBP-C) with Actin and Sequence Identification of a Possible Actin-Binding Domain." *Journal of Molecular Biology* 331 (3): 713–24.
- Srikakulam, R. and Winkelmann, D.A., 2004. "Chaperone-Mediated Folding and Assembly of Myosin in Striated Muscle." *Journal of Cell Science* 117 (4): 641–52.
- Srikakulam, R., Liu, I. and Winkelmann, D.A., 2008. "Unc45b Forms a Cytosolic Complex with Hsp90 and Targets the Unfolded Myosin Motor Domain." Edited by Hilal Lashuel. *PLoS ONE* 3 (5): e2137.
- Srikakulam, R. and Winkelmann, D.A., 1999. "Myosin II Folding Is Mediated by a Molecular Chaperonin." *Journal of Biological Chemistry* 274 (38): 27265–73.
- Starr, R. and Offer, G., 1978. "The Interaction of C-Protein with Heavy Meromyosin and Subfragment-2." *The Biochemical Journal* 171 (3): 813–16.
- Stein, L.A., White, M.P. and Annis, D.T., 1989. "Biochemical Kinetics of Porcine Cardiac Subfragment-1. II. Pre-Steady-State Studies of the Initial Phosphate Burst." *Circulation Research* 65 (2): 515–25.
- Steinmetz, P.R.H., Kraus, J.E.M., Larroux, C., Hammel, J.U., Amon-Hassenzahl, A., Houliston, E., Wörheide, G., Nickel, M., Degnan, B.M. and Technau, U., 2012. "Independent Evolution of Striated Muscles in Cnidarians and Bilaterians." *Nature* 487 (7406): 231–34.
- Stewart, M.A., Franks-Skiba, K., Chen, S. and Cooke, R., 2010. "Myosin ATP Turnover Rate Is a Mechanism Involved in Thermogenesis in Resting Skeletal Muscle Fibers." *Proceedings of the National Academy of Sciences* 107 (1): 430–35.
- Sung, J., Nag, S., Mortensen, K.I., Vestergaard, C.L., Sutton, S., Ruppel, K., Flyvbjerg, H. and Spudich, J.A., 2015. "Harmonic Force Spectroscopy Measures Load-Dependent Kinetics of Individual Human  $\beta$ -Cardiac Myosin Molecules." *Nature Communications* 6 (1): 7931.
- Sweeney, H.L. and Houdusse, A., 2010. "Structural and Functional Insights into the Myosin Motor Mechanism." *Annual Review of Biophysics* 39 (1): 539–57.
- Teare, D., 1958. "Asymmetrical Hypertrophy of the Heart in Young Adults." *British Heart Journal* 20 (1): 1–8.

- Tester, D.J. and Ackerman, M.J., 2011. "Genetic Testing for Potentially Lethal, Highly Treatable Inherited Cardiomyopathies/Channelopathies in Clinical Practice." *Circulation* 123 (9): 1021–37.
- Thompson, R.F. and Langford, G.M., 2002. "Myosin Superfamily Evolutionary History." *The Anatomical Record* 268 (3): 276–89. <https://doi.org/10.1002/ar.10160>.
- Tilney, L.G., 1976. "The Polymerization of Actin. II. How Nonfilamentous Actin Becomes Nonrandomly Distributed in Sperm: Evidence for the Association of This Actin with Membranes." *The Journal of Cell Biology* 69 (1): 51–72.
- Toepfer, C., Caorsi, V., Kampourakis, T., Sikkil, M.B., West, T.G., Leung, M.C., Al-Saud, S.A., et al. 2013. "Myosin Regulatory Light Chain (RLC) Phosphorylation Change as a Modulator of Cardiac Muscle Contraction in Disease." *The Journal of Biological Chemistry* 288 (19): 13446–54.
- Toniolo, L., Patruno, M., Maccatrozzo, L., Pellegrino, M.A., Canepari, M., Rossi, R., D'Antona, G., Bottinelli, R., Reggiani, C. and Mascarello, F., 2004. "Fast Fibres in a Large Animal: Fibre Types, Contractile Properties and Myosin Expression in Pig Skeletal Muscles." *The Journal of Experimental Biology* 207 (Pt 11): 1875–86.
- Tripathi, S., Schultz, I., Becker, E., Montag, J., Borchert, B., Francino, A., Navarro-Lopez, F., et al. 2011. "Unequal Allelic Expression of Wild-Type and Mutated  $\beta$ -Myosin in Familial Hypertrophic Cardiomyopathy." *Basic Research in Cardiology* 106 (6): 1041–55.
- Trivedi, D.V., Adhikari, A.S., Sarkar, S.S., Ruppel, K.M. and Spudich, J.A., 2018. "Hypertrophic Cardiomyopathy and the Myosin Mesa: Viewing an Old Disease in a New Light." *Biophysical Reviews* 10 (1): 27–48.
- Ujfalusi, Z., Vera, C.D., Mijailovich, S.M., Svicevic, M., Yu, E.C., Kawana, M., Ruppel, K.M., Spudich, J.A., Geeves, M.A. and Leinwand, L.A., 2018. "Dilated Cardiomyopathy Myosin Mutants Have Reduced Force-Generating Capacity." *Journal of Biological Chemistry* 293 (23): 9017–29.
- Vale, R.D., 2003. "The Molecular Motor Toolbox for Intracellular Transport." *Cell* 112 (4): 467–80.
- Varnava, A.M., Elliott, P.M., Sharma, S., McKenna, W.J. and Davies, M.J., 2000. "Hypertrophic Cardiomyopathy: The Interrelation of Disarray, Fibrosis, and Small Vessel Disease." *Heart (British Cardiac Society)* 84 (5): 476–82.
- Venolia, L. and Waterston, R.H., 1990. "The Unc-45 Gene of *Caenorhabditis Elegans* Is an Essential Muscle-Affecting Gene with Maternal Expression." *Genetics* 126 (2): 345–53.
- Venolia, L., Ao, W., Kim, S., Kim, C. and Pilgrim, D., 1999. "Unc-45 Gene Of *Caenorhabditis Elegans* Encodes a Muscle-Specific Tetratricopeptide Repeat-Containing Protein." *Cell Motility and the Cytoskeleton* 42 (3): 163–77.
- Vinson, V.K., De La Cruz, E.M., Higgs, H.N. and Pollard, T.D., 1998. "Interactions of *Acanthamoeba* Profilin with Actin and Nucleotides Bound to Actin." *Biochemistry* 37 (31): 10871–80.
- Walker, M.G., 2001. "Pharmaceutical Target Identification by Gene Expression Analysis." *Mini Reviews in Medicinal Chemistry* 1 (2): 197–205.
- Walklate, J., Vera, C., Bloemink, M.J., Geeves, M.A. and Leinwand, L.A., 2016. "The Most Prevalent Freeman-Sheldon Syndrome Mutations in the Embryonic Myosin Motor Share Functional Defects." *Journal of Biological Chemistry* 291 (19).
- Walklate, J., Ujfalusi, Z. and Geeves, M.A., 2016. "Myosin Isoforms and the Mechanochemical Cross-Bridge Cycle." *The Journal of Experimental Biology* 219 (2): 168–74.

- Walro, J.M. and Kucera, J., 1999. "Why Adult Mammalian Intrafusal and Extrafusal Fibers Contain Different Myosin Heavy-Chain Isoforms. Trends Neurosci 22: 180 –184, 1999." Trends in Neurosciences 22: 180–84.
- Walsh, R., Rutland, C., Thomas, R. and Loughna, S., 2010. "Cardiomyopathy: A Systematic Review of Disease-Causing Mutations in Myosin Heavy Chain 7 and Their Phenotypic Manifestations." Cardiology 115 (1): 49–60.
- Wang, J, Wang, Y., Zou, Y., Sun, K., Wang, Z., Ding, H., Yuan, J., et al. 2014. "Malignant Effects of Multiple Rare Variants in Sarcomere Genes on the Prognosis of Patients with Hypertrophic Cardiomyopathy." European Journal of Heart Failure 16 (9): 950–57.
- Weiss, A., Schiaffino, S. and Leinwand, L.A., 1999. "Comparative Sequence Analysis of the Complete Human Sarcomeric Myosin Heavy Chain Family: Implications for Functional Diversity." Journal of Molecular Biology 290 (1): 61–75.
- Weiss, A., 1996. "The mammalian myosin heavy chain gene family." Annual Reviews LEINCHPT.DUN AR18-14 Annu. Rev. Cell Dev. Biol. Vol. 18.
- Weiss, S., Rossi, R., Pellegrino, M.A., Bottinelli, R. and Geeves, M.A., 2001. "Differing ADP Release Rates from Myosin Heavy Chain Isoforms Define the Shortening Velocity of Skeletal Muscle Fibers." Journal of Biological Chemistry 276 (49): 45902–8.
- Weith, A.E., Previs, M.J., Hoeprich, G.J., Previs, S.B., Gulick, J., Robbins, J. and Warshaw, D.M., 2012. "The Extent of Cardiac Myosin Binding Protein-C Phosphorylation Modulates Actomyosin Function in a Graded Manner." Journal of Muscle Research and Cell Motility 33 (6): 449–59.
- Wesche, S., Arnold, M. and Jansen, R.P., 2003. "The UCS Domain Protein She4p Binds to Myosin Motor Domains and Is Essential for Class I and Class V Myosin Function." Current Biology : CB 13 (9): 715–24.
- Whalen, R.G., Sell, S.M., Butler-Browne, G.S., Schwartz, K., Bouveret, P. and Pinset-Härström, I., 1981. "Three Myosin Heavy-Chain Isozymes Appear Sequentially in Rat Muscle Development." Nature 292 (5826): 805–9.
- White, H.D., Belknap, B. and Webb, M.R., 1997. "Kinetics of Nucleoside Triphosphate Cleavage and Phosphate Release Steps by Associated Rabbit Skeletal Actomyosin, Measured Using a Novel Fluorescent Probe for Phosphate †." Biochemistry 36 (39): 11828–36.
- Wieczorek, D.F, Periasamy, M., Butler-Browne, G.S., Whalen, R.G. and Nadal-Ginard, B., 1985. "Co-Expression of Multiple Myosin Heavy Chain Genes, in Addition to a Tissue-Specific One, in Extraocular Musculature." Journal of Cell Biology 101: 618–29.
- Willott, R.H., Gomes, A.V., Chang, A.N., Parvatiyar, M.S., Pinto, J.R. and Potter, J.D., 2010. "Mutations in Troponin That Cause HCM, DCM AND RCM: What Can We Learn about Thin Filament Function?" Journal of Molecular and Cellular Cardiology 48 (5): 882–92.
- Woodward, S.K., A., Geeves, M.A. and Manstein, D.J., 1995. "Kinetic Characterization of the Catalytic Domain of Dictyostelium Discoideum Myosin." Biochemistry 34 (49): 16056–64.
- Woody, M.S., Winkelmann, D.A., Capitanio, M., Ostap, E.M. and Goldman Y.E., 2019. "Single Molecule Mechanics Resolves the Earliest Events in Force Generation by Cardiac Myosin." ELife 8 (September).
- Yetman, AT. and McCrindle, B.W., 2005. "Management of Pediatric Hypertrophic Cardiomyopathy." Current Opinion in Cardiology 20 (2): 80–83.

Yilmaz, A., Kindermann, I., Kindermann, M., Mahfoud, F., Ukena, C., Athanasiadis, A., Hill, S. et al., 2010. "Comparative Evaluation of Left and Right Ventricular Endomyocardial Biopsy: Differences in Complication Rate and Diagnostic Performance." *Circulation* 122 (9): 900–909.

Yu, H., Ma, L., Yang, Y. and Cui, Q., 2007. "Mechanochemical Coupling in the Myosin Motor Domain. I. Insights from Equilibrium Active-Site Simulations." *PLoS Computational Biology* 3 (2): e21.

Yu, Q. and Bernstein., S.I., 2003. "UCS Proteins: Managing the Myosin Motor." *Current Biology* : CB 13 (13): R525-7.

Zhou, Y., Liu, D. and Kaminski, H.J., 2010. "Myosin Heavy Chain Expression in Mouse Extraocular Muscle: More Complex than Expected. Investig." *Investigative Ophthalmology & Visual Science* 51: 6355–63.